

Thèse de Doctorat

Abdul ROCHIM

*Mémoire présenté en vue de l'obtention du
grade de Docteur de l'Université de Nantes
sous le label de l'Université Nantes Angers Le Mans*

École doctorale : Sciences pour l'Ingénieur, Géosciences, Architecture

Discipline : Sciences pour l'Ingénieur

Spécialité : Génie Civil

Unité de recherche : Génie Civil et Mécanique UMR CNRS 6183

Soutenue le 3 décembre 2015

Thèse N° :

Characterization of suffusion susceptibility of granular soils

JURY

Rapporteurs :

M. Stéphane BONELLI, Directeur de Recherche, HDR, IRSTEA, Aix en Provence
M. Éric VINCENS, Maître de Conférences, HDR, Ecole Centrale de Lyon

Examineurs :

M. Didier MAROT, Professeur, Université de Nantes
M. Luc SIBILLE, Maître de Conférences, Université Joseph Fourier, Grenoble
M. Luc THOREL, Directeur de Recherche, HDR, IFSTTAR, Bouguenais
M. Moulay Saïd EL YOUSOUFI, Professeur, Université de Montpellier
M. S. Imam WAHYUDI, Maître de Conférences, Sultan Agung Islamic University, Indonesia

Directeur de Thèse :

M. Didier MAROT, Professeur, Université de Nantes

Co-encadrant de Thèse :

M. Luc SIBILLE, Maître de Conférences, Université Joseph Fourier, Grenoble

TABLE OF CONTENTS

Table of contents	i
List of figures	iv
List of tables	x
List of symbols	xi
Résumé	xiii
INTRODUCTION.....	1
1-Background.....	1
2-Research Objectives.....	3
3-Thesis Layout.....	3
CHAPTER I Literature Review	5
1.1 Definitions and phases of internal erosion	5
1.1.1 Definitions of internal erosion.....	5
1.1.2 Phases of internal erosion.....	6
1.2 Suffusion.....	9
1.2.1 Definitions of suffusion.....	9
1.2.2 Instability and failure of hydraulic structures regarding suffusion	10
1.2.3 Recent experimental studies on suffusion.....	11
1.2.4 Identification of suffusion	12
1.2.5 Control parameters for likelihood of suffusion	13
1.3 Coupling of geometry, mechanical and hydraulic condition.....	16
1.4 Criteria for likelihood of suffusion.....	17
1.4.1 Geometric criteria to assess soils likelihood to suffusion	17
1.4.2 Hydraulic criteria to assess soils likelihood to internal erosion	22
1.5 Soils susceptibility	26
1.5.1 Erodimeter for soil susceptibility testing	26
1.5.2 Interpretation of soil erodibility	34
1.5.3 Recent soil susceptibility classification for interface erosion	35
1.6 Mechanical response of soils to suffusion.....	36
CHAPTER II Suffusion Susceptibility	42
2.1 Introduction	42
2.2 Tested gradations.....	42

2.3	Downward seepage test	45
2.3.1	Erodimeter	45
2.3.2	Experimental procedures	48
2.4	Tested specimens	49
2.5	Repeatability check and phenomenological analysis	52
2.5.1	Evolution of hydraulic conductivity and erosion rate	52
2.5.2	Identification of predominant processes	59
2.6	Study of hydraulic loading history	60
2.6.1	Influence on the onset of suffusion	60
2.6.2	Influence on the development of suffusion	63
2.7	Grain size distribution of post-test.....	77
2.8	Proposition of classification of suffusion susceptibility.....	79
2.8.1	Approach of erosion coefficient k_d versus critical hydraulic shear stress (τ_c) ...	79
2.8.2	Energy-based approach	81
2.9	Comparison of gradation-based criteria and suffusion resistance index (I_β).....	91
2.9.1	Kezdi (1979) criterion versus suffusion resistance index (I_β).....	91
2.9.2	Kenney and Lau (1985) criteria versus suffusion resistant index (I_β).....	91
2.9.3	Wan and Fell (2008) criterion versus suffusion resistance index (I_β).....	92
2.9.4	Chang and Zhang (2013) criterion versus suffusion resistant index (I_β)	92
2.10	The effect of fine content and density	94
2.11	Synthesis.....	95
CHAPTER III Small Scale Model of Dike		97
3.1	Introduction	97
3.2	Seepage test	97
3.2.1	Description of the device.....	97
3.3	Properties of tested soil.....	102
3.4	Mechanical properties resulted from triaxial compression tests	103
3.4.1	Experimental procedures.....	104
3.5	Experimental results	107
3.5.1	Settlement during saturation phase	107
3.5.2	Settlement during seepage test	108
3.5.3	Cumulative loss mass	109
3.5.4	Downstream flow rate	110
3.5.5	Spatial distribution of fine and density after seepage test.....	112
3.5.6	Displacement during seepage test	113

3.5.7	Expended energy and erodibility classification	114
3.6	Numerical simulation	116
3.6.1	Introduction	116
3.6.2	Methodology	116
3.6.3	Geometry (specimen <i>B-90s</i>).....	116
3.6.4	Input of soil properties	117
3.6.5	Initial phase	118
3.6.6	Seepage test phase	119
3.6.7	Calculation phase	120
3.6.8	Numerical results.....	120
3.6.9	Settlement in saturation process	120
3.6.10	Flow network.....	122
3.6.11	Global safety factor	123
3.6.12	Comparison between experimental and numerical results	124
3.6.13	Downstream flow rate	124
3.6.14	Initiation of sliding and slip surface	126
3.6.15	Local hydraulic head	127
3.7	Synthesis	131
CONCLUSION and PERSPECTIVES		133
REFERENCES.....		137
List of Publication		141
Annex 1	– Summary of suffusion test performed	142
Annex 2	– Properties of the suffusion test	143
Annex 3	– Tested specimens: G5A, G5B, G6, P1, P2, P3 and P4.....	144
Annex 4	– Tested specimens: L1, L2, L3, L4Ai, L4Aii, L4C, L4D and L5.....	148
Annex 5	– Tested specimens: D1, D2, D3B, M1, M3, M4, S1 and S2.....	153
Annex 6	– Tested specimens: B-90f, C-90a, Chav-1, Chav-2i, Chav-2ii, R1-90b, R2-97f and R2-97g.....	158
Annex 7	– Small scale model of dike: Summary of small scale model of dike.....	164
Annex 8	– Small scale model of dike: specimen <i>B-90s</i>	165
Annex 9	– Small scale model of dike: specimen <i>B-75s</i>	170
Annex 10	– Small scale model of dike: specimen <i>B-90u</i>	175

LIST OF FIGURES

Figure 1 Failure of Teton dam.....	3
Figure I.1 Illustration of initiation of internal erosion by four modes (Chang, 2012)	6
Figure I.2 Phenomena initiating internal erosion in embankment dam (Blais, 2005)	6
Figure I.3 Model for the development of failure by piping in the embankment (Foster & Fell, 1999).....	7
Figure I.4 Model for the development of failure by piping (Foster & Fell, 1999)	8
Figure I.5 The diagram of failure path for failure by piping through the embankment (Foster, 1999).	8
Figure I.6 Classification of suffusion (Ziems, 1996) (a) internal suffusion (b) external suffusion (c) contact suffusion	10
Figure I.7 Factors Affecting the Initiation of Internal Erosion (Garner and Fannin, 2010).....	14
Figure I.8 Classification of the grain size distribution of soils (Lafleur et al. 1989)	16
Figure I.9 Parallel cylindrical tubes	20
Figure I.10 H/F curve to assess instability by Kenney & Lau (1985).....	20
Figure I.11 Method for assessing internal instability by Burenkova (1993).....	21
Figure I.12 Method for assessing internal instability of broadly graded silt-sand-gravel soils (Wan and Fell, 2008).....	21
Figure I.13 Method for assessing internal instability of soils (Li and Fannin, 2008)	21
Figure I.14 Hydraulic criterion for horizontal flow (Adel et al. 1988)	22
Figure I.15 Test arrangement of seepage test using permeameter cell (a) 245 mm, (b) 580 mm (Kenney and Lau, 1985).....	30
Figure I.16 Permeameter for screen tests (Lafleur, 1989).....	30
Figure I.17 Apparatus of seepage test (Skempton and Brogan, 1994).....	31
Figure I.18 Experimental setup for seepage test (Sterpi, 2003)	31
Figure I.19 Permeameter apparatus (Moffat and Fannin, 2006) (a) component of the large permeameter, (b) arrangement of the instrumentation	31
Figure I.20 Schematic diagram of downflow seepage test apparatus (Wan and Fell, 2008) ...	32
Figure I.21 Schematic representation of experimental triaxial cell (Bendahmane et al., 2008).....	32
Figure I.22 Schematic of testing apparatus (Chang and Zhang, 2011)	32
Figure I.23 The apparatus of oedo-permeameter (Sail et al., 2012).....	33
Figure I.24 Schematic diagram of seepage test assembly (Ke and Takahashi, 2012)	33
Figure I.25 Seepage test apparatus (Marot et al. 2012): (a) General view of the IFSTTAR centrifuge bench, (b) schematic diagram of downward seepage flow test apparatus	33

Figure I.26 Classification of interface erosion measured by JET proposed by Hanson and Simon (2001).....	35
Figure I.27 Classification of soil erodibility by Briaud (2005) a) erosion rate and hydraulic shear stress , b) erosion rate and water velocity	36
Figure I.28 Grain size distribution curve with depth before and after erosion (Ke and Takahashi, 2012)	37
Figure I.29 Cone resistance before and after erosion (Ke and Takahashi, 2012)	37
Figure I.30 Mohr-Coulomb failure envelopes before and after erosion with DEM approach (Scholtes et al., 2011).....	38
Figure I.31 Side view of experiment developed by Horikoshi et al. (2012).....	40
Figure I.32 Cross section of levee experiments developed by Beek et al. (2010).....	40
Figure I.33 Relationship between critical gradient and g-level	41
Figure I.34 Side view of test apparatus (Tanaka et al. 2014).....	41
Figure II.1 Tested grain size distributions (a) G5 to P4 (sandy gravel), (b) L1 to L5 (silt-sand-gravel).....	44
Figure II.2 Tested grain size distributions (a) D1 to S2 (silt-sand-gravel) and (b) A to R2 (sandy gravel).....	45
Figure II.3 Schematic diagram of the erodimeter	47
Figure II.4 Modified erosion cell: (a) metal mold keeping the specimen standing (b)Funnel-shaped draining system and 4 mm pore opening grid.....	47
Figure II.5 Soil collecting system: (a) effluent tank and rotating sampling system (b) beakers to catch eroded mass.....	48
Figure II.6 Water collecting system: (a) downstream overflow outlet (b) mass balance.....	48
Figure II.7 (a) schematic diagram of piston mold of 50 mm specimen, (b) pictures of piston mold (with top and bottom pistons; and a 1750 mm piston to expel the specimen).....	49
Figure II.8 Multi-stage and single-stage hydraulic gradients.....	50
Figure II.9 Grain size distribution of soils D3, A, B, C and R2.....	52
Figure II.10 Variation of hydraulic conductivity of tested specimens subjected to multi-stage hydraulic gradients A-90a,b,a_rep; D3A and D3Arep.....	53
Figure II.11 Variation of hydraulic conductivity of tested specimens subjected to multi-stage hydraulic gradients B-90a; B-97a,b; C-97a,b.....	53
Figure II.12 Variation of hydraulic conductivity of tested specimens subjected to multi-stage hydraulic gradients R2-90a,b; R2-97b	54
Figure II.13 Variation of hydraulic conductivity of tested specimens subjected to multi-stage hydraulic gradients B-90h,k	54
Figure II.14 Time series of erosion rate – specimens subjected to multi-stage hydraulic gradient (A-90a,a_rep,b ; R2-90a,b ; R2-97b)	55
Figure II.15 Time series of erosion rate – specimens subjected to multi-stage hydraulic gradient (B-90a; B-97a,b ; C-97a,b).....	56

Figure II.16 Time series of erosion rate – specimens subjected to multi-stage hydraulic gradient (R2-90a,b ; R2-97b)	56
Figure II.17 Time series of erosion rate – specimens subjected to multi-stage hydraulic gradient (B-90h,k)	57
Figure II.18 Variation of hydraulic conductivity of tested specimens subjected to single-stage hydraulic gradients and flow rate condition (A-90c; B-90c,e; R2-97d)	58
Figure II.19 Time series of erosion rate– specimens subjected to single-stage hydraulic gradient and flow rate condition (A-90c; B-90c,e; R2-97d)	58
Figure II.20 The change of hydraulic gradient of tested specimens subjected to imposed flow rate condition (B-90e and R2-97d).....	59
Figure II.21 Two categories of soil response to hydraulic loadings	60
Figure II.22 Hydraulic gradient versus average flow velocity (specimens A-90a,a_rep,b; R2-90a,b).....	61
Figure II.23 Hydraulic gradient versus average flow velocity (specimens B-90a,h; B-97a,b).....	62
Figure II.24 Hydraulic gradient versus average flow velocity (specimens C-97a,b).....	62
Figure II.25 Erosion rate versus hydraulic shear stress (B-90a to B-97b)	63
Figure II.26 Determination of erosion coefficient, k_d (linear - linear scale)	64
Figure II.27 Erosion rate versus hydraulic shear stress (A-90a,a_rep,b)	65
Figure II.28 Erosion rate versus hydraulic shear stress (D3A, D3Arep)	66
Figure II.29 Erosion rate versus hydraulic shear stress (B-90a; B-97a,b)	66
Figure II.30 Erosion rate versus hydraulic shear stress (B-90h)	67
Figure II.31 Erosion rate versus hydraulic shear stress (R2-90a,b)	67
Figure II.32 Erosion rate versus hydraulic shear stress (C-97a,b)	68
Figure II.33 Erosion rate versus hydraulic shear stress (A-90c – R2-97b).....	69
Figure II.34 Erosion rate versus flow power (A-90a,a_rep,b)	71
Figure II.35 Erosion rate versus flow power (D3A, D3Arep)	71
Figure II.36 Erosion rate versus flow power (B-90a; B-97a,b)	72
Figure II.37 Erosion rate versus flow power (B-90h)	72
Figure II.38 Erosion rate versus flow power (R2-90a,b)	73
Figure II.39 Erosion rate versus flow power (C-97a,b)	73
Figure II.40 Cumulative eroded dry mass per unit volume versus cumulative expanded energy per unit volume (A-90a,a-rep,b,c).....	74
Figure II.41 Cumulative eroded dry mass per unit volume versus cumulative expanded energy per unit volume (D3A, D3Arep)	75
Figure II.42 Cumulative eroded dry mass per unit volume versus cumulative expanded energy per unit volume (B-90a,c,e,h,k).....	75

Figure II.43 Cumulative eroded dry mass per unit volume versus cumulative expanded energy per unit volume (B-97a,b)	76
Figure II.44 Cumulative eroded dry mass per unit volume versus cumulative expanded energy per unit volume (R2-90a,b; R2-97a,b)	76
Figure II.45 Cumulative eroded dry mass per unit volume versus cumulative expanded energy per unit volume (C-97a,b)	77
Figure II.46 Grain size distribution after test (A-90b)	78
Figure II.47 Grain size distribution after test (B-90b)	78
Figure II.48 Grain size distribution after test (C-97a).....	79
Figure II.49 Proposed classification of suffusion susceptibility based on the approach of erosion coefficient k_d versus critical hydraulic shear stress (A-90a – R2-97b)	80
Figure II.50 Proposed classification of suffusion susceptibility based on the approach of erosion coefficient k_d versus critical hydraulic shear stress (G5A – L5)	80
Figure II.51 Proposed classification of suffusion susceptibility based on the approach of erosion coefficient k_d versus critical hydraulic shear stress (D1 – S2)	81
Figure II.52 Grain size distribution of soils K10L90, K20L80 and KPR25F75 (After Bendahmane et al., 2008 and Nguyen et al., 2012)	81
Figure II.53 Cumulative eroded dry mass versus cumulative energy (A1 – A8).....	82
Figure II.54 Cumulative eroded dry mass versus cumulative energy (A11 – A28).....	83
Figure II.55 Cumulative eroded dry mass versus cumulative energy (F10 – F23).....	83
Figure II.56 Proposed classification diagram of suffusion susceptibility - energy-based approach (A-90c – C-97b)	84
Figure II.57 Proposed classification diagram of suffusion susceptibility - energy-based approach (Chav-2i – R2-97g)	84
Figure II.58 Proposed classification diagram of suffusion susceptibility - energy-based approach (G5A – L5)	85
Figure II.59 Proposed classification diagram of suffusion susceptibility - energy-based approach (D1 – S2)	85
Figure II.60 Proposed classification diagram of suffusion susceptibility - energy-based approach (A1 – F23)	86
Figure II.61 Effect of hydraulic loading history on suffusion susceptibility classification	90
Figure II.62 Suffusion resistance index (I_β) versus D_{15}/d_{85}	91
Figure II.63 Suffusion resistance index (I_β) versus H/F_{min}	92
Figure II.64 Suffusion resistance index (I_β) versus Wan and Fell criterion.....	93
Figure II.65 Effect of fine content on suffusion susceptibility classification	94
Figure III.1 Schematic diagram of the dike apparatus	99
Figure III.2 Front view of transparent box	99
Figure III.3 Pressure ports: a) in the bottom side, b) in the back side of the box	99

Figure III.4 Fibre mess to separate dike soil and upstream water reservoir.....	100
Figure III.5 Water supply system: a) 200 lt capacity water tank, b) pump and connection gates	100
Figure III.6 Upstream overflow outlet to maintain upstream water level	101
Figure III.7 Soil collecting system: a) funnel-shaped draining outlet b) effluent tank with 8 beaker rotating sampling device	101
Figure III.8 Water collecting system: a) downstream water outlet b) flow rate measurement equipped with a balance	102
Figure III.9 Measurement system: water head pipes.....	102
Figure III.10 Grain size distribution of tested soil	103
Figure III.11 Picture of sand and gravel from Sabliere Palvadeau	103
Figure III.12 Drained triaxial compression on tested soil: determination of Young's modulus of tested soil	104
Figure III.13 Drained triaxial compression on tested soil: determination of dilatancy angle of tested soil	105
Figure III.14 Shear strength parameters of tested soil	105
Figure III.15 Saturation process of water pressure ports	106
Figure III.16 Production of specimen	106
Figure III.17 Schematic diagram of the method to saturate the specimen	107
Figure III.18 Saturation process of the specimen.....	107
Figure III.19 Schematic diagram of seepage test method	108
Figure III.20 Picture of a dike model after a seepage test: the dike is deformed because of settlements and sliding occurring during the test	108
Figure III.21 Settlement of the dike crest during the saturation process.....	109
Figure III.22 Settlement of the dike crest during seepage test.....	109
Figure III.23 Cumulative dry eroded mass versus times (captured by beakers only).....	110
Figure III.24 Cumulative dry eroded mass versus times (beakers + outside beakers).....	110
Figure III.25 The onset of suffusion (B-90 _{s-rep}).....	111
Figure III.26 The variation of downstream flow rate during the test.....	112
Figure III.27 The variation of corrected downstream flow rate during the test	113
Figure III.28 Initial downstream flow rate versus corrected downstream flow rate	113
Figure III.29 Fine fraction and dry density in several locations after the seepage test (B-90 _{s-rep}).....	114
Figure III.30 Sliding in the downstream slope t = 2.25 to 2.50 min (B-90 _{s-rep})	114
Figure III.31 Sliding in the downstream slope t = 2.75 to 6.75 min (B-90 _{s-rep})	115
Figure III.32 Evolution of the shape of the downstream slope during the seepage test (B-90 _{s-rep})	115

Figure III.33 Area of the soil where water go through (B-90 _{s-rep}).....	116
Figure III.34 Cumulative eroded dry mass versus cumulative flow energy	116
Figure III.35 Classification of suffusion susceptibility - energy-based approach.....	117
Figure III.36 The front view of tested specimen	118
Figure III.37 The geometry condition of dike model.....	118
Figure III.38 Two initial conditions: (a) saturation phase, (b) seepage test.....	120
Figure III.39 Seepage test on tested dike	120
Figure III.40 Settlement measured experimentally on the test B-90s-rep of the dike during the saturation process.....	121
Figure III.41 Settlement of the dike simulated with Plaxis due to (a) gravity loading, (b) saturation phase	121
Figure III.42 Equipotential drops of the dike (in meter) at minutes 3.75, computed with Plaxflow.....	122
Figure III.43 Equipotential drops of the dike (in meter) at minutes 17, computed with Plaxflow.....	122
Figure III.44 Equipotential drops of the dike (in meter) at minutes 360, computed with Plaxflow.....	123
Figure III.45 Condition where FoS = 1.00	124
Figure III.46 Flow field at 360 minutes: (a) Flow velocity, (b) flow rate section A-A*	125
Figure III.47 Comparison of downstream flow rate between experimental study and numerical study (B-90s-rep).....	125
Figure III.48 Displacement of at minutes 2.25 in cm (experimental vs. numerical study)....	126
Figure III.49 Displacement of at minutes 2.50 in (experimental vs. numerical study).....	126
Figure III.50 Displacement of at minutes 2.75 (experimental vs. numerical study) in cm....	126
Figure III.51 Displacement of at minutes 3.75 (experimental vs. numerical study) in cm....	126
Figure III.52 Displacement of at minutes 6.75 (experimental vs. numerical study) in cm....	127
Figure III.53 Measured and simulated values of total head (in meter) at 3.75 minutes.....	127
Figure III.54 Measured and simulated values of total head (in meter) at 17 minutes.....	128
Figure III.55 Measured and simulated values of total head (in meter) at 6 hours	128
Figure III.56 Comparison of total water head within the dike between real test and simulation G5-E4 (B-90 _{s-rep}).....	129
Figure III.57 Comparison of total water head within the dike between real test and simulation F3-B3 (B-90 _{s-rep}).....	129
Figure III.58 Comparison of total water head within the dike between real test and simulation G1-A1 (B-90 _{s-rep})	130
Figure III.59 Time series of evolution of deviation values within the dike soil (G5-B3).....	130
Figure III.60 Time series of evolution of deviation values within the dike soil (G1-A1)	131

LIST OF TABLES

Table I.1 Erosion rate index, I_{HET} (Wan and Fell, 2004).....	36
Table I.2 Erosion resistance index, I_{α} (Marot et al., 2011)	36
Table II.1 Properties of tested gradations.....	46
Table II.2 Assessment of soil internal stability by recent criteria.....	47
Table II.3 Properties of tested specimens.....	51
Table II.4 Erosion coefficient and critical hydraulic shear stress for specimens subjected to multi-stage hydraulic gradients	69
Table II.5 Properties of reference specimens by Bendahmane et al., 2008 and Nguyen et al., 2012.....	82
Table II.6 Proposed classification of suffusion resistance index, I_{β}	86
Table II.7 Comparison of proposed classification of suffusion susceptibility based on $kd-\tau_c$ method and energy-based method (G5A to B-97b).....	87
Table II.8 Comparison of proposed classification of suffusion susceptibility based on $kd-\tau_c$ method and energy-based method (C-90a to F23).....	88
Table II.9 Given grain size distributions with different hydraulic loading histories	89
Table II.10 Chang and Zhang (2013) criterion versus suffusion resistant index (I_{β}).....	93
Table III.1 Properties of tested specimens	104
Table III.2 Tested soil properties	119
Table III.3 Computation stages of tested dike.....	120
Table III.4 Displacement and global safety factor	124

LIST OF SYMBOLS

C_e	Coefficient of soil erosion
C_u	Uniformity coefficient
d_x	Sieve size for which X% of the sample by weight passes (mm)
D_{xf}	Diameter of the X% mass passing in the coarse part (mm)
D_{xs}	Diameter of the X% mass passing in the fine part (mm)
d_0	Average capillary tube diameter of the coarser fraction (mm)
D_h^c	Kozeny effective diameter of the coarse fraction (mm)
D_i^c	Average diameter of grains in the i th interval of the particle size distribution curve of the coarse fraction (mm)
e	Void ratio
E_{ther}	Thermal energy exchange between the system and the environment (J)
e_{int}	Internal energy of the fluid ($J.kg^{-1}$)
F_n	Mass percentage of the finer fraction (%)
G_s	Specific gravity of the soil
g	Gravity acceleration ($m.s^{-2}$)
G^*	Geometric-based factor that determines the proportion of stress transferred to the particles of the fine soil fraction
I_{HET}	Erosion index
i_c	Critical upward hydraulic gradient for heaving
I_α	Erosion resistance index for surface erosion
K	Intrinsic permeability (m^2)
k_d	Erodibility coefficient ($g.N^{-1}.s^{-1}$)
k	Hydraulic conductivity ($m.s^{-1}$)
L	Length of the specimen (m)
m	Eroded dry mass (kg)
\dot{m}	Soil erosion rate ($kg.s^{-1}.m^{-2}$)
M	Mass of fluid (kg)
N_p	Average number of pore
\vec{n}	Surface normal vector directed to the fluid
n	Porosity of soil
n_c	Porosity of the coarse fraction
P	Percentage of particles finer than 0.063 mm
Q	Fluid flow rate ($l.min^{-1}$)

r_p	Average radius of pores (m)
R	Correlation coefficient
r	Constant radius (m)
S	Cross section of the specimen (m ²)
S_p	Average pore area (m ²)
T	Tortuosity, the ratio between the shortest distance of two points in flow direction and the effective length of the flow path following the winding pore channels
t	Duration (min)
U	Velocity of the fluid (m.s ⁻¹)
V	Volume of fluid (l)
$v_{p,av}$	Mean pore velocity (m.s ⁻¹)
v_f	Darcian flow velocity (m.s ⁻¹)
W	Mechanical work between upstream and downstream (J)
z	Coordinate (m)
ΔF_i^c	Fraction of grains in the i th interval of the particle size distribution curve of the coarse fraction.
Δh	Hydraulic head drop (m)
ΔL	Distance between two sections (m)
ΔP	Pressure drop (Pa)
Δz	Altitude change for a one dimensional flow between two inlets (m)
Δz	Thickness of soil specimen (m)
α_D	Shape coefficient
α	Ratio of cumulative eroded mass to cumulative expanded energy
τ	Hydraulic shear stress at the soil-water interface (Pa)
τ_c	Critical hydraulic shear stress at initiation of erosion (Pa)
ρ	Density (kg.m ³)
ρ_d	Dry density (kg.m ³)
μ	Dynamic viscosity (Pa.s)
γ'	Submerged unit weight of soil (kg.m ⁻³)
γ_w	Unit weight of water (kg.m ⁻³)
α	Stress reduction factor in the finer fraction
σ'_{to}	Vertical effective stress on top of specimen (kPa)
σ'_{vm0}	Mean vertical stress in the middle of soil layer (kPa)

Résumé

Introduction et étude bibliographique

Les ouvrages hydrauliques tels que les barrages et les digues ont des fonctions primordiales pour notre société. Ils sont en effet construits afin de protéger les populations et les biens des inondations, afin de créer des retenues d'eau pour la production d'hydroélectricité et la constitution de réserves d'eau pour la consommation ou l'irrigation. A l'échelle mondiale, la Commission Internationale des Grands Barrages (ICOLD) indique que le nombre de barrages est de l'ordre de 45 000 dont 569 en France (Building Research Establishment, 2002). Par ailleurs en France sont recensés 8 000 km de digues de protection des inondations, 6 700 km de digues de canaux de navigation et plus de 1 000 km de digues pour l'optimisation de la gestion de l'eau.

Les ouvrages hydrauliques en terre et d'une manière générale les fondations de tout ouvrage peuvent être le siège d'écoulements interstitiels qui peuvent générer le détachement, puis le transport de certaines particules constitutives des sols considérés. Dans certaines conditions, ces phénomènes, nommés érosion interne peuvent aboutir à la rupture de l'ouvrage (Fry et al., 2012). Parmi les quatre phénomènes d'érosion interne (Fell et Fry, 2013), la suffusion mobilise la fraction fine du sol qui peut migrer dans les vides interstitiels de la fraction grossière. Le développement de la suffusion peut alors modifier notablement la porosité du sol et donc ses propriétés hydrauliques et mécaniques. Il convient également de souligner que le développement de la suffusion peut générer une deuxième phase d'érosion caractérisée par un fort débouillage de particules fines qui s'accompagne d'un tassement important et d'un fort accroissement de la conductivité hydraulique (Sibille et al., 2015). L'étude de la suffusion est complexe car ce processus est gouverné par plusieurs paramètres qui sont couplés : la microstructure du milieu poreux, la sollicitation mécanique et la sollicitation hydraulique.

L'étude bibliographique réalisée permet de faire un bilan des travaux sur l'érosion interne qui sont publiés dans la littérature et plus particulièrement ceux portant sur la suffusion. Les approches ont été multiples avec des analyses expérimentales, numériques ou analytiques. Ces travaux sur l'initiation et le développement de la suffusion ont notamment porté sur l'identification de critères basés sur (i) la géométrie (distribution granulométrique, forme des grains, densité), (ii) les caractéristiques physico-chimiques du sol et du fluide interstitiel, (iii) le chargement mécanique externe et (IV) le chargement hydraulique.

Cependant plusieurs limitations de ces recherches et plusieurs questions restées ouvertes peuvent être identifiées :

1. L'expression du gradient hydraulique critique proposée par Li (2008) est inversement proportionnelle à la longueur de l'écoulement. De ce fait, le gradient critique diminue avec l'épaisseur de l'échantillon considéré ce qui s'oppose à la gestion des risques à l'échelle des ouvrages,
2. L'étude de l'effet de l'historique de chargement hydraulique apparaît limitée à l'étude de Luo et al. (2013) qui concluent que les essais de longue durée aboutissent à la sensibilité d'un mélange de sable –gravier plus importante vis-à-vis de la suffusion,
3. Plusieurs classifications de sensibilité à l'érosion d'interface ont été proposées (Hanson et Simon, 2001, Wan et Fell, 2004, Marot et al., 2011) mais jusqu'à maintenant aucune pour la suffusion. Donc en regard de la gestion des risques associés à la suffusion, une classification de sensibilité des sols apparaît nécessaire,

4. L'effet de la suffusion sur le comportement mécanique des sols requiert des recherches complémentaires car certains travaux décrits dans la littérature aboutissent à des conclusions opposées (par exemple : Ke et Takahashi, 2014 et Sterpi, 2003).

Dans ce contexte scientifique, les objectifs de cette thèse sont : (1) de caractériser le processus de suffusion, (2) de définir une méthodologie systématique pour l'identification de la sensibilité des sols à la suffusion, (3) de proposer une classification de sensibilité des sols à la suffusion, (4) de contribuer à la compréhension de la suffusion et des mécanismes induits à l'échelle d'un modèle réduit de digue.

La démarche scientifique associée à ces objectifs comprend tout d'abord la réalisation et l'interprétation d'essais de suffusion réalisés à l'aide d'un dispositif spécifique existant. Par ailleurs un modèle physique est développé afin de réaliser des essais sur un modèle réduit de digue. Enfin des simulations numériques sont effectuées à l'aide du logiciel Plaxis et leurs résultats sont comparés avec les mesures obtenues avec le modèle réduit de digue.

Sensibilité à la suffusion

Afin d'étudier le processus de suffusion et de proposer une classification de sensibilité des sols à ce phénomène d'érosion interne, 26 sols non cohésifs ont été étudiés. En utilisant les critères granulométriques présentés dans la littérature, l'analyse de la distribution granulométrique des sols testés montre d'une part, que la majeure partie d'entre eux semble être instable et que d'autre part, les résultats de cette analyse dépendent des critères granulométriques utilisés. En conséquence, cette analyse granulométrique ne peut constituer qu'une détermination préalable de la susceptibilité des sols à la suffusion. La caractérisation précise de la sensibilité à la suffusion nécessite donc la réalisation et l'interprétation d'essais dédiés.

Suivant cet objectif, une cinquantaine d'essais est réalisée à l'aide d'un érodimètre triaxial développé au sein de notre équipe de recherche (Bendahmane et al. 2008). La réponse des échantillons à la sollicitation hydraulique est caractérisée par le suivi au cours du temps de la conductivité hydraulique, du taux d'érosion et de la masse érodée cumulée. La sollicitation hydraulique est modélisée par le gradient hydraulique, la contrainte de cisaillement hydraulique ou par la puissance dissipée par le fluide interstitiel (Marot et al., 2012). L'intégration temporelle de cette puissance permet alors de déterminer l'énergie dissipée. Une attention particulière porte sur la répétitivité des essais et plusieurs types d'historique de chargement hydraulique sont appliqués. Quatre historiques de chargement hydraulique consistent à accroître le gradient hydraulique suivant différentes fréquences et différents incréments de gradient. Un historique de chargement est à gradient hydraulique unique et deux valeurs de débits imposés sont également utilisées.

Lors des essais réalisés sous gradient hydraulique contrôlé avec accroissement par paliers de celui-ci, trois étapes successives peuvent être identifiées en comparant l'évolution au cours du temps de la conductivité hydraulique d'une part, et du taux d'érosion d'autre part. La première étape se caractérise par un faible taux d'érosion et la diminution de la conductivité hydraulique, ce qui indique que la filtration d'une partie des grains détachés apparaît comme le processus prédominant. Au cours de la deuxième étape, le processus prédominant est l'érosion qui se caractérise par un accroissement du taux d'érosion et de la conductivité hydraulique. La troisième étape est marquée par la constance de la conductivité hydraulique qui indique qu'un état permanent est atteint. Au cours des essais à palier unique de gradient hydraulique ou à débit imposé, seules les étapes 1 puis 3 sont observées et l'érosion se développe très peu. La complexité de la suffusion est également illustrée par l'analyse

granulométrique après essais de suffusion. En comparaison de la distribution granulométrique initiale, la partie amont de l'échantillon érodé a un pourcentage de fines moins élevé, alors que la partie aval de l'échantillon peut subir qu'une très légère diminution de ce pourcentage de fines, voire même un accroissement.

La caractérisation de l'initiation de la suffusion, est tout d'abord réalisée conformément à la méthode de Skempton et Brogan (1994) qui consiste à identifier l'initiation par l'accroissement de la conductivité hydraulique et d'en déduire la valeur correspondante de gradient hydraulique critique. Pour les différents sols testés, la valeur du gradient hydraulique critique apparaît plus faible dans le cas d'un accroissement faible du chargement hydraulique (faible incrément de gradient hydraulique ou durée importante des paliers) en comparaison des essais réalisés avec un accroissement plus intense du chargement hydraulique. L'application d'un débit imposé ne permet pas de définir une valeur de gradient hydraulique critique. L'initiation et le développement de la suffusion sont également étudiés à l'aide de la loi d'érosion utilisée dans le cas de l'érosion d'interface (Hanson et Simon, 2001 ; Wan et Fell, 2004). Cette interprétation souligne tout d'abord la grande difficulté rencontrée dans le cas de la suffusion, pour établir précisément une loi linéaire entre le taux d'érosion et l'excès de contrainte par rapport à la contrainte de cisaillement hydraulique critique. Cette détermination n'est d'ailleurs possible que lors d'un essai réalisé à gradient hydraulique croissant par paliers. Par ailleurs, le coefficient d'érosion apparaît systématiquement plus faible lorsque l'accroissement du chargement hydraulique est plus faible. L'influence de l'historique de chargement hydraulique apparaît donc déterminante sur l'initiation et le développement de la suffusion, ce qui rend difficile l'élaboration d'une classification de la sensibilité des sols à ce processus d'érosion interne.

Afin de prendre en compte la complexité de la suffusion, une nouvelle approche est développée. Elle consiste à déterminer la masse érodée sèche cumulée et l'énergie correspondante dissipée par le fluide interstitiel au cours du temps, jusqu'au régime permanent qui est caractérisé par la constance de la conductivité hydraulique. L'analyse des résultats montre que pour les sols testés suivant les différents historiques de chargement hydraulique, il est possible d'obtenir une même classification relative de sensibilité à la suffusion. L'étendue de sensibilité des sols testés ainsi que la prise en compte de résultats publiés sur des sols cohésifs permettent la proposition d'une classification de sensibilité à la suffusion qui est divisée en 6 catégories, de très résistant à très érodable.

Modèle réduit de digue

Un modèle physique est développé afin de pouvoir tester un modèle réduit de digue qui est réalisé par compactage en 5 couches d'épaisseur et de densité contrôlées. Pour limiter la taille du dispositif, seule la moitié d'une digue est modélisée (avec une plateforme en crête et un seul talus du côté aval, d'inclinaison 30°). Le dispositif permet la mesure de : la charge hydraulique en plusieurs points, le tassement en crête, le débit d'eau qui traverse la digue et la masse érodée au cours du temps. Après essai, la densité et la distribution granulométrique sont déterminées en différents points. Par analyse d'images (PIV) les déplacements longitudinaux sont également étudiés.

Quatre essais sont ainsi effectués sur un mélange sable-gravier préalablement testé à l'érodimètre triaxial. L'analyse des résultats met en évidence la diminution de la densité et du pourcentage de fines, notamment le long du talus aval et de la base de la digue, ce qui souligne l'influence des conditions aux limites. L'accroissement de l'écart de charge amont-aval génère un glissement le long du talus aval. L'analyse par approche énergétique de la

sensibilité à la suffusion du sol testé à l'échelle du modèle réduit aboutit à la même classification que celle obtenue à partir de l'essai réalisé avec l'érodimètre triaxial. Cette concordance de classification semble donc indiquer la possibilité d'utiliser l'approche énergétique suivant plusieurs échelles spatiales.

La simulation des différentes étapes des essais est menée à l'aide du logiciel Plaxis. Le couplage entre le comportement du sol et la redistribution de la pression interstitielle est pris en compte. Toutefois, aucune loi d'érosion n'est introduite dans Plaxis et les caractéristiques mécaniques et hydrauliques du sol sont supposées constantes. Quelques différences apparaissent entre les valeurs simulées et les mesures du champ de pression interstitielle, par contre la simulation permet de prédire de manière précise l'initiation du glissement observé expérimentalement. Donc ces résultats ne permettent pas de conclure qu'en à l'influence de la suffusion sur la dégradation de la stabilité du talus de digue.

Conclusion

L'étude bibliographique et l'analyse de la cinquantaine d'essais réalisés dans le cadre de cette thèse mettent en exergue la complexité du phénomène de suffusion qui est composé de trois processus couplés : le détachement, le transport et la filtration de la fraction fine. Les analyses des résultats montrent également que l'initiation et le développement de la suffusion sont fortement influencés par l'historique de chargement hydraulique. Pour prendre en compte cette influence, une méthode d'interprétation est définie à partir de la masse érodée, de l'énergie dissipée par le fluide interstitiel et l'évolution temporelle de la conductivité hydraulique. Grâce aux essais réalisés à l'érodimètre triaxial sur un large panel de sols non cohésifs et à des essais publiés sur des sols cohésifs, l'approche énergétique permet de proposer une classification des sols à la suffusion en 6 catégories. Un modèle physique est développé et est utilisé pour réaliser 4 essais sur modèle réduit de digue. L'interprétation des essais suivant l'approche énergétique aboutit à la même classification de sensibilité du sol qu'à l'échelle de l'érodimètre triaxial. Enfin ces essais mettent en évidence la génération d'un glissement du talus aval qui est également simulée par le logiciel Plaxis.

L'ensemble des résultats obtenus dans le cadre de cette thèse permet d'ouvrir plusieurs perspectives notamment pour l'étude d'ouvrages en vraie grandeur et pour l'étude de l'influence de la suffusion sur le comportement mécanique des sols.

INTRODUCTION

1-Background

Hydraulic structures such as dams and levees or dikes provide many benefits for our society. They are built with the aim to protect people and property against flood and to provide water supply and the need of electricity. In worldwide scale, the number of large dams in a database given by International Commission on Large Dams (ICOLD) is around 45.000 which 569 are located in France (Building Research Establishment, 2002). Moreover in France, these works represent: 8,000 km of levees as protection against floods, 6700 km of navigation or hydropower canals, and more than 1000 km of dikes and water management dams.

Since hydraulic structures are submerged or partially submerged in water, they are subjected to some seepage passing through them. This can lead to a generation of the detachment and transport of certain constituent particles of the structures (if they are made of soil) or their foundations. In the worst cases, it may lead to failure. This problem is called internal erosion. The terminology of “failure” here is not an accident that destroys a whole hydraulic structure but rather collapse or movement of a part of a structure or its foundations so that the structure cannot retain the stored water (ICOLD, 1995). Flood resulting from the failure of hydraulic structures can produce some devastating disasters, not only certain property damage but also loss of life.

The dam failure population worldwide due to internal erosion that caused loss of life can be huge as presented by several researchers. In Charles (2011), it is reported British dam failures in the period before 1924 have caused 356 deaths. Some international dams have also shown failures that have caused 516 deaths in the period between 1959 and 2009. This includes a failure in Situ Gintung dam situated in Indonesia in the year of 2009 that caused a hundred of deaths. According to Comité Français des Grands Barrages, (CFGB,1997) since 1970 no failure of a major dam in France has been existed. However, there have been 70 internal erosion incidents in which ten serious incidents occurred at small dams, including three that breached the embankment (Charles, 1998). In addition, it was reported in Fry et al. (2012) during 2010-2012 period the 6 failures recorded in France were caused by concentrated leak erosion or by backward erosion but no fatalities occurred. According to Foster et al. (2000) among 11.192 surveyed dams before the year of 1986, 136 experienced failure or dysfunction or instabilities with 48% due to overtopping, 46% due to piping (or internal erosion), and 5.5% due to sliding. Internal erosion can also induce overtopping (due to settlement induced by erosion) that considered as major causes of failures as reported in Costa (1985). Sixty percent of the more than 11.100 loss of life related to all dam failures worldwide have occurred in just three failures as follow: overtopping of concrete arch dam by landslide-generated wave in Vajont, Italy in 1963 that caused loss of life 2.600 deaths, overtopping of embankment dam in Johnstown Dam, Pennsylvania in 1889 that brought 2.200 deaths and overtopping of embankment dam during construction in Machhu II, India in 1974 that caused more than 2.000 deaths. From aforementioned fatalities, piping and seepage amounting to 28 percent have been indicated to cause overtopping. From latest inquiry over the world reported in Fry et al. (2012) 432 failures of water retaining structures were owing to internal erosion comprising 111 large dams, 259 small dams and 61 channel dikes, levees or flood embankments and one unknown type.

Fell (2003) also indicated that overtopping and internal erosion are the two main causes of earthen embankment failure. The other examples of notable failures of hydraulic structures in United States caused by internal erosion are Teton dam in Idaho, in 1976 as displayed in Figure 1, Baldwin Hills dam in California in 1963 and Quail Creek dike in Utah in

1989. Teton dam was reclamation dam that catastrophically failed on June 5, 1976 during first filling of the reservoir causing 11 deaths and damages estimated to range from 400 million to 1 billion US dollars (US Army Corps of Engineering, 2012).

Suffusion, as one type of internal erosions, refers to detachment and transport of finer particles through a coarser soil matrix due to seepage flow. The development of suffusion can modify hydraulic and mechanical characteristic of soils. This may trigger the other aforementioned erosions, for instance backward erosion, that can be the catalyst for significant instabilities. The study of suffusion is a complex matter as governed by several criteria such as geometrical criteria, mechanical and hydraulic criteria. The difficulty to determine the most important parameters is present.

Many researchers have been carried out studies on internal erosion (by suffusion) by experimental, numerical or analytical studies. Their work on the initiation and development of the phenomenon (of suffusion) generally associated considerations about: (i) geometrical criteria (gradation distribution, grain shape, density of the granular packing) (Istomina, 1957; Kezdi, 1979; Kenney and Lau, 1985; Burenkova, 1993; Li and Fannin, 2008; Wan and Fell, 2008; and Chang and Zhang, 2013), (ii) physicochemical characteristic of medium and interstitial fluid (Arulanandan and Perry, 1983; Reddi et al, 2000), (iii) external mechanical loading (Bendahmane et al, 2008), (iv) hydraulic criteria (Skempton and Brogan, 1994; Reddi et al., 2000; Perzlmaier, 2007; Li, 2008; and Marot et al., 2011) and (v) erosion susceptibility classification.

The study to investigate and characterize the initiation and development of suffusion on sand-gravel soils has been conducted by a number of investigators including Lafleur et al. (1989), Kenney and Lau (1986), Burenkova (1993), Skempton and Brogan (1994), Sterpi (2003), Moffat and Fannin (2006), Wan and Fell (2008), Sail et al. (2012), Chang and Zhang (2011), Ke and Takahashi (2012), Horikoshi et al. (2012) and Luo et al. (2013). However, from several approaches using critical hydraulic gradient, it is found the expression given are a function of the thickness of the soil specimen. Due to scale effect, the critical hydraulic gradient becomes lower for the increase of the thickness of soil specimen that is contrast with risk management. Based on this, a new approach regarding hydraulic loading will be used. Moreover, to the present several soil susceptibility classifications were proposed only for interface erosion (Hanson and Simon, 2001; Wan and Fell, 2004; and Marot et al, 2011). The study on characterization of soil susceptibility due to suffusion is far to be completed. Thus for the safety of assessment of a soil, suffusion susceptibility classification is needed.

The consequences of suffusion on mechanical soil properties can vary. Suffusion may increase or decrease soil shear strength. Sterpi (2003) shows after suffusion the stiffness and shear strength increase whereas Ke and Takahashi (2012) demonstrate that suffusion results in the decrease of soil shear strength. It is worth noting that Sterpi (2003) carried out triaxial tests to determine stiffness and shear strength properties of the soils by using replicated soils that may represent post-test soils whereas Ke and Takahashi (2012) used post-test soils. The result of Sterpi (2003) different from that of Ke and Takahashi (2012) may be attributed to their different gradings or tested soils for determination soil shear strength after erosion. However, effect of suffusion on hydraulic and mechanical soil properties on the whole structures such as slope stability may be still a few. Thus the study of the effect of suffusion on hydraulic and mechanical soil properties is required.



Figure 1 Failure of Teton dam

(http://www.geol.ucsb.edu/faculty/sylvester/Teton_Dam/Teton%20Dam.html)

2-Research Objectives

This research aims for investigating the initiation and development of the mechanism of suffusion on the body of dikes. The objectives of this research are:

1. to characterize suffusion mechanisms.
2. to provide a new methodology for identification of suffusion susceptibility of soils.
3. to propose suffusion susceptibility classification.
4. to establish better understanding of the mechanism of initiation and development of suffusion process on the body of dikes, in small scale model.
5. to characterize the effects of suffusion on mechanical and hydraulic soil properties.

This research focuses mainly on suffusion that comprises experimental studies on soil susceptibility tests and small scale model of dike tests, and simulation of the small scale model of dike using PLAXFLOW that can be briefly explained as follows.

1. Modified triaxial erodimeter tests are performed in order to characterize the suffusion susceptibility of a soil. The soil specimens are subjected to downward seepage flow to erode the soils. Three kinds of hydraulic loading are used: constant hydraulic gradient, multi-stage hydraulic gradients and constant flow rate. Their result data are to characterize mechanism of initiation and development of suffusion, to provide proposition of suffusion susceptibility classification and a new methodology for suffusion susceptibility.
2. Small scale model of dike tests are carried out to characterize the effects of suffusion on the mechanical behaviour of soils.
3. Simulation using PLAXFLOW program to compare with experimental study of small-scale model dike.

3-Thesis Layout

This thesis comprises three chapters.

Chapter 1: describes definition and phases of internal erosion, suffusion, instability of hydraulic structures due to suffusion, coupling of several criteria to suffusion occurs, commonly-used methods to assess the potential of internal instability based on geometric and hydraulic aspects, soil susceptibility, mechanical response of soils and soil susceptibility and previous work on internal instability in dikes.

Chapter 2: describes tested grading and specimen used, the experimental procedure and test results obtained with a modified triaxial erodimeter. Then we explain how we characterized from the constituted experimental data base the suffusion mechanism in order to propose a new methodology for the evaluation of suffusion susceptibility and suffusion susceptibility classification.

Chapter 3: describes the grading of specimens tested, the experimental procedure and test results concerning the small scale model of dike. Development of suffusion in this reduce scale soil structure is characterized and effects on its hydro-mechanical behaviour is evaluated thanks, among others, to comparisons with simulations with PLAXFLOW.

Finally we conclude the study. Theoretical and experimental works presented in this thesis are summarized, and the recommendations provided for future research are given.

CHAPTER I LITERATURE REVIEW

1.1 Definitions and phases of internal erosion

1.1.1 Definitions of internal erosion

The term “erosion” according to Sterpi (2003) customarily indicates the detachment of a particle from the soil structure, under the mechanical or chemical action of a fluid flow, in the form of surface flow (surface erosion) or internal seepage (internal erosion). Thus erosion can be divided into internal erosion and external erosion. The terminology of internal erosion generally develops in the presence of two conditions: the detachment and transport of particles. Fell and Fry (2007) defined internal erosion as condition when soil particles within an embankment dam or its foundation, are carried downstream by seepage flow. Another definition of internal erosion used by Bureau of Reclamation and US Army Corps of Engineers (USACE) as a generic term to describe erosion of particles by water passing through a body of soil.

Fell & Fry (2007) classify internal erosion (initiation) into several types of soil erosion, that are, concentrated leak erosion or piping, suffusion, contact erosion (or surface suffusion) and backward erosion (or piping) as illustrated in the Figure I.1. The difference among these erosions can be explained as follows.

Concentrated leak erosion: erosion in a concentrated leak may occur in a crack or pipe in an embankment dam or its foundation caused by differential settlement, desiccation, freezing, thawing and hydraulic fracture; or it may occur in a continuous permeable zone containing coarse and/or poorly compacted materials which form an interconnected voids system.

Backward erosion involves the detachment of soil particles when the seepage exits to a free unfiltered surface, such as the ground surface downstream of a soil foundation or the downstream face of a homogeneous embankment, or a coarse rockfill zone immediately downstream from the fine grained core. The detached particles are carried away by the seepage flow and the process gradually works its way towards the upstream side of the embankment or its foundation until a continuous pipe is formed.

Contact erosion is, also described as external or surface suffusion, a form of internal erosion which involves selective erosion of fine particles from the contact with a coarser layer, for instance along the contact between silt and gravel sized particles. In presence of flow parallel to the interface, particles from fine material layer are eroded, and transported through the pores of the coarse material.

Suffusion involves selective erosion of fine particles from the matrix of coarse particles (coarse particles are not floating in the fine particles). The fine particles are removed through the voids between the larger particles by seepage flow, leaving behind an intact soil skeleton formed by the coarser particles.

Moreover, Schuler and Brauns (1996) indicate several phenomena that may initiate internal erosion in embankment dams. These phenomena include: piping by heave, suffusion, backward erosion, dispersion, dissolution, entrainment, suffusion by exsolution, scour as shown in the Figure I.2.

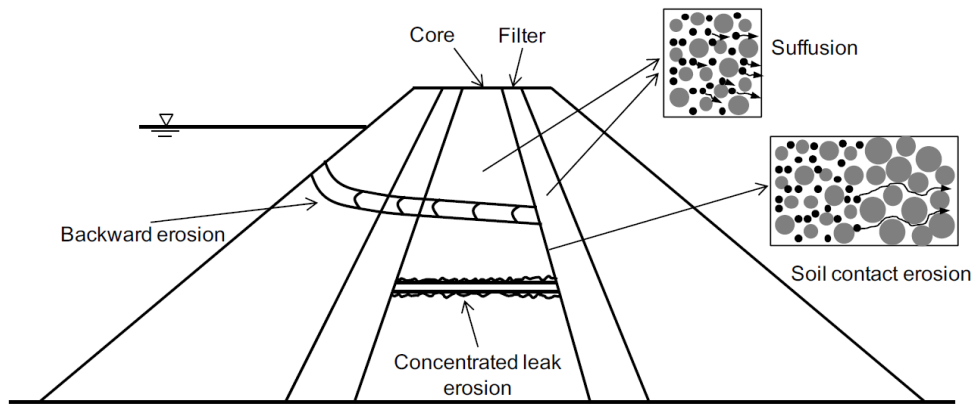


Figure I.1 Illustration of initiation of internal erosion by four modes (Chang, 2012)

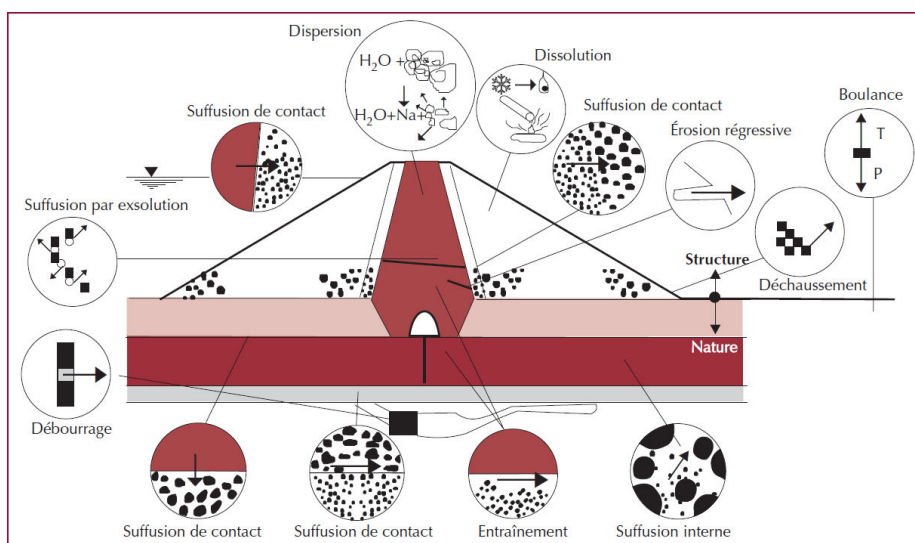


Figure I.2 Phenomena initiating internal erosion in embankment dam (Blais, 2005)

1.1.2 Phases of internal erosion

In general, internal erosion modes that lead to failure in a dam can be categorized into three groups: (i) internal erosion in the dam embankment, (ii) internal erosion in the foundation and (iii) internal erosion from the dam embankment into the foundation.

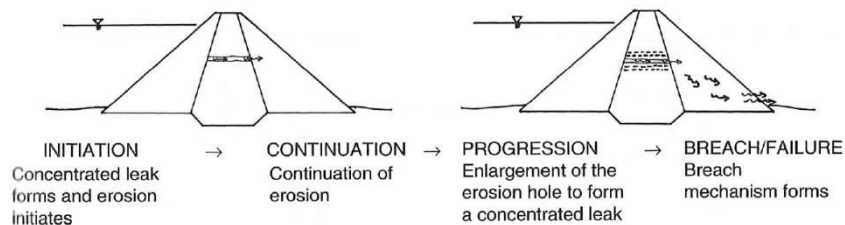
The process of internal erosion in embankments dams and their foundations according to Foster and Fell (1999) can be represented by four phases: initiation of erosion, continuation of erosion, progression of erosion and development of a breach. Conceptual models for development of failure by piping for the aforementioned modes are illustrated in the Figure I.4 with all four phases definitions are given as follows. In addition the diagram of failure path for failure by piping through the embankment is shown in the Figure I.5.

- Phase I (initiation) is the first phase of internal erosion when one of the phenomena of the detachment of particles occurs. These four initiations are concentrated leak, backward erosion, suffusion and soil contact erosion.

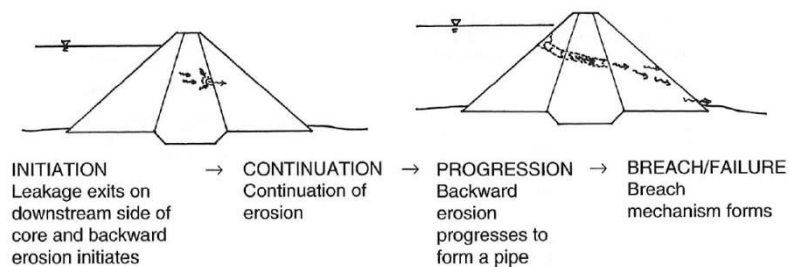
The way to detect when the initiation of internal erosion by suffusion starts is intricate as in the field the real evidence disappears within the failure of the structures. The

initiation of suffusion for instance may be attributed by the detachment of finer soil particles from its coarse matrix and become transported through sufficiently large voids and constrictions. Detachment and migration of soil particles require an adequate seepage force against the intergranular friction and constriction.

- Phase II (continuation) is the phase where the relationship of the particle size distribution between the base (core) material and the filter controls whether or not erosion will continue. In soil base-filter system, if the coarse fraction cannot act as a good filter to the soil base thus erosion process continues. For internal erosion to continue, it depends on the condition of the exit point in downstream side. Whether the exit point is free or filtered may result differently. When the exit point is free, continuation of internal erosion may occur.
- Phase III (progression) is indicated by pipe forming. This third phase of internal erosion occurs where hydraulic shear stresses in the eroded soil may or may not lead to enlargement of the pipe. The increase in pore pressure and seepage are the main causes of regressive erosion and enlargement of the duct. In Fell and Fry (2007), it is reported that with respect to structure instability, suffusion was not generally likely to lead to a piping failure since the flows were unlikely to be sufficient to erode the coarse soil remaining after suffusion had occurred. However slope instability was triggered by the increase of the phreatic surface level in the downstream slope of the embankment due to the increase in seepage flows in the soil in which suffusion had occurred. Moreover, backward erosion will not progress if layers of soil or embankment materials into which the seepage is flowing act as a no-erosion filter.
- Phase IV (development of breach) is the final phase of internal erosion. It may occur in one of four phenomena: pipe enlargement, downstream slope instability, loosening of the downstream face and overtopping.

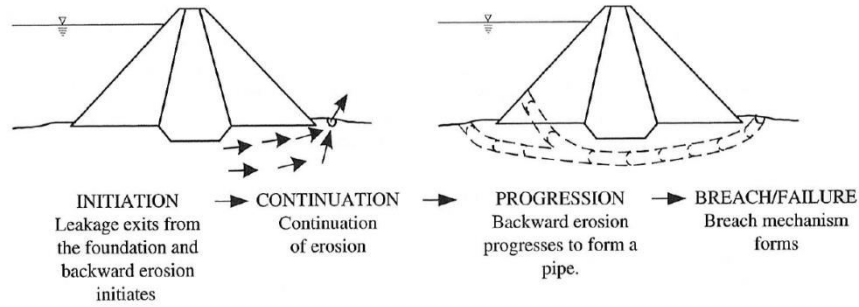


(a) Piping in the embankment initiated by concentrated leak erosion

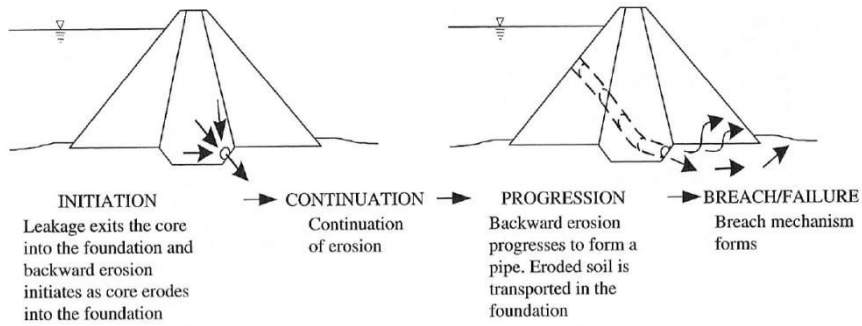


(b) Piping in the embankment initiated by backward erosion

Figure I.3 Model for the development of failure by piping in the embankment (Foster & Fell, 1999)



(a) Piping in the foundation initiated by backward erosion



(b) Piping from embankment to foundation initiated by backward erosion

Figure I.4 Model for the development of failure by piping (Foster & Fell, 1999)

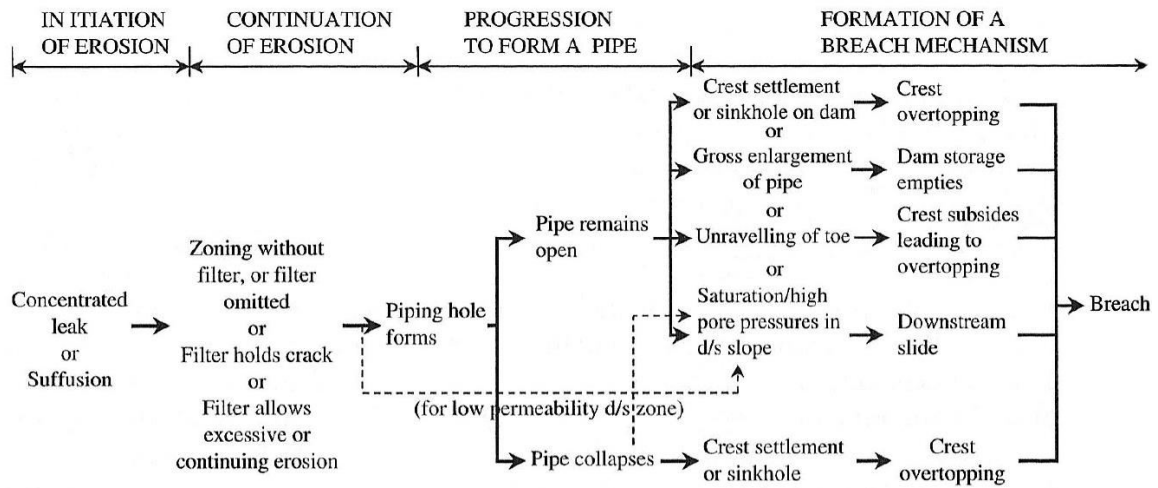


Figure I.5 The diagram of failure path for failure by piping through the embankment (Foster, 1999).

1.2 Suffusion

1.2.1 Definitions of suffusion

In the literature, different terms are used interchangeably to define the phenomena of the detachment of finer fractions from its parent material and transported through its pore spaces. These terms include “suffusion”, “suffosion” “suffossion” (with double “s”) and “internal stability” as defined by several researchers as follow Kézdi (1979), Kovacs (1981), Kenney and Lau (1985), Chapuis (1992), Chapuis et al. (1996), Moffat (2006), Wan and Fell (2008) and US. Department of the Interior (2012).

Kezdi (1979) defined “suffusion” as a phenomenon where water, while seeping through the pores, carries along the finer particles without destroying the soil structure. The other description of suffusion defined by Kovacs (1981) is the motion of fine particles. He defined it as redistribution of fine grains within the layer, when the solid volume of the layer is not changed only the local permeability is altered. Kenney and Lau (1985) defined “suffosion” to describe the transport of small particles from a soil. They also defined the term “internal stability” as the ability of a granular material to prevent loss of its own small particles due to disturbing agents such as seepage and vibration. Chapuis (1992) defined “suffusion” as the transport of small particles from a soil, which leaves large openings between the particles and later in 1996 Chapuis et al. defined “suffossion” (with double “s”) as a migration of fine particles of a soil within its own pore space”. Moffat (1996) used the term “suffusion” to describe migration of the fine fraction simultaneously with the coarse fraction (skeleton). Wan and Fell (2008) defined “suffusion” as the process by which finer soil particles are moved through constrictions between larger soil particles by seepage forces. Moffat et al. (2011) made distinctions between the phenomena of suffusion and suffosion to describe spatial and temporal progression of internal instability in laboratory permeameter test. They defined “suffusion” as phenomenon where the finer fraction of an internally unstable soil moves within the coarser fraction without any loss of matrix integrity or change in total volume whereas “suffosion” is where particle migration yields a reduction in total volume and a consequent potential for collapse of the soil matrix. Department of the Interior (2012) defined both “suffusion” and “suffosion” differently with respect to volume change in a soil. Suffusion involves selective erosion of finer particles from the matrix of coarser particles (that are in point-to-point contact) in such a manner that the finer particles are removed through the voids between the larger particles by seepage flow, leaving behind a soil skeleton formed by the coarser particles. With suffusion there is typically little or no volume change. Whereas suffosion is a similar process, but results in volume change (voids leading to sinkholes) because the coarser particles are not in point-to-point contact. Suffosion is less likely under the stress conditions and gradients typically found in embankment dams. According to Fell and Fry (2013) “suffusion” occurs when the small particles of soil are transported by the seepage flow through the pores of the coarser particles. The coarser particles are not transported and the effective stresses are largely transferred through the matrix of the coarser particles. Movement of particles occurs throughout the soil, not just from the downstream surface as in backward erosion. Sail et al. (2011) and Sibille et al. (2015) demonstrate that the development of suffusion can lead to a large settlement. It means suffusion also corresponds to a volume change or a deformation of the coarse skeleton. It seems that the distinction between suffusion and suffosion is very difficult to realize. Finally this distinction seems to be mainly influenced by the boundary conditions at the downstream part of the tested specimen. The definitions of aforementioned terms refer to movement of fine particles within the coarse matrix. Thus the term “suffusion” is used in this thesis to

describe the detachment and transport of fine particles even in the case where there a volume change or a deformation of the coarse skeleton.

According to the actual location of particle movement within the soil matrix, Kezdi (1979) classified suffusion into three types: internal suffusion, external suffusion and contact suffusion as shown in the Figure I.6. Internal suffusion has been used to describe a movement of fine fraction within the soil matrix that affect only the local permeability without any change in volume of soil structure. In contrast, external suffusion occurs at free surface where fine particles are carried from one layer (base soil layer) into an adjacent layer (filter layer). Contact suffusion occurs at the contact interface between different materials of soil. The fine material particles carried in the pores of the coarse material, under the action of a flow parallel or perpendicular to the interface.

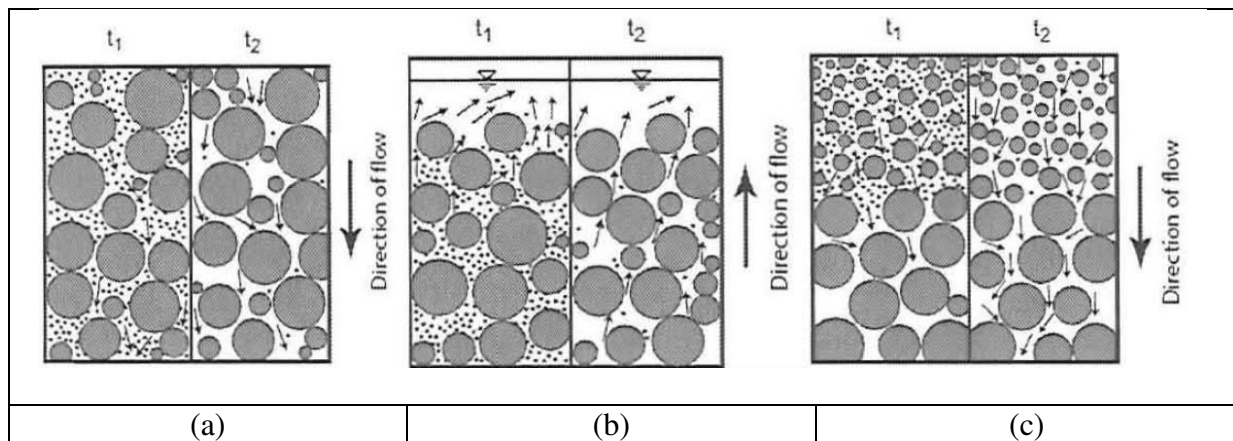


Figure I.6 Classification of suffusion (Ziems, 1996)
(a) internal suffusion (b) external suffusion (c) contact suffusion

1.2.2 Instability and failure of hydraulic structures regarding suffusion

There are a few instances of failures and incidents in embankment dams over the world indicated by suffusion but it is worth noting that suffusion may trigger backward erosion or piping as one of the main catalysts of dam instability and failures. From historical record of embankment dam failures and accidents until 1979 for dams of heights 50 feet or greater reported by Kollgaard and Chadwick (1988), it is indicated 14 failures from 17 incidents. According to Charles (1998), the failure of the Sapin embankment, homogeneous embankment composed of a sand fill, in 1988 was attributed to suffusion within the embankment. Ten years after first filling, flows of water and a shallow slip occurred in the lower part of the downstream slope of the 16 m high, embankment. Engemoen and Redlinger (2009) lists 99 incidents and failures by several types of failure mechanism, 17 incidents due to suffusion that are associated with dams constructed on, or of, glacial soils. In US. Department of Interior (2012), it was reported there were 17 dam failures caused by suffusion mechanism (8 failures with definitive particle transport and the other 9 incidents with excessive seepage). Moreover, most (60 to 75%) of the incidents involving internal migration, scour, and suffusion occur in the first 25 years of operational history. During the recent investigation over the world in the period 2010-2012, from 432 failures of hydraulic structures (including large and small dams, dikes and levee), 4% was supported by suffusion (Fry et al. 2012).

1.2.3 Recent experimental studies on suffusion

The study of suffusion is a complex matter. Different from interface erosion with respect to the transport of fine fractions, the evolution of suffusion involves iterative and complicated process that induce variations in erosion rate, hydraulic conductivity, and deformation. When fine fractions are detached and transported by seepage flow, they will pass through the soil but on the other hand they filtrate somewhere within the soil and clog the pores. This can be attributed to the constriction size. As the successive fine particles also clog the pores, the local hydraulic gradient may increase and then decrease hydraulic conductivity and erosion rate. Only large enough seepage flow can push the clogging and re-transport the fine fractions. This relates to the action of hydraulic loading. All the process depends much on the coupling of geometrical, mechanical and hydraulic condition that will be explained later in the following section.

Several experimental studies were carried out to investigate the initiation of internal erosion (suffusion) under hydraulic or hydro-mechanical condition as follow.

Skempton and Brogan (1994) presented a test under upward seepage on gap-graded soil, highly unstable sandy gravel with H/F minimum = 0.14 (where H is mass fraction measured between D and $4D$ and F is mass fraction smaller than D), porosity $n = 34\%$, and $d_{15}/d_{85} = 11$. Skempton and Brogan (1994) used a method of the increase of hydraulic conductivity to define the onset of suffusion. It is shown from the results that when the hydraulic gradient was 0.10, the coefficient of permeability kept constant value of 0.45 cm/s. With further increase of hydraulic gradient, the hydraulic gradient 0.2 initiates strong erosion with a permeability increased by a factor 2 with respect to the initial one. When the hydraulic gradient is increased to 0.28, violent erosion was observed and the coefficient of permeability increased to 1.6 cm/s, which was approximately 4 times of the initial value.

Tomlinson and Vaid (2000) carried out filtration tests to study piping erosion using artificial granular soils or glass bead (gap graded) having filter soil size 2-3 mm in diameter and base soil (finer fraction) size in ranges 0.18-0.425mm subjected to downward seepage. Two kinds of differential water head in the first minute are applied to study their effect to critical hydraulic gradient. Tomlinson and Vaid (2000) used a method of the sudden decrease of hydraulic gradient to define the onset of instability. The first tests were conducted by increasing water head difference up to 2 cm gradually in the first minute. In contrast for the second tests, a water head difference up to 23 cm was rapidly applied within the first minute was rapidly applied. For both tests the head was maintained for the first 10 minutes and then increased of additional 2 cm every 10 minutes. The result showed that the critical hydraulic gradient is lower if the head is rapidly increased, as a filtration zone is inhibited from forming. Soil samples for which the water head has been rapidly increased eroded and settled for a much lower hydraulic gradient than those of gradually increased water head. This indicated that with the same given hydraulic gradient, a soil may become unstable if the gradient is rapidly imposed. The grain-size ratio is the most important parameter affecting the stability of the soil/filter interface. The stability corresponds to piping erosion ratio D_{15f}/D_{85s} where d_{15c} is the diameter of the 15% mass passing in the coarse part; d_{85f} is the diameter of the 85% mass passing in the fine part. The ratio $D_{15f}/D_{85s} < 8$, will not fail, $D_{15f}/D_{85s} > 12$, will not be able to retain base soil, and $8 < D_{15f}/D_{85s} < 12$, piping will occur.

Sterpi (2003) carried out suffusion tests under upward hydraulic loading. The soil used was well graded compacted sand (continues particle size distribution) with fine particle content (<0.08 mm) of 23% but without clay particles. Maximum and minimum values of void ratio were $e_{max} = 0.94$ and $e_{min} = 0.33$, respectively. Sterpi (2003) defined the initiation of suffusion by the increase of eroded mass on the sample head using gentle flow of air. A sudden increase

of water outflow was at a gradient equal to 0.39 observed 5 hours after the beginning of the seepage flow, which indicates an appreciable increase of hydraulic conductivity.

Conducting suffusion tests, Moffat & Fannin (2006) used a large permeameter to test cohesionless granular soil subjected to downward hydraulic loading. A gap-graded soil with a filter ratio $d_{15}/d_{85} = 7.4$ that exceeds Kezdi's criterion was used here. They used a method of the sudden decrease of hydraulic gradient to define the onset of suffusion. Moffat and Fannin (2006) introduced gradients from 1 with increment of 1. Erosion started at gradient of 1.9 and continued to onset of failure at gradient of 8.3. Failure was determined by rapid decrease of local gradient hydraulic.

Wan & Fell (2008), by introducing upward seepage to soil specimens, revealed that erosion in internally unstable soils will begin at a gradient lower than the Terzaghi's critical effective stress gradient. Wan & Fell (2008) used measurement of eroded mass by effluent turbidity to define the onset of erosion. Most of the tested soils began to erode at gradients of 0.8 or less, and for several soils less than 0.3. Soils with higher porosity begin to erode at lower hydraulic gradients. Loosest soil tested began to erode at gradients less than 0.3, while soils with plastic fines required higher gradients to begin to erode. Gap-graded soils tended to begin to erode at lower gradients than non gap-graded soils with the same fines content.

Conducting test on soils subjected to downward seepage, Chang and Zhang (2011) used gap-graded soils with H/F minimum = 0.75, uniformity coefficient, $C_u=16.7$, and $d_{15c}/d_{85f}=10.2$ where d_{15c} is the diameter of the 15% mass passing in the coarse part; d_{85f} is the diameter of the 85% mass passing in the fine part. To determine the onset of suffusion, they used a method of increased of eroded mass and hydraulic conductivity. They showed suffusion initiated at low gradient of 1.2 and continued with sudden increase in flow rate and hydraulic conductivity at gradient of 3.15.

Sail et al. (2011) conducted suffusion tests in permeameter on cohesionless granular soil subjected to downward hydraulic loading. Using gap-graded soil of glass mixture called G4-C that referred to Moffat and Fannin (2006) with $C_u = 1.4$ and $d_{85} = 0.19$ mm for the fine fraction (40%) and $C_u = 1.7$ and $d_{10} = 1.4$ mm for the coarse fraction (60%), Sail et al. (2011) defined the onset of suffusion by the decrease of local hydraulic gradients. They demonstrated that erosion commenced at gradient of 0.2 and the onset of failure was at gradient 4.9.

From the aforementioned studies, the methods to determine the onset of internal erosion (suffusion) can vary. Most of the studies used hydraulic gradient approach to represent the hydraulic loading imposed to the soils.

1.2.4 Identification of suffusion

Identifying whether or not the test soil is internally unstable from the results is an important step. There is no general rules to judge the instability of soils based on the testing results. Different investigators followed different identification methods. Here, four identification methods are summarized according to: a) the evolution of hydraulic conductivity, b) the change of hydraulic gradient, c) the mass of the soil fraction loss, and d) the change in gradation curve, and failure. Some of the investigators consider only a single identification, but the others combine several identifications to characterize internal instability.

In the first method, the onset of suffusion is detected if a significant change in hydraulic conductivity occurs during the testing process. This can be recognized from a hydraulic conductivity - time relationship. When the hydraulic conductivity of a soil progressively or

suddenly increases, the suffusion initiates. Lafleur (1989), Skempton and Brogan (1994), Chapuis et al. (1996) and recently Ke and Takahashi (2012) adopted this method.

In the second method, the onset of suffusion is detected by sudden decrease of a local hydraulic gradient, as considered by Moffat and Fannin (2006), Perzlmaier (2007), Sail et al. (2011), Li (2008), Moffat et al. (2011). When a local hydraulic gradient within porous medium increases, it may be attributed to a clogging process. Once such this large hydraulic gradient can push the clogging, the fine fraction is washed out accompanied by increase hydraulic conductivity and the drop of hydraulic gradient.

In the third method, the suffusion initiation can be indicated by continuous loss of fine particles or significant settlement of the sample. However, Lafleur et al. (1989), Bendahmane et al. (2005), Fannin and Moffat (2006), and Li (2008), Chang and Zhang (2012), Sail et al. (2011), Luo et al. (2013) followed this method. However, no quantitative stability thresholds have been proposed, but Lafleur et al. (1989) set out the minimum loss of fine fraction for an unstable soil equals to 0.25 g/cm^2 .

In the fourth method, soil instability is reflected from the after-test gradation curves. Kenney and Lau (1985), Lafleur (1989), Ke and Takashi (2012), Chang (2012) judged their testing results from the changes in the grain size distribution curves at different layers of the soil samples before and after the seepage tests. The soils are considered as internally unstable when there is a significant change between the grain size distribution curves before and after the seepage test.

1.2.5 Control parameters for likelihood of suffusion

The study of suffusion depends on (i) geometry of the porous medium, (ii) physicochemical characteristic of medium and interstitial fluid, (iii) mechanical loading conditions and (iv) hydraulic loading condition.

Garner and Fannin (2010) developed a Venn diagram, as shown in the Figure I.7 to illustrate that erosion is generated by three factors: the susceptibility to erosion of the material, the critical hydraulic load and condition of critical stress. Material susceptible to internal erosion is related to the likelihood for finer fraction to detach from its parent matrix and migrate out of the soil. These detachment and migration relate to grain size distribution, the shape of grains and pores. In case of cohesive soil, the physicochemical characteristic of solid medium such as dispersiveness should be taken into account. The critical hydraulic load is associated with the action of seepage flow that is sufficient enough to invoke the initiation of internal erosion. This factor can relate to the seepage gradients, velocities or hydraulic shear stress present in the embankment or foundation. The critical stress condition is related to the inability to resist internal erosion due to the magnitude of effective stress within the body of the dam. The coupling of material susceptibility, hydraulic loading and critical stress yields to the detachment and transport of soil grains.

According to Schuler (1995), parameters influencing the susceptibility of a soil to suffusion are as follow: (i) from the geometric point of view: grain-size and their distribution, pore size and their distribution, grain shape, and pore shape; (ii) from the mechanical point of view: degree of compaction, cohesion, and effective stress; (iii) from the hydraulic point of view: hydraulic gradient, seepage direction, pore fluid velocity, chemical property of the fluid.

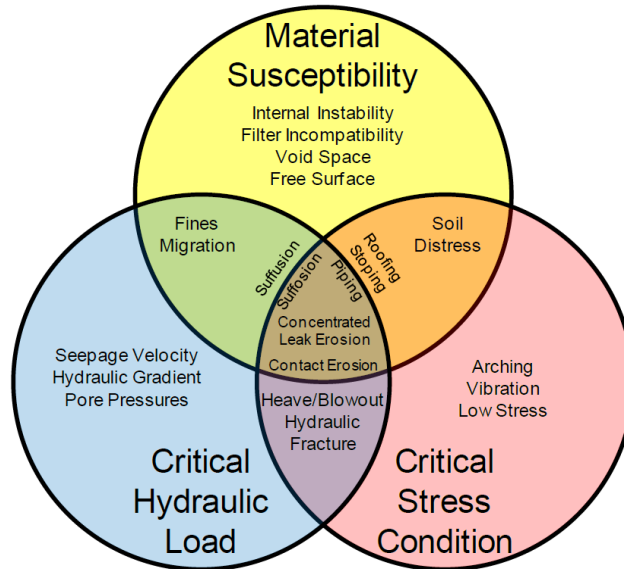


Figure I.7 Factors Affecting the Initiation of Internal Erosion (Garner and Fannin, 2010)

Geometry of the porous medium

In entire suffusion process, the detachment of finer particles from its parent material and migration by seepage flow requires constriction size that is sufficiently large. Filtration within the soil matrix due to the impediment of small constriction can induce clogging and result in decreasing hydraulic conductivity. When large seepage power can sufficiently push the clogging then the finer fractions will remigrate. This constriction size is conditioned by gradation distribution, the grains shape and the density of granular packing.

According to Lafleur et al. (1989), the shape of the grading curves can be divided into three groups: linear distribution (curves 1 and 2), discontinuous distribution (curve 3) and upwardly concave distribution (curve 4) as shown in the Figure I.8.

Based on gradation information, according to Burenkova (1993) and Wan and Fell (2008), soils with a steep slope on coarse fraction and gentle slope on the finer fraction (curve 4) were likely to be internally unstable. Moreover as indicated by Fell and Fry (2007), soil gradation types which are susceptible to suffusion or internally unstable are either discontinuous (or gap-graded) distribution (curve 3) and upwardly concave distribution (curve 4).

For granular soils, the phenomenon of suffusion occurs only if some criteria are satisfied. According to Wan and Fell (2008) and Fell and Fry (2013), there are three criteria for suffusion to occur:

- 1). the size of the fine soil particles must be smaller than the size of the constrictions between the coarser particles, which form the basic skeleton of the soil,
- 2). the amount of fine soil particles must be less than enough to fill the voids of the basic skeleton formed by the coarser particles. If there are more than enough fine soil particles for void filling, the coarser particles will be “floating” in the matrix of fine soil particles, instead of forming the basic soil skeleton,
- 3). the velocity of flow through the soil matrix must be high enough to move the loose fine soil particles through the constrictions between the larger soil particles.

The first two criteria are associated with geometric criteria that may control the likelihood for suffusion, whereas the third is related to the action of hydraulic flow with respect to seepage power required to migrate the fine particles.

Kenney and Lau (1985) indicate whether cohesionless soils are internally stable or not depending on (1) particle size distribution curve of the whole material, (2) density of the compacted material, and (3) severity of the disturbing force. Furthermore, Li and Fannin (2008) stated that to assess internal instability of soils, the two aspects to be considered are (1) the susceptibility to internal instability, which is influenced by the grain size distribution of the soil, and (2) the onset of any instability, which is governed by hydromechanical influences.

With respect to the grain shape, Kovacs (1981) distinguished shape coefficient between spherical and angular particles. He proposed to compute the diameter of the average pore by using shape coefficient whose values ranging between 6 for the spherical particles and from 7 to 9 for the more angular particles. Marot et al. (2012a) clearly demonstrate that suffusion process relies on the grain angularity of coarse fraction. Given a same grain size distribution, angularity of coarse fraction grains contributes to increase the suffusion resistance.

In the case of cohesive soil, physicochemical characteristic of medium and interstitial fluid should be taken into account in the process of detachment and transport of fine particles. Arulanandan and Perry (1983) indicated that eroded aggregate size was a function of the state flocculation or deflocculation of clay soil. This state depends particularly on the chemical composition of the interstitial fluid, as well as on the quantity and nature of the clay. The reduction of suffusion could be attributed to the influence of sodium chlorate on the flocculation of the soil. When sodium absorption is high then the physicochemical interaction forces decrease. This can cause deflocculation and thus suffusion resistance decrease. Reddi et al. (2000) indicated that the increase of sodium chlorate concentration contributed to the decrease of suffusion rate erosion.

Mechanical conditions

The changes of the density of granular packing or modification of effective stress within porous medium by external loads can create grain arrangement. When the effective stress or the soil density of a soil increases, suffusion resistance of the soil also increases. The effective stress of the soil is an important factor with respect to the soil shear strength. The stress condition plays a role in internal instability due to the influence of the stress on the microstructure of the soil and in turn it responses to a hydraulic loading. The combination of material susceptibility, hydraulic loading and critical stress condition (see the early part of section 2.2.4 for detail definition) induce detachment, and migration of soil grains. According to Moffat and Fannin (2006) and Bendahmane et al. (2008), a rise of effective stress in porous medium resulted in increasing suffusion resistance.

Hydraulic loading condition

Even if the transport fine particles is geometrically feasible, the action of hydraulic flow should be studied. Given soils having the same properties but different grain shapes for instance, the critical hydraulic flow may differ. The critical hydraulic flow is related to the lowest hydraulic action on soil particles required to detach, migrate and push the finer fraction. The hydraulic loading on the grains is often described by three distinct approaches: hydraulic gradient (Skempton and Brogan, 1994 and Li, 2008), hydraulic shear stress (Reddi et al., 2000) and pore velocity (Perzlsmaier, 2007). Recently Marot et al. (2011) proposed energy-based approach to characterize hydraulic loading.

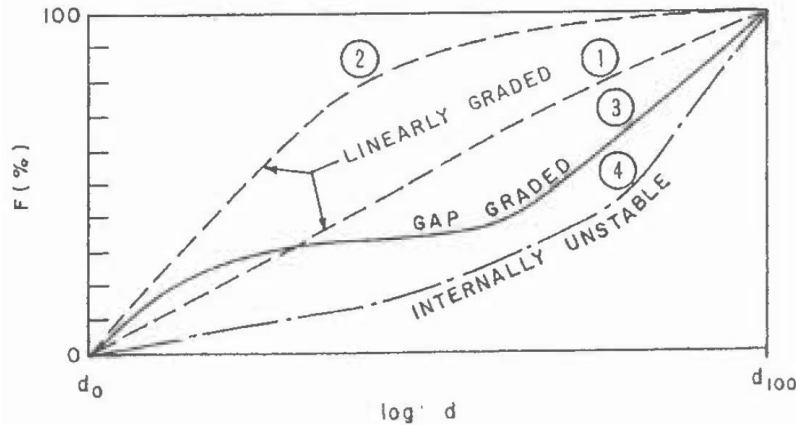


Figure 1.8 Classification of the grain size distribution of soils (Lafleur et al. 1989)

1.3 Coupling of geometry, mechanical and hydraulic condition

Likelihood of internal erosion of a soil is governed by coupling of geometric conditions, mechanical conditions, and hydraulic conditions of a soil. Among the three factors, it is difficult to decide which one is the most important variable to control the soil susceptibility to suffusion as they are coupled. Regarding the geometric conditions, the likelihood of migration of fine particles is possible but both mechanical condition and hydraulic condition also support the initiation of suffusion. Given that the same soils have the same gradation properties but different relative density or subjected to under different stress states within the soil, the hydraulic gradients that induce the onset of suffusion may be different. From the point of view of effective stress, under large stress of hydraulic conditions (confining pressure), the microstructures of a soil tend to consolidate and become denser, and locking of fines with respect to the coarse granular fraction is improved. Thus larger critical hydraulic gradients inducing migration of fine particles within the pore structures and constrictions are required.

Over the years a large number of researchers have been conducting interpretations on suffusion by taking into account coupling of geometrical conditions, mechanical condition and hydraulic conditions, such as Tomlinson and Vaid (2000), Bendahmane et al. (2008), Bandini and Sathiskumar (2009), Moffat and Fannin (2011), Chang and Zhang (2011), Marot et al. (2012) and Moffat and Herrera (2014).

Tomlinson and Vaid (2000) showed the effect of hydraulic loading rate imposed to gap-graded soils in filtration test. Given a hydraulic gradient value, a soil may become unstable if the hydraulic gradient is rapidly imposed i.e. the critical gradient becomes lower for a high hydraulic loading rate. Bendahmane et al. (2008) reported that given gradation distribution and confining pressure, larger hydraulic gradient resulted larger erosion rate, but given gradation distribution and hydraulic gradient, larger confining pressure resulted decrease of erosion rate. In Bandini and Sathiskumar (2009), the saturated hydraulic conductivity and the coefficient of consolidation of clean sands can be two orders of magnitude bigger than those of sand with 25% of non-plastic silt. Moreover, a given silt content, the hydraulic conductivity varies mostly within one order of magnitude depending on the void ratio of the soil. Moffat and Fannin (2011) pointed out that the critical hydraulic gradient increases with the increase of effective stress and the onset of internal erosion can be governed either by increasing hydraulic gradient or decreasing the effective stress. Chang and Zhang (2011) demonstrated that the maximum erosion rate, the evolution in soil permeability and the total deformation of the soil specimen increase with the increase of deviatoric stress. With the aim

to investigate the effect of angularity to suffusion, Marot et al. (2012a) carried out a series of tests on clayey sand subjected to hydraulic gradient. Given gradation distribution and confinement pressure, it was shown that the angularity of coarse fraction may influence the increase of suffusion resistance of tested soils by a factor 5. Moffat and Herrera (2014) proposed a theoretical model with the aim to indicate an approximate value of critical hydraulic gradient to the onset of suffusion in a cohesionless soil of known grain size distribution curve. The model to enhance the criterion proposed by Kezdi (1979) used parameters: the effective stress, the porosity of the soil, the friction angle between the coarse and fine fractions, and G^* (a geometric-based factor that determines the proportion of stress transferred to the particles of the fine soil fraction).

1.4 Criteria for likelihood of suffusion

1.4.1 Geometric criteria to assess soils likelihood to suffusion

Geometric condition of a soil may control the likelihood of internal erosion. Several researchers have proposed methods to assess the susceptibility of a soil to internal erosion based only on the gradation information of a soil. Geometric criteria can be divided into (i) gradation-based internal stability criteria (USACE 1953, Istomina 1957, Kezdi 1979, Sherard 1979, Kenney and Lau 1985, Burenkova 1993, Wan and Fell 2008, Li and Fannin 2008, Chang and Zhang 2013); and (ii) constriction-based internal erosion criteria (Indraratna et al. 2011, Shire and Sullivan 2013 and Moffat and Herrera 2014).

USACE criterion

The U.S. Army Corps of Engineers, USACE (1953) carried out suffusion test on sandy gravel soils subjected to downward flow. They proposed that the onset of suffusion requires: turbulent flow conditions, a hydraulic gradient ≥ 5 , and a coefficient of uniformity of $C_u > 20$.

Istomina criterion

Istomina (1957) developed a simple method to evaluate internal stability of sand-gravel soils based on the uniformity of the grain-size distribution curve. The coefficient of uniformity, C_u , is as an indicator to assess internal stability. Soils with $C_u < 10$ are internally stable, and those with $C_u > 20$ are likely to be internally unstable. Those with $10 < C_u < 20$ fall into the transitional zone.

Kezdi criterion

Kezdi (1979), presents a method that splits curve into its coarse and fine components at an arbitrary grain diameter. This method follows the Terzaghi's idea of filtration criterion. Self-filtering is the process where the coarse particles of a cohesionless soil prevent erosion of the fine particles. The soil is internally unstable if it satisfies $(d_{15c}/d_{85f})_{\max} > 4$ where d_{15c} is the diameter of the 15% mass passing in the coarse part; d_{85f} is the diameter of the 85% mass passing in the fine part. The difficulty of Kezdi criterion is at which point precisely splitting the grain size distribution. However later Li (2008) indicated that the limit between finer and coarser fractions corresponds to the minimum value of the Kenney and Lau's (1985) ratio H/F , where H is mass fraction measured between D and $4D$ and F is mass fraction smaller than D . Moffat and Fannin (2006) proposed a soil considered as stable if it satisfied $(d_{15c}/d_{85f})_{\max} \leq 4$, and as unstable if $(d_{15c}/d_{85f})_{\max} \geq 7$.

Sherard criterion

Similar to the concept of Kezdi (1979) arbitrarily splitting the gradation distribution curve in two, Sherard (1979) indicated that suffusion or internal instability can be attributed to $(D_{15coarse}/d_{85fine}) > 4$ to 5.

Kovacs (capillary tube model)

Kovacs (1981) proposed average pore diameter by representing porous medium as capillary tube model to assess internal stability. Pore space of the soil is represented as a bundle of parallel cylindrical tubes (see Figure I.9). The average pore diameter of the coarse fraction d_0 is computed in the idealized soil skeleton based on the following expression:

$$d_0 = 4 \frac{n_c}{1-n_c} \frac{D_h^c}{\alpha_D} \quad (I.1)$$

where n_c is porosity of the coarse fraction, D_h^c is the Kozeny effective diameter of the coarse fraction and α_D is the shape coefficient (6 for rounded particles, 7 to 9 for angular particles).

n_c and D_h^c can be computed by :

$$n_c = n + F_n(1 - n) \quad (I.2)$$

$$D_h^c = \frac{1}{\sum \frac{\Delta F_i^c}{D_i^c}} \quad (I.3)$$

where n is porosity of the soil, F_n is the mass percentage of the finer fraction, ΔF_i^c and D_i^c are the weight and average diameter of grains in the i th interval of the particle size distribution curve of the coarse fraction.

Kenny and Lau method

According to the test results on 16 soil samples, Kenney and Lau (1985) present a method of geometric criterion to assess internal instability of soil. Determination of whether soils are internally unstable or stable in the method is based on the shape of particle size grading curve. Kenney & Lau defined the ratio of F and H where F denotes mass fraction smaller than and particle diameter D , and H measured the mass fraction between D and $4D$. Soil with a ratio $H/F < 1$ shown in the Figure I.10 are defined as internally unstable soils. Kenney & Lau (1985) choosed a size interval with a ratio equals to four times because the size of predominant constriction in the void network of a filter is approximately one-fourth the size of the smallest particle making the filter. This means particles of size D can pass through constriction in a filter formed by particles of size $4D$ and larger.

Burenkova approach

The Burenkova (1993) method is based on ratios of d_{90}/d_{60} and d_{90}/d_{15} , where d_{90} is the sieve size for which 90% of the sample by weight passes. The d_{90}/d_{60} ratio denotes the slope of the coarse part of the particle size distribution, whereas the d_{90}/d_{15} can be regarded as a measure of the filter action between the coarse fraction and the finer fraction. Internally stable soil, should satisfy the Equation II.4 as follows. For couples of ratios belonging to area II in the Figure I.11, corresponding soils are considered as internally stable, while for areas I and III soils are internally unstable. This method is not able to identify the internal instability of gap-graded soils but broadly graded soils.

$$0.76 \log \left(\frac{d_{90}}{d_{15}} \right) + 1 < \frac{d_{90}}{d_{60}} < 1.86 \log \left(\frac{d_{90}}{d_{15}} \right) + 1 \quad (I.4)$$

Wan and Fell method

Conducting tests on 20 soil samples, Wan and Fell (2008) stated that the most widely used methods were conservative as most of the soil samples tested in University of New South Wales (UNSW) were stable whereas they were predicted as unstable by those methods. Wan and Fell (2008) proposed a method for assessing internal instability of broadly graded silt-sand-gravel soils. Defining couple ratios between d_{90}/d_{60} and d_{20}/d_5 , this method classifies soils into three categories stable, transition, and unstable, as presented in the Figure I.12. However, this method is not appropriate for soils having finer fraction less than 15%. This method is not able to identify the internal instability of gap-graded soils but broadly graded soils.

Li and Fannin method

Li and Fannin (2008) proposed a method to assess internal stability based on the filtering capacity of the coarse particles to the fine particles after comparing two methods proposed by Kezdi (1979) and Kenney and Lau (1985). Li and Fannin (2008) method based on experimental tests and compilation of a database from the findings of eight laboratory studies on a total of 57 gradations. Comparison indicates the filter ratio (D'_{15}/d'_{85}) of the Kezdi method is relatively more conservative for $F < 15\%$, and the stability index $(H/F)_{\min}$ of the Kenney and Lau method is more conservative for $F > 15\%$ as shown in the Figure I.13.

Indraratna et al. approach

The size of controlling constriction in the pore network must be larger than maximum diameter of the loose particles, affording these particles the possibility of being moved by seepage flow. Indraratna et al. (2011) proposed a criterion based on a probabilistic method on a broadly-graded soil. The grading information and relative density of soil are parameters required to obtain constriction size distribution curve. By dividing a soil into a coarse component and a fine component, the controlling constriction size could be obtained from the coarse component. The ratio between controlling constriction size of coarse particles and fine fraction component, D_{c35}/d_{85f} , was deduced to distinguish stable to unstable soils. D_{c35}/d_{85f} where D_{c35} is defined as 35% constrictions of a given constriction size distribution curve are smaller that is chosen as the controlling constriction size of the coarse component, and d_{85f} is used to represent diameter of 85% mass passing in the fine component. If a soil satisfies $D_{c35}/d_{85f} < 0.73$, it is considered as internally stable. If $D_{c35}/d_{85f} > 0.82$, the soil can be judged as internally unstable. Within these two boundaries, further laboratory testing is needed. The criterion proposed by Indraratna et al. (2011) is based on the porosities influenced by grain size distribution and degree of compaction. This method assumed that the coarse particles contact each other in which the pore formed by the coarse is filled by the fine particles. However, for soil specimens compacted by moisture tamping, which is a common compaction method in dam engineering practice, some fine particles could also form the matrix.

Chang and Zhang method

Chang and Zhang (2013) proposed three geometric criteria for well-graded soils and gap-graded soils with respect to the percentage of particles finer than 0.063 (named P). For well-graded soils the stability is assessed with Kenney and Lau's criterion $(H/F)_{\min}$. For $P < 5\%$, it is stable if $(H/F)_{\min} > 1.0$. With $5\% \leq P \leq 20\%$, soil is stable if $(H/F)_{\min} > 4/3 - P/15$ and a soil with $P > 20\%$ is stable. For gap-graded soils, the stability is assessed with gap ratio that Chang and Zhang (2013) defined as: $G_r = d_{\max}/d_{\min}$ (d_{\max} and d_{\min} : maximal and minimal

particle size respectively of the missing fraction). With $P < 10\%$, a soil is stable if only $G_r < 3$. A soil with $P > 35\%$ is considered stable, and with $10\% \leq P \leq 35\%$ the soil is stable if $G_r < 0.3P$. This is only applicable to low plasticity soils.

Moffat and Herrera approach

Moffat and Herrera (2014) proposed a criterion based on ratio D_{15}/d_{85} (Kezdi method) and stress factor G^* where G^* is a geometric-based factor that determines the proportion of stress transferred to the particles of the fine soil fraction. The proposed model aims to enhance the criterion proposed by Kezdi (1979) and uses the following parameters: the effective stress, the porosity of the soil, the friction angle between the coarse and fine fractions, and G^* . Their conclusions are:

- (i) the most important parameters to define the onset of suffusion are effective stress and hydraulic gradient,
- (ii) factor G^* decreases as the value of D_{15}/d_{85} (D_{15} is the diameter of the 15% mass passing in the coarse part; d_{85} is the diameter of the 85% mass passing in the fine part) increases that means for soils having values of $D_{15}/d_{85} > 4.0$ according to Kezdi (1979), the critical hydraulic gradient i_{cr} becomes smaller under the same effective stress conditions.

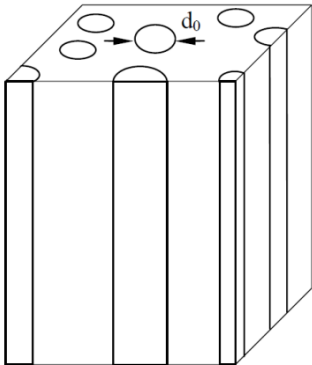


Figure I.9 Parallel cylindrical tubes

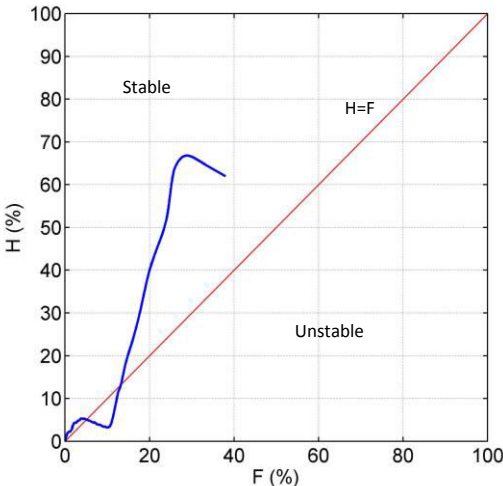


Figure I.10 H/F curve to assess instability by Kenney & Lau (1985)

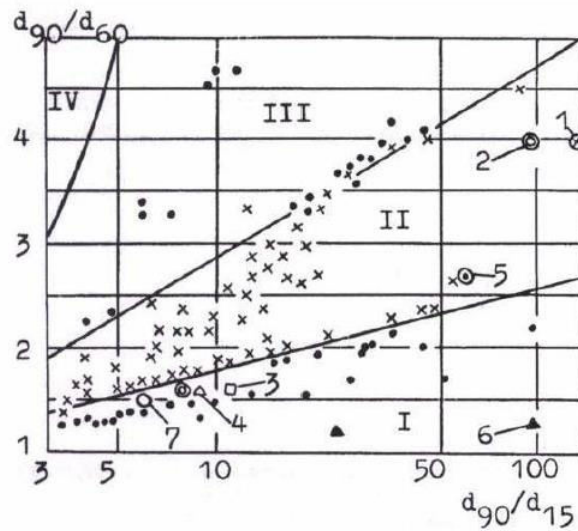
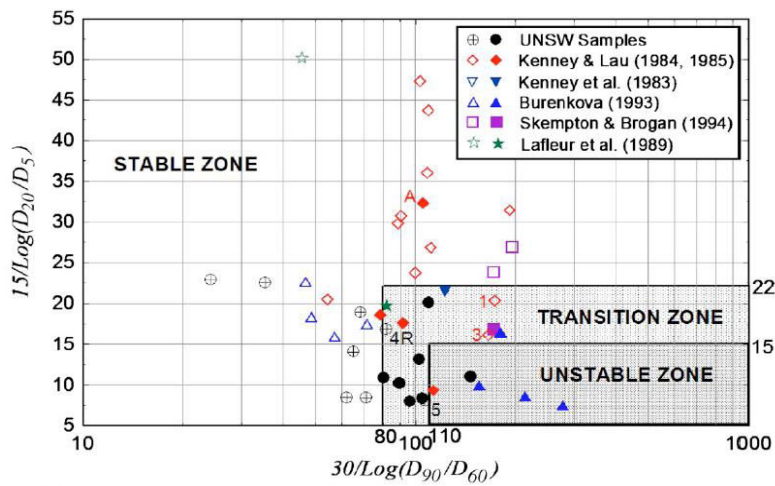


Figure I.11 Method for assessing internal instability by Burenkova (1993)



Notes:
 1. Hollow symbol represents internally stable sample.
 2. Solid symbol represents internally unstable sample.

Figure I.12 Method for assessing internal instability of broadly graded silt-sand-gravel soils (Wan and Fell, 2008)

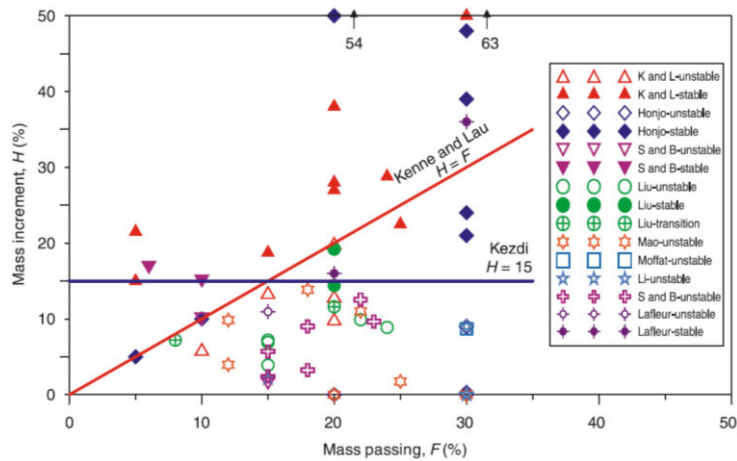


Figure I.13 Method for assessing internal instability of soils (Li and Fannin, 2008)

1.4.2 Hydraulic criteria to assess soils likelihood to internal erosion

The study of hydraulic conditions, as external triggers, is required to investigate the onset of suffusion even if the soil is geometrically feasible to suffusion. The hydraulic loading applied on a soil is often described by the hydraulic gradient, the hydraulic shear stress and the pore velocity or the Darcy velocity. In the literature, several investigators have proposed the concept of hydraulic loadings to initiate internal erosion or suffusion: Terzaghi (1939), Adel et al. (1988), Skempton and Brogan (1994), Reddi et al. (2000), Perzlmaier (2007), Li et al. (2008) and Li and Fannin (2011). Recently Marot et al. (2011) proposed an energy-based approach to characterize hydraulic loading.

1.4.2.1 Hydraulic gradient criteria

Terzaghi approach.

The classical theory of zero vertical effective stress in sand column was proposed by Terzaghi (1939). Seepage in an upward direction can reduce the effective stress within the soil. Zero effective stress is defined when total stress at a soil point equals to pore water pressure. The vertical effective stress becomes zero within the layer when the upward hydraulic gradient is equal to the critical gradient, then heave failure occurs. Terzaghi (1939) proposed critical upward hydraulic gradient for heaving, $i_c (= \gamma'/\gamma_w)$ equal to 1.0, where γ' is submerged unit weight of soil and γ_w is unit weight of water. It is worth stressing that this criterion was initially introduced to describe the hydraulic heave and not correspond to internal soil erosion phenomenon.

Adel et al. criterion

Adel et al. (1988) carried out three seepage tests on minestones imposed to horizontal flow. The specimen had a length of 105 cm. Eroded mass of finer particles was collected in a sandtrap. Erosion rate was used to determine a value for critical hydraulic gradient, with the threshold defined equal to $1\text{g/m}^2\cdot\text{s}$ that was measured during 30 minutes. A linear relation was proposed between critical hydraulic gradient (i_{cr}) and Kenney and Lau's criterion $(H/F)_{min}$ as shown in the Figure I.14.

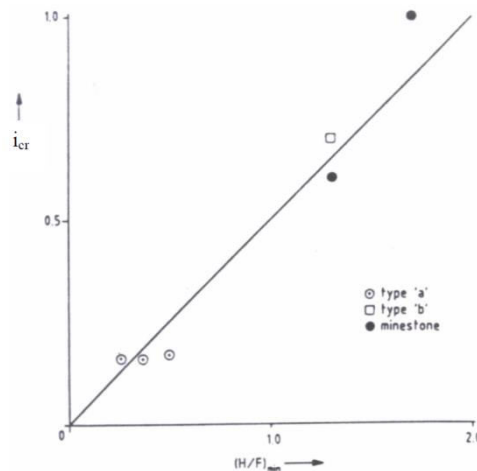


Figure I.14 Hydraulic criterion for horizontal flow (Adel et al. 1988)

Skempton and Brogan method

Skempton and Brogan (1994) presented tests under upward seepage on gap-graded soil, highly unstable sandy gravel. The results indicated that the critical hydraulic gradient can be much lower than the theoretical values by Terzaghi (1939). This can be explained that the overburden load is taken predominantly by the coarse fraction, leaving the finer fraction under relatively small stress. The critical hydraulic gradient required to initiate suffusion, i_{cr} , by Skempton and Brogan (1994) is expressed:

$$i_{cr} = (1 - \alpha) \left(\frac{\gamma'}{\gamma_w} \right) \quad (I.5)$$

where α is stress reduction factor in the finer fraction that less than 0.1 for sandy gravel and its value needed to be determined by internal erosion tests.

The use of such a criterion to characterize suffusion may be questionable since it is directly derived from Terzaghi's criterion for initiation of hydraulic heave.

Li method

Li (2008) performed suffusion tests on cohesionless soils with a large permeameter (inner diameter: 279 mm and the length: 310 mm) and a small permeameter (inner diameter: 100 mm and the length: 108 mm). He evaluated the suffusion initiation due to a temporal variation of local hydraulic gradient and observed that the critical hydraulic gradient can be seven times higher with the small permeameter than with the large one for a same type of tested specimen and a same mean vertical effective stress. The difference was attributed to scale effects. From Skempton and Brogan's (1994) concept of stress reduction and with the objective to eliminate scale effect, Li (2008) expressed the critical hydraulic gradient for upward seepage flow, i_{cr} , as a function of a normalized vertical effective stress and the thickness of specimen as:

$$i_{cr} = \alpha \left(\frac{\sigma'_{to}}{\gamma_w g \Delta z} + \frac{\gamma'}{\gamma_w} \right) = \alpha \left(\frac{\sigma'_{vm0}}{\gamma_w g \Delta z} + 0.5 \frac{\gamma'}{\gamma_w} \right) \quad (I.6)$$

where σ'_{to} is the vertical effective stress on top of specimen; Δz is the thickness of soil specimen; g is gravity; and σ'_{vm0} is the mean vertical stress in the middle of soil layer ($\sigma'_{vm0} = \sigma'_{to} + 0.5 \rho' g \Delta z$). It is worth noting that the thickness of the soil specimen corresponds to the seepage path in the case of vertical seepage flow.

The value of stress reduction factor α depends on the granular distribution and the shape of particles as presented in the Equation II.7.

$$\alpha = 3.85 \left(\frac{d'_{85}}{d_0} \right) - 0.616 \quad (I.7)$$

where, d'_{85} is the representative diameter of the finer fraction (d'_{85} : sieve size for which 85% of the weighed fine fraction is finer) and d_0 is the average capillary tube diameter of the coarser fraction. The expression of d_0 defined by Kovacs (1981) can be seen in the geometry criteria section.

Li and Fannin approach

Li and Fannin (2012) proposed a theoretical hydromechanical envelope to characterize the critical hydraulic gradient of a soil under overburden stress. The critical hydraulic gradient for an internally unstable soil subjected to an effective vertical stress can be expressed as

$$i_c = \frac{\alpha}{1-0.5\alpha} \left(\bar{\sigma}'_{vm} + \frac{0.5(G_s-1)}{(1+e)} \right) \quad (I.8)$$

where α is the stress transformation coefficient; G_s is the specific gravity of the soil; e is the void ratio; and $\bar{\sigma}'_{vm}$ is the effective vertical stress of the soil.

1.4.2.2 Hydraulic shear stress

Regarding hydraulic shear stress, Reddi et al. (2000) proposed to represent the porous medium by a system of parallel capillary tubes each of a constant radius r . Assuming that hydraulic loading can be represented by a shear stress, the hydraulic shear stress for a horizontal flow between upstream section A and downstream section B of the system can be expressed by the Equation II.9.

$$\tau = 1.414 \left(\frac{\Delta P}{\Delta L} \right) \left(\frac{r}{2} \right) \quad (I.9)$$

Where $\Delta P = P_A - P_B$ is the pressure drop between sections A and B, ΔL is the distance between section A and B.

This concept of hydraulic shear stress can be reformulated in the case of a vertical flow by:

$$\tau = \left(\frac{\Delta h \gamma_w}{\Delta z} \right) \sqrt{\frac{2k\mu}{\gamma_w n}} \quad (I.10)$$

where Δh is the hydraulic head drop, Δz the altitude change for a one dimensional flow between an inlet section A and an outlet section B, k the hydraulic conductivity, μ the dynamic viscosity, and n the porosity.

1.4.2.3 Flow velocity

Perzmaier (2007) assuming the hydraulic gradient cannot sufficiently describe the transport of particles along the flow path, proposed a hydraulic criterion based on critical pore velocity. The actual mean pore velocity $v_{p,av}$ can be derived from the Darcian flow velocity v_f , the porosity n and the tortuosity T as shown in the Equation II.11. The value of mean pore velocity can be 4 to 8 times higher than the Darcian flow velocity.

$$v_{p,av} = \frac{v_f}{n.T} \quad (I.11)$$

The tortuosity describes the ratio between the shortest distance of two points in flow direction and the effective length of the flow path following the winding pore channels.

This approach of the erosion process for instance can describe the effect of boiling at an unfiltered exit of seepage. A particle which partially blocks a pore of the soil at the surface, is lifted by the pore velocity. Once the particle is transported away from the surface, velocity reduces as porosity approaches 1 and the particle sinks back to the surface.

1.4.2.4 Energy-based approach

Marot et al. (2011) proposed a new method based on the energy dissipated by the fluid and the mass loss of the sample. The energy and the mass loss are attributed to seepage flow and the response of the soil, respectively. For illustration, for a given volume V of fluid that comprises a mass M and density ρ , mass M has a contact surface S with its environment (soil and wall).

The external surface of the volume is oriented by its normal vector \vec{n} from fluid to environment. The temporal variation of the energy of seeping fluid is equal to the sum of the variation of its thermal energy and the variation of mechanical work of external forces to the volume. This variation of the energy is expressed by:

$$\frac{dE}{dt} = \frac{d}{dt} \iiint_{Mass} \left(e_{int} + \frac{w^2}{2} + \vec{g}\vec{z} \right) dM \quad (I.12)$$

$$\frac{dE}{dt} = \frac{\partial}{\partial t} \iiint_{Volume} \left(e_{int} + \frac{w^2}{2} + \vec{g}\vec{z} \right) \rho dV + \oint_S \left(e_{int} + \frac{w^2}{2} + \vec{g}\vec{z} \right) \rho (\vec{U}\vec{n}) \cdot dS \quad (I.13)$$

and

$$\frac{dE}{dt} = \frac{dE_{Ther}}{dt} + \frac{dW}{dt} \quad (I.14)$$

Where t is the time, E_{ther} is the thermal energy exchange between the system and the environment, W is the mechanical work between upstream and downstream, e_{int} is the internal energy of the fluid, U is the velocity of the fluid, with components (u, v, w) , g is gravity, \vec{n} is surface normal vector directed to the fluid, and z indicates coordinates.

To simplify the equation, three assumptions are used here: (i) the system is considered as adiabatic, energy variations with time are neglected, only the mechanical work between the upstream and the downstream sides of the system is considered, (ii) the temperature and the internal energy with time are assumed to be constant for the volume, (iii) the flow is in steady state condition, thus the temporal variation of kinetic energy can be neglected and the density of the fluid is assumed to be constant.

Thus using the given assumptions, the equations may be rewritten as:

$$\frac{dW}{dt} = \oint_S \left(\frac{w^2}{2} + \vec{g}\vec{z} \right) \rho (\vec{U}\vec{n}) dS \quad (I.15)$$

The mechanical work is defined as the sum of mechanical work by pressure ($W_{pressure}$), by erosion at the fluid-solid interface ($W_{erosion}$) and by viscosity and turbulence in the fluid ($W_{intrafluid}$). The dissipation of total energy in the system can be written as:

$$\frac{dW}{dt} = \frac{dW_{pressure}}{dt} + \frac{dW_{intrafluid}}{dt} + \frac{dW_{erosion}}{dt} \quad (I.16)$$

The temporal derivative of work done by pressure, P , is expressed by :

$$\frac{dW_{pressure}}{dt} = - \oint_S P (\vec{U}\vec{n}) dS \quad (I.17)$$

Substituting the Equation (I.15) and (I.17) to (I.16) lead to:

$$\frac{dW_{intrafluid}}{dt} + \frac{dW_{erosion}}{dt} = \oint_S \left(\frac{w^2}{2} + \vec{g}\vec{z} + \frac{P}{\rho} \right) \rho (\vec{U}\vec{n}) dS \quad (I.18)$$

The flow conservation with a same specimen section on the whole length leads to assume the same average velocity in the upstream section A and downstream section B. The Equation II.18 becomes:

$$\frac{dW_{Intrafluid}}{dt} + \frac{dW_{erosion}}{dt} = \oint_S \left(\vec{g}\vec{z} + \frac{P}{\rho} \right) \rho(\vec{U}\vec{n})dS = \rho g \Delta z Q + Q \Delta P \quad (I.19)$$

Where $\Delta P = P_A - P_B$; $\Delta z = Z_A - Z_B$; Q is the fluid flow rate.

In the case of the suffusion process, due to relatively low value of the Reynolds number, it is assumed that the energy dissipation by viscosity is mainly transformed into erosion and the erosion dissipation representing the transfer of energy from the fluid phase to the solid one is neglected (Sibille et al. 2014). In consequence, the temporal derivative of mechanical work through erosion called as “erosion power” can be expressed by:

$$\frac{dW_{erosion}}{dt} = \rho g \Delta z Q + Q \Delta P \quad (I.20)$$

With $\Delta z > 0$ if the flow is in downward direction, $\Delta z < 0$ if the flow is upward and the temporal derivative of erosion work is equal to $Q \Delta P$ if the flow is horizontal.

The energy dissipation is the temporal integration of the instantaneous erosion power for the test duration.

1.5 Soils susceptibility

1.5.1 Erodimeter for soil susceptibility testing

To obtain better understanding of the mechanisms of initiation and progression of erosion, experimental studies have been carried out by scientists and engineers in the hydraulic and geotechnical fields. The aim of these studies was to provide the tools to evaluate the soil susceptibility, to understand the mechanism of the onset and the development of erosion that occurs in hydraulic structures subjected to seepage flow and thus complete the necessary data. To assess the susceptibility of soils to internal erosion, over the years, a number of different laboratory methods have been developed such as permeameter erodimeter, modified triaxial erodimeter, among others.

In the literature, several researchers have designed specific devices to investigate the onset and development of suffusion for instance: Kenney and Lau (1985), Lafleur et al. (1989), Skempton and Brogan (1994), Sterpi et al. (2003), Moffat and Fannin (2006), Wan and Fell (2008), Sail et al. (2011), Ke and Takashi (2012), and Marot et al. (2012). However, some researchers who designed modified triaxial erodimeter are Bendahmane et al. (2008), Chang and Zhang (2011), and Luo et al. (2013).

Kenney and Lau (1985)

Following the basic experimental approach used by U.S Army Corps of Engineers, Kenney and Lau (1985) carried out filtration tests on cohesionless soils subjected to downward seepage flow and vibration to erode the soils. Using permeameter cells having dimension: 245 mm in diameter and 450 mm high; and 580 mm in diameter and 860 mm high, coarse particles were chosen as drainage layers for base soils that were placed at the bottom of cells (see Figure I.15). The seepage water supplied by upper reservoir flowed through the specimen, depositing particles in the sedimentation tank, and was returned by pump to the

upper reservoir. In order to move loose particles towards the bottom of the samples, the specimens were vibrated lightly by manually tapping the horizontal beams that spanned the sedimentation tank with a rubber hammer.

Lafleur et al. (1989)

To get a better understanding of the behavior of filtration and the likelihood of the onset of suffusion in cohesionless soil, Lafleur et al. (1989) conducted tests on an artificial material (spherical glass beads) that had three different grain size distribution curves: linear, broadly-graded and gap-graded. The tests are performed with a cylindrical permeameter cell subjected to a downward direction flow by imposing hydraulic gradients between 2.5 and 6.5 m / m (see Figure I.16). An array of piezometer tubes was installed to monitor pore water pressure. During these tests, the mass loss was screened by metal wire mesh that was placed at the bottom of the test soils.

Skempton and Brogan (1994)

Skempton and Brogan (1994) carried out infiltration tests using highly unstable sandy gravel soils that were subjected to upward seepage flow in a rigid cell 139 mm in diameter and about 155 mm in length as shown in the Figure I.17. The objective was to determine a critical hydraulic gradient corresponding to the onset of suffusion and to validate the test by Kenney and Lau (1985). After being thoroughly mixed and moistened, the soil was placed into the cell in four layers each about 40 mm thick and then tipped in and packed by hand. To ensure uniform flow across the area of sample, gravel and coarse sand layer was placed at the bottom of soil. Small head flow was induced until reaching the top edge of cell to saturate the test soil and over flow was captured by the lower basin allowing to measure the discharge. Hydraulic gradients were imposed by upward vertical flow and increased until failure of the sample.

Sterpi (2003)

Sterpi (2003) carried out suffusion test under upward hydraulic loading. The 7 cm in diameter and 14 cm high samples of well graded silt-sand-gravel soils were reconstituted by the moist tamping procedure of Ladd (1978) into a membrane held by a vacuum in a cylindrical mold. The test soils were then subjected to the upward seepage flow by hydraulic head difference between the upper reservoir and the overflow valve as illustrated in the Figure I.18. In order to control and monitor direct evaluation of the hydraulic gradient, a manometer is connected to the base of the sample. A porous stone was placed at the base of specimen to ensure a uniform flow. A collecting system comprised wire mesh #200 and containers in which the wire mesh is to separate the fine particles from coarser grains possibly eroded from the soil primary fabric and the container is to collect water outflow. The container was removed and replaced at constant time intervals to capture the quantity of water. This enables one to evaluate the changes of the soil hydraulic conductivity during the test. The weight of the eroded particles is also measured, after sedimentation and oven drying.

Moffat & Fannin (2006)

Conducting suffusion tests, Moffat & Fannin (2006) used a device as shown in the Figure I.19 to test cohesionless granular soil subjected to downward hydraulic loading. The device comprises permeameter cell, axial loading system, hydraulic control system, collecting system, and data acquisition system. The test specimen having dimension of 279 mm in diameter and about 450 mm in length was placed in the transparent rigid-wall permeameter to observe the specimen during the test. Downward seepage flow is introduced and controlled through an inlet port on top plate that is supplied by tap water and reservoir of 270 L capacity.

The collecting system to capture the outflow is placed in the base plate. The axial loading is applied to the test specimen by piston through rod and loading plate and measured using load cell. To monitor the local hydraulic gradients changes within the specimen due to seepage flow, a series of transducers was used. In order to monitor axial displacement, a Linear Variable Differential Transducer (LVDT) was also used.

Wan and Fell (2008)

A schematic diagram of the laboratory tests carried out by Wan and Fell (2008) is shown in the Figure I.20. The device comprises a cylindrical cell of 300-mm internal diameter containing the tested soil, hydraulic control system to supply seepage flow, collecting system to capture loss particles and flow rate, piezometers to monitor water pore pressure, and data acquisition system provided by transducers and a computer. The tested soil 300-mm thick was placed in between top filter layer of 25 mm single-sized aggregates and bottom filter layer of 20 mm single-sized aggregates. The soil was subjected to downward direction flow supplied from a constant head tank located 2.5 m above the seepage cell. The seepage cell was placed inside a transparent overflow tank to maintain a constant water head at the downstream side of the apparatus. A seepage gradient, $i \approx 8$ was maintained across the tested soil. Water pore pressure were measured by piezometers embedded at different depths of the soil sample and recorded by transducers, electronic data logger, and a computer. Overflow was collected in bottom tank to facilitate measurement of flow rate.

Bendahmane et al. (2008)

Bendahmane et al. (2008) performed suffusion tests on clay-sand soils using a modified triaxial testing apparatus (Figure I.21). Using single-layer semistatic compaction, a soil specimen of 50 mm both in diameter and in height was wrapped with flexible membrane and was placed in the pedestal base of the triaxial. To avoid leakage between the soil and the membrane, 20 kPa confining pressure was injected to the cell. Saturation of the soil specimen then continued by injecting carbon dioxide and deaerated water from the bottom side. Afterward, to consolidate the specimen, increased confining pressures were applied to the specimen until stabilization was reached. The specimen was subjected to downflow seepage water. Three controlling parameters (hydraulic gradient, kaolinite percentage, and confining pressure) were used to characterize the onset and the development of suffusion. In order to measure the clay erosion, an optical sensor was installed in the drainage tube underneath the funnel shaped outlet. The outflow and eroded mass were measured using balance.

Chang and Zhang (2011)

Chang and Zhang (2011) conducted suffusion test on gap-graded sand-gravel soils subjected to downward seepage. The apparatus as shown in the Figure I.22 is composed of a triaxial system, a pressurized water supply system, soil collection system, and water collection system. The soil specimen 100 mm both in diameter and height was wrapped by flexible membranes. The computer-controlled triaxial testing apparatus was modified to allow the control of hydraulic gradient and stress state. During the erosion process, to measure the soil specimen deformation owing to vertical load, LVDT and digital camera were used. Three transparent water tanks 200 mm in diameter and 400 mm in height were used to provide sufficient water as inflow into soil specimen. For the collecting system, a transparent funnel-shaped tube, eroded mass containers, and water containers. To separate eroded mass and outflow, T-fitting was used by putting steel wire mesh 0.064 mm in the inlet of drainage tube of outflow. The eroded mass captured in the container was then dried and measured while the outflow was measured by a balance to measure the flow rate.

Sail et al. (2011)

Sail et al. (2011) carried out suffusion tests on cohesionless soils to characterize the onset and development of suffusion. The apparatus used comprised oedo-permeameter cell, collecting system, axial loading system, hydraulic control system, and data acquisition system (see Figure I.23). The transparent rigid wall cell of 280-mm in internal diameter and 600-mm high was equipped with fourteen pressure ports to monitor water pore pressure across the soil specimen. The tested soil was supported by 15 mm thick mesh screen that has a 10 mm pore opening size in order to allow the migration of all grains. Mass loss was migrated through the cell base and captured by the collecting system. The cell base has a vertical funnel-shaped draining system, specially designed to avoid clogging, while the collecting system is composed of an effluent tank which has an overflow outlet with a 0.08 mm mesh in order to catch the extracted fine particles. Effluent tank is equipped with a rotating sampling system containing several beakers for the effluent sampling. The axial load was applied through the piston mounted on the top of the cell and the piston displacement was measured by a LVDT and data acquisition recorded by a computer. Hydraulic control system is composed of two reservoirs of 1500 L capacity and a pump. A 200 L tank equipped with an air pressure controller supplied the water for seepage flow induced to the specimen. The water head applied on the specimen top face is measured by a pressure transducer connected to the pressure port on the piston base. The seepage flow is measured with two electromagnetic flowmeters (of different capacities 120 L/min and 480 L/min) located between the pressure tank and the oedo-permeameter cell.

Ke & Takashi (2012)

Ke & Takashi (2012) conducted a series of one-dimensional upward seepage tests using sand-gravel soils subjected to constant water head. Three controlling parameters were used to investigate their effect to suffusion: (i) the percentage of finer fraction, (ii) the relative density of the soils, and (iii) the maximum hydraulic gradient. The tested soils were placed in the transparent cell having dimension of 100 mm in internal diameter and 300 mm in height to permit the observation of migration of soils (Figure I.24). For hydraulic control system, the water head in downstream side was control by constant head tank which can be raised or lowered to provide hydraulic gradient across the specimen. To capture the overflow, the top of the cell was equipped with a pipe connected to a cylinder container. The evolution of water pore pressures across the soil specimen due to imposed hydraulic gradient were measured with four piezometers embedded in four different layers.

Marot et al. (2012)

Marot et al. (2012) carried out suffusion test using centrifuge machine. The tested specimen was a broadly-graded clayey sand having dimension 73 mm in diameter and 60 – 120 mm in height. The device used comprises a rigid wall cylinder cell, a hydraulic control system, and effluent sampling system. The whole device was placed in the IFSTTAR centrifuge swinging basket to reproduce full-scale stress state as shown in the Figure I.25. A downward seepage flow supplied by a 245 mm tank is imposed to the small scale model under a constant hydraulic head. To ensure uniform flow across the soil specimen, a glass bead layer was placed in the top of the specimen. For the collecting system, the bottom of the funnel-shaped draining system was equipped to permit the transport of eroded particles. A wire mesh 0.1 mm pore opening size was placed under the specimen to allow only the migration of fine particles. The cell outlet was connected with an effluent sampling system by a drainage pipe and needle valve. The opening of upstream and downstream valves was achieved in flight when the selected centrifuge acceleration is reached. A rotating effluent system composing of

several beakers was developed to catch the effluent during the test duration and it is controlled remotely from the centrifuge operator's room through a camera.

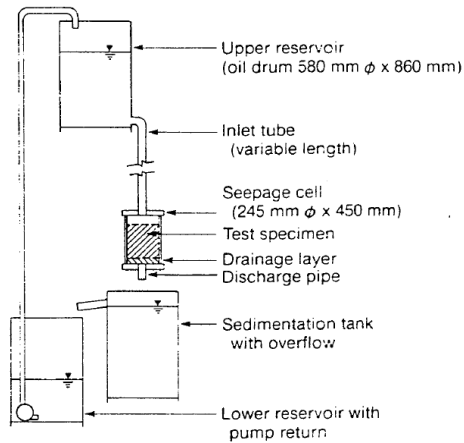


Fig. 2. Test arrangement using 245 mm diameter seepage

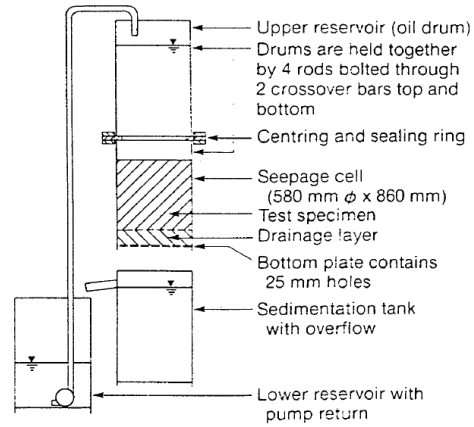


Fig. 3. Test arrangement using 580 mm diameter seepage

(a) (b)
Figure I.15 Test arrangement of seepage test using permeameter cell
(a) 245 mm, (b) 580 mm (Kenney and Lau, 1985)

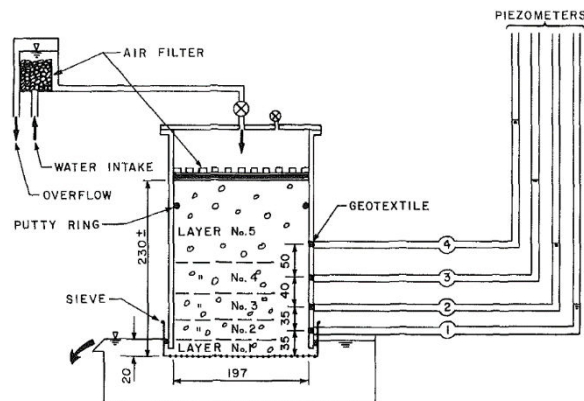


Figure I.16 Permeameter for screen tests (Lafleur, 1989)

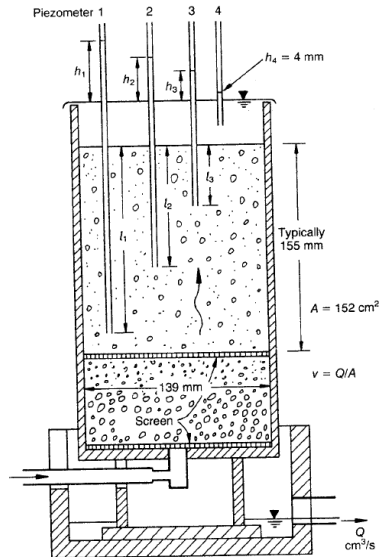


Figure I.17 Apparatus of seepage test (Skempton and Brogan, 1994)

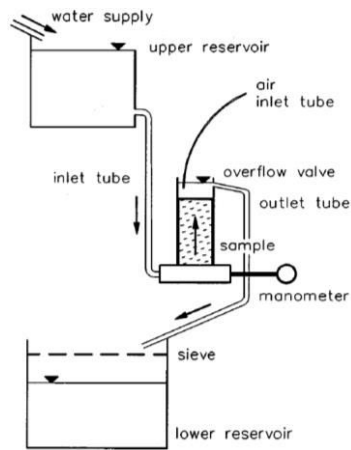


Figure I.18 Experimental setup for seepage test (Sterpi, 2003)

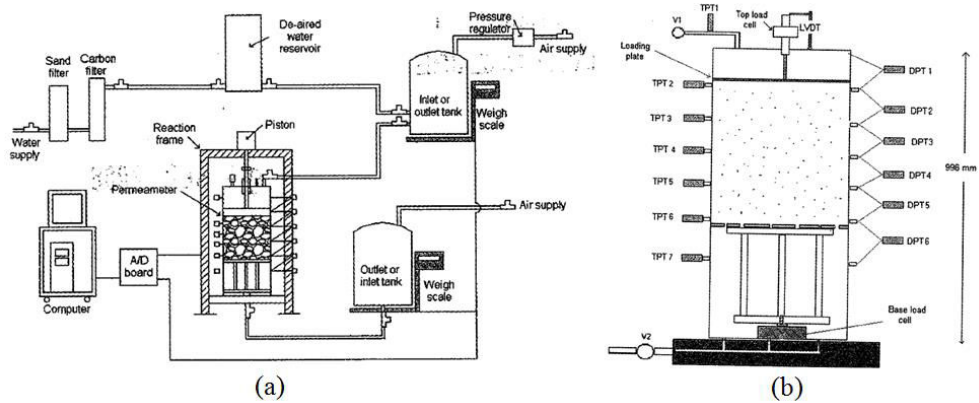


Figure I.19 Permeameter apparatus (Moffat and Fannin, 2006)
 (a) component of the large permeameter, (b) arrangement of the instrumentation

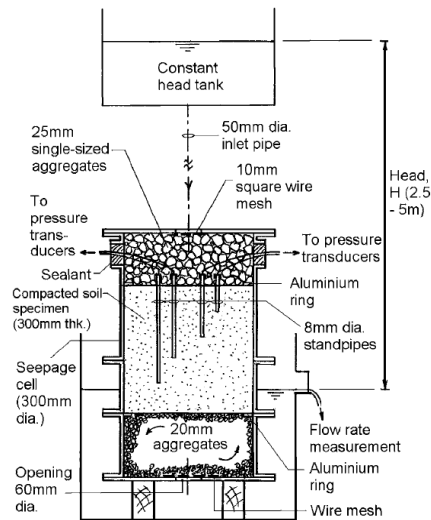


Figure I.20 Schematic diagram of downflow seepage test apparatus (Wan and Fell, 2008)

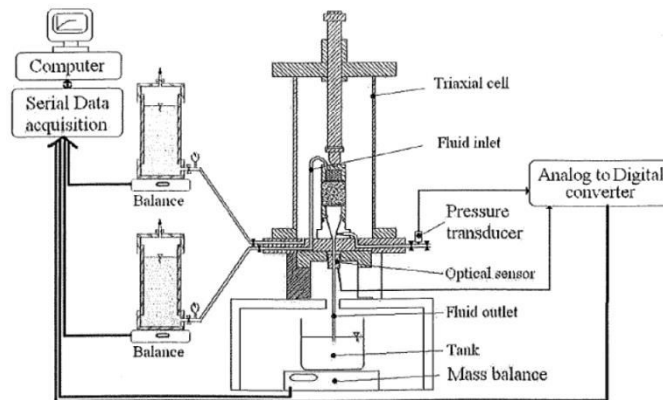


Figure I.21 Schematic representation of experimental triaxial cell (Bendahmane et al., 2008)

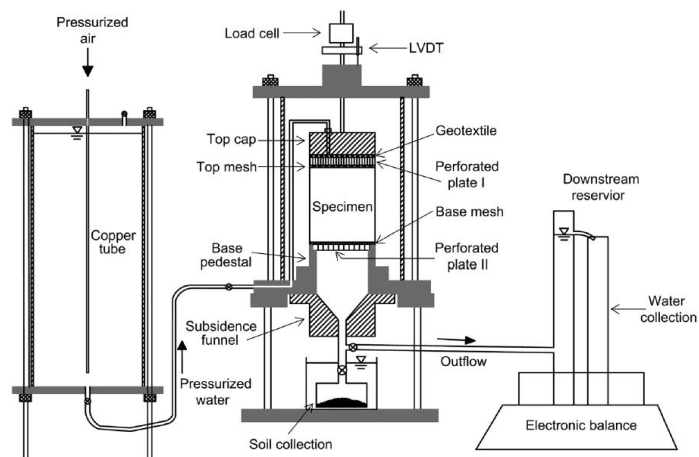


Figure I.22 Schematic of testing apparatus (Chang and Zhang, 2011)

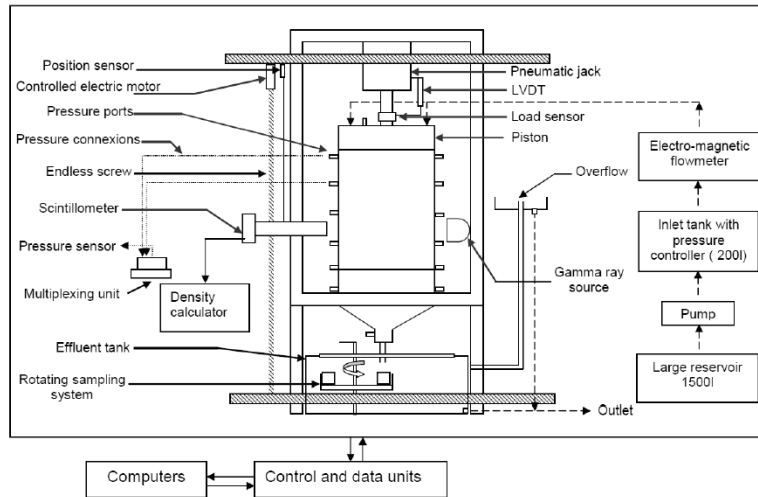


Figure I.23 The apparatus of oedo-permeameter (Sail et al., 2012)

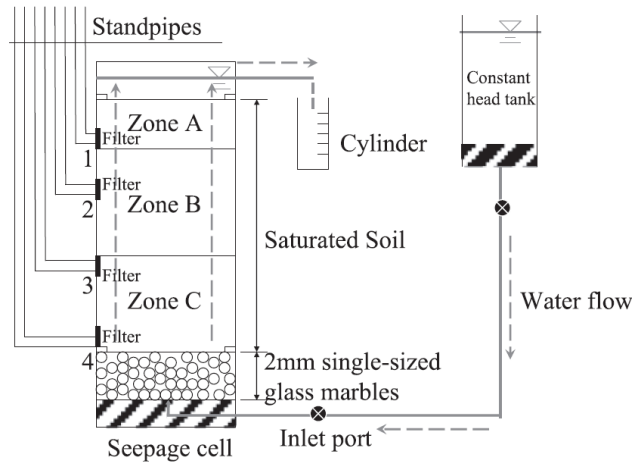


Figure I.24 Schematic diagram of seepage test assembly (Ke and Takahashi, 2012)

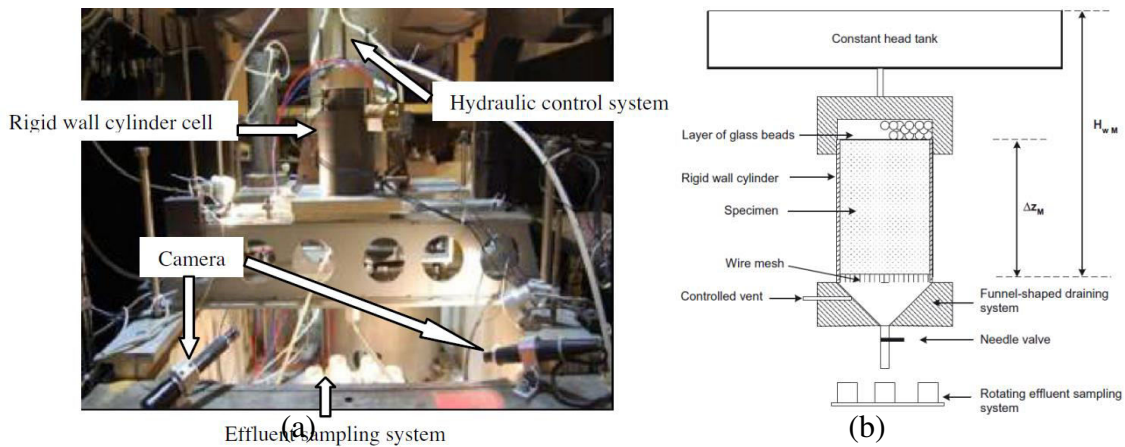


Figure I.25 Seepage test apparatus (Marot et al. 2012): (a) General view of the IFSTAR centrifuge bench, (b) schematic diagram of downward seepage flow test apparatus

1.5.2 Interpretation of soil erodibility

Erosion rate

Erodibility represents the erosion resistance of a soil subjected to water flow (a high erodibility corresponds to a low resistance). The action of the water on the soil can be evaluated through the shear stress induced by the water on the soil at the water-soil interface. Hanson (1989) and Wan and Fell (2004) proposed, the cases of hole erosion or piping erosion, the expression (Equation II.21) to describe soil erosion using shear stress term called erosion function.

$$\dot{m} = k_d(\tau - \tau_c) \quad (\text{I.21})$$

Where \dot{m} is the soil erosion rate; k_d is the erodibility coefficient; τ is the hydraulic shear stress at the soil-water interface; and τ_c is the critical hydraulic shear stress at initiation of erosion.

From the equation, soil erodibility can be described by two parameters: critical erosive shear stress and erodibility coefficient. Critical erosive shear stress corresponds to the initiation of erosion, which means a soil erodes when the shear stress exerted by the flowing water exceeds the critical erosive shear stress. Erodibility coefficient indicates the amount of soils eroded at a time interval under a given shear stress. The critical erosive shear stress reflects the ease of initiation of erosion in the soil, while the erodibility coefficient represents how fast the soil erodes.

The value of erosion rate per unit of surface area much depends on the definition of surface area. Considering the surface of pores is more representative than surface of the cross section of the sample for suffusion process, the erosion rate of soils per unit of pore area (\dot{m}) defined by Reddi et al. (2000) as presented in Equation (II.22) – (II.26) was used (pore are presented by a series of capillaries tubes).

$$\dot{m}(t) = \frac{m(t)}{N_p S_p t} \quad (\text{I.22})$$

where m is eroded dry mass, N_p the average number of pore, S_p the average pore area, and t the duration.

$$N_p = \frac{S n}{\pi r_p^2} \quad (\text{I.23})$$

$$S_p = 2 \pi r_p L \quad (\text{I.24})$$

where S is the cross section of the specimen, r_p the average radius of pores, L length of the specimen.

$$r_p = \sqrt{\frac{8K}{n}} \quad (\text{I.25})$$

$$K = k \frac{\mu}{\gamma_w} \quad (\text{I.26})$$

where K is the intrinsic permeability.

1.5.3 Recent soil susceptibility classification for interface erosion

According to Wan and Fell (2004), the susceptibility of a soil can be described in two aspects: (i) the rate of erosion when a given hydraulic shear stress is applied to the soil, and (ii) the ease of initiating erosion in the soil.

Instead of just classifying soils in internally stable or unstable soils according to some criteria, several researchers, Hanson and Simon (2001), Wan & Fell (2004), Briaud (2005), and Marot (2011) presented classifications of erosion susceptibility, but such classifications are related to interface erosion processes, and up to now, there is no classification for suffusion susceptibility.

Hanson and Simon (2001) proposed the classification of soil susceptibility to erosion, shown in Figure I.26, based on the values of erosion coefficient k_d and hydraulic shear stress τ_c measured using the JET (Jet Erosion Test). The classification is divided into five classes from highly resistant to highly erodible. Using Hole Erosion Test (HET), Wan & Fell (2004) proposed an expression of erosion index (I_{HET}) ranging from 1 to 6 as shown in the Table I.1. I_{HET} is a function of C_e where C_e is coefficient of soil erosion corresponding to ratio of erosion rate per unit surface area of the slot or hole at time to hydraulic shear stress along the hole at time.

$$I_{HET} = -\log(C_e) \quad (I.27)$$

Briaud (2005) has classified erodibility of soil into 6 groups from non-erosive to very high erodibility, based on ratio between erosion rate and hydraulic shear stress, and ratio between erosion rate and water velocity as shown in

Figure I.27. Marot et al. (2011) proposed an equation of erosion resistance index, I_α for surface erosion as follows and ranged soils from highly resistant to highly erodible (see Table I.2).

$$I_\alpha = -\log_{10}(\alpha) = -\log_{10}\left(\frac{\text{dry eroded mass}}{\text{total dissipated flow energy}}\right) \quad (I.28)$$

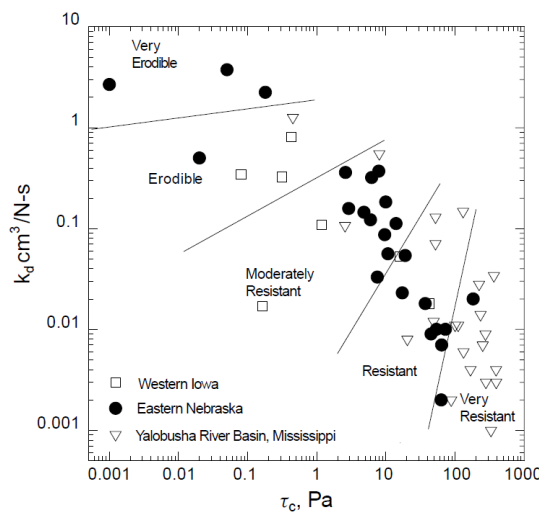


Figure I.26 Classification of interface erosion measured by JET proposed by Hanson and Simon (2001)

Table I.1 Erosion rate index, I_{HET} (Wan and Fell, 2004)

Index of erosion rate, I_{HET}	Description of erosion rate	Ranking of erosion
< 2	Very highly fast	1
2 - 3	Very fast	2
3 - 4	Moderately fast	3
4 - 5	Moderately slow	4
5 - 6	Slow	5
> 6	Very slow	6

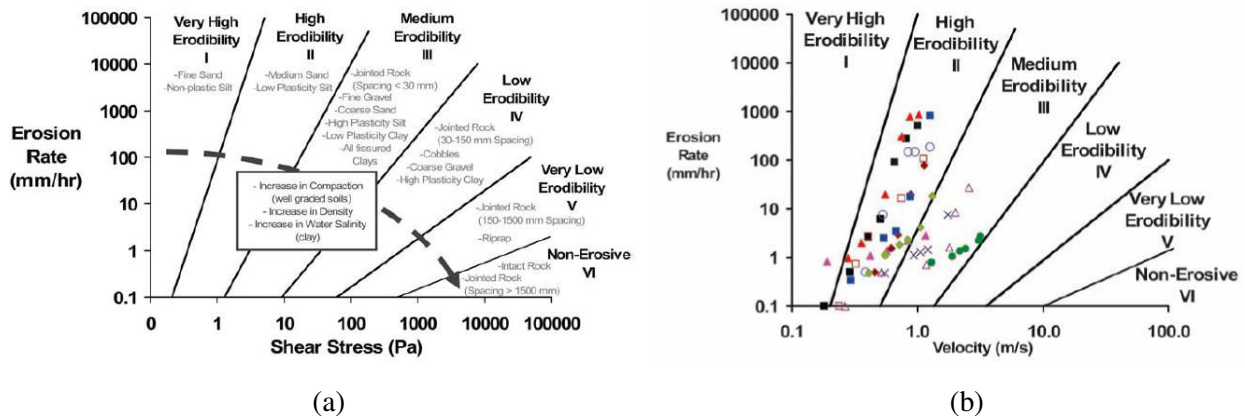


Figure I.27 Classification of soil erodibility by Briaud (2005)
a) erosion rate and hydraulic shear stress, b) erosion rate and water velocity

Table I.2 Erosion resistance index, I_{α} (Marot et al., 2011)

Index of erosion resistance, I_{α}	Description of erosion rate	Ranking of erosion
$I_{\alpha} < 1$	Highly erodible	1
$1 \leq I_{\alpha} < 2$	Erodible	2
$2 \leq I_{\alpha} < 3$	Moderately erodible	3
$3 \leq I_{\alpha} < 4$	Moderately resistant	4
$4 \leq I_{\alpha} < 5$	Resistant	5
$I_{\alpha} \geq 5$	Highly resistant	6

1.6 Mechanical response of soils to suffusion

Mechanical response of homogeneous soil samples

Within the complicated and iterative process of suffusion, the migration of fine particles through the voids between the larger particles by seepage flow, leaving behind the granular materials, can induce changes in the mechanical behavior of soils. This loss mass of fine particles can change porosity and induce a significant decreases the shear strength of the soils. Loss of fine fractions locally may also deform the crest of the dike or even the whole structures.

Horikoshi et al. (2011) Ke and Takashi (2012) from a series of tests of suffusion aim to investigate the mechanical consequences of internal erosion on non-cohesive soils. They pointed that the migration of fine particle can induce the reduction of soil shear strength. One of the approaches to assess the vulnerability of a soil to suffusion is by comparing particle grain size distribution before and after erosion. As shown in the Figure I.28, there was the indication of loss mass of fine particles that induce the decrease of the soil shear strength. An in-situ testing technique was carried out by Ke and Takahashi (2012) on disturbed samples after erosion using miniature cone penetration test to evaluate the soil shear strength. The cone tip resistance (N) profile as presented in the Figure I.29 can indicated the reduction of soil shear strength.

Scholtes et al. (2011), with the aim to assess the effect of internal erosion on the mechanical properties of granular assembly, followed a multi-scale approach based upon numerical experiments. Two kinds of approach were performed: three-dimensional numerical model based on the discrete element method (DEM) and a micromechanical constitutive relation. It was indicated that the shear strength was strongly modified by the loss mass of soil particles. The study showed that the internal friction angle decreased from 24.2° for intact material to 20.8° for degraded material as shown in the Figure I.30.

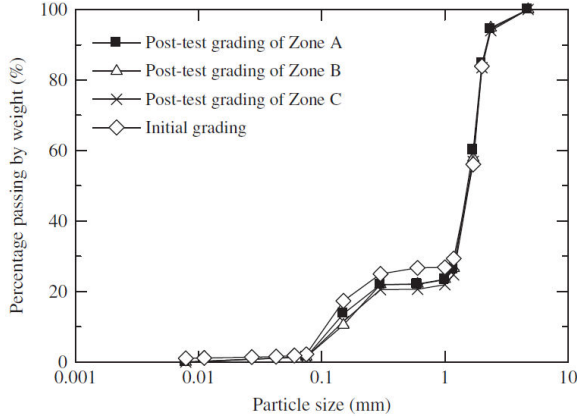


Figure I.28 Grain size distribution curve with depth before and after erosion (Ke and Takahashi, 2012)

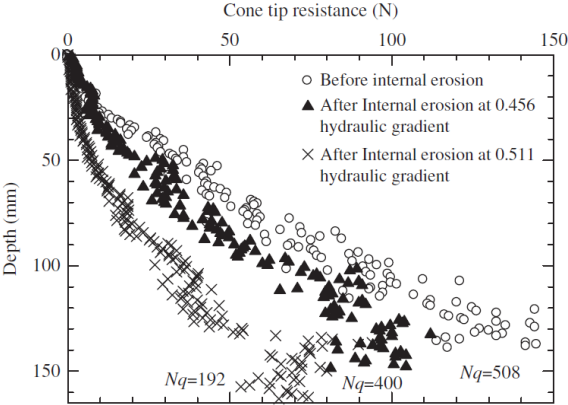


Figure I.29 Cone resistance before and after erosion (Ke and Takahashi, 2012)

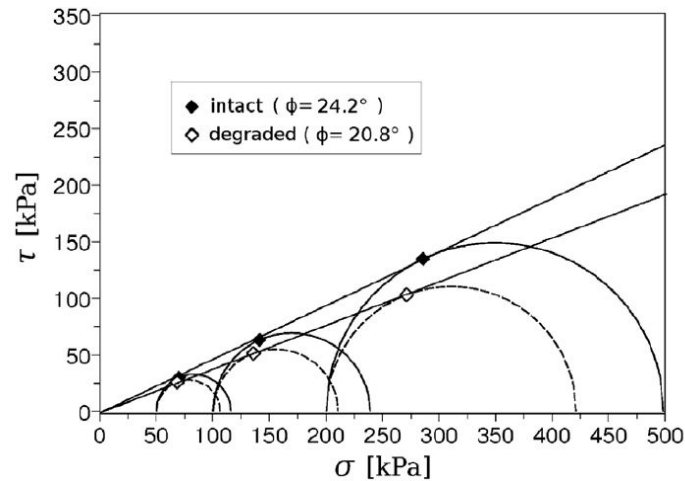


Figure I.30 Mohr-Coulomb failure envelopes before and after erosion with DEM approach (Scholtes et al., 2011)

Response of hydraulic structure based on small scale dike model

In the case of hydraulic structures such as earth dams and levees, the effect of the water seepage on the stability of an earth structure are the following: a) internal soil erosion or piping by removing and transporting soil particles, starting a duct that might increase rapidly, producing a complete failure; b) water pressure increase that will decrease the effective stresses and therefore decrease the shear strength of the soil; c) larger water flow forces due to the increase of hydraulic gradient might significantly decrease the safety factor and produce a slope failure (Berrones and Acosta, 2011). Numerous researchers have carried out experimental and numerical studies on suffusion or internal erosion using small model dike or levee.

Horikoshi et al. (2012). Presenting suffusion process in gap-graded cohesionless soils in a small scale model levee as displayed in Figure I.31, Horikoshi et al. (2012) carried out six different tests with respect to the percentage of fine fraction and hydraulic boundary condition. This study aims to determine the mechanism of suffusion and to examine the effect of this phenomenon on the stability of soil structures. Three different values of fine fractions were used to investigate their effect to the process of suffusion and mechanical behaviour of the soils. All the tests were subjected to either constant flow rate or constant head. The approach of suffusion mechanism was deduced by measuring eroded mass, rate of discharge at toe during elapsed time and spatial fine fraction distribution before and after suffusion tests. The variation of permeability was computed using Dupuit assumption with the visually observed phreatic surface that was captured by photographic images and measured discharge. Given hydraulic boundary conditions, the lower percentage of fine fractions 10% resulted in larger erosion rate than that of 15% in the early time. However after a certain elapsed time the erosion rate for the soil with a fine fraction of 15% drastically increased to become larger than what was observed for 10% of fines. This drastic increase of erosion rate of the soil with a fine fraction of 15% widens the flow channel and the internal erosion rate increases and suffusion is progressively broadened from the toe to middle of the embankment as in the backward erosion. Later Horikoshi and Takahashi (2014) investigated the effects of seepage time and repeated water infiltration in the small scale model of dike using the same apparatus, and the same procedures and measurement. They demonstrated the change in the spatial distribution within the dike as the effect of seepage time and water infiltration. In early stage, the development of temporal suffusion under the constant head may be attributed to the

interaction between the migration of fines eroded from embankment and its deposit into the bottom of the base. The bottom deposit may lead to a decrease in hydraulic conductivity and induces clogging. Within times, suffusion may proceed upstream along the phreatic surface from downwards in embankments. The migration of fine fraction may be associated to not only with seepage flow but also by effects of gravity forces.

Beek et al. (2010). With the objective to study piping erosion, Beek et al. (2010) carried out a test on small scale levee model using centrifugal method which the side view model is shown in the Figure I.32. The approach of hydraulic gradient was used to characterize the internal erosion mechanism. The sand used as foundation is Baskarp sand which is coloured to estimate the length of piping erosion. The seepage length is 0.35 m and the thickness of the sand sample (excluding the foam bed) is 0.10 m. This model represents a one scale prototype with a 5 m high embankment that is 28 m wide at the base lying on an 8 m thick sand layer. The tests were run at a scale factor of 80. To generate the collapse of the levee, the upstream head of the levee was increased until piping occurred. However, this was not possible, due to the length scaling effects in the piping process, the critical gradient increases with decreasing length. For a length of 0.35 m, as used in the experiments, the expected critical head exceeds the height of the clay levee. Thus a screen and a stabilising fill have been added to the set-up to have a possibility to increase water head exceeding the crest of the levee. During the experiment, the upstream head was increased in steps of 0.01 m per 5 minutes until sand boil is observed on the downstream side. The increase of gradient was continued resulting in progressive increase of sand transport in the foundation of the levee. Beek et al. (2010) revealed that the higher g-level, the lower critical gradient as shown in Figure I.33. The highest g-level 80 g resulted in the lowest critical hydraulic gradient. The sand boiling initiation was observed at gradient of 0.14-0.22 and after sand transport progressively increased, the levee collapsed at hydraulic gradient equaling to 0.43.

Tanaka et al. (2014). With the aim to investigate the mechanisms and features of piping, Tanaka et al. (2014) carried out levee model tests using uniform fine sand. To characterize the mechanism of piping erosion, the approach of hydraulic gradient was used. The Finite Element Method FEMFRSD3 for tracing a free surface was used to compute seepage lines and exit gradients on the downstream seepage surface. Three tested models with the differences in downstream slope, the length of the base of levee and relative density were performed. The side view of apparatus is shown in the Figure I.34. The test procedures comprised building the specimen, saturation for one night and seepage test by dewatering downstream side with very small rate. The result showed that when the water head difference between the upstream and downstream side reached a critical value, piping occurs on the downstream slope surface just above the downstream water level (or just on the surface of seepage). Piping occurs entirely on the downstream slope just above seepage line. After a certain elapsed time, piping progressively proceeded upstream to the storage water level that changed the shape of embankment surface and failure occurred after 17 hours. It can be noticed the a steeper downstream slope led to reduce the time until the collapse of the structure.

Acosta et al. (2013). Dewatering in downstream side of submerged slopes of protection levees can generate drawdown condition. Acosta et al. (2013) presented the safety of a protection levee under rapid drawdown conditions studied by numerical modeling based on finite element method by using the PLAXFLOW program. Drawdown phenomenon was modelled as a coupled problem of transient seepage-deformation in a saturated/unsaturated medium. The PLAXFLOW was performed for transient seepage analysis and the PLAXIS

program for deformation, consolidation and stability analyses. In this work, the details of the proposed methodology were also presented. The results demonstrated that the stability of a submerged slope under drawdown conditions (partial or total) was mainly affected by the properties of the material of the levee and the drawdown rate and drawdown ratio. From results of parametric analyses it was observed that the *fully rapid drawdown* condition occurs when the water level of the reservoir descends more quickly than the remaining pore water pressures dissipated within the levee precisely caused by the drawdown, and no necessarily due to a total decrease of the water surface in a given period of time (minutes, hours or days). Finally, from slope stability analyses the safety factor was observed to decrease when the drawdown ratio increased.

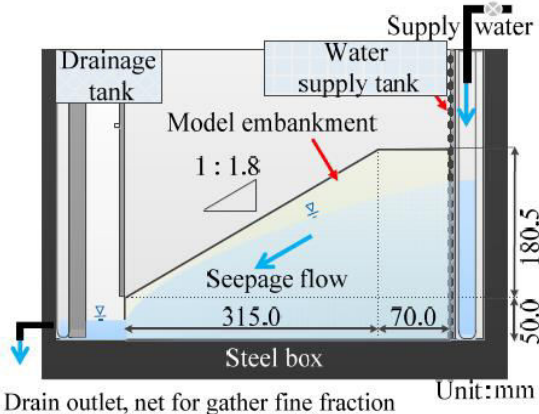


Figure I.31 Side view of experiment developed by Horikoshi et al. (2012)

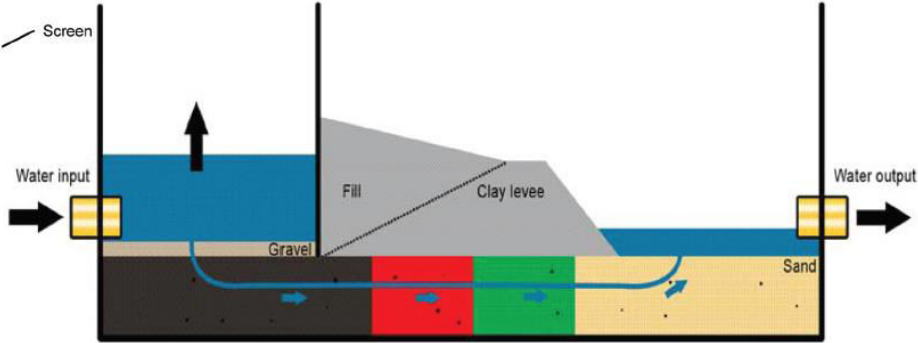


Figure I.32 Cross section of levee experiments developed by Beek et al. (2010)

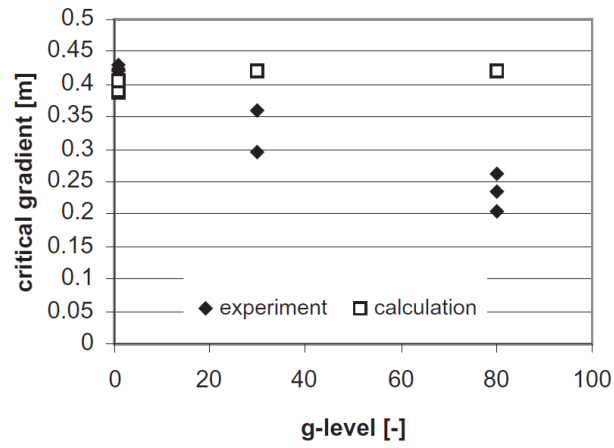


Figure I.33 Relationship between critical gradient and g-level

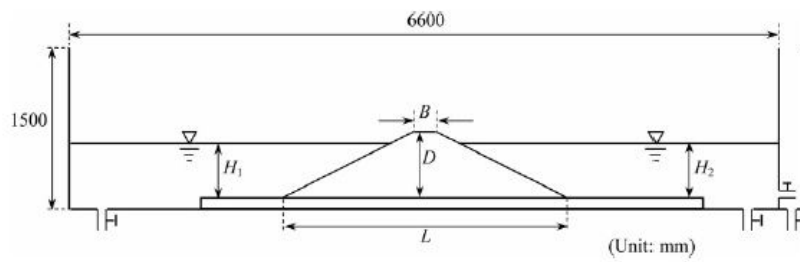


Figure I.34 Side view of test apparatus (Tanaka et al. 2014)

CHAPTER II SUFFUSION SUSCEPTIBILITY

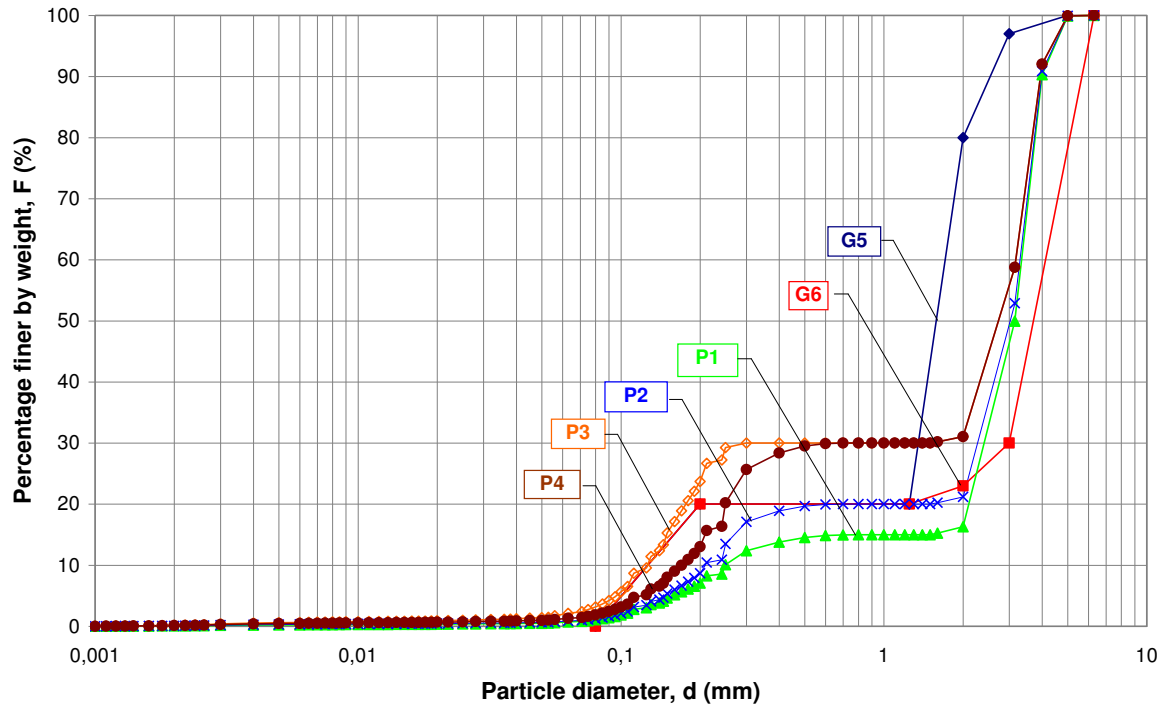
2.1 Introduction

In order to investigate the mechanism of suffusion on cohesionless soils and to provide a classification of suffusion susceptibility, a series of tests is performed using an erodimeter. In a first time the susceptibility classification is carried out by taking into account only the grain size distribution thanks to different existing gradation based-criteria. Later in this chapter the results of suffusion tests are also taken into account for the building of a classification of suffusion susceptibility. It is worth noting that since almost all the gradation distributions used in this study are discontinuous or gap-graded distribution, the recent criteria by Chang and Zhang (2013) that specifically provide the assessment for gap-graded soil, will be of particular interest. To characterize soil response and the action of hydraulic loading, specimens are subjected to a water flow in downward direction. Three kinds of hydraulic loading history on several grain size distributions are used here with the aim to investigate the effect of hydraulic loading history. These hydraulic loadings are multi-stage hydraulic gradients, single-stage hydraulic gradient and controlled injected flow rate.

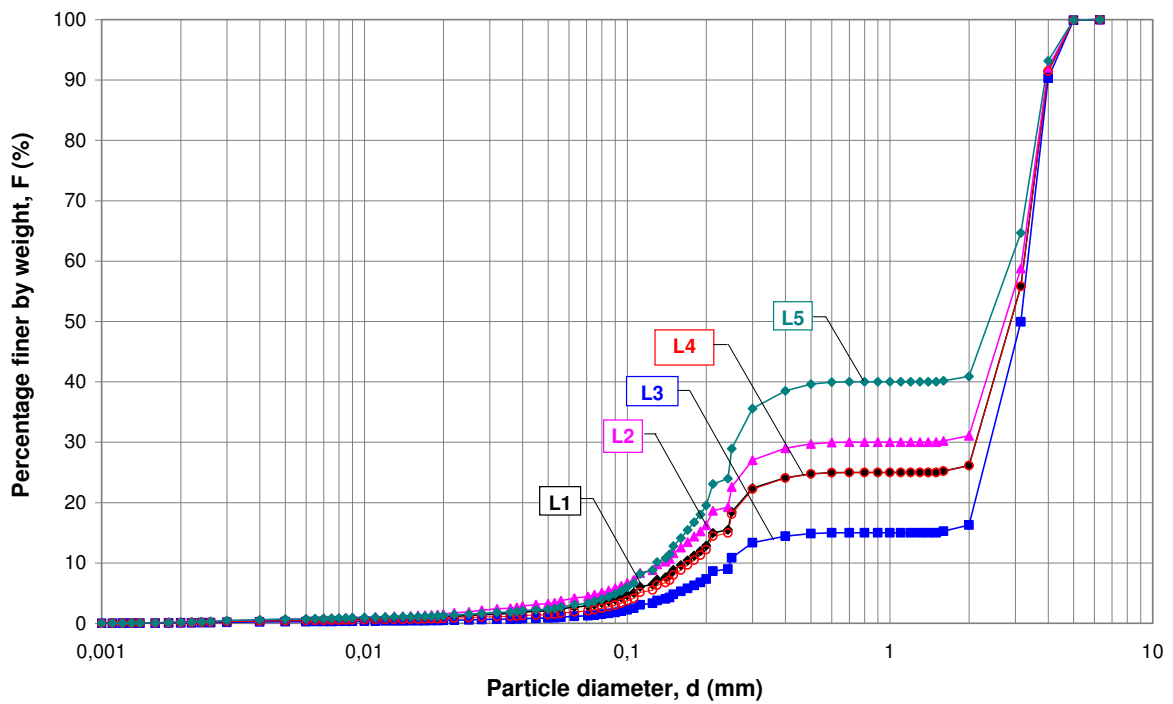
The response of the specimens is investigated through the changing of hydraulic conductivity and erosion rate versus time respectively, and also the changing of erosion rate versus hydraulic shear stress or stream power in order to characterize the suffusion mechanism. As to the present a classification of suffusion susceptibility has not been yet established, the first approach (to classify suffusion susceptibility) using previous methods proposed by several researchers in case of interface erosion to investigate the evolution of erosion rate versus hydraulic shear stress can be conducted. Determination of erosion coefficients k_d and α (where k_d is erosion rate coefficient and α is ratio of cumulative eroded mass to cumulative expanded energy) is also presented. Erosion rate computed here is erosion rate of a soil per unit of pore surface defined by Reddi (2000). To have conformity with erosion rate, the expressions of hydraulic shear stress given by Reddi et al. (2000) are also used. Afterward the energy-based approach proposed by Marot et al. (2011) based on two independent cumulative quantities is used. Finally based on the results, the classification of suffusion susceptibility and the methodology to evaluate the suffusion susceptibility are proposed. This chapter comprises four sections: (i) the description of tested gradation distributions and tested specimens, (ii) the apparatus for downward seepage test and test procedure, (iii) results and discussion and (iv) proposition of suffusion susceptibility classification and methodology.

2.2 Tested gradations

The gradations used in this study can be identified as discontinuous or gap-graded distribution and widely-graded distributions as presented in the Figure II.1 and Figure II.2. Twenty six grain size distributions consisting of silt, sand and gravel soils, and sandy gravel soils are tested. The properties of the given gradations are summarized in Table II.1. As the first study to assess the susceptibility of a soil to suffusion, the grain size distributions can be confronted with several gradation-based criteria. It is worth noting that the gradation-based criteria do not take into account the other important parameters such as grain shape and soil density. The result of the assessment of internal stability is shown in Table II.2. Six latest criteria based on gradation distribution to assess the stability of soils are used in Table II.2.

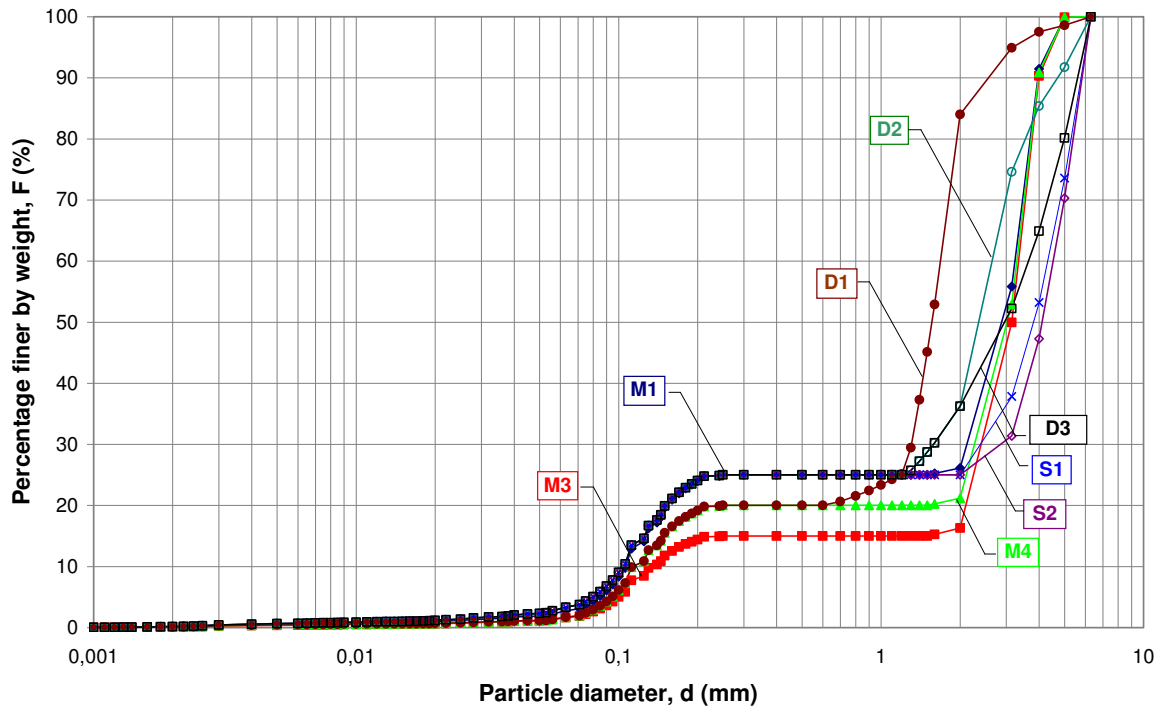


(a)

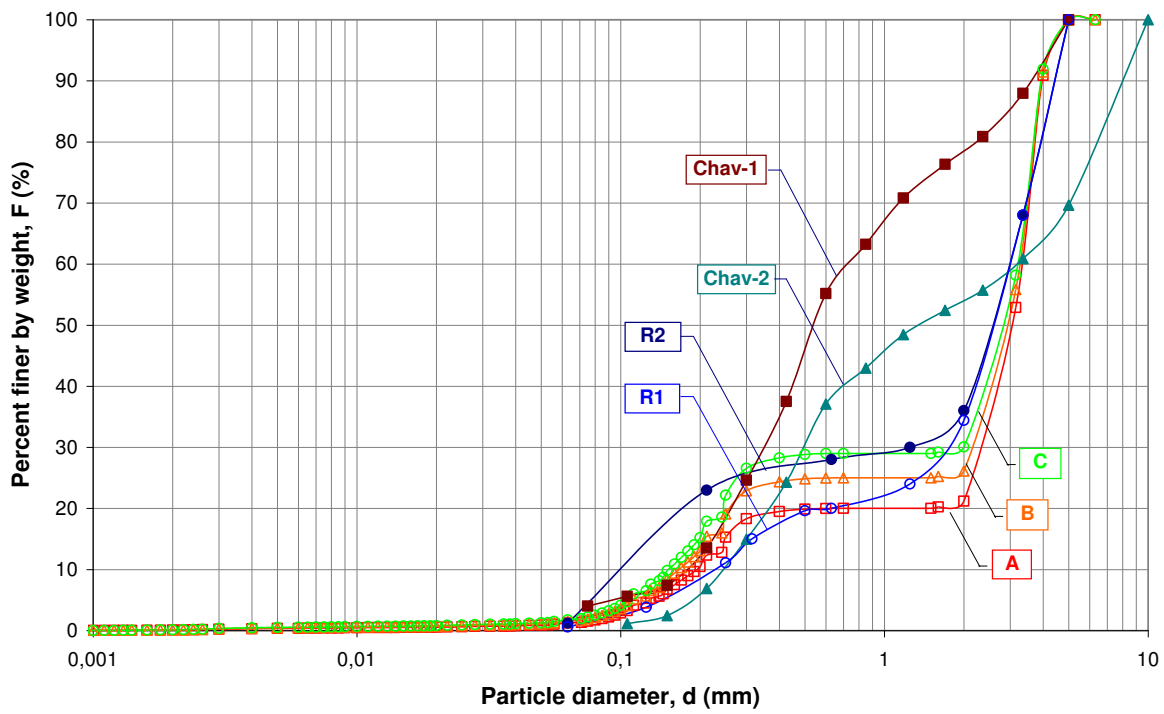


(b)

Figure II.1 Tested grain size distributions
 (a) G5 to P4 (sandy gravel), (b) L1 to L5 (silt-sand-gravel)



(a)



(b)

Figure II.2 Tested grain size distributions
(a) D1 to S2 (silt-sand-gravel) and (b) A to R2 (sandy gravel)

Table II.1 Properties of tested gradations

Tested gradation	Cu	Gr	P (%)	d ₅ (mm)	d ₁₀ (mm)	d ₁₅ (mm)	d ₂₀ (mm)	d ₃₀ (mm)	d ₆₀ (mm)	d ₉₀ (mm)	(H/F) _{min}	d (H/F=min) (mm)	d ₁₅ /d ₈₅
G5	12.50	6.25	0	0.110	0.140	0.170	0.200	1.375	1.750	2.588	0	0.200	7.692
G6	31.53	6.25	0	0.110	0.140	0.170	0.200	3.000	4.414	5.829	0	0.200	17.002
P1	13.47	1.667	0.722	0.157	0.250	0.900	2.127	2.470	3.361	3.993	0.107	0.400	8.245
P2	15.84	1.875	0.877	0.147	0.208	0.271	0.800	2.319	3.309	3.980	0.070	0.400	8.256
P3	25.22	3.75	2.119	0.096	0.126	0.149	0.177	0.400	3.181	3.948	0.0004	0.300	11.546
P4	18.70	1.875	1.316	0.119	0.170	0.209	0.250	0.800	3.181	3.948	0.052	0.500	8.060
L1	19.75	2.143	2.706	0.104	0.164	0.214	0.270	2.150	3.250	3.965	0.047	0.400	8.562
L2	23.49	2.143	4.188	0.078	0.135	0.187	0.244	0.700	3.181	3.948	0.042	0.400	8.627
L3	13.65	2.143	1.153	0.154	0.246	0.700	2.127	2.469	3.362	3.993	0.057	0.400	11.486
L4	18.65	2.143	1.922	0.111	0.174	0.242	0.273	2.150	3.250	3.965	0.049	0.400	8.479
L5	23.24	2.143	3.075	0.091	0.129	0.167	0.202	0.258	3.011	3.906	0.033	0.500	8.319
D1	14.91	2.40	2.698	0.094	0.113	0.148	0.250	1.307	1.692	2.633	0.109	0.212	8.159
D2	26.03	4.80	5.336	0.080	0.104	0.126	0.151	1.584	2.712	4.727	0	0.250	12.409
D3	35.24	4.80	3.336	0.080	0.104	0.126	0.151	1.584	3.671	5.645	0	0.250	12.409
M1	30.53	6.0	2.729	0.084	0.106	0.127	0.153	2.150	3.250	3.965	0	0.250	14.661
M3	25.04	6.0	1.638	0.099	0.134	0.250	2.127	2.469	3.362	3.993	0	0.250	14.661
M4	29.17	6.0	1.698	0.094	0.113	0.148	0.250	2.319	3.309	3.980	0	0.250	14.501
S1	41.60	8.0	3.336	0.080	0.104	0.126	0.151	2.448	4.333	5.807	0	0.250	18.667
S2	43.70	8.0	3.336	0.080	0.104	0.126	0.151	2.901	4.552	5.862	0	0.250	21.160
A	17.06	2.14	1.227	0.128	0.194	0.249	0.700	2.319	3.309	3.980	0.038	0.400	8.761
B	19.52	2.14	1.533	0.111	0.166	0.210	0.262	2.150	3.250	3.965	0.035	0.400	8.741
C	21.07	2.14	1.779	0.107	0.152	0.198	0.245	1.969	3.196	3.952	0.033	0.400	8.724
Chav-1	4.25	WG	4.026	0.094	0.176	0.224	0.263	0.352	0.750	3.629	0.406	1.180	3.159
Chav-2	12.92	WG	0	0.186	0.246	0.301	0.368	0.503	3.178	8.354	0.383	1.180	2.109
R1	13.11	WG	0.590	0.145	0.231	0.315	0.630	1.683	3.029	4.483	0.601	0.315	5.483
R2	24.46	WG	1.200	0.094	0.123	0.157	0.263	1.250	3.013	4.484	0.165	0.212	9.653

Among all the grain size distributions only gradation distribution *Chav* and *R* are considered as widely-graded soils (see Figure II.2). According to Lafleur (1979) a soil having discontinuous or gap-graded distribution is internally unstable. The considered gradation criteria (except Wan and Fell's criterion) indicate all identically an unstable (or suffusive) behaviour for ten gap-graded soils (*G5*, *G6*, *P3*, *D2*, *D3*, *M1*, *M3*, *M4*, *S1* and *S2*). In case of gap-graded soils three criteria, Kezdi, and Kenney and Lau, seem to be the most conservative since they qualify these gradations as unstable. In case of widely-graded soils, gradation distribution *Chav-1* and *Chav-2* are identical for all the criteria (except Kenny and Lau criterion). Finally, the classification of the rest of the gradation distributions seems to depend on the used criterion.

2.3 Downward seepage test

2.3.1 Erodimeter

A specific testing apparatus as shown in Figure II.3 is used to characterize the susceptibility of soils. It comprises an erosion cell, a water supply system, a soil collection system, and a water collection system. The testing device comprises a modified cell to saturate the sample in upward direction (Figure II.4), and to force fluid through the sample in downward direction during the erosion phase. An upstream water tank 2 as a supply of demineralized water is provided at the inlet of the soil specimen during the erosion phase. The funnel-shaped draining system is connected to the effluent tank by a glass pipe (Figure II.5). The effluent tank is equipped with an overflow outlet (Figure II.6) in order to control the downstream hydraulic head and a rotating sampling system containing 8 beakers for the sampling of eroded particles. Overflow water is continuously weighed by mass balance in order to determine injected flow rate (Figure II.6).

Table II.2 Assessment of soil internal stability by recent criteria

Tested gradation	Assessment method				
	Kezdi (1979)	Kenney and Lau (1985)	Li and Fannin (2008)	Wan and Fell (2008)	Chang and Zhang (2013)
G5	unstable	unstable	unstable	stable	unstable
G6	unstable	unstable	unstable	stable	unstable
P1	unstable	unstable	stable	unstable	stable
P2	unstable	unstable	stable	transition	stable
P3	unstable	unstable	unstable	stable	unstable
P4	unstable	unstable	stable	stable	stable
L1	unstable	unstable	stable	stable	stable
L2	unstable	unstable	stable	stable	stable
L3	unstable	unstable	stable	unstable	stable
L4	unstable	unstable	stable	stable	stable
L5	unstable	unstable	stable	stable	stable
D1	unstable	unstable	stable	stable	stable
D2	unstable	unstable	unstable	stable	unstable
D3	unstable	unstable	unstable	stable	unstable
M1	unstable	unstable	unstable	stable	unstable
M3	unstable	unstable	unstable	unstable	unstable
M4	unstable	unstable	unstable	stable	unstable
S1	unstable	unstable	unstable	stable	unstable
S2	unstable	unstable	unstable	stable	unstable
A	unstable	unstable	unstable	unstable	stable
B	unstable	unstable	unstable	stable	stable
C	unstable	unstable	unstable	stable	stable
Chav-1	stable	unstable	stable	stable	stable
Chav-2	stable	unstable	stable	stable	stable
R1	unstable	unstable	unstable	stable	stable
R2	unstable	unstable	unstable	stable	stable

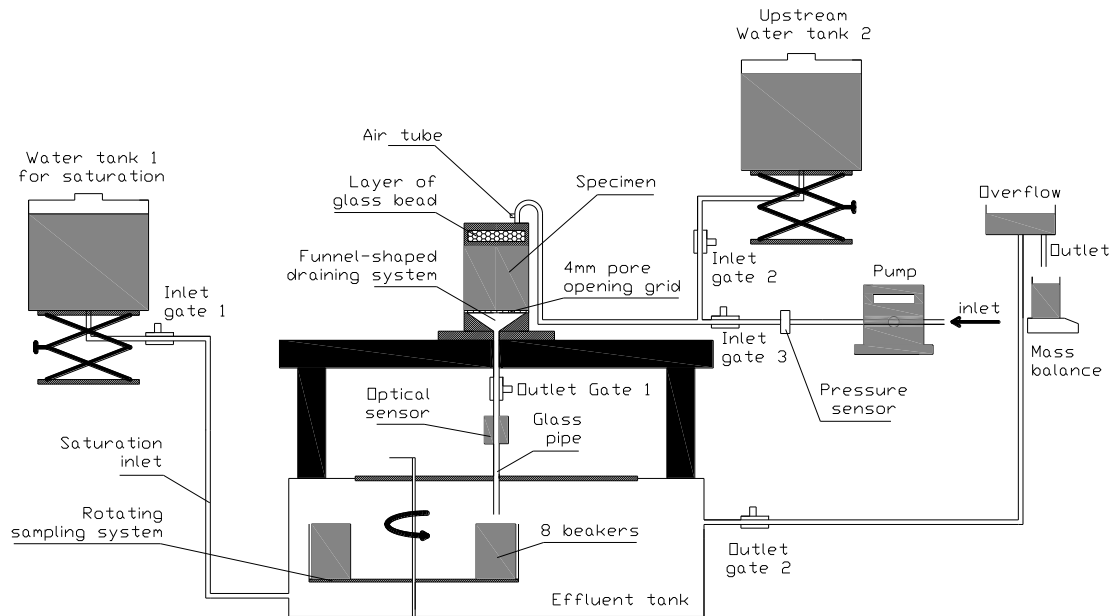
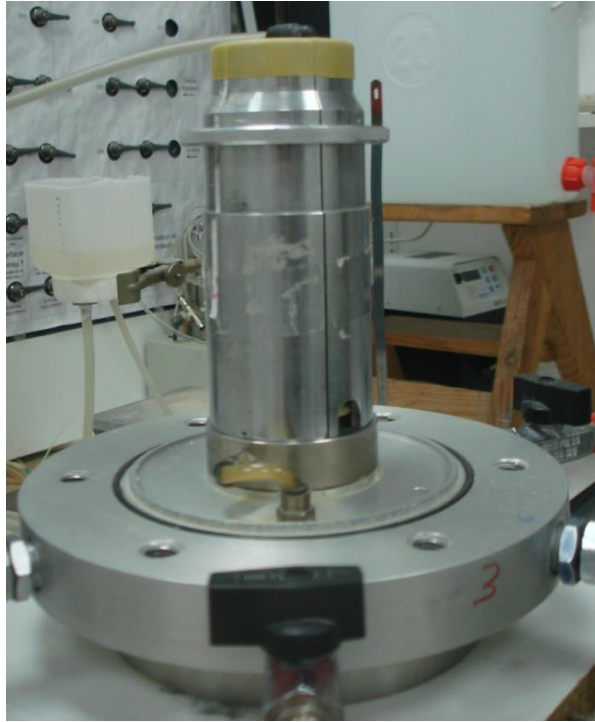
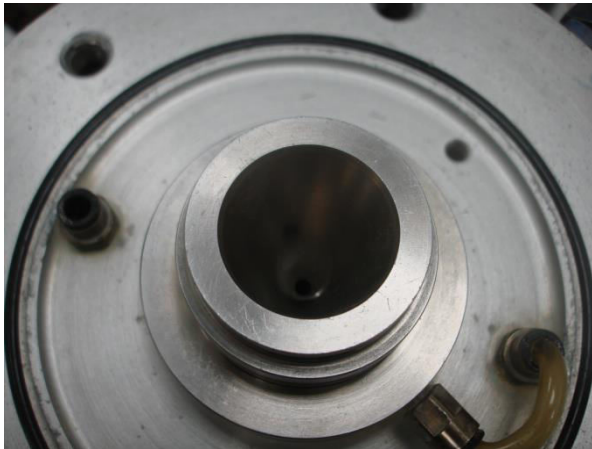


Figure II.3 Schematic diagram of the erodimeter



(a)



(b)

***Figure II.4 Modified erosion cell: (a) metal mold keeping the specimen standing
(b) Funnel-shaped draining system and 4 mm pore opening grid***



(a)



(b)

**Figure II.5 Soil collecting system: (a) effluent tank and rotating sampling system
(b) beakers to catch eroded mass**



(a)



(b)

**Figure II.6 Water collecting system: (a) downstream overflow outlet
(b) mass balance**

2.3.2 Experimental procedures

A series of tests was carried out in three steps: specimen production, saturation and downward seepage test.

The specimen preparation phase can be divided into two steps: production of the specimen, and saturation. The finer grain and gravel are first mixed with a water content (4%, 6%, 7.8%, 9%) for 3 minutes as presented in Table II.3. The specimens are produced using a single layer semi-static compaction technique as shown in Figure II.7. The mixture is placed in a mould of 50 mm diameter and 50 mm height and subsequently compressed under the action of two pistons until the initial fixed dry density is reached. In the erosion cell device, the specimen is

placed on a 4 mm pore opening grid and wrapped with a layer of membrane, then closed with the metal mold. The pore opening of the grid allows the migration of all particles of silt and sand. The saturation phase begins with injection of carbon dioxide (from the bottom) for the duration of 5 minutes to improve dissolution of gases into water, and afterward the specimen is saturated using demineralised water by gradually increasing the level of the *water tank 1* (for saturation) through a saturation inlet until water appears in the air tube. During saturation process, only the saturation *inlet gate 1*, *outlet gates 1 and 2* and the *air tube* are opened. The air tube is provided to control that the water level reaches the top of sample and saturation is finished. The whole saturation phase requires approximately one night. Finally the saturation inlet gate is closed.

The specimen is subjected to a water flow in a downward direction using demineralized water. During downward seepage test, the *outlet gate 1* are kept opened and the *upstream inlet gate 2* is opened. The seepage pressure is exerted by raising the upstream water tank step by step for multi-staged hydraulic gradients (Figure II.8), then a downward seepage flows into the specimen and discharges from the funnel-shaped drainage system. It is underlined that the *upstream inlet gate 2* is always opened during the increase of hydraulic gradients. In case of hydraulic loading with flow-rate condition, the water supply system comprises a *gear pump* connected to a *pressure sensor*. The outlet overflow water mass is recorded in this process, and eroded mass is captured by beakers. The beakers are rotated each time the hydraulic gradient is increased. The dry eroded mass is obtained by drying the beakers containing water and the eroded soil mass in an oven for 24 hours. The flow rate (Darcy velocity) is then computed by the measured outlet water mass, time and the sectional area of specimen.

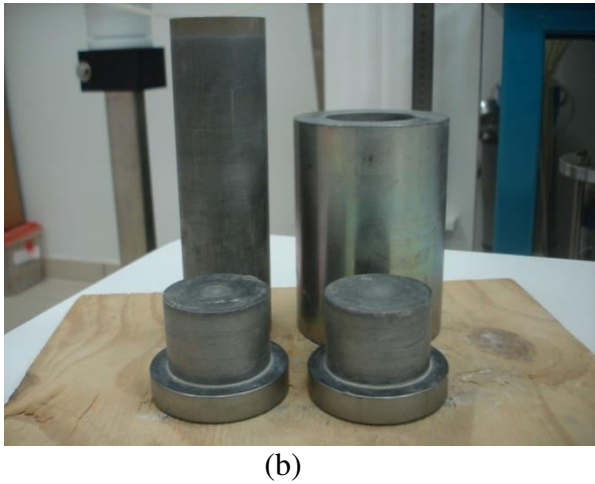
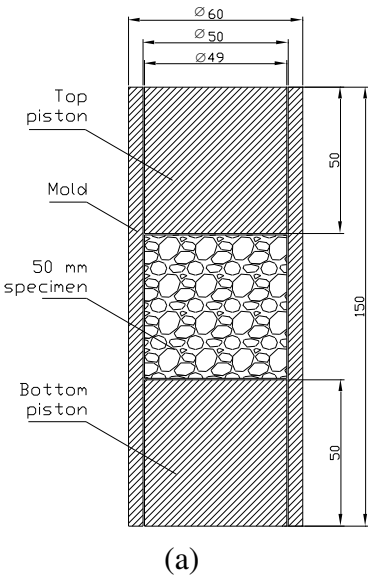


Figure II.7 (a) schematic diagram of piston mold of 50 mm specimen, (b) pictures of piston mold (with top and bottom pistons; and a 1750 mm piston to expel the specimen)

2.4 Tested specimens

Table II.3 summarizes tested specimens with the description of parameters defining the testing conditions. A number of 50 specimens can be divided into two groups with respect to

specimen dry density ρ_d : 16 kN/m³ (specimens *G5A* to *S2*) and larger than 16 kN/m³ (specimens *A-90a* to *R2-97g*). With respect to confinement, only four specimens are subjected to a confinement pressure 15 kPa (*G5A*, *G5B*, *G6* and *P1*), whereas the others are without confinement. For several specimens, gradation, initial density and hydraulic loading conditions are embedded in the specimen name. For instance *B-90a* the letter “B” represents the gradation B, “90” the initial dry density: 90% of maximum dry density (from standard proctor test, ASTM D698-12e1) and “a” refer to hydraulic loading history applied.

A series of tests was subjected to three kinds of hydraulic loading history: multi-stage hydraulic gradient (41 specimens), single-stage hydraulic gradient (4 specimens) and injected flow rate condition (5 specimens) (see Table II.3). Figure III.8 shows a diagram of hydraulic gradients subjected to several specimens for instance hydraulic gradient “a” (*A-90a*, *B-90a*, *B-97a*, *R2-90a*), hydraulic gradient “b” (*A-90b*, *B-97b*, *R2-90b*, *R2-97b*), hydraulic gradient “h” (*B-90h*), hydraulic gradient “k” (*B-90k*), hydraulic gradient “D3” (*D3A*, *D3Arep*) and hydraulic gradient “c” (*A-90c*, *B-90c*). The hydraulic loading “a” consist of increasing the hydraulic head by steps of 0.1 until 2, then by steps of 0.5 between 2 and 4 and by steps of 1 beyond. Steps are directly equal to 1 for the hydraulic loading “b”. The hydraulic loading “h and D3” consist of increasing the hydraulic head by steps of 0.2 until 1, then by steps of 1 beyond, whereas the long-term hydraulic loading “k” only consist of hydraulic gradient 0.5 and 1 which each was kept constant during 12 hours. For each step the hydraulic gradient “a” and “b” were kept constant during 10 minutes, “D3” were kept constant during 20 minutes whereas “h” each step was maintained for 60 minutes. The hydraulic loadings for the other specimens can be seen in the “Annex” section.

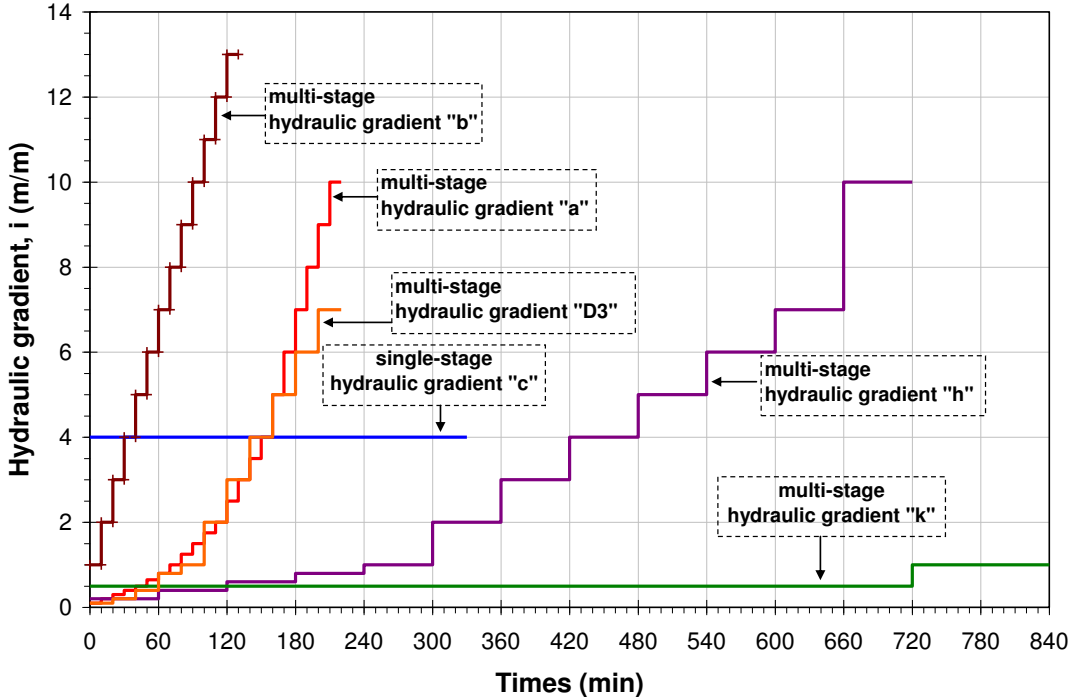


Figure II.8 Multi-stage and single-stage hydraulic gradients

Table II.3 Properties of tested specimens

Tested gradations	Tested specimens	Initial dry density (kN/m ³)	Preparation water content (%)	Applied hydraulic gradient, i (m/m)	Injected flow (ml/min)	Test duration (min)
G5	G5A	16	9	1 - 16	-	479
	G5B	16	9	0.1 - 9	-	584
G6	G6	16	9	0.1 - 12	-	361
P1	P1	16	9	1 - 16	-	478
P2	P2	16	9	1 - 15	-	422
P3	P3	16	9	1 - 10	-	299
P4	P4	16	9	1 - 9	-	272
L1	L1	16	9	0.1 - 3	-	420
L2	L2	16	9	0.1 - 3	-	420
L3	L3	16	9	0.1 - 3	-	420
L4	L4Ai	16	9	0.1 - 4	-	480
	L4Aii	16	9	0.1 - 3	-	140
	L4C	16	9	0.8	-	420
	L4D	16	9	2	-	420
L5	L5	16	9	0.1 - 3	-	420
D1	D1	16	9	0.1 - 16	-	340
D2	D2	16	9	0.1 - 7	-	220
D3	D3A	16	9	0.1 - 7	-	220
	D3Arep	16	9	0.1 - 7	-	220
	D3B	16	9	0.5 - 6.5	-	160
M1	M1	16	9	0.1 - 5	-	181
M3	M3	16	9	0.1 - 6	-	200
M4	M4	16	9	0.1 - 8	-	240
S1	S1	16	9	0.1 - 9	-	260
S2	S2	16	9	0.1 - 9	-	260
A	A-90 _a	17.39	7.8	0.1 - 15	-	270
	A-90 _a rep	17.39	7.8	0.1 - 13	-	250
	A-90 _b	17.39	7.8	1 - 15	-	130
	A-90 _c	17.39	7.8	4	-	300
B	B-90 _a	17.39	7.8	0.1 - 6	-	180
	B-90 _c	17.39	7.8	4	-	300
	B-90 _e	17.39	7.8	-	1.641	270
	B-90 _f	17.39	7.8	-	12	210
	B-90 _h	17.39	7.8	0.2 - 10	-	720
	B-90 _k	17.39	7.8	0.5 - 1	-	1440
	B-97 _a	18.74	7.8	0.1 - 12	-	240
	B-97 _b	18.74	7.8	1 - 9	-	90
C	C-90 _a	17.39	7.8	0.1 - 4	-	160
	C-97 _a	18.74	7.8	0.1 - 9	-	210
	C-97 _b	18.74	7.8	1 - 7	-	70
Chav-1	Chav-1	16.54	6	0.1 - 14	-	320
Chav-2	Chav-2 _i	16.54	4	0.1 - 9	-	260
	Chav-2 _{ii}	18.90	4	0.1 - 16	-	340
R1	R1-90 _b	17.39	7.8	0.1 - 11	-	110
R2	R2-90 _a	17.39	7.8	0.1 - 6	-	180
	R2-90 _b	17.39	7.8	1 - 8	-	80
	R2-97 _b	18.74	7.8	1 - 12	-	120
	R2-97 _d	18.74	7.8	-	1.247	210
	R2-97 _f	18.74	7.8	-	12	270
	R2-97 _g	18.74	7.8	-	48	210

Confining pressure (G5A - P1) = 15 kPa

Confining pressure (P2 - R2-97f) = 0 kPa

2.5 Repeatability check and phenomenological analysis

In order to provide a better description of the proposed methodology of the classification of suffusion susceptibility, a series of 19 specimens are selected to an interpretation. They are

- sandy-gravel soils that consist of 15 specimens subjected to multi-stage hydraulic gradients (*D3A*, *D3Arep*, *A-90a*, *A-90a_rep*, *A-90b*, *B-90a*, *B-90h*, *B-90h*, *B-97a*, *B-97b*, *C-97a*, *C-97b*, *R2-90a*, *R2-90b*, *R2-97b*),
- 2 specimens subjected to single-stage hydraulic gradient (*A-90c*, *B-90c*),
- 2 specimens subjected to an imposed flow rate condition (*B-90e*, *R2-97d*).

Figure III.9 shows the grading of these specimens that can be identified as gap-graded soils which contain fine content 20%, 23%, 25% and 29% for the grading A - R2- B and D3 - C respectively. Their properties can be seen in Table II.3 whereas the hydraulic loading history in terms of hydraulic gradients imposed to selected specimens is shown in Figure III.8. The other specimens can be seen in the **Annex** section. A repeatability test named *D3Arep* and *A-90a_rep* were carried out to investigate the methodology used is reliable and repeatable.

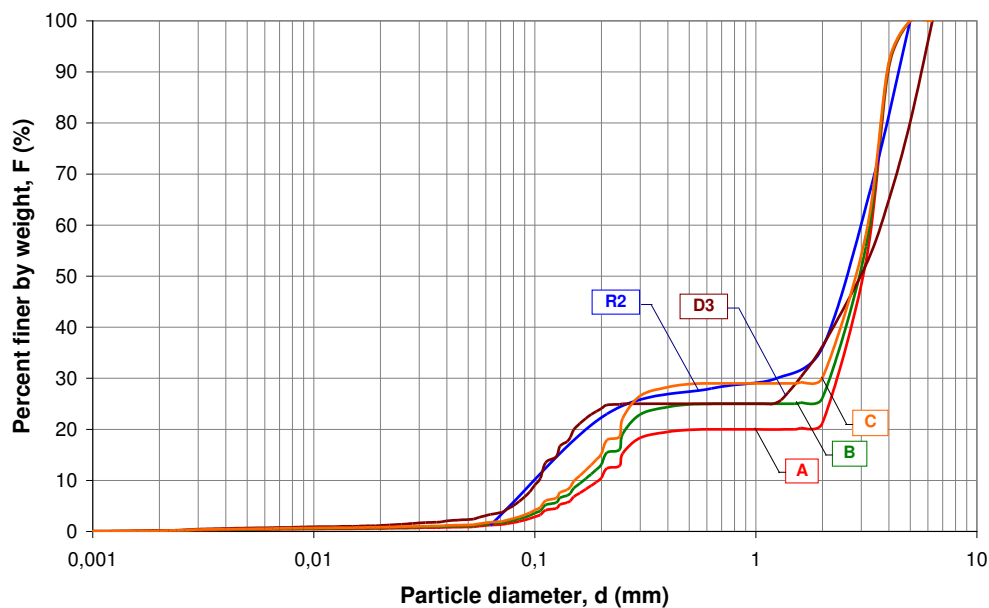


Figure II.9 Grain size distribution of soils D3, A, B, C and R2

2.5.1 Evolution of hydraulic conductivity and erosion rate

2.5.1.1 Multi-stage hydraulic gradient condition tests

All the computation of hydraulic conductivity are based on the Darcy's formula. The arrow signs in Figure II.10 highlights the time when hydraulic conductivity stabilizes at a constant value. There is a clear typical trend of an initial decrease of hydraulic conductivity before it turns to progressively increases and finally reaches a constant value from the arrow signs. We assume this decrease of the hydraulic conductivity is attributed to some fine particles, detached and transported under the imposed water seepage and filtered within the soil itself. This filtration thus makes a partial clogging and decreases the hydraulic conductivity. Hydraulic conductivity increases only latter, for much larger hydraulic gradients possibly pushing the clogging. A similar behaviour is observable in Figure II.11 to Figure II.13 for samples B, C, and R2. Figure II.10 shows that repeatability is fairly good, as representation points are close for tests *D3A* and *D3Arep*; *A-90a* and *A90a_rep*.

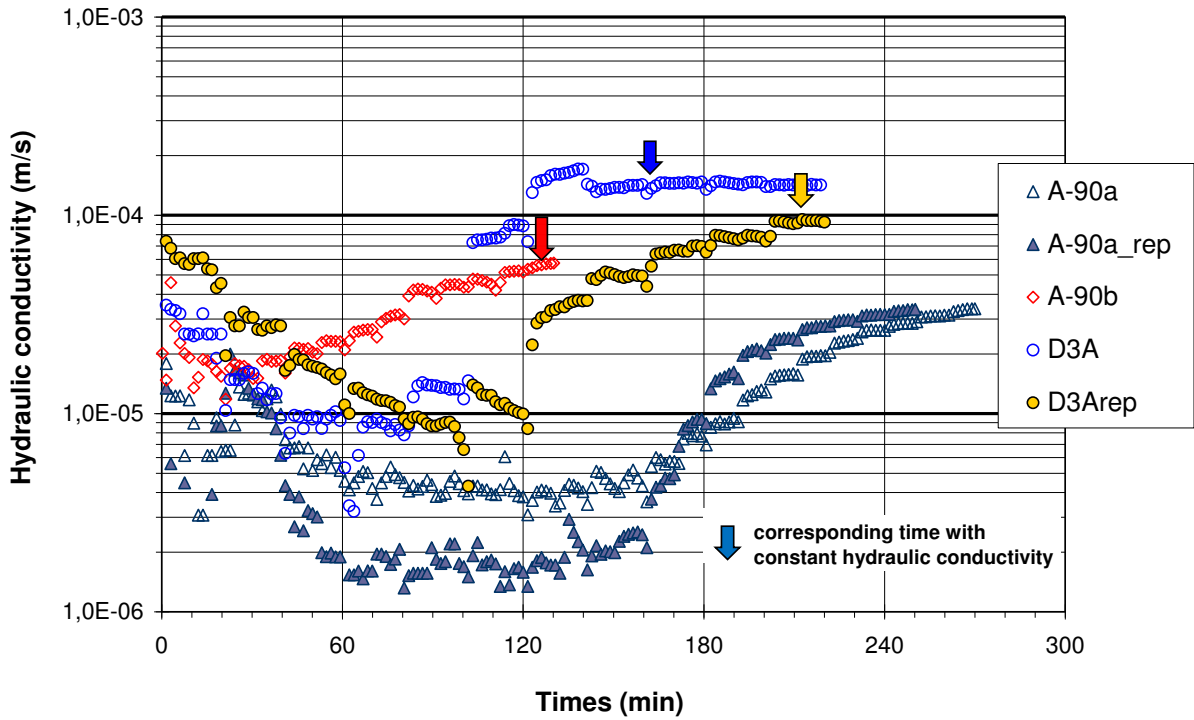


Figure II.10 Variation of hydraulic conductivity of tested specimens subjected to multi-stage hydraulic gradients A-90a,b,a_rep; D3A and D3Arep

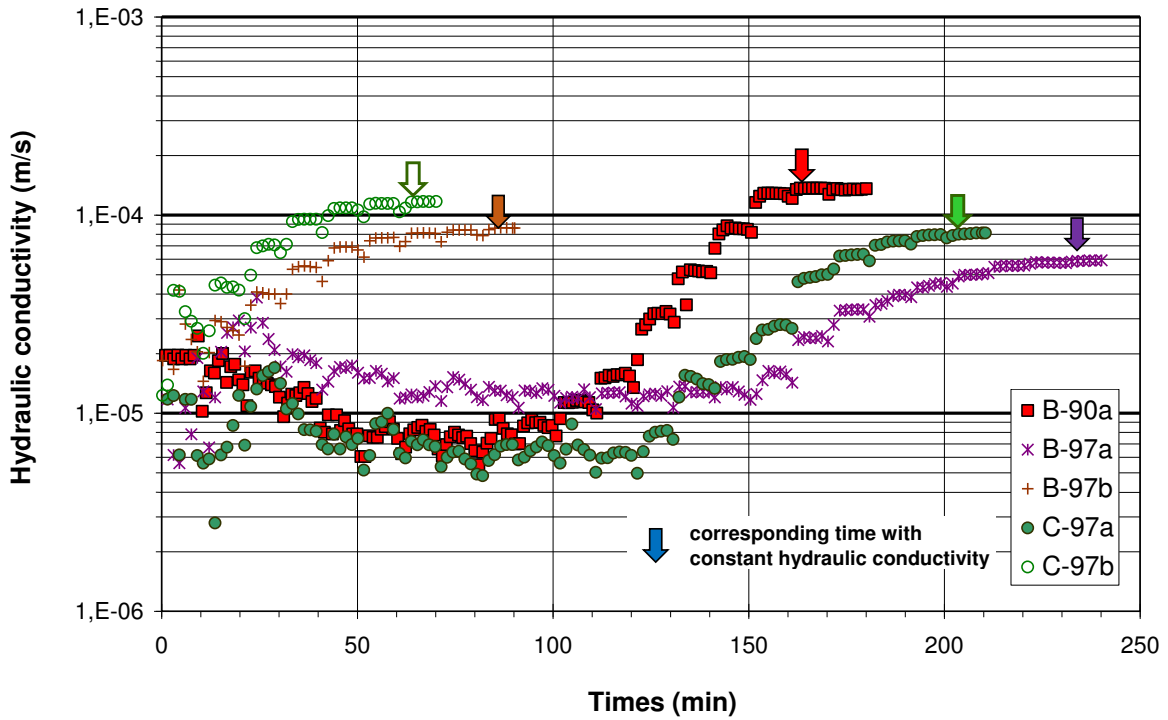


Figure II.11 Variation of hydraulic conductivity of tested specimens subjected to multi-stage hydraulic gradients B-90a; B-97a,b; C-97a,b

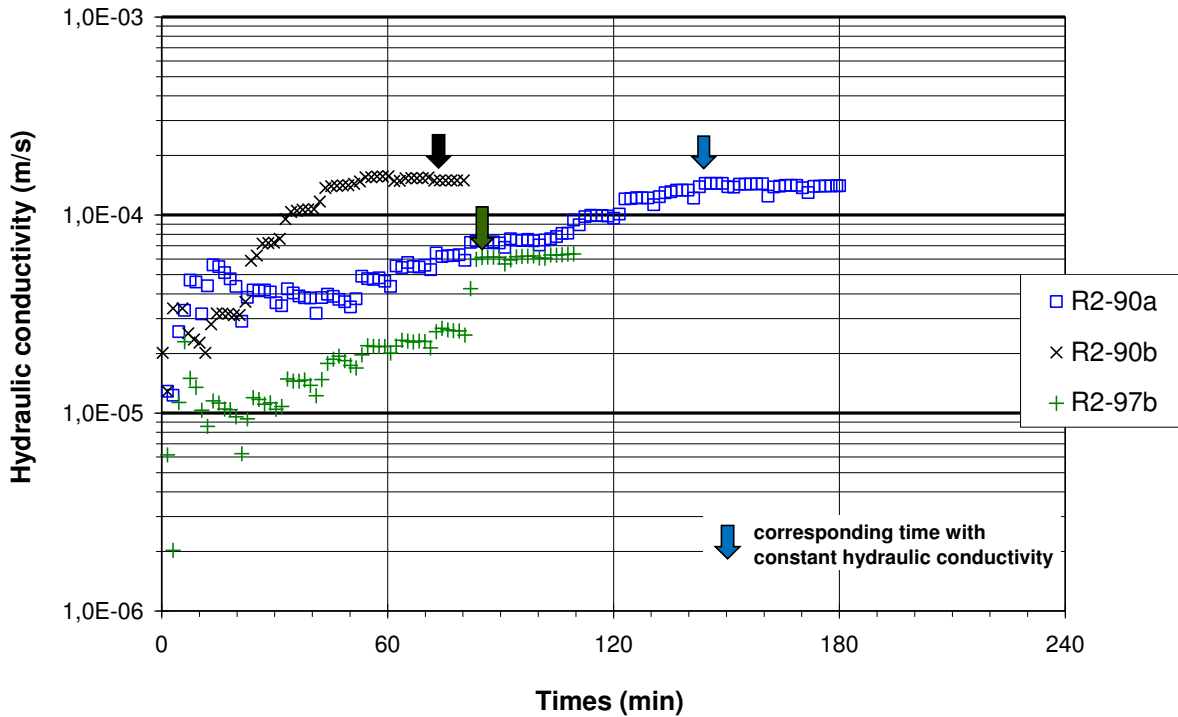


Figure II.12 Variation of hydraulic conductivity of tested specimens subjected to multi-stage hydraulic gradients R2-90a,b; R2-97b

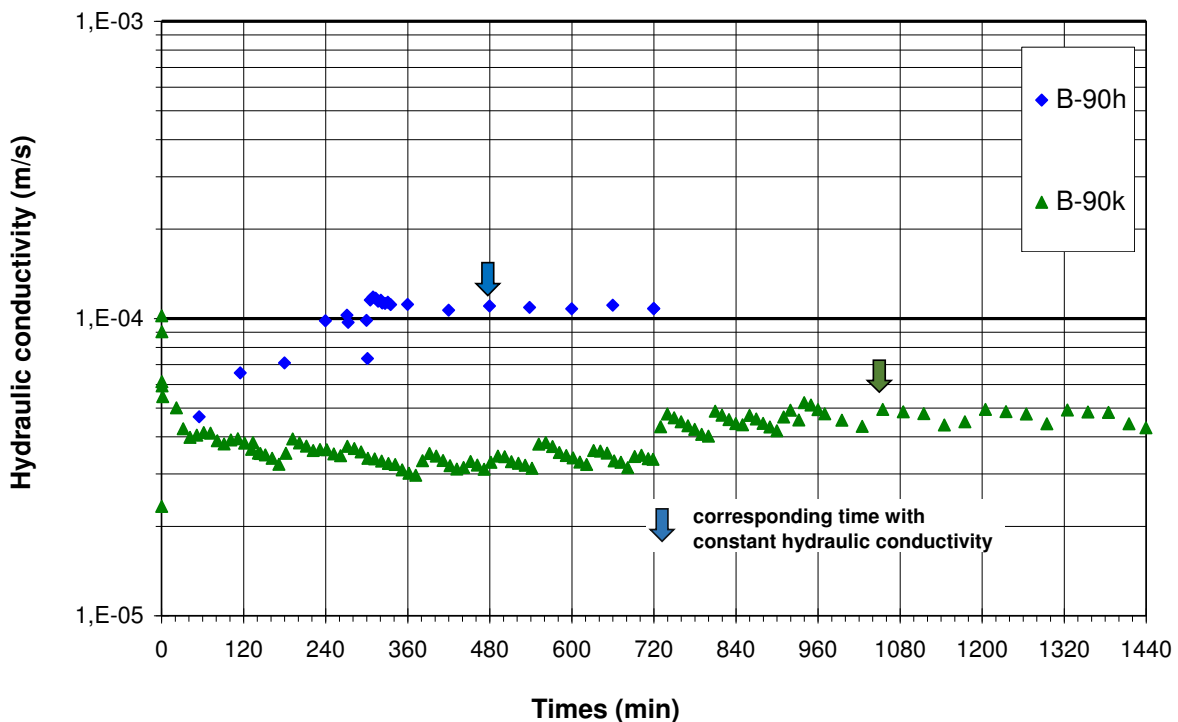


Figure II.13 Variation of hydraulic conductivity of tested specimens subjected to multi-stage hydraulic gradients B-90h,k

Figure II.14 to Figure II.17 show the variation of erosion rate versus time for several specimens. It is underlined that erosion rate here is not an “instantaneous” erosion rate, but a mean erosion rate over each hydraulic step. Each point in the diagrams of time series of

erosion rate corresponds to the dry eroded mass collected each step of application of hydraulic gradient. The corresponding hydraulic gradient at any time can be retrieved by comparing the times in the x-axis in Figure II.14 - Figure II.17 with the hydraulic gradients in Figure II.8.

The value of erosion rate per unit of surface area depends importantly on the definition of surface area. Considering the surface of pores is more representative than surface of the cross section of the sample for suffusion process, thus the erosion rate computed here is the erosion rate of a soil per unit surface of pore (\dot{m}) defined by Reddi et al. (2000) as presented in the Eq. II.22 – II.26. This expression assumes by representing porous medium as capillary tube model and pore space of the soil is represented as a bundle of parallel cylindrical tubes.

The arrow signs in the Figure II.14 to Figure II.17 point out the time of stabilized hydraulic conductivity. It is shown in these figures, erosion rate does not always increase when hydraulic gradient increases. In the first minutes given increased hydraulic gradients, the specimens imposed to multi-stage hydraulic gradients show the decrease of erosion rate. This is because the detachment of finer particles is transported and filtrated somewhere within the soil. This filtration thus induces a partial clogging and decreases the erosion rate. After the soil is subjected to a larger enough hydraulic gradient to blow the clogging, the erosion rate then increases until maximum value is reached. From this stage the erosion rate then tends to decrease again. However, Figure II.14 shows that the repeatability test of specimens *D3A* and *A-90a* is fairly good, as representation points are close.

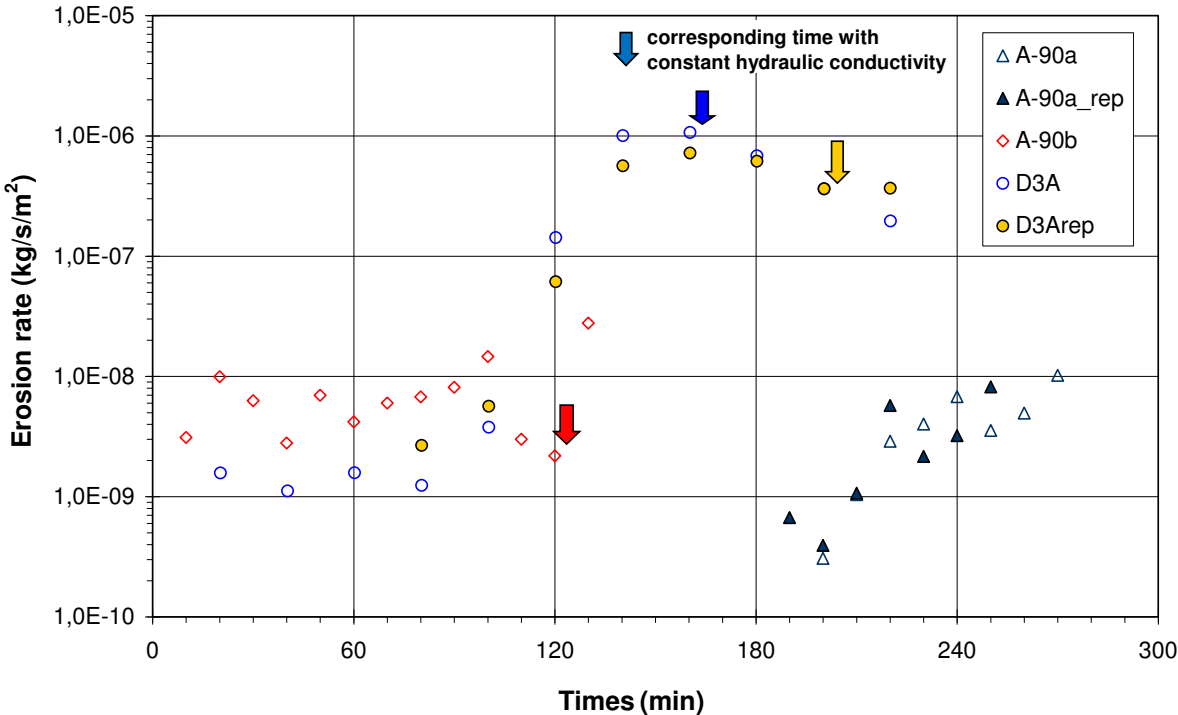


Figure II.14 Time series of erosion rate – specimens subjected to multi-stage hydraulic gradient (A-90a,a_rep,b ; R2-90a,b ; R2-97b)

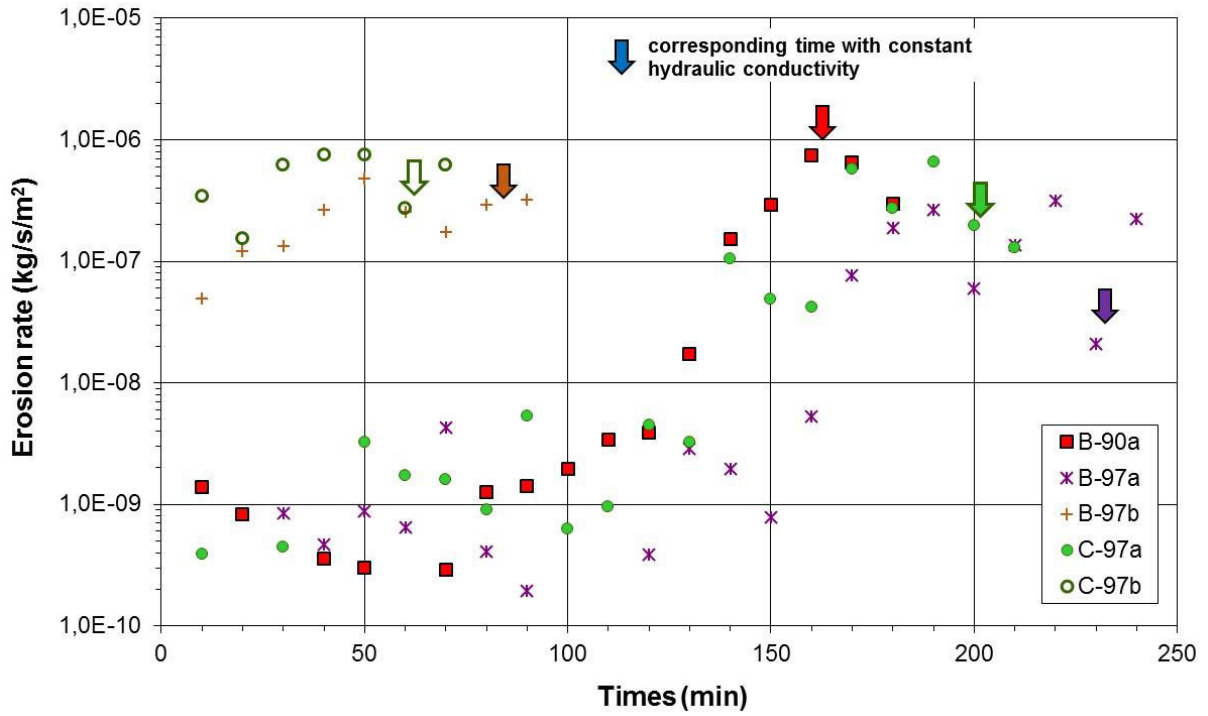


Figure II.15 Time series of erosion rate – specimens subjected to multi-stage hydraulic gradient (B-90a; B-97a,b ; C-97a,b)

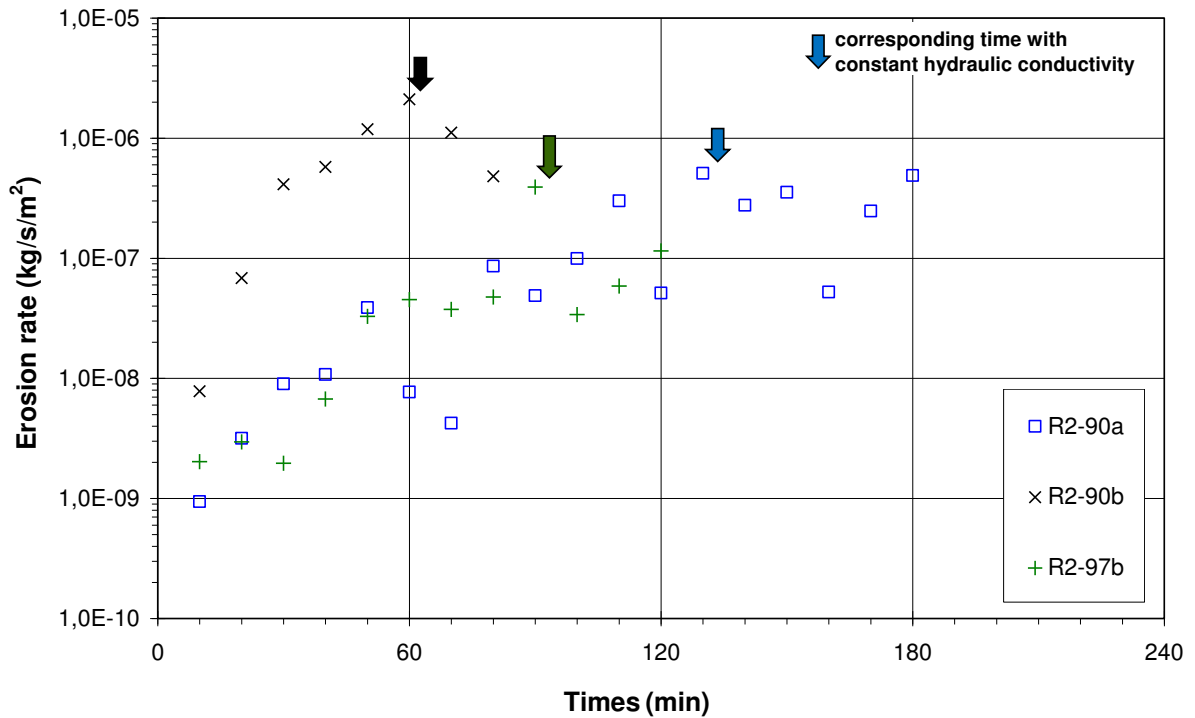


Figure II.16 Time series of erosion rate – specimens subjected to multi-stage hydraulic gradient (R2-90a,b ; R2-97b)

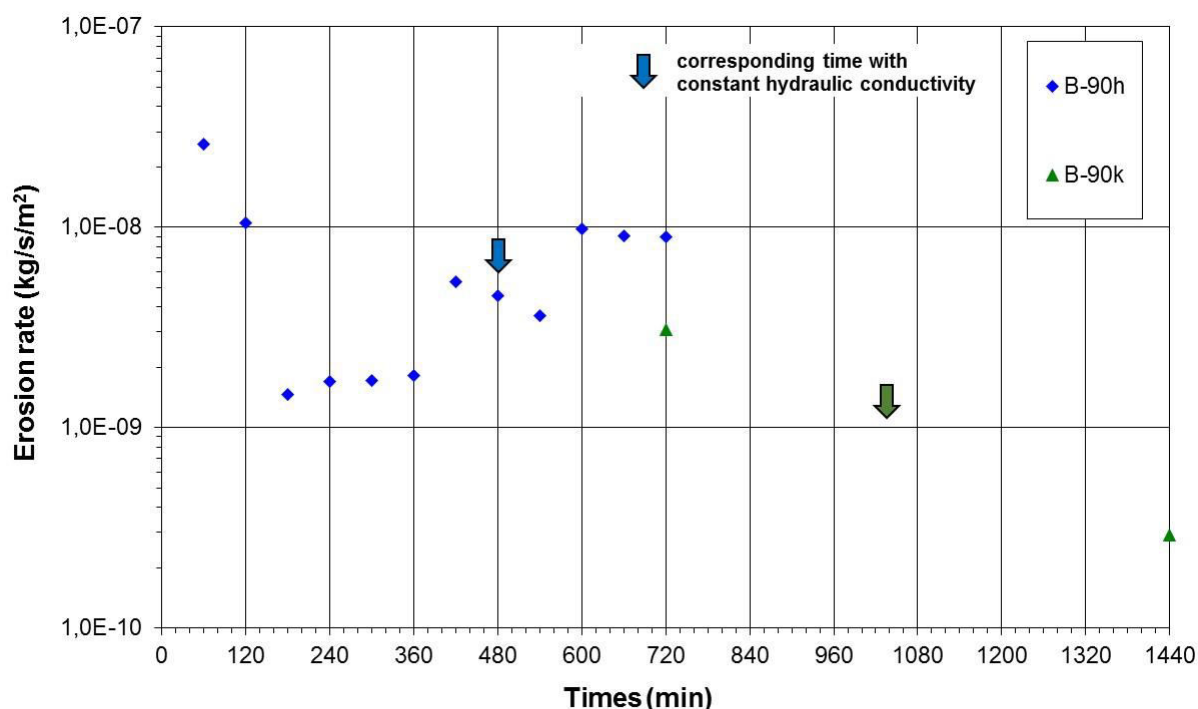


Figure II.17 Time series of erosion rate – specimens subjected to multi-stage hydraulic gradient (B-90h,k)

For all the tested specimens subjected to multi-stage hydraulic gradients, the hydraulic conductivity gradually decreases during the first several minutes while the mass erosion rate is relatively low and itself decreases. An important increase of the erosion rate then occurs simultaneously with the increase of the hydraulic conductivity, confirming the assumption of a clogging firstly restricting the water flow and then blown by the seepage flow itself. Finally hydraulic conductivity tends to stabilize while a maximum erosion rate is reached. This last phase can be explained by the fact that after reaching such eroded mass, the soil becomes more porous than before due to larger volume of void. There may still be concentration of fine fraction in one part of soil but not in another part. The latter condition may create preferential flow path for seeping water where there is no more particles to erode.

2.5.1.2 Single stage hydraulic gradient and constant flow rate condition tests

Figure II.18 shows the evolution of hydraulic conductivity of tested specimen during elapsed time and Figure II.19 depicts the variation of erosion rate during the times.

Hydraulic conductivities of the specimens subjected to single-stage hydraulic (A-90c and B-90c) and injected flow rate condition (B-90e and R2-97d) decrease during the given times. The decrease of hydraulic conductivity presented in Figure II.18 can be attributed to a process of filtration within the soils that induces the decrease of erosion rate as shown in Figure II.19. It is worth noting that during the filtration process, erosion process also occurred but bringing only few eroded mass.

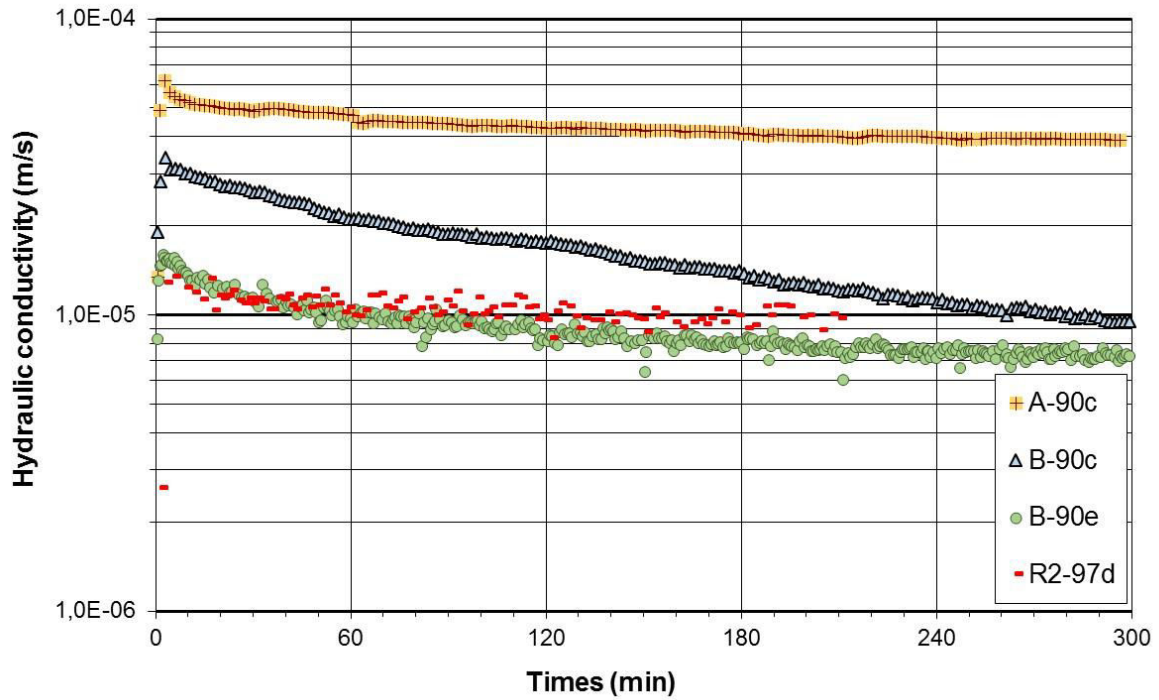


Figure II.18 Variation of hydraulic conductivity of tested specimens subjected to single-stage hydraulic gradients and flow rate condition (A-90c; B-90c,e; R2-97d)

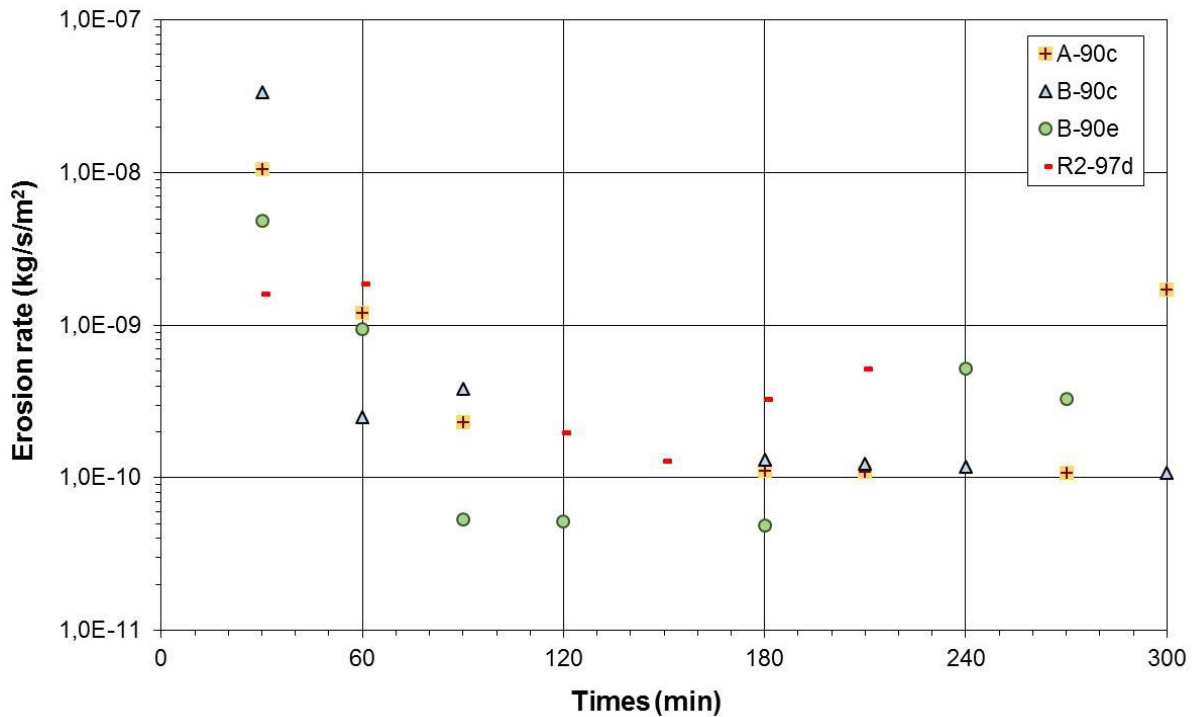


Figure II.19 Time series of erosion rate—specimens subjected to single-stage hydraulic gradient and flow rate condition (A-90c; B-90c,e; R2-97d)

Comparing to the specimens subjected to multi-stage hydraulic gradients characterized by three predominant phases, filtration seems to be predominant phase for the specimens subjected to a single-stage hydraulic gradient and flow rate condition. Given the specimens it is obvious that the different hydraulic loadings can significantly change the soil responses.

Figure II.20 shows the time series of computed hydraulic gradients for corresponding injected flow rate condition (*B-90e* and *R2-97d*). From the variation of computed hydraulic gradient, it seems that the computed hydraulic gradient of the specimen *B-90e* equals to 1.3 could not initiate erosion corresponding to the decrease of the hydraulic conductivity (Figure II.18). However, with the same hydraulic gradients 1.3, the specimen *B-90a* that was subjected to multi-stage hydraulic gradient appear to initiate the erosion as shown in the time series of hydraulic conductivity (Figure II.11). Thus, the hydraulic loading history in term of multi-stage hydraulic gradient shows the ability to follow the development of suffusion.

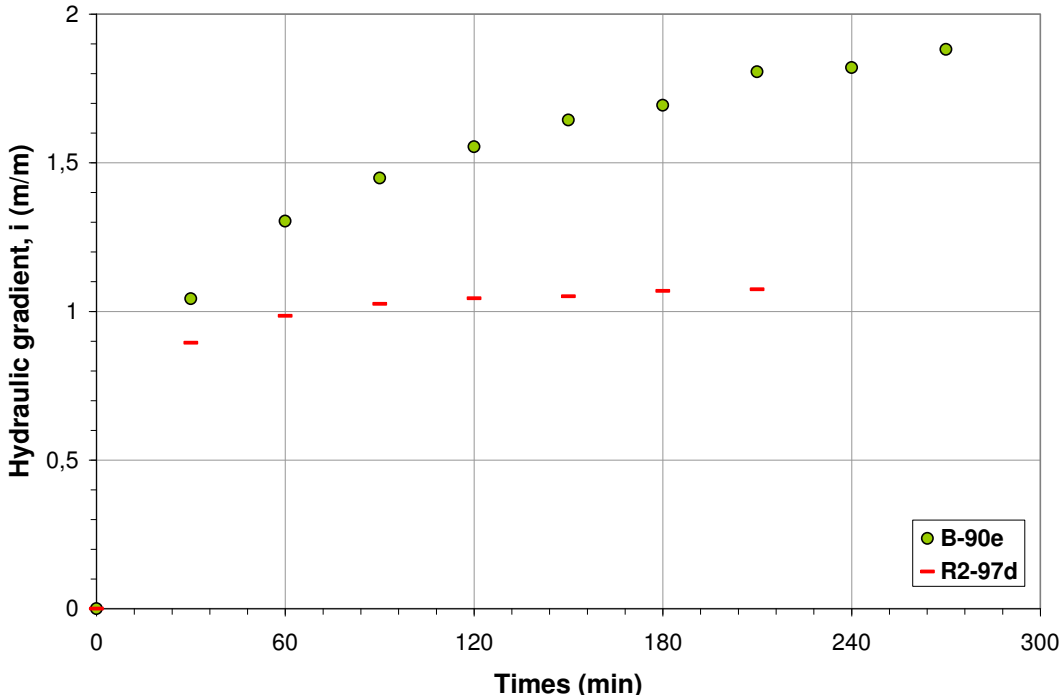


Figure II.20 The change of hydraulic gradient of tested specimens subjected to imposed flow rate condition (*B-90e* and *R2-97d*)

2.5.2 Identification of predominant processes

From the evolution of hydraulic gradient versus time for all the specimens it can be deduced that the variation of hydraulic conductivity with respect to the hydraulic loading history can be grouped into two categories as shown in Figure II.21.

The variation of hydraulic conductivity of specimen *B-90a* can be a representative of all the specimens imposed by multi-staged hydraulic gradients. With such hydraulic loading history an evolution into three predominant phases can be drawn: filtration, process of erosion and finally failure (represented by constant value of hydraulic conductivity). It seems with this approach, the possibility to follow all the evolutions such as initiation and development of suffusion is obvious. With the objective to classify the suffusion susceptibility of soils investigated that will be explained later in this chapter, this method is easier to determine erosion coefficient k_d than the two other methods (single-stage hydraulic gradient and injected flow rate). Thus, the likelihood to follow all the evolutions is difficult using the other

hydraulic loading histories, i.e., with single-stage hydraulic gradient or with a flow-rate controlled condition. The time series of hydraulic conductivity of the specimen *B-90c* can represent all the specimens subjected to single-stage hydraulic gradient and the specimen *B-90e* can represent all the specimens subjected to flow-rate controlled condition. In the latter cases, filtration that induces clogging occurs during elapsed time until the test is stopped. In case of methods of single-stage hydraulic gradient and flow-rate controlled condition, we do not know if the occurrence of erosion is just delayed beyond the duration of the tests, or if it would never happen (in this case it would mean that suffusion cannot develop). Considering test *B-90a*, by increasing progressively the applied hydraulic gradients from 1.3 to 4 the hydraulic conductivity increases by a factor of 20. Whereas in the case of test *B-90c*, performed with a single-stage hydraulic gradient, even by applying hydraulic gradient of 4, the hydraulic conductivity continuously decreases.

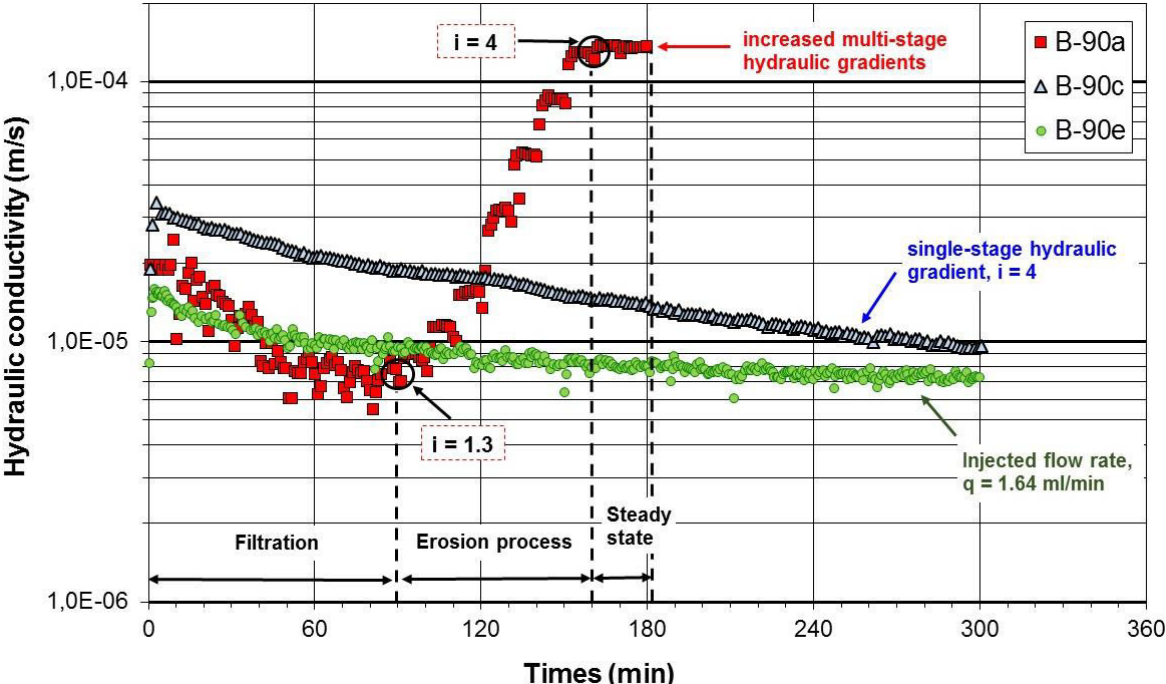


Figure II.21 Two categories of soil response to hydraulic loadings

In all cases it is clear that the susceptibility of soils to suffusion is highly dependent on the history of the hydraulic loading. For the need to the classification of suffusion susceptibility, we prefer the method by increasing the hydraulic gradient by steps because it is the one (among the different histories we tested) leading to the most damageable response of the soil in term of erosion. It may be also the most representative of the history of the hydraulic loading experienced by a dike or a levee, where local hydraulic gradients will increase gradually due to the increase of the water level behind the water retaining structure.

2.6 Study of hydraulic loading history

2.6.1 Influence on the onset of suffusion

Determination of the onset of suffusion can be identified by several approaches. In this study, as proposed by Skempton and Brogan (1994), the onset of suffusion is determined by the change of the hydraulic conductivity. The diagram of relationship between the hydraulic gradient and the average flow velocity (representing hydraulic conductivity) of specimens

which were tested under multistage hydraulic gradient conditions is shown in Figure II.22 (specimens A and R2), in Figure II.23 (specimens B) and in Figure II.24 (specimens C). The arrow signs point out a critical hydraulic gradient as at this hydraulic gradient suffusion starts to occur (as highlighted here after). The linear relationship between the hydraulic gradient and the average flow velocity before the sign of arrow indicates the permeability stays constant and is not influenced by some detached of filtered particles. Thus the erosion is almost negligible during this stage as presented in Figure II.15 for the specimen *B-90a*. During this stage, the detachment of fine particle by the action of water flow is transported and filtrated somewhere within the soil that provokes a clogging thus decreases the hydraulic conductivity. After reaching critical hydraulic gradient, the flow induced by hydraulic gradient can push the clogging and washes out the fine fraction, leading to larger porosity, and thus increases hydraulic conductivity. This can be then presented by the sharp increase of the curve slope. Regarding the specimen *B-90a*, the initiation of the sharp increase of the curve slope (Figure II.23) corresponds to the time when hydraulic conductivity presents a minimum value as shown in Figure II.21. This point corresponds to a hydraulic gradient equal to 1.3. For several specimens (*B-97b*, *B-90h*, and *C-97b*), the significant change of slope was not clearly observed, thus determination of critical hydraulic gradient (i_{cr}) with this approach is not easy. In this case, small change of slope may be determined as critical hydraulic gradient.

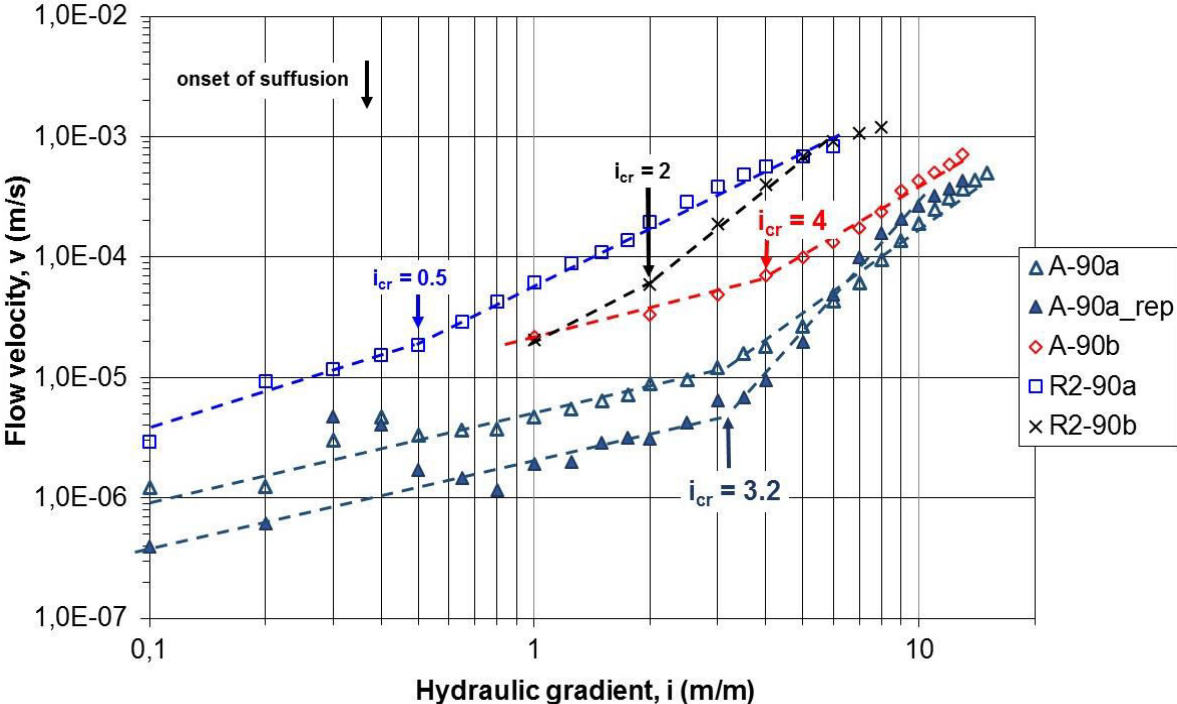


Figure II.22 Hydraulic gradient versus average flow velocity (specimens A-90a,a_rep,b; R2-90a,b)

From the determination of the critical hydraulic gradient as presented in Figure II.22 to Figure II.24, it can be deduced that $i_{cr a} < i_{cr b}$. Under hydraulic loading history *a*, suffusion starts easier than in the case of hydraulic loading history *b*.

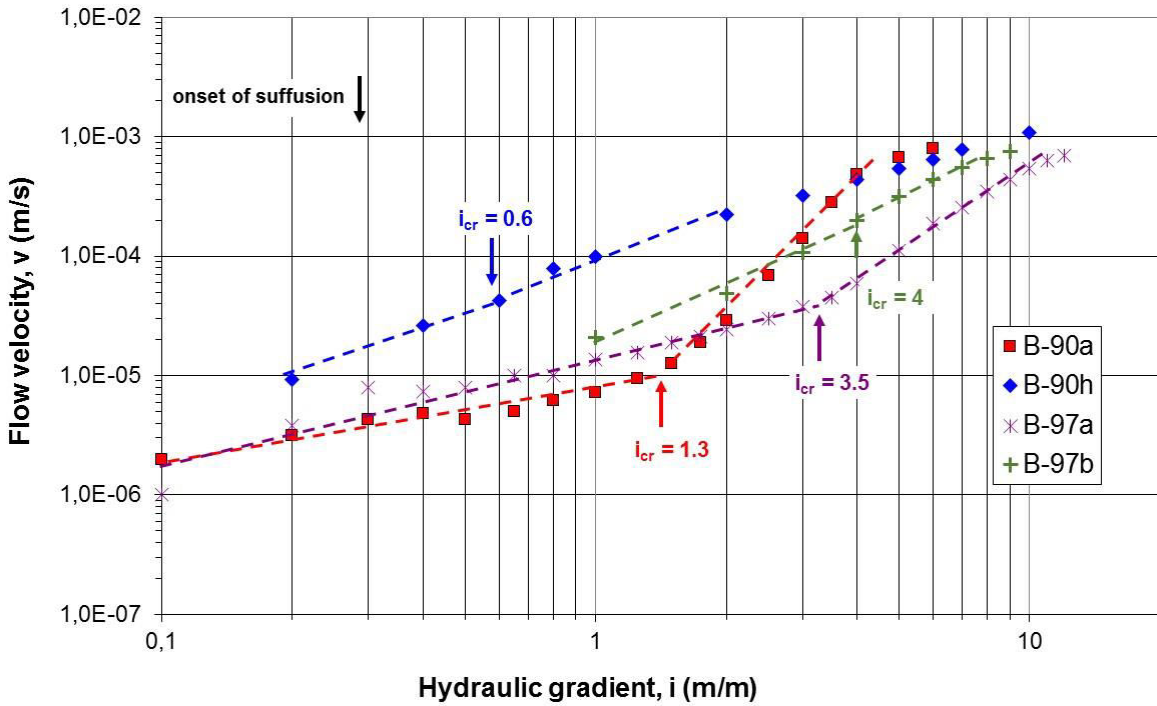


Figure II.23 Hydraulic gradient versus average flow velocity (specimens B-90a,h; B-97a,b)

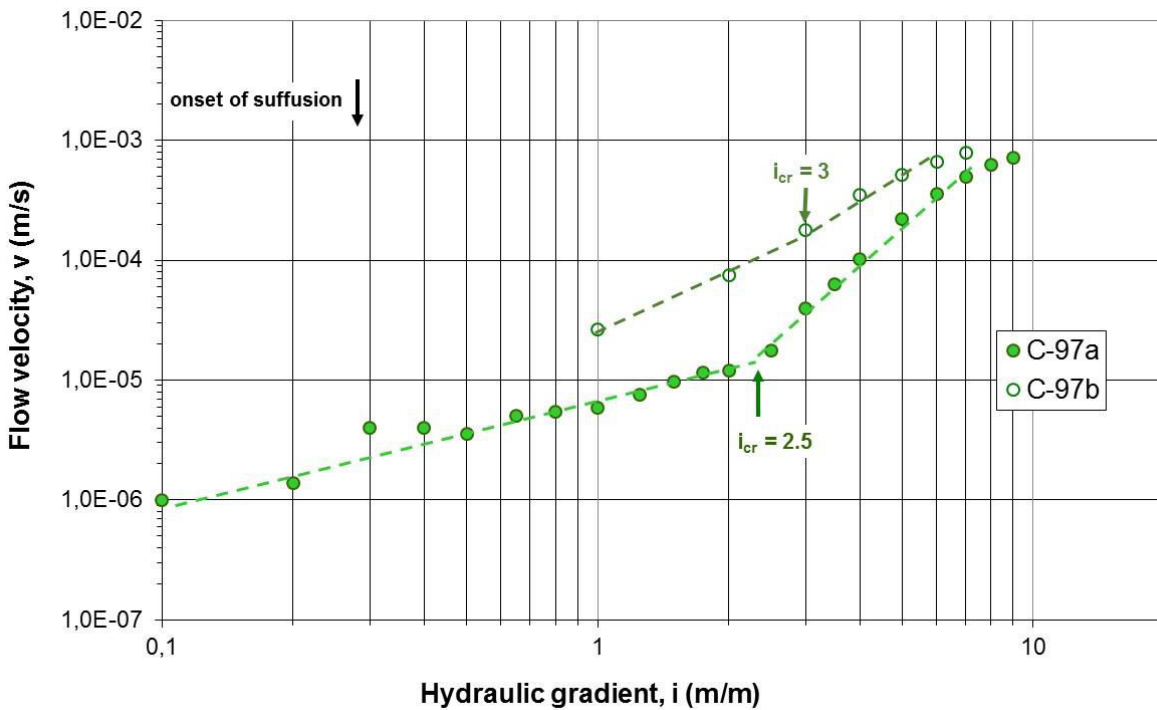


Figure II.24 Hydraulic gradient versus average flow velocity (specimens C-97a,b)

2.6.2 Influence on the development of suffusion

2.6.2.1 Hydraulic shear stress based method

In conformity with methods proposed for interface erosion classification, a first approach to define a suffusion susceptibility classification can consist to investigate the variation of the erosion rate with the hydraulic shear stress. It is worth stressing that the expression (Equation II.21) proposed by Hanson (1989) and Wan and Fell (2004) has been developed only for interface or contact erosion. However one can try to apply it to suffusion case. For that one can use the expression of the hydraulic shear stress within a soil defined by Reddi et al. (2000). For a vertical flow the shear stress is presented in Equation II.10.

The variation of hydraulic shear stress to erosion rate is displayed in Figure II.25, for tests realized under multistage hydraulic gradient condition. For single stage hydraulic gradient condition tests and imposed controlled flow rate condition test, it is shown in **Annex** section. For suffusion process, no clear relation appears between erosion rate and hydraulic shear stress for all hydraulic loading conditions.

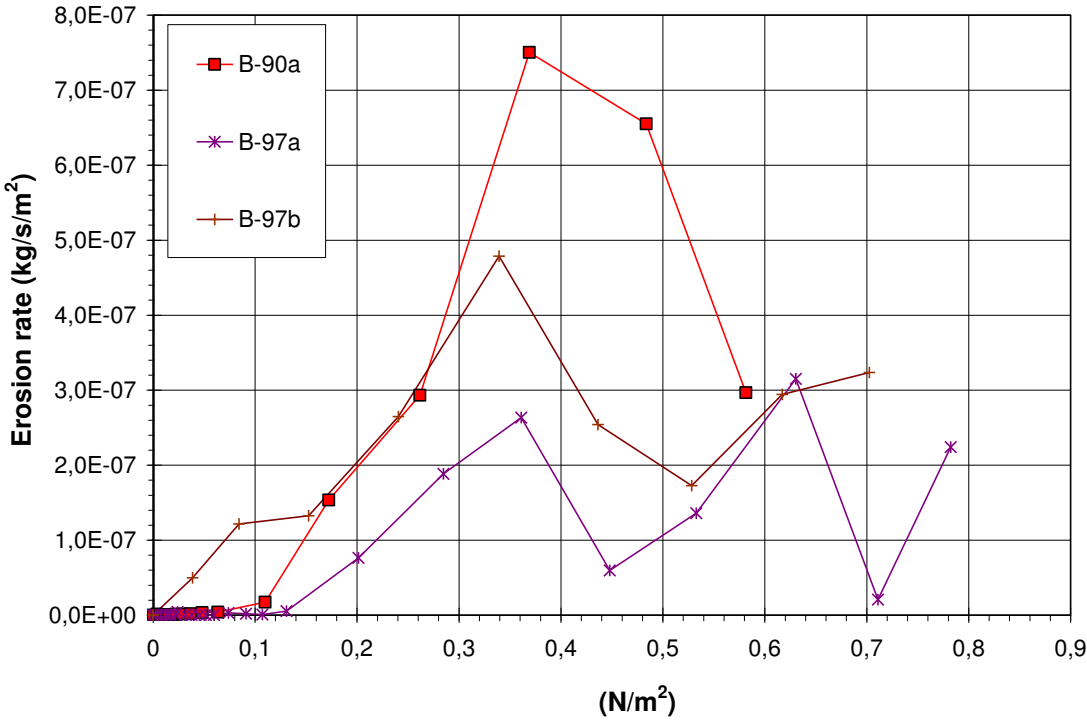


Figure II.25 Erosion rate versus hydraulic shear stress (B-90a to B-97b)

It is shown that erosion rate does not always increase when hydraulic shear stress increases. Similar to the evolution of hydraulic conductivity, it is worth noting that the evolution of all the specimens imposed by multi-staged hydraulic gradients in the diagram of hydraulic shear stress versus erosion rate can be split into three phases. In the first minutes the erosion rate progressively decreases (attributed to a clogging process) then it gradually increases (attributed to clogging blow) and after sometimes erosion rate decreases again (attributed to steady state). However such phases do not seem to appear in the specimens subjected to single-stage hydraulic gradient and injected flow rate. The erosion rate continuously decreases (B90c) as displayed in Figure II.19.

The erodibility, or erosion susceptibility, can be estimated with respect to the hydraulic shear stress (as assumed to be representative of the hydraulic loading). The erosion rate coefficient k_d is assumed to be representative of the erosion susceptibility. In the necessity to build a classification of suffusion susceptibility of tested specimens a first approach proposed by Hanson and Simon (2001) and Wan and Fell (2004) can be used. This approach is based on the determination of k_d coefficient. In order to apply such approach for suffusion process, the value of k_d is defined from linear approximation of the plot of the erosion rate with respect to the hydraulic shear stress. Concerning erosion coefficient “ k_d ”, in the literatures, erosion coefficient k_d is proposed by several researchers in case of interface erosion where in such erosion processes there is no filtration phase or clogging event. Since suffusion comprises the detachment, the transport and the filtration of fine particles, the selection of k_d as the linear correlation between erosion rate and hydraulic shear stress (following the previous method in case of interface erosion) for suffusion should only corresponds to erosion mode.

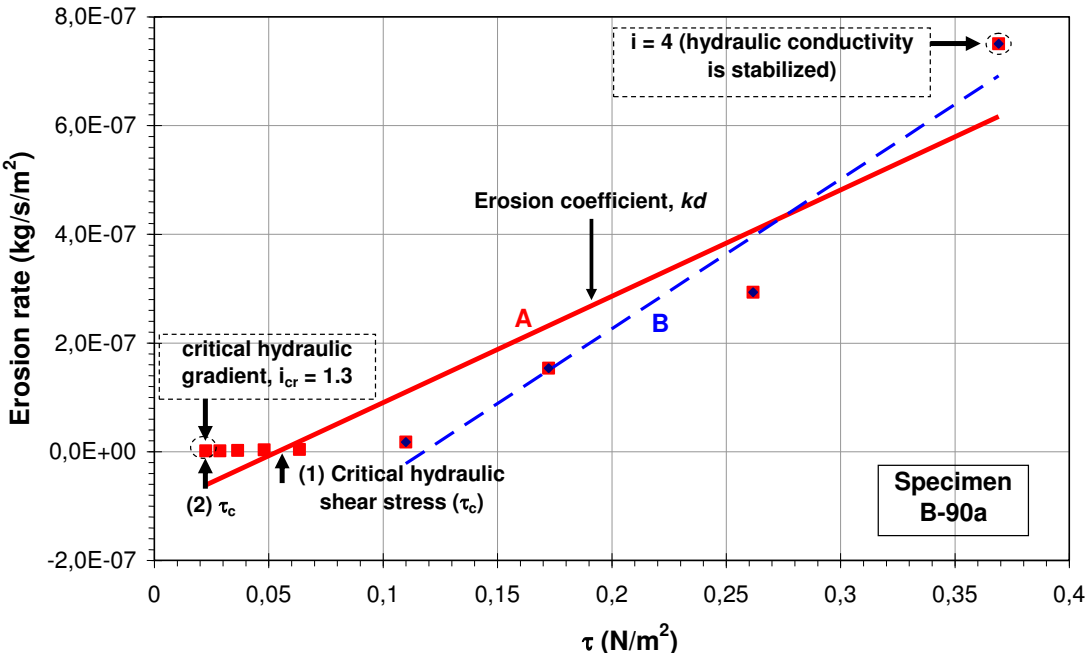


Figure II.26 Determination of erosion coefficient, k_d (linear - linear scale)

Due to temporal measurement of erosion rate that for suffusion process, no clear relation appears between erosion rate and hydraulic shear stress (Figure II.25), the determination of k_d becomes difficult. The initial point where to start the linear approximation can vary. The different starting point may result in a different k_d value. As shown in Figure II.26, different slopes of k_d (A and B) can be produced if the starting point is different. Due to this, a proposition to determine k_d value using a methodology of the slope A is chosen. This linear approximation A is defined from an initial point where hydraulic conductivity presents a minimum value (later it is named critical hydraulic gradient) to a last point where the hydraulic conductivity is stabilized and erosion rate vanishes. However, for some specimens where hydraulic conductivity does not reach constant value until the end of the test, the final point is used as a last point. For instance, for specimen B-90a the initial point corresponds to a critical hydraulic gradient equals to 1.3 and the last point corresponds to hydraulic gradient equals to 4 as shown in Figure II.26.

With the objective to establish a threshold in term of critical hydraulic shear stress, the determination of critical hydraulic shear stress is achieved by two different approaches (see k_d slope A in Figure II.26). Later it is shown that for several specimens, it is not possible to use the first approach as a single threshold as follows then the second approach can be the other alternative.

- 1) From the plot of the linear approximation of hydraulic shear stress versus erosion rate (k_d slope A) with the initial point corresponds to critical hydraulic gradient (representing the onset of erosion) and final point corresponds to stabilized hydraulic conductivity, the critical hydraulic shear stress is defined by extending the slope line until crossing x-axis (hydraulic shear stress axis) at y-axis equals to 0 as shown in Figure II.26. However, the possibility for the slope lines crossing the negative x-axis (negative hydraulic shear stress) at y-axis equals to 0 may appear. Thus, their critical hydraulic shear stresses are assumed equals to 0.
- 2) Critical hydraulic shear stress is directly computed from critical hydraulic gradient (see k_d slope A).

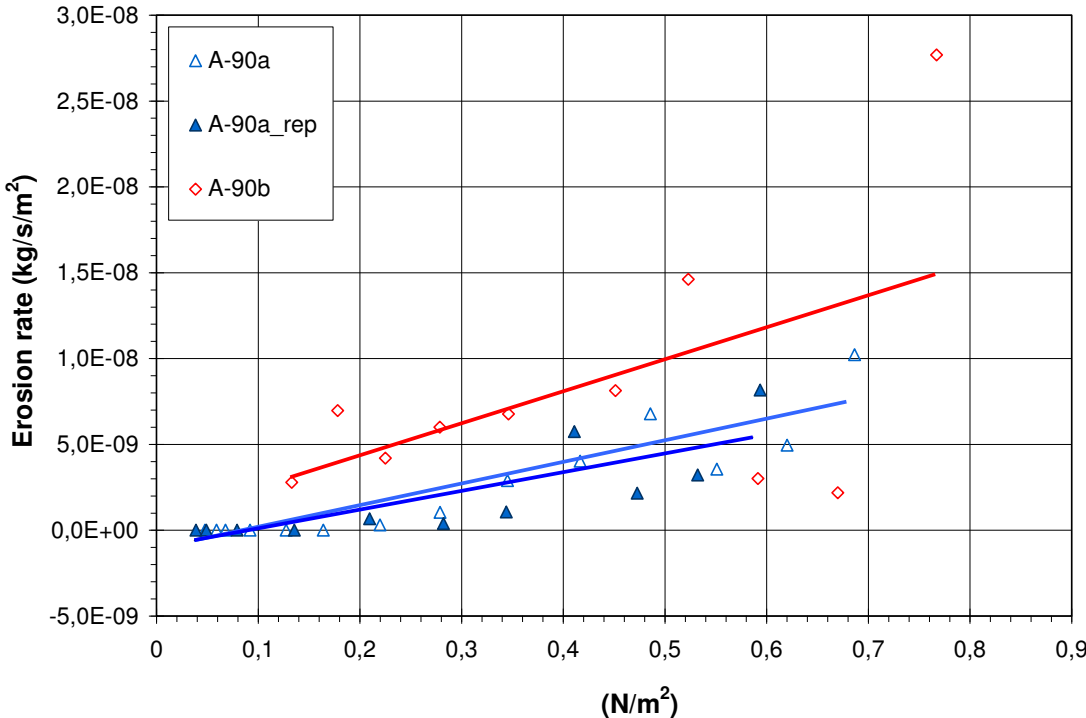


Figure II.27 Erosion rate versus hydraulic shear stress (A-90a,a_rep,b)

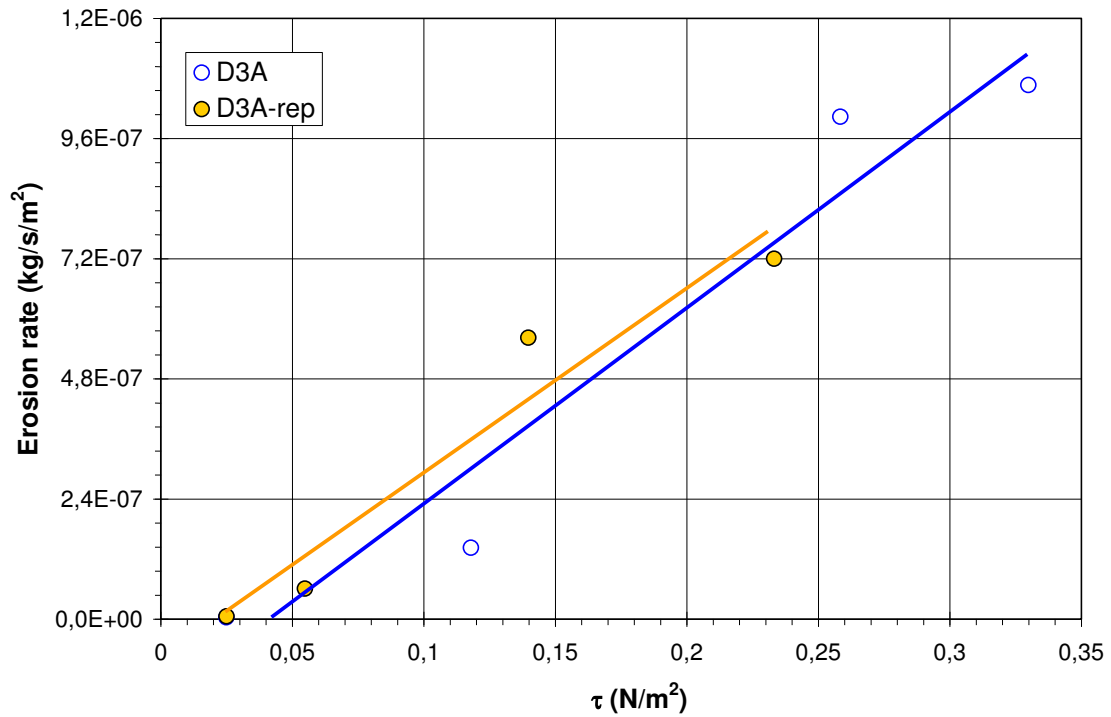


Figure II.28 Erosion rate versus hydraulic shear stress (D3A, D3Arep)

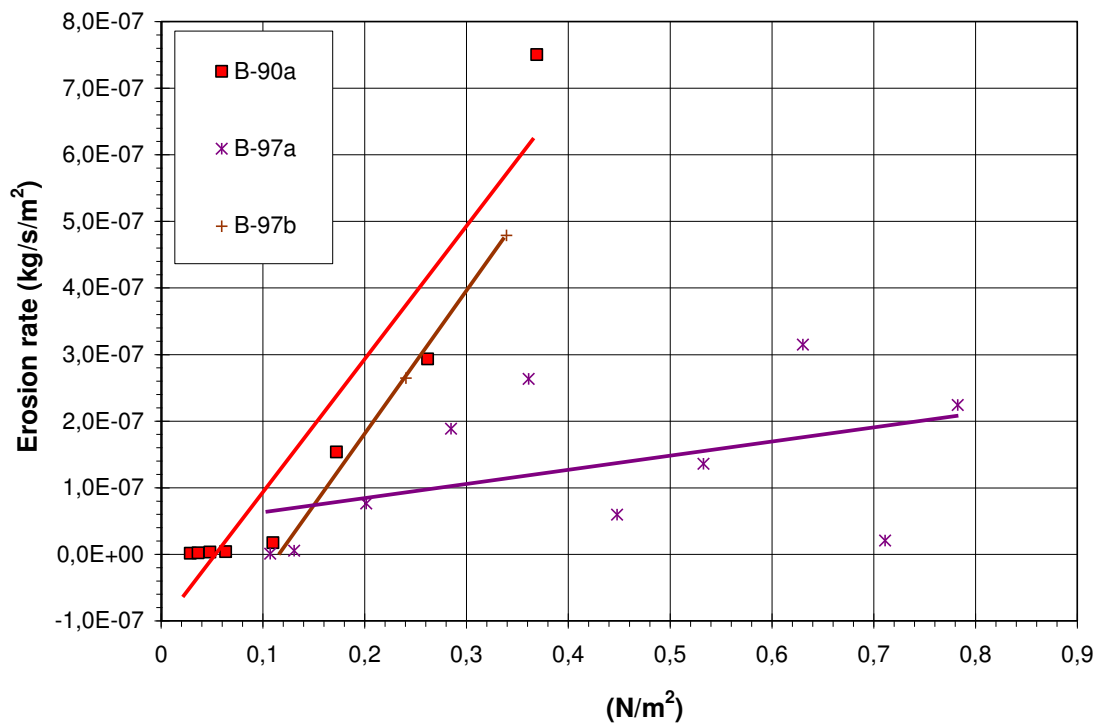


Figure II.29 Erosion rate versus hydraulic shear stress (B-90a; B-97a,b)

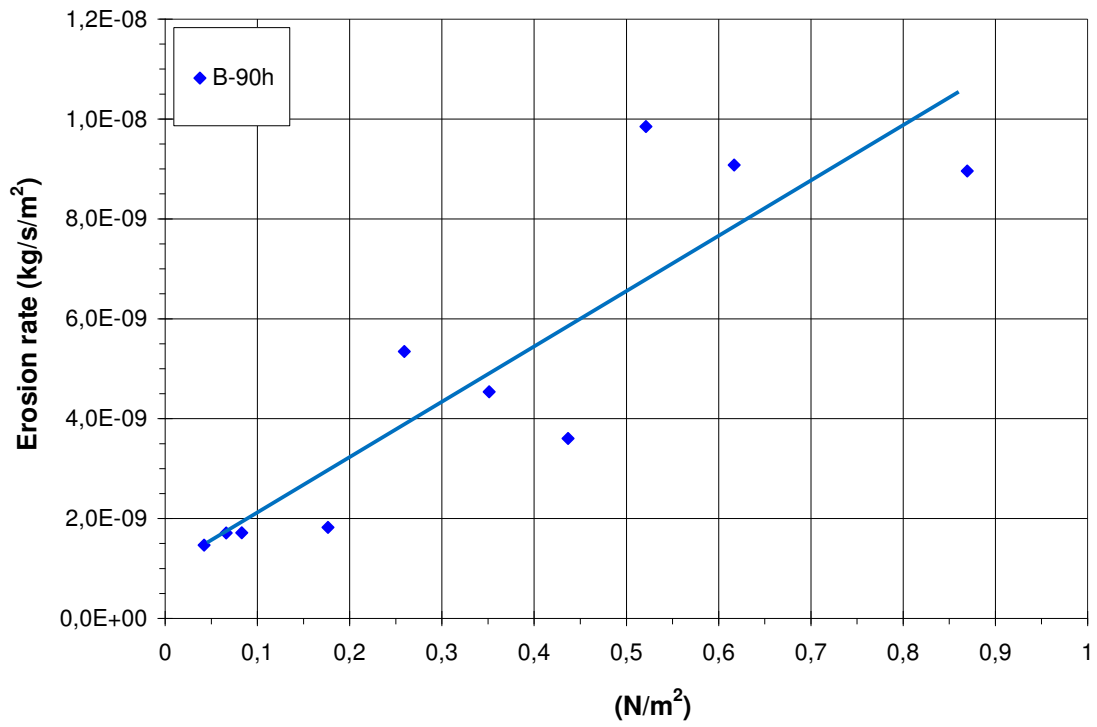


Figure II.30 Erosion rate versus hydraulic shear stress (B-90h)

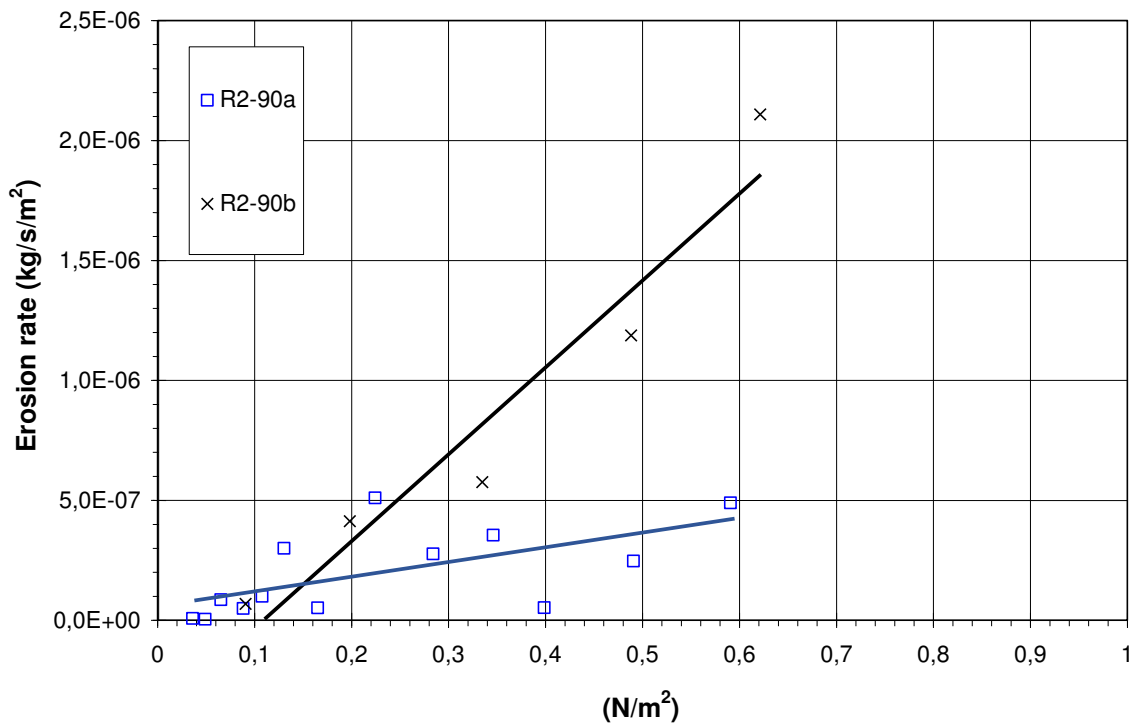


Figure II.31 Erosion rate versus hydraulic shear stress (R2-90a,b)

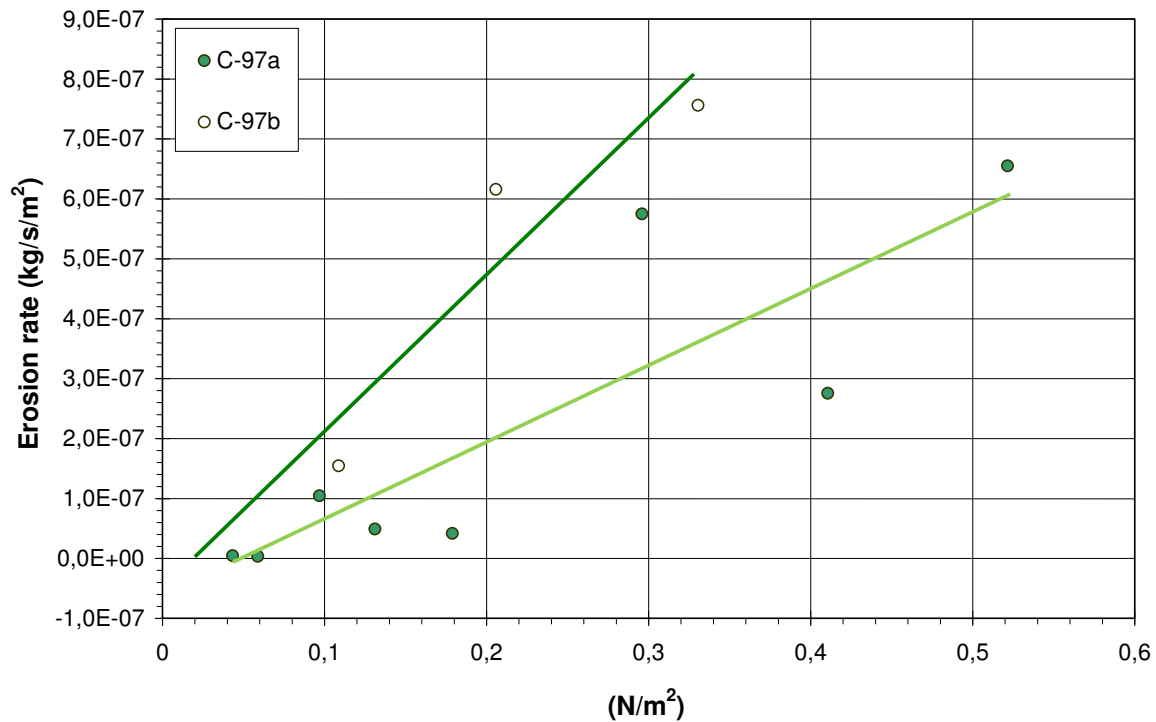


Figure II.32 Erosion rate versus hydraulic shear stress (C-97a,b)

Figure II.27 to Figure II.32 show determination of erosion coefficient k_d from linear correlation between hydraulic shear stress and erosion rate. To investigate the effect of hydraulic loading history to k_d and critical hydraulic loading history, only given specimens with different hydraulic loading history are presented. It is shown that for several specimens (A-90b, B-97a, B-90h, R2-90a), their extended slope lines cross the negative x-axis. Thus their critical hydraulic shear stresses are assumed equals to 0 for first approach (see Table II.4). The repeatability test of the specimen A-90a as shown in Figure II.27 is good, as the magnitude of the k_d slopes are similar.

However, due to predominant-filtration phase in a single-stage hydraulic gradient and imposed controlled flow rate condition tests, the determination of k_d value is more difficult as shown in Figure II.33. Thus only tests realized under multistage hydraulic gradient condition permit to draw a linear correlation between erosion rate and hydraulic shear stress to determine erosion coefficient k_d .

It is worth stressing the for the proposition of the classification of suffusion susceptibility, this hydraulic shear stress method in term of k_d value is not easy in the case of multi-stage hydraulic gradient and does not work in the case of single-stage hydraulic gradient and imposed controlled flow rate condition test.

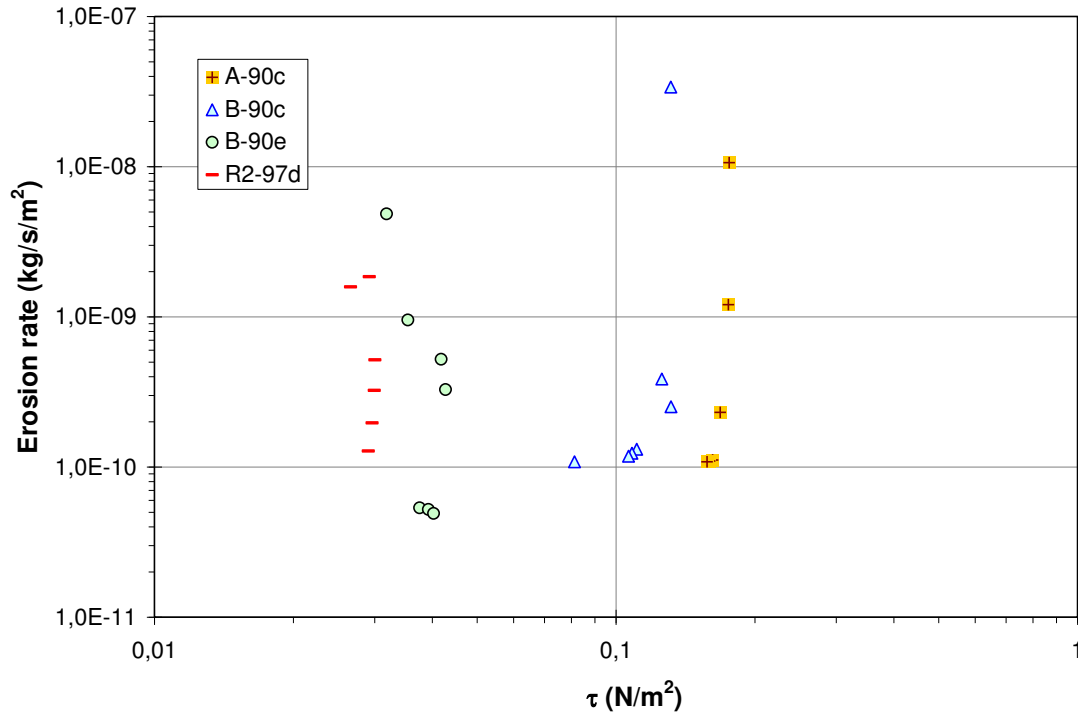


Figure II.33 Erosion rate versus hydraulic shear stress (A-90c – R2-97b)

Table II.4 Erosion coefficient and critical hydraulic shear stress for specimens subjected to multi-stage hydraulic gradients

Specimen	Erosion coefficient k_d			Critical hydraulic shear stress τ_c	
	(s/m)			(Pa)	
	Value	R^2	n	(1)	(2)
A-90a	1,00E-08	0.824	14	0.10	0.048
A-90b	2,00E-08	0.283	10	0	0.133
B-90a	2,00E-06	0.900	8	0.05	0.029
B-90h	1,00E-08	0.780	10	0	0.042
B-97a	2,00E-07	0.207	10	0	0.107
B-97b	1,00E-06	1	2	0.05	0.241
C-97a	1,00E-06	0.742	8	0.07	0.059
C-97b	3,00E-06	0.869	3	0.02	0.109
R2-90a	6,00E-07	0.405	14	0	0.026
R2-90b	4,00E-06	0.929	5	0.10	0.091

R : correlation coefficient, n : number of points

Table II.4 shows the comparison of erosion coefficient k_d and critical hydraulic shear stress τ_c of given specimens subjected to different hydraulic loading history in term of hydraulic gradient. With respect to hydraulic loading history, the erosion coefficient k_d of the specimens subjected to hydraulic gradient a is smaller than those of hydraulic gradient b ($k_d a < k_d b$). It can be noticed that the critical hydraulic shear stress of the specimens subjected to hydraulic gradient a is smaller than those of hydraulic gradient b ($\tau_c a < \tau_c b$) with the second approach. It is in a good agreement with the results of in term of hydraulic gradients. It seems that the development of suffusion appears smaller under hydraulic loading history a in term of both hydraulic gradient and hydraulic shear stress.

In regard with fine content, the k_d value specimen A (20%) is smaller than that of specimen B (25%) and C (29%). In addition, given soil density and hydraulic loading history, the critical hydraulic shear stress τ_c of specimen $A-90a$ is smaller that of $B-90a$, $\tau_c B-97a < \tau_c C-97a$, and $\tau_c B-97b < \tau_c C-97b$. Thus, it seems that specimens with lower fine content are more resistant.

2.6.2.2 Power based method

The hydraulic loading acting on grains can also be expressed by hydraulic erosion power as presented in the Eq. II.20. Figure II.34 to Figure II.39 show the relationship between erosion rate and erosion power for all the specimens.

With such approach, the evolution of erosion rate versus erosion power seems to be similar to those of erosion rate versus hydraulic shear stress. It is shown that erosion rate does not always increase when erosion power increases. The evolution of all the specimens imposed by multi-stage hydraulic gradients in the diagram of erosion power versus erosion rate can be also distinguished into three phases. However, the specimens subjected to single-stage hydraulic gradients and flow rate condition erosion rate progressively decreases (see in **Annex** section). Similar to hydraulic shear stress method, for the proposition of the classification of suffusion susceptibility, the flow power approach in term of the determination of slope is not easy in the case of multi-stage hydraulic gradient and does not work in the case of single-stage hydraulic gradient and imposed controlled flow rate condition test.

In conclusion, from the interpretation of methods both hydraulic shear stress and flow power, the approach of erosion rate seems not to work. This is because temporal measurement cannot follow all suffusion process from initiation to development.

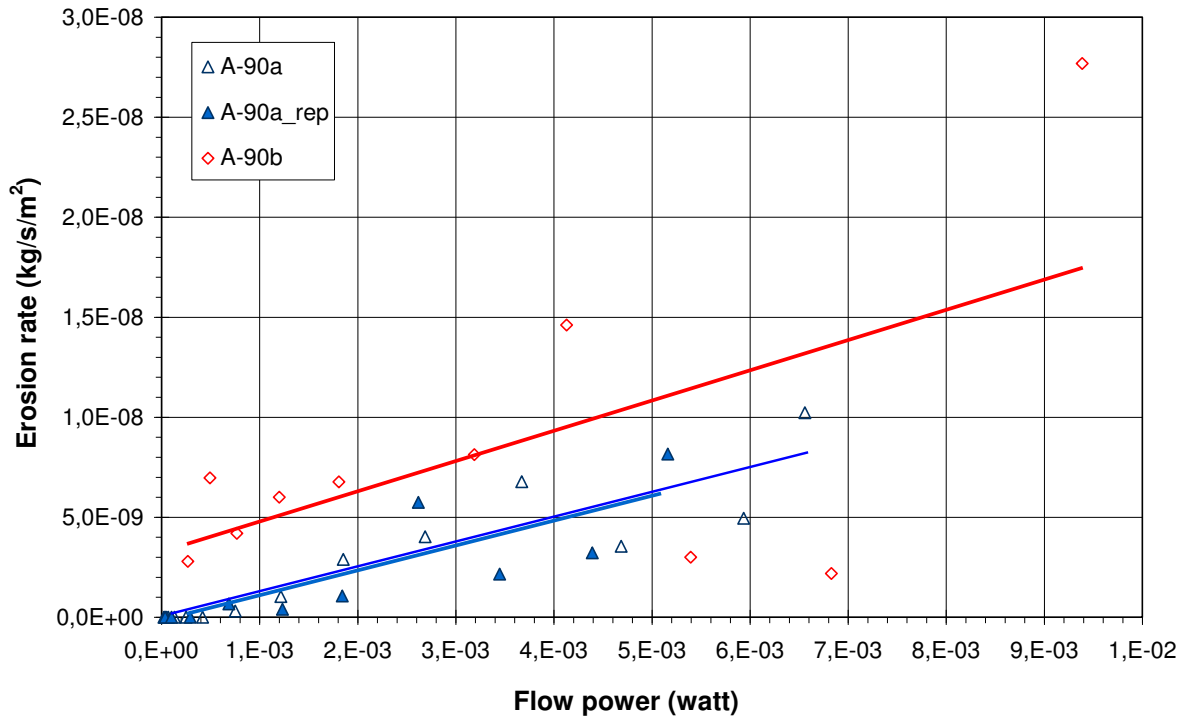


Figure II.34 Erosion rate versus flow power (A-90a,a_rep,b)

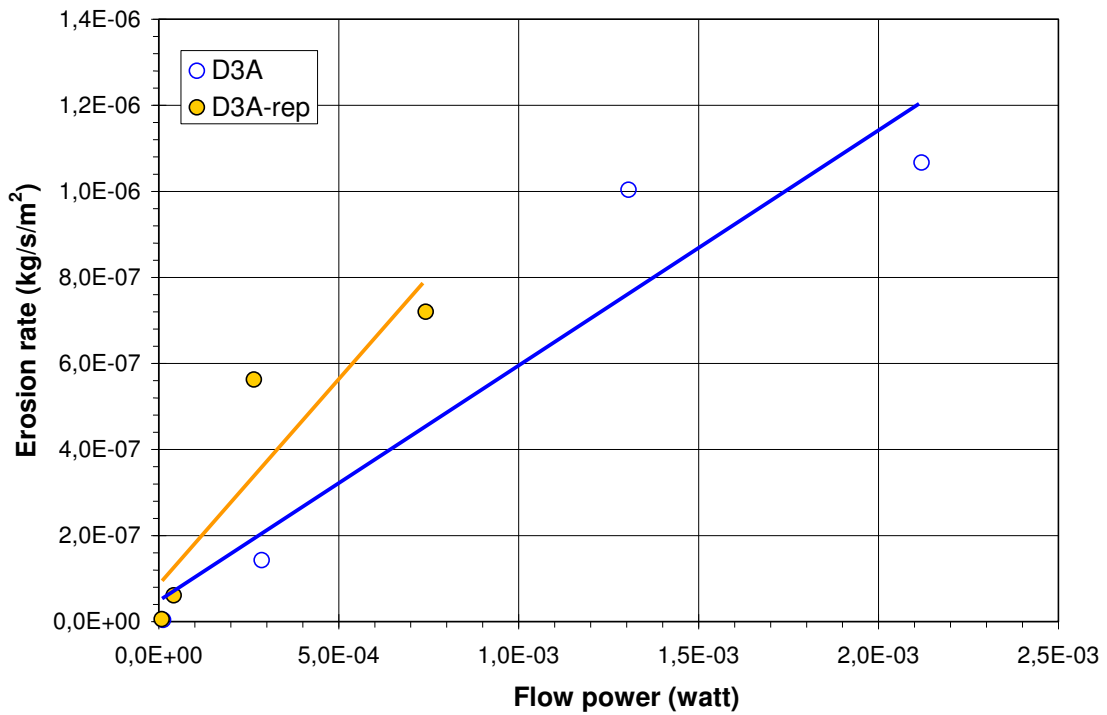


Figure II.35 Erosion rate versus flow power (D3A, D3Arep)

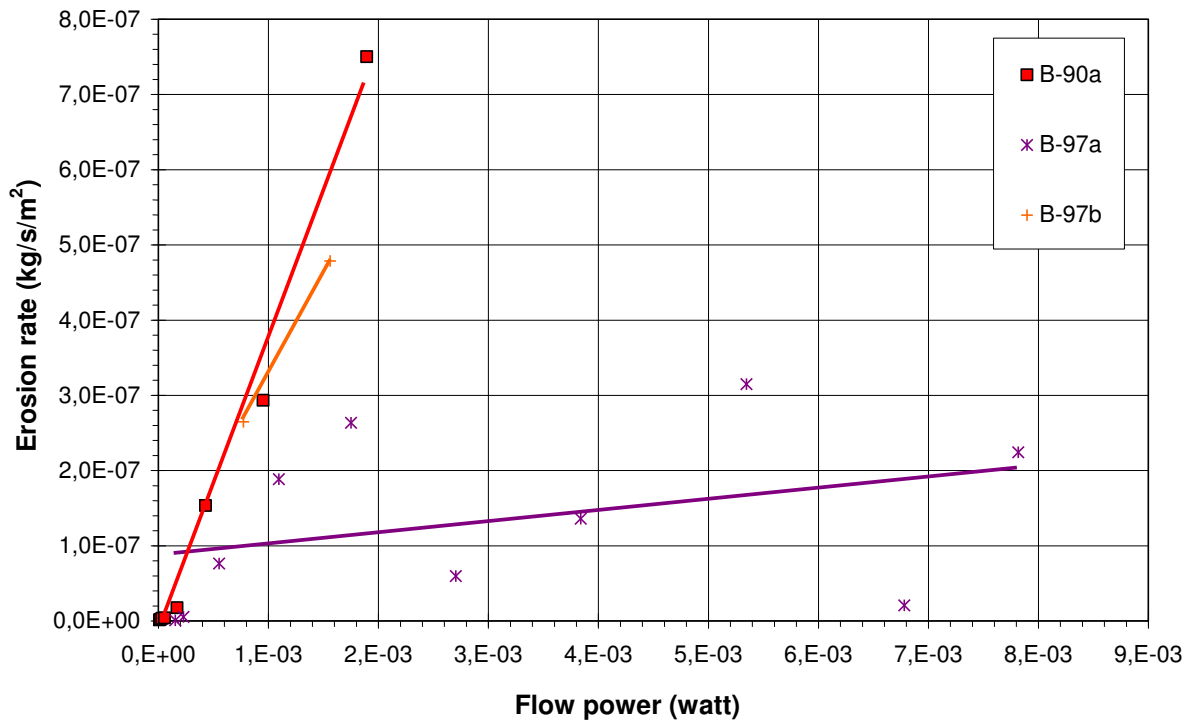


Figure II.36 Erosion rate versus flow power (B-90a; B-97a,b)

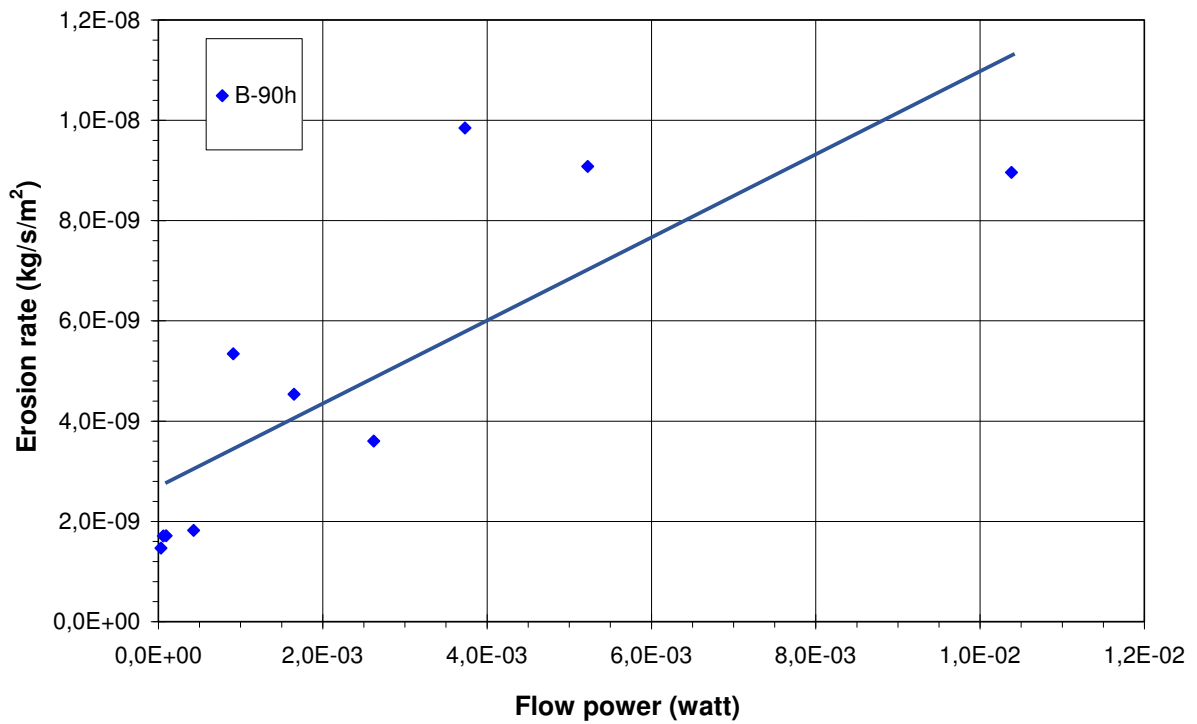


Figure II.37 Erosion rate versus flow power (B-90h)

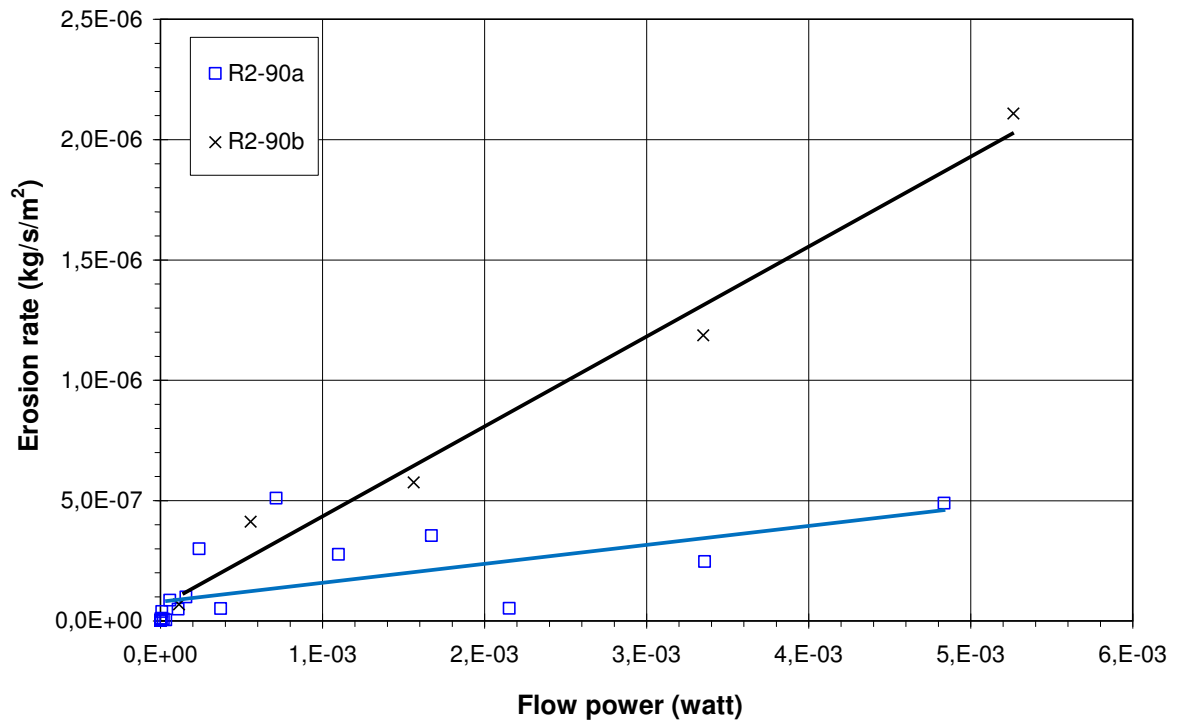


Figure II.38 Erosion rate versus flow power (R2-90a,b)

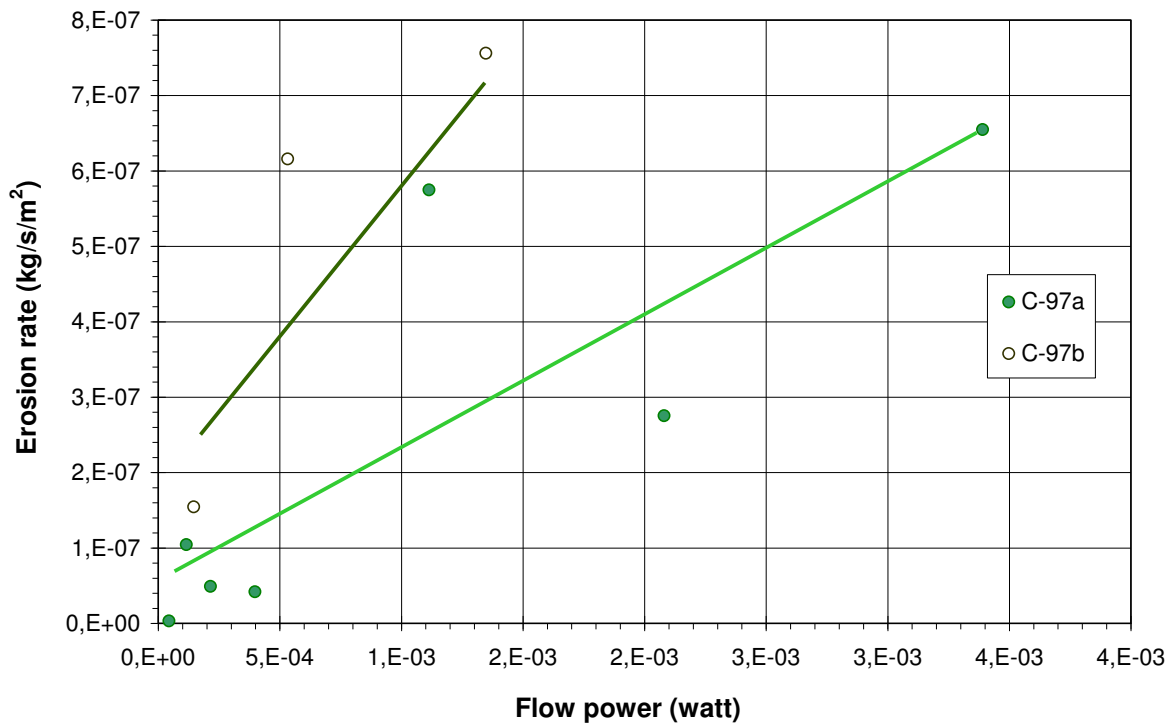


Figure II.39 Erosion rate versus flow power (C-97a,b)

2.6.2.3 Energy based method

With the objective to take into account the complexity of suffusion process, Marot et al. (2011) proposed a new method in order to take into account the whole hydraulic loading history based on the energy dissipated by the fluid seepage. This method use two different independent parameters: (i) the cumulative expanded energy to characterize hydraulic loading and (ii) the cumulative eroded dry mass to characterize soil response. This approach is based on the assumptions: 1) the system is considered as adiabatic, 2) the temperature and 3) the internal energy with time are assumed to be constant for the volume, the flow is in steady state condition. In the case of the suffusion process, due to relatively low value of the Reynolds number, it is assumed that intrafluid energy dissipation by turbulence is neglected and energy is mainly dissipated at the vicinity of the fluid-solid interface (Marot et al., 2011). Energy-based approach is related to the water seepage power called as “erosion power” that can be expressed by Eq. II.20. The energy dissipation, $E_{erosion}$ is the temporal integration of the instantaneous erosion power for the test duration.

Figure II.40 to Figure II.45 show the relationship between cumulative expanded energy and cumulative eroded mass in log-log scale. However such relationship for other tested specimens is presented in **Annex** section. The points highlighted by arrows correspond to the end of development of suffusion (i.e. time from which hydraulic conductivity is stabilized) in order to classify the soil susceptibility. It is worth noting that the points before and after the arrows do not represent the soil susceptibility. The eroded mass in the beginning may be attributed to loss mass during saturation phase and during filtration process. The after-arrow points also do not represent the soil susceptibility since they correspond to the steady state. If the series of final points is taken into account, the soil susceptibility may become less erodible. For some tests without arrows, their susceptibility is defined at the last point. For the specimens subjected to single-stage hydraulic gradient and imposed controlled flow rate condition test, the last point is taken into account as a representative of the soil susceptibility.

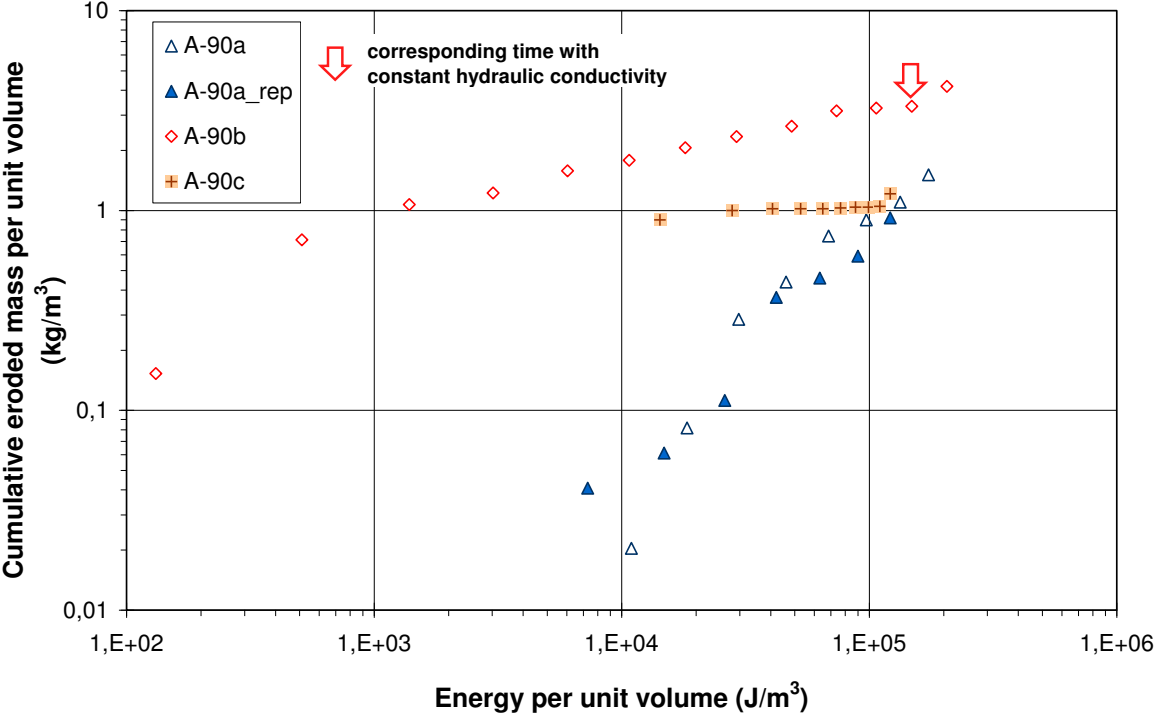


Figure II.40 Cumulative eroded dry mass per unit volume versus cumulative expanded energy per unit volume (A-90a,a-rep,b,c)

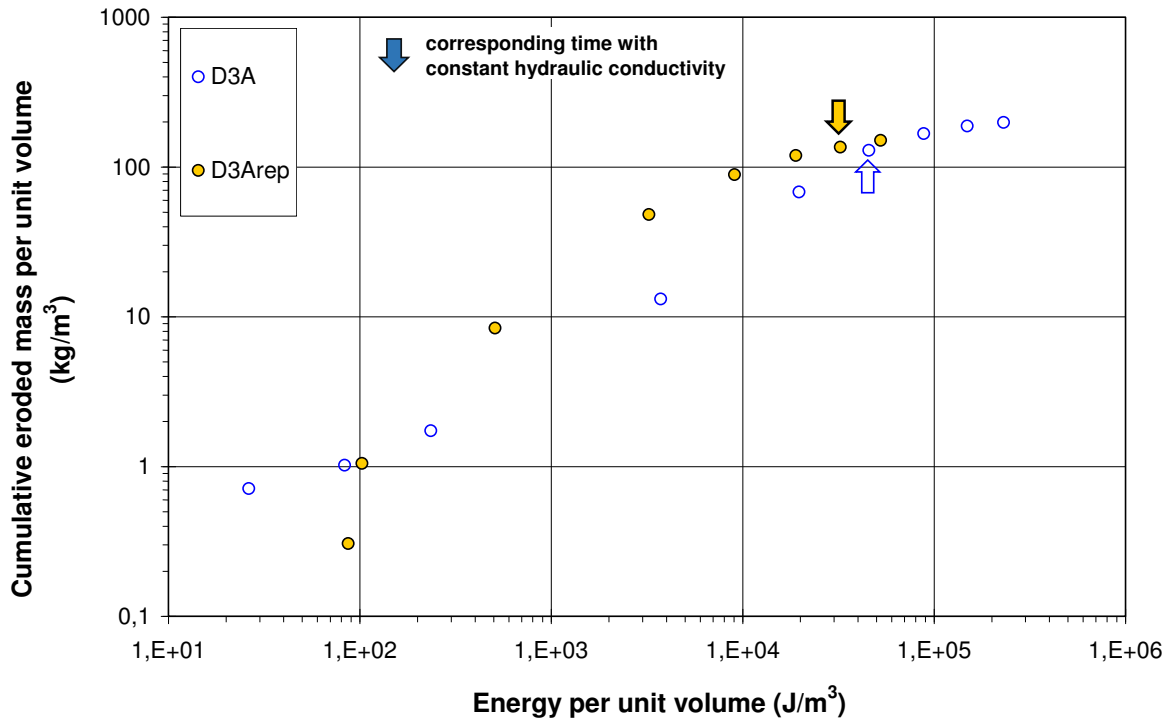


Figure II.41 Cumulative eroded dry mass per unit volume versus cumulative expanded energy per unit volume (D3A, D3Arep)

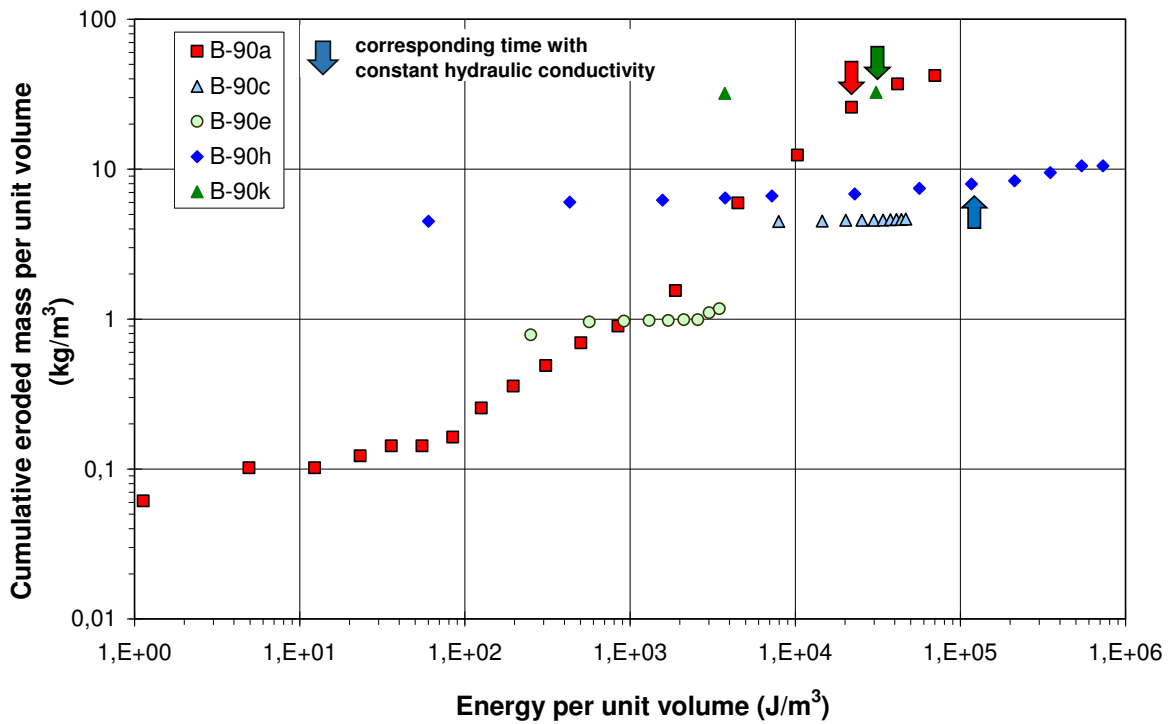


Figure II.42 Cumulative eroded dry mass per unit volume versus cumulative expanded energy per unit volume (B-90a,c,e,h,k)

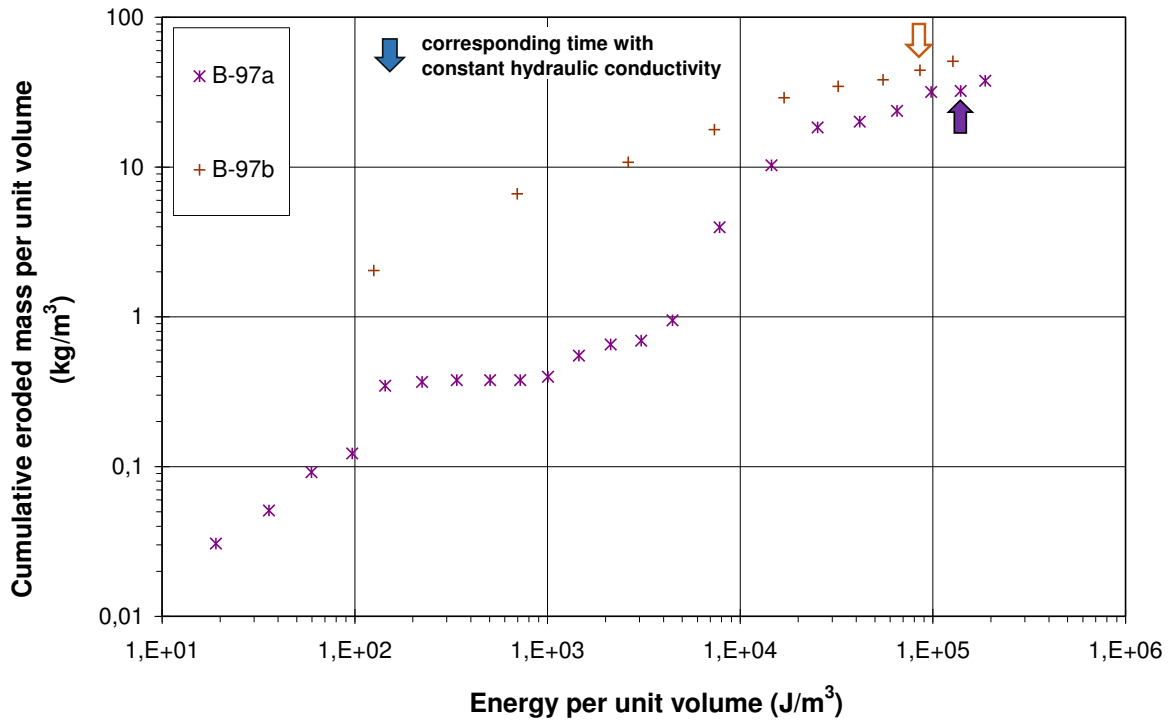


Figure II.43 Cumulative eroded dry mass per unit volume versus cumulative expanded energy per unit volume (B-97a,b)

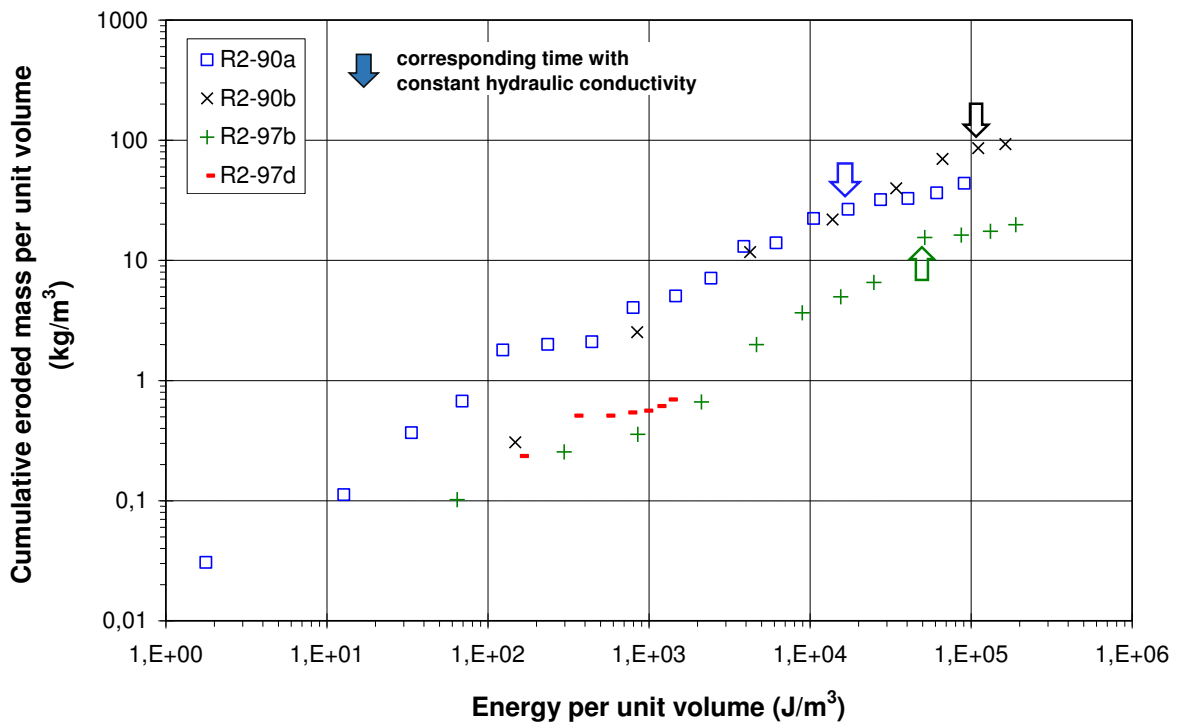


Figure II.44 Cumulative eroded dry mass per unit volume versus cumulative expanded energy per unit volume (R2-90a,b; R2-97a,b)

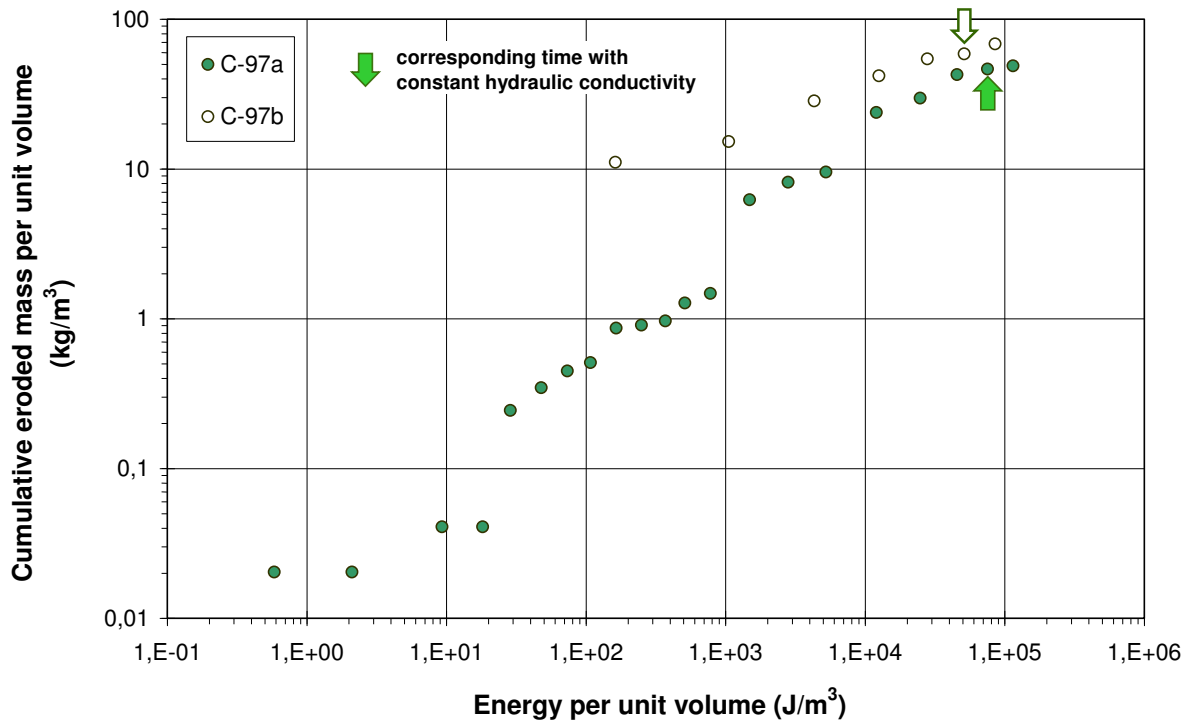


Figure II.45 Cumulative eroded dry mass per unit volume versus cumulative expanded energy per unit volume (C-97a,b)

The energy-based method that uses cumulative values can follow all the evolution of suffusion process from initiation to development. Thus the determination of erosion coefficient (from the plot of linear approximation of cumulative eroded mass and cumulative energy) is more possible and easier than that of the methods of hydraulic shear stress and flow power. All tests in single stage hydraulic gradient condition tests and constant flow rate condition tests can be studied with energy based method, but they do not work if tests are carried out under hydraulic shear stress method or flow power based method.

2.7 Grain size distribution of post-test

In order to follow the process of suffusion with respect to the transport of the fine fraction within the soil, a test on grain size distribution after test was carried out. After seepage test, the soil was divided into two parts: top and base with the same portions. Figure II.46 to Figure II.48 show soil gradings of the post-test of the specimens *A-90b*, *B-90a* and *C-97a*. Each diagram shows the grain size distributions of before (initial condition) and after seepage test. Given the specimen *A-90b* consisting 20% fine fraction, fine fraction in the top side decreases whereas in the base side increases. It seems that the water flow imposed during seepage test can detach and transport some fine fraction to the base level. The percentage of fine fraction in the base level higher than that of the initial condition can be attributed to the supply of fine fraction from the top level whereas only small quantity of fine fraction erosion in the base level. Thus the supply and filtration induce the increase of the fine fraction in the base level.

However, given the specimens *B-90a* (25% fine fraction) and *C-97a* (29% fine fraction), the percentage of fine fraction in both top and base level decreases (less than that of initial condition). In the base level, even though there is a supply of fine fraction from the top level, the percentage of fine fraction still decreases. This can be attributed to a significant erosion of fine fraction in the base level.

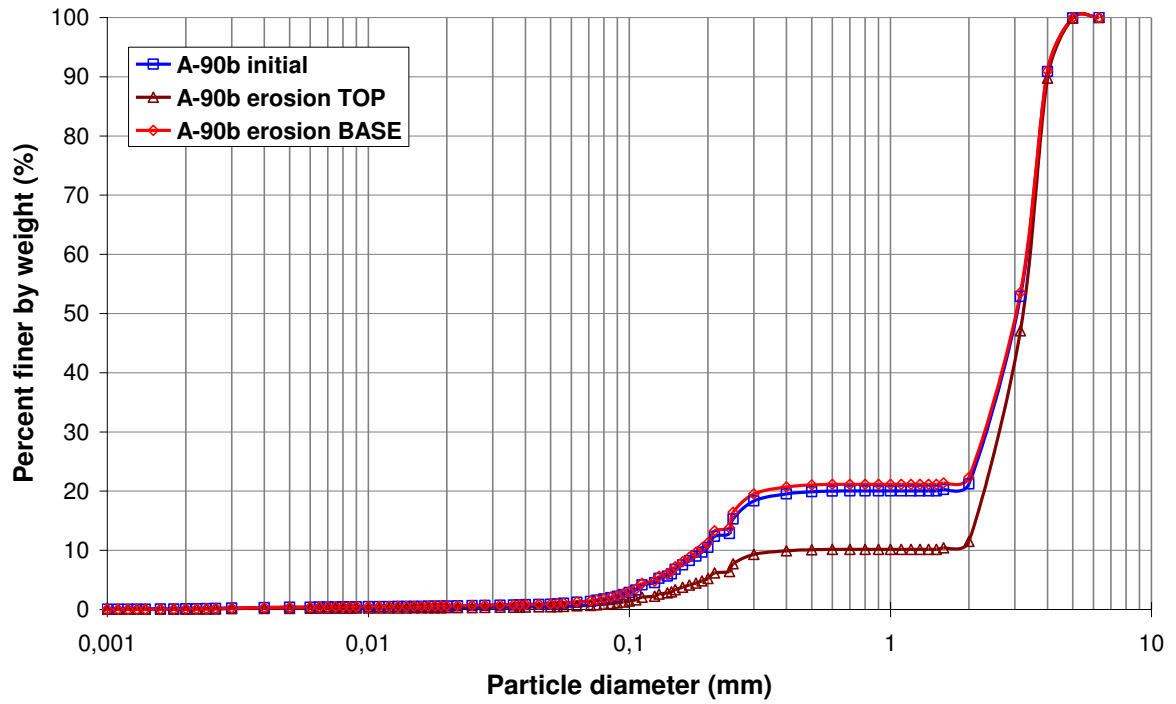


Figure II.46 Grain size distribution after test (A-90b)

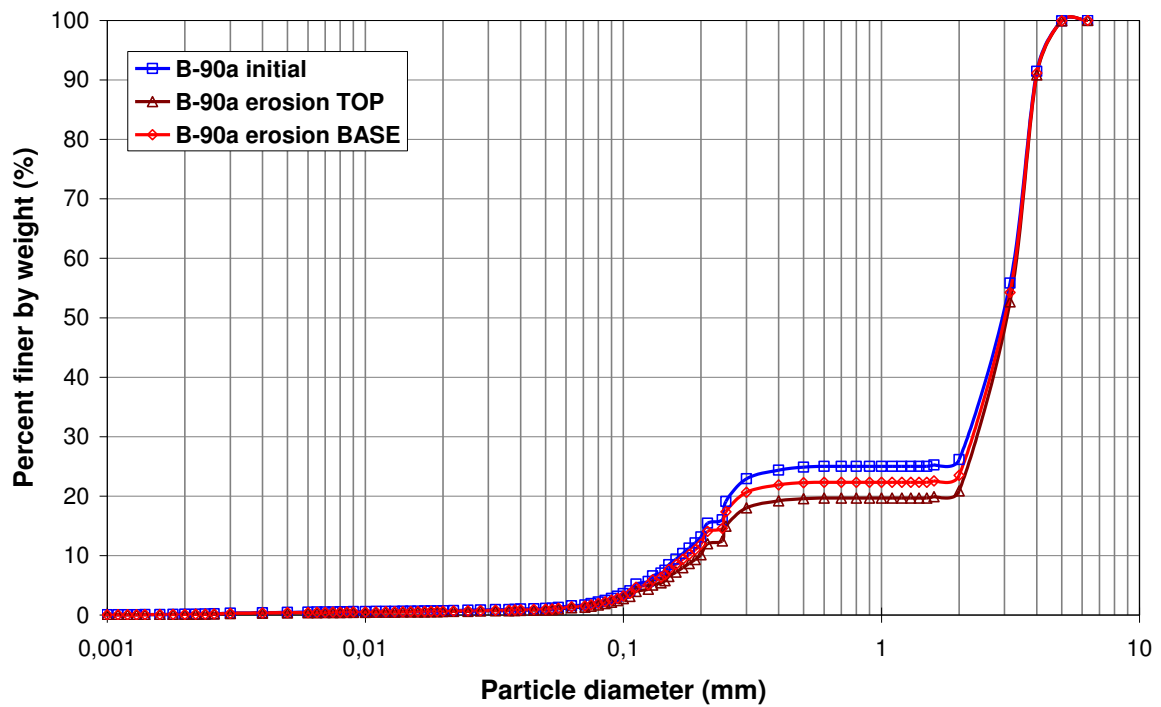


Figure II.47 Grain size distribution after test (B-90b)

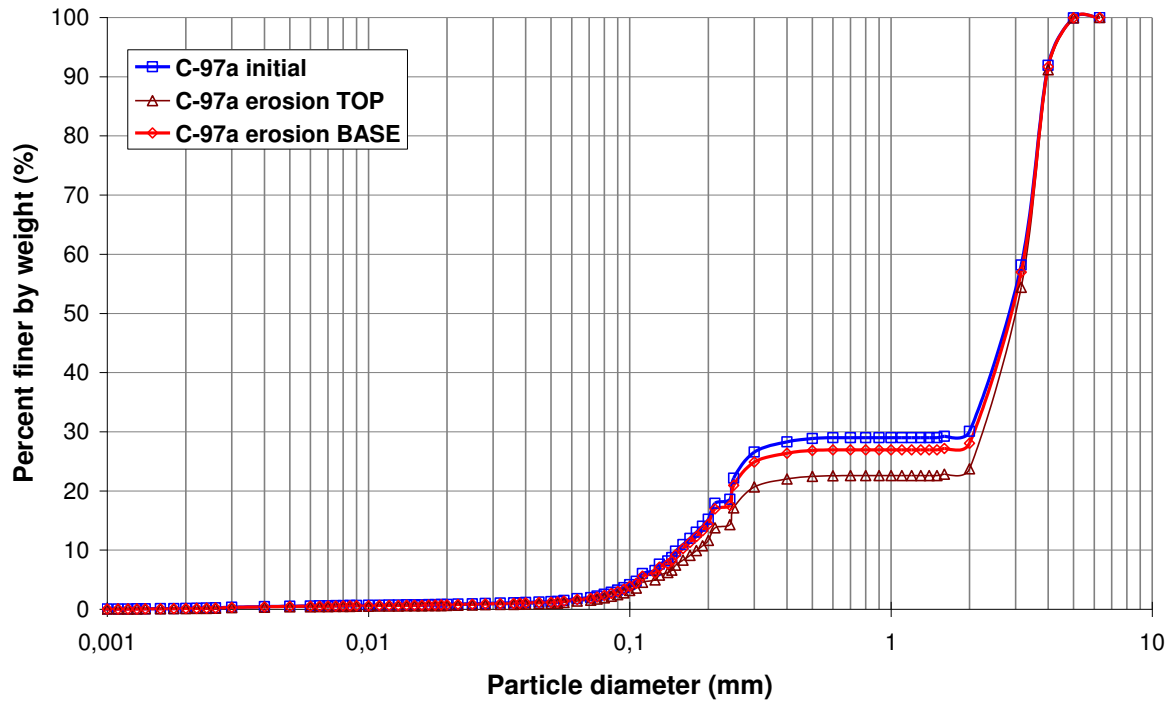


Figure II.48 Grain size distribution after test (C-97a)

2.8 Proposition of classification of suffusion susceptibility

Erosion susceptibility classifications were proposed by different methods in the case of interface erosion. Thus the study on characterization of suffusion susceptibility and its classification are far to be completed.

With the objective to propose a classification of suffusion susceptibility, two approaches are used: 1) the approach of the relation between erosion coefficient k_d and critical hydraulic shear stress 2) energy-based approach. Based on the test results on a series of tested specimens (for the first approach) and with the addition of the test results by other researchers (for the second approach), the authors propose two classification diagram of suffusion susceptibility based on the aforementioned approaches.

2.8.1 Approach of erosion coefficient k_d versus critical hydraulic shear stress (τ_c)

We propose a classification of suffusion susceptibility that is divided into five classes from resistant to highly erodible as presented in Figure II.49 to Figure II.51. It is worth stressing that erosion coefficient k_d is defined from linear correlation between erosion rate and hydraulic shear stress in which critical hydraulic shear stress determined as an initial point corresponding to the onset of suffusion. Due to the difficulty of determination of erosion coefficient k_d for the specimens subjected to single-stage hydraulic gradient and flow rate condition, thus only the specimens subjected to multi-stage hydraulic gradients are presented.

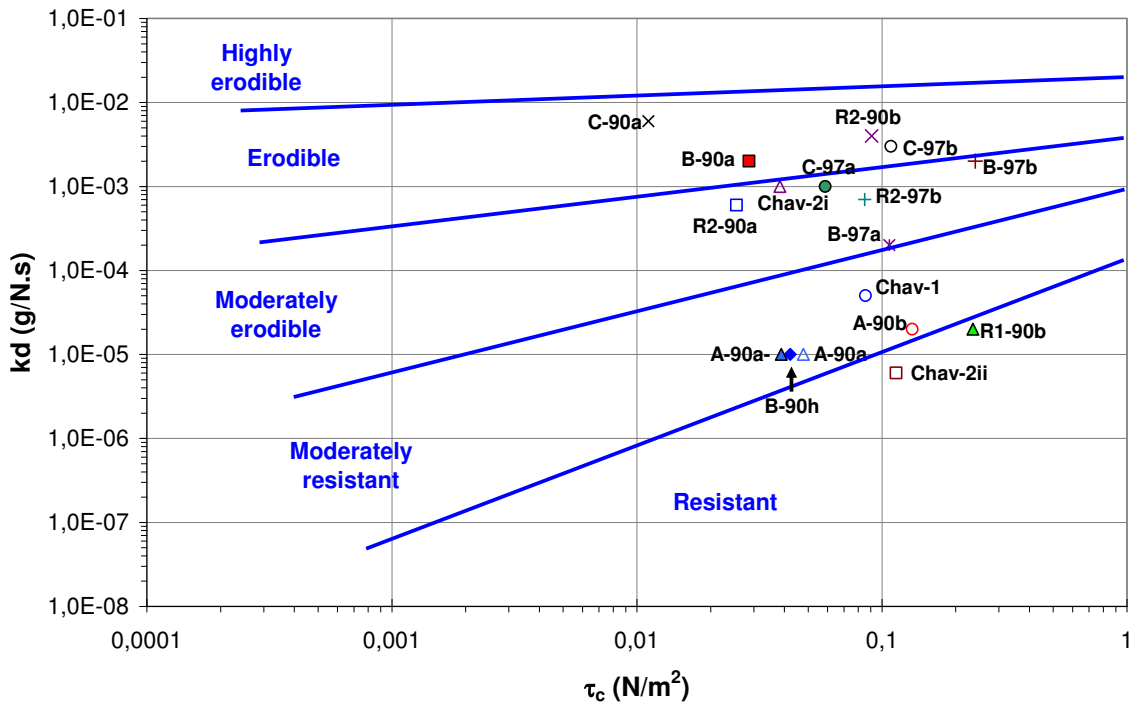


Figure II.49 Proposed classification of suffusion susceptibility based on the approach of erosion coefficient k_d versus critical hydraulic shear stress (A-90a – R2-97b)

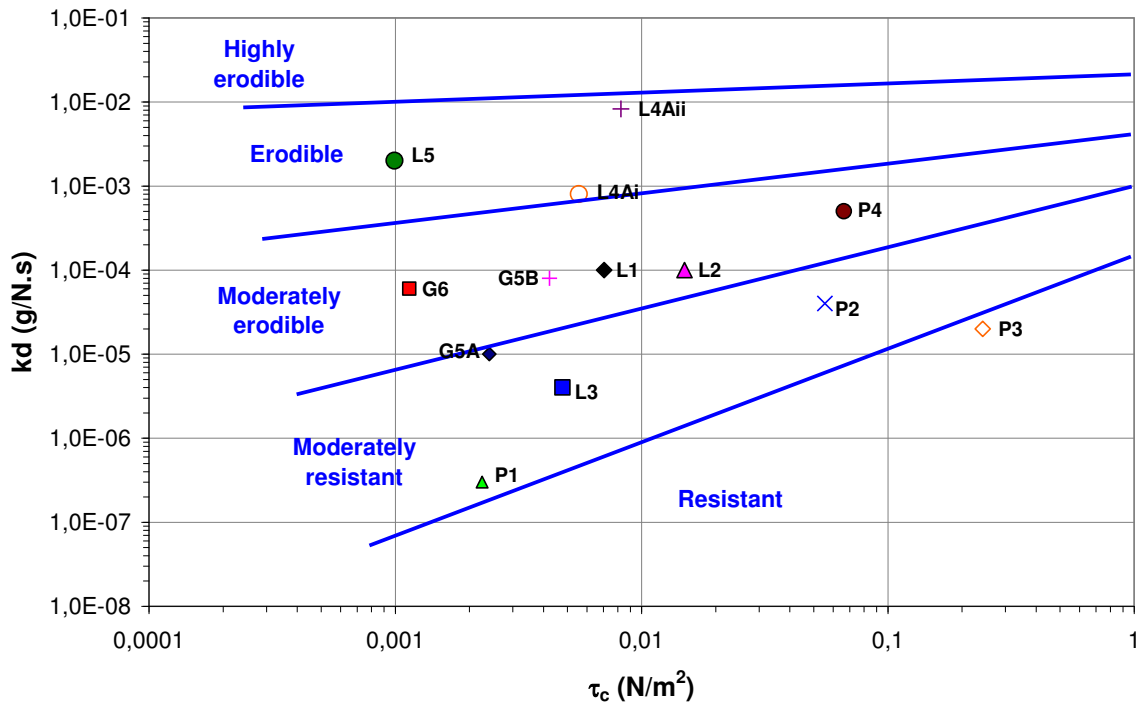


Figure II.50 Proposed classification of suffusion susceptibility based on the approach of erosion coefficient k_d versus critical hydraulic shear stress (G5A – L5)

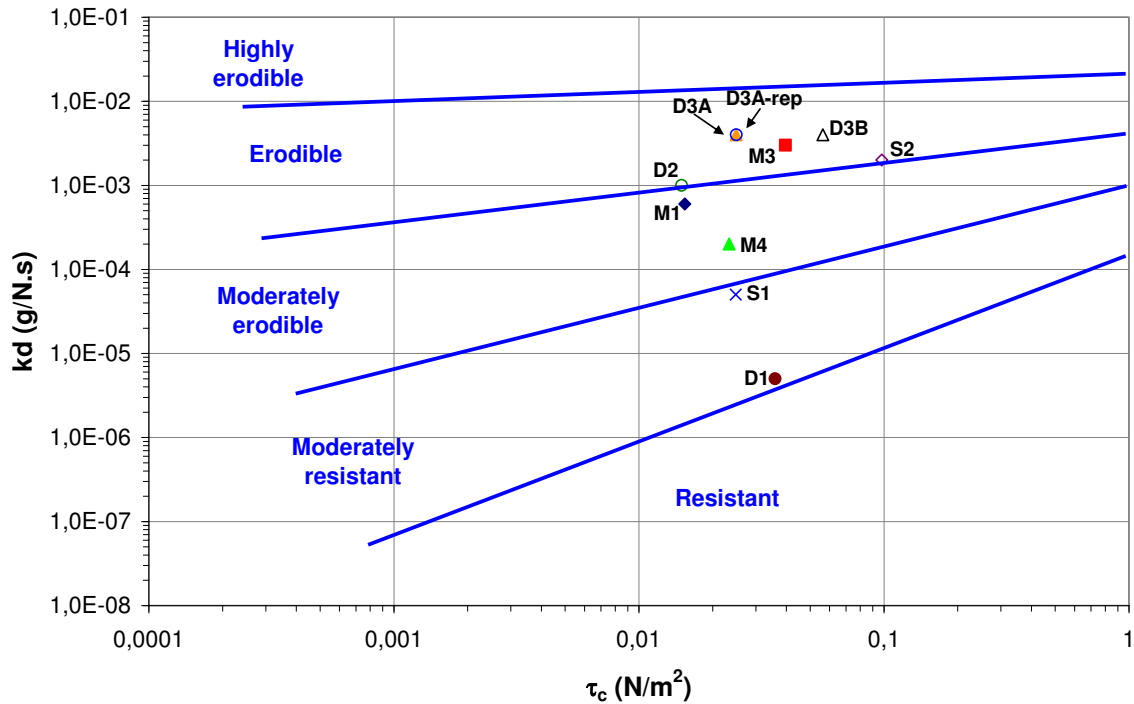


Figure II.51 Proposed classification of suffusion susceptibility based on the approach of erosion coefficient k_d versus critical hydraulic shear stress (D1 – S2)

2.8.2 Energy-based approach

In order to provide a classification of suffusion susceptibility, results from all tested specimens and also results of reference specimens from Bendahmane et al. (2008) and Nguyen et al. (2012) are presented. Three grain size distribution of reference soils: *K10L90* and *K20L80* (Bendahmane et al., 2008) and *KPR25F75* (Nguyen et al., 2012) are shown in Figure II.52. All the reference soils are mixtures of sand and clay that consist of 10% to 25% of clay, respectively. Table II.5 shows the properties of specimens subjected to single-stage hydraulic gradient (13 specimens) and flow rate controlled condition (3 specimens).

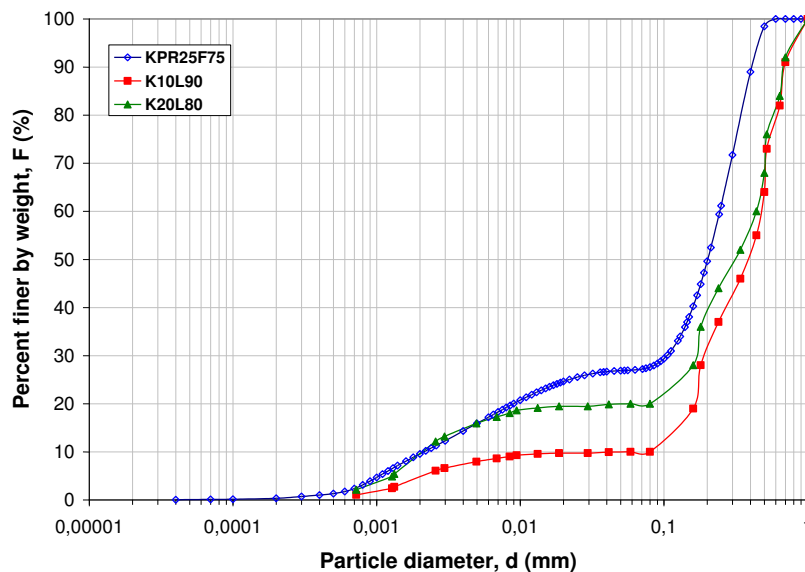


Figure II.52 Grain size distribution of soils *K10L90*, *K20L80* and *KPR25F75* (After Bendahmane et al., 2008 and Nguyen et al., 2012)

Table II.5 Properties of reference specimens by Bendahmane et al., 2008 and Nguyen et al., 2012

Soil reference in paper	Specimen reference in paper	Initial dry density (kN/m ³)	Applied hydraulic gradient i	Injected flow (ml/min)	Confining pressure (kPa)	Test duration (min)
K10L90 ⁽¹⁾	A1	17	20	-	200	10
	A2	17	20	-	200	18
	A4	17	40	-	200	43
	A5	17	2	-	100	32
	A8	17	20	-	100	33
	A11	17	60	-	100	32
	A14	17	100	-	100	36
K20L80 ⁽¹⁾	A27	17	20	-	100	30
	A28	17	60	-	100	34
KPR25F75 ⁽²⁾	F14	16	5	-	15	42
	F15	16	7	-	15	88
	F13	16	10	-	15	121
	F10	16	18	-	15	1395
	F20	16	-	1.2	15	385
	F17	16	-	1.4	15	210
	F23	16	-	1.6	15	200

⁽¹⁾ Bendahmane et al. (2008) and ⁽²⁾ Nguyen et al. (2012)

Figure II.53 to Figure II.55 show the variation of cumulative eroded mass and cumulative expanded energy per volume for all the reference specimens. The arrow signs correspond to stabilized hydraulic conductivity. It can be noticed that if we compare the tested specimens and the reference specimens, the cumulative eroded mass of cohesive soil is much less than that of sandy-gravel soil with a factor of 100.

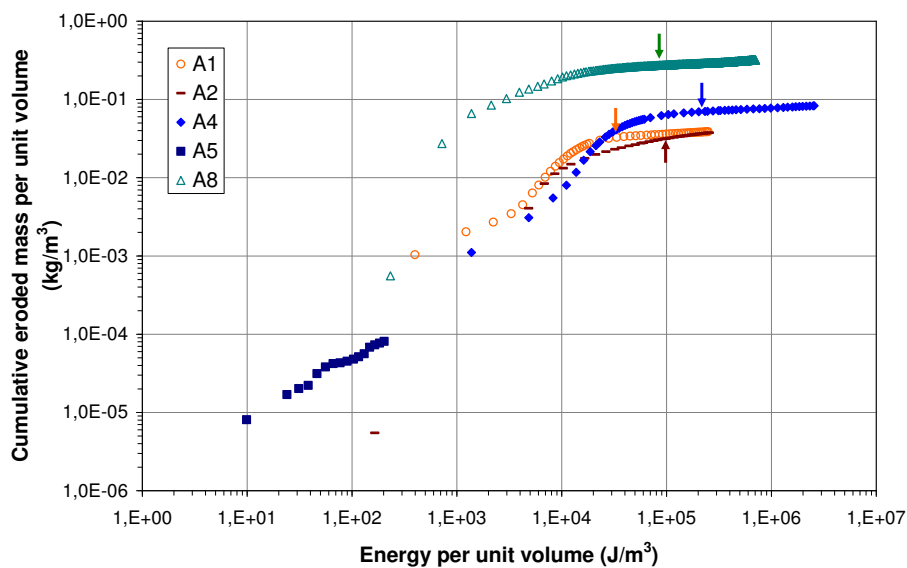


Figure II.53 Cumulative eroded dry mass versus cumulative energy (A1 – A8)

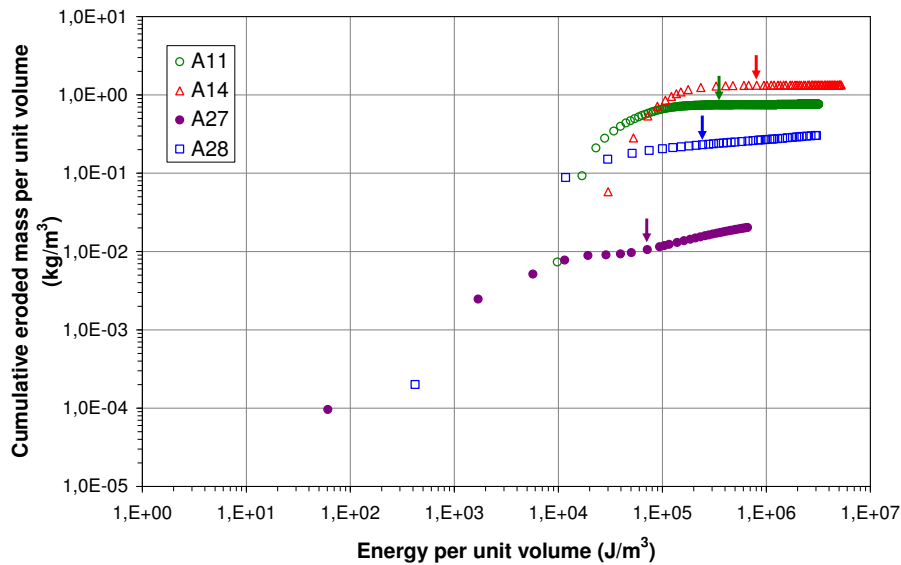


Figure II.54 Cumulative eroded dry mass versus cumulative energy (A11 – A28)

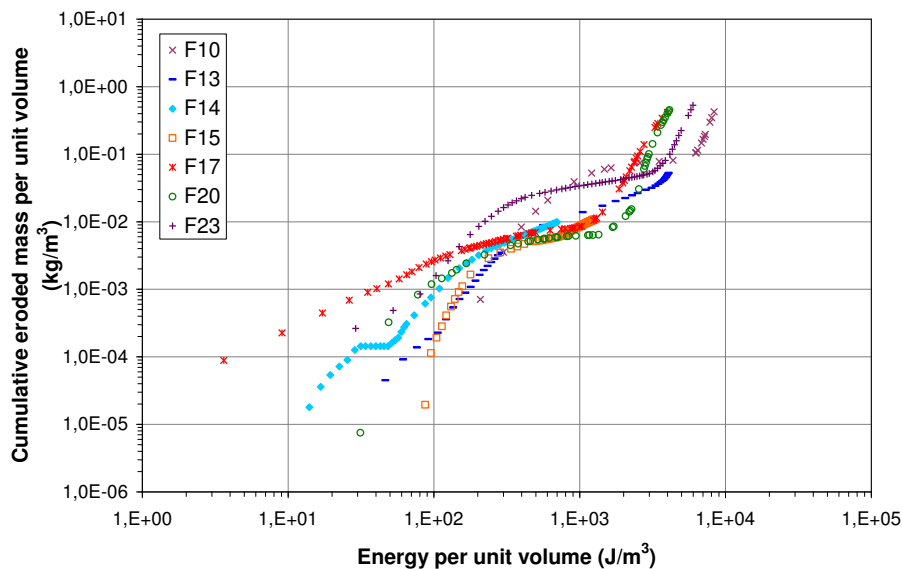


Figure II.55 Cumulative eroded dry mass versus cumulative energy (F10 – F23)

For the size of tested specimens and the duration of realized tests, a large range of cumulative expanded energy and a large range of cumulative eroded mass are obtained: from 200.8 J/m^3 to $1.218 \cdot 10^6 \text{ J/m}^3$ and from $8.071 \cdot 10^{-5} \text{ kg/m}^3$ to 150.48 kg/m^3 , respectively. According to these results, six categories of soil susceptibility for suffusion process are proposed: from highly resistant to highly erodible. Figure II.56 to Figure II.60 shows the classification of suffusion susceptibility for all the tested specimens and the reference specimens.

From the classification diagram, Index of suffusion resistance, I_β based on the equation of energy-based approach by Marot et al. (2011) (see Eq. II.28) is proposed as presented in Table II.6. Six ranges of suffusion resistance index, I_β are proposed, with I_β smaller than 2 defined as highly erodible and larger than 6 as highly resistant.

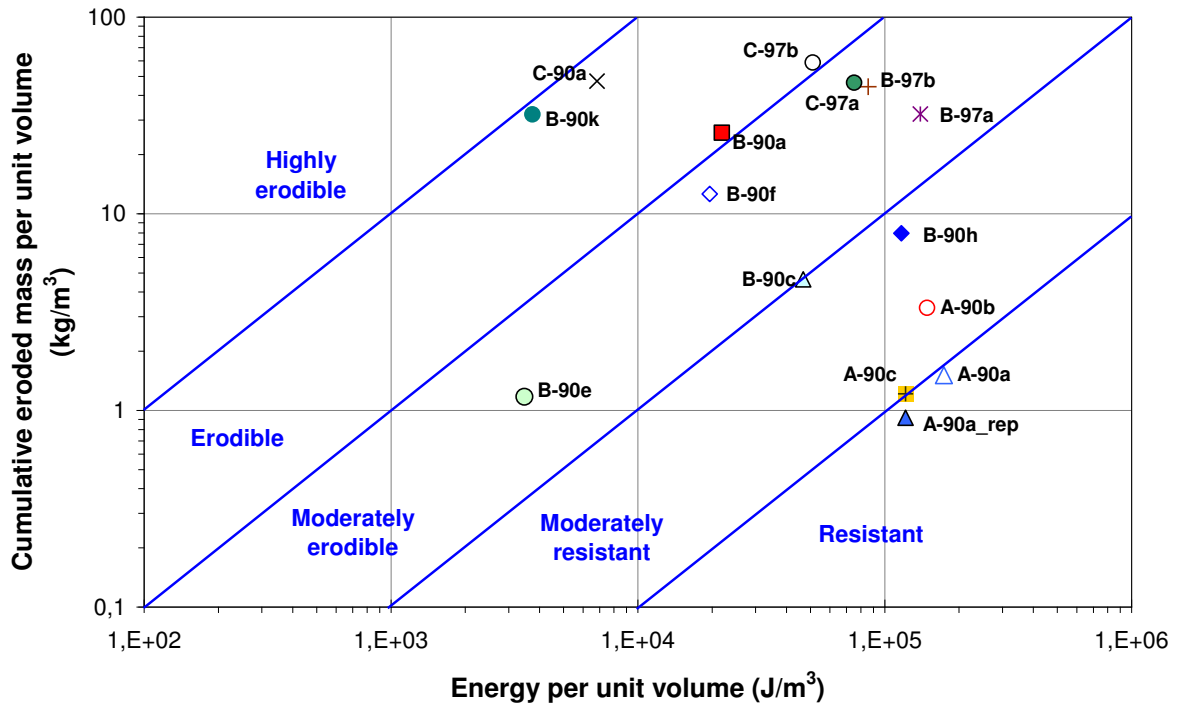


Figure II.56 Proposed classification diagram of suffusion susceptibility - energy-based approach (A-90c – C-97b)

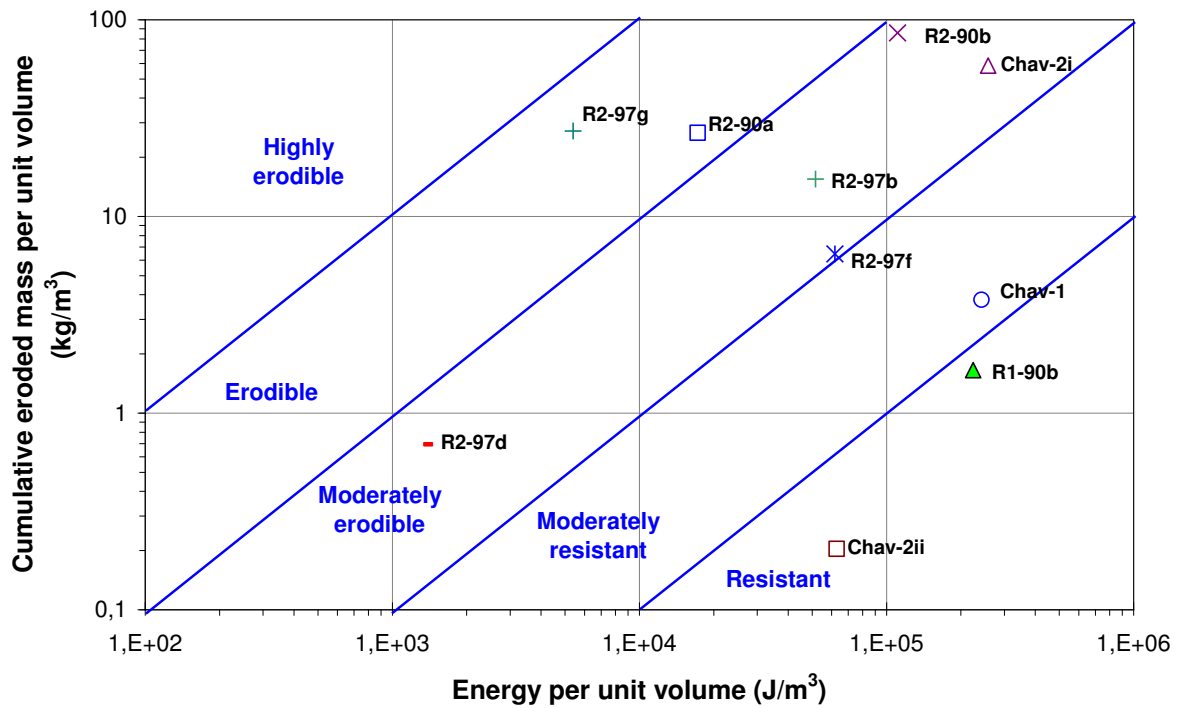


Figure II.57 Proposed classification diagram of suffusion susceptibility - energy-based approach (Chav-2i – R2-97g)

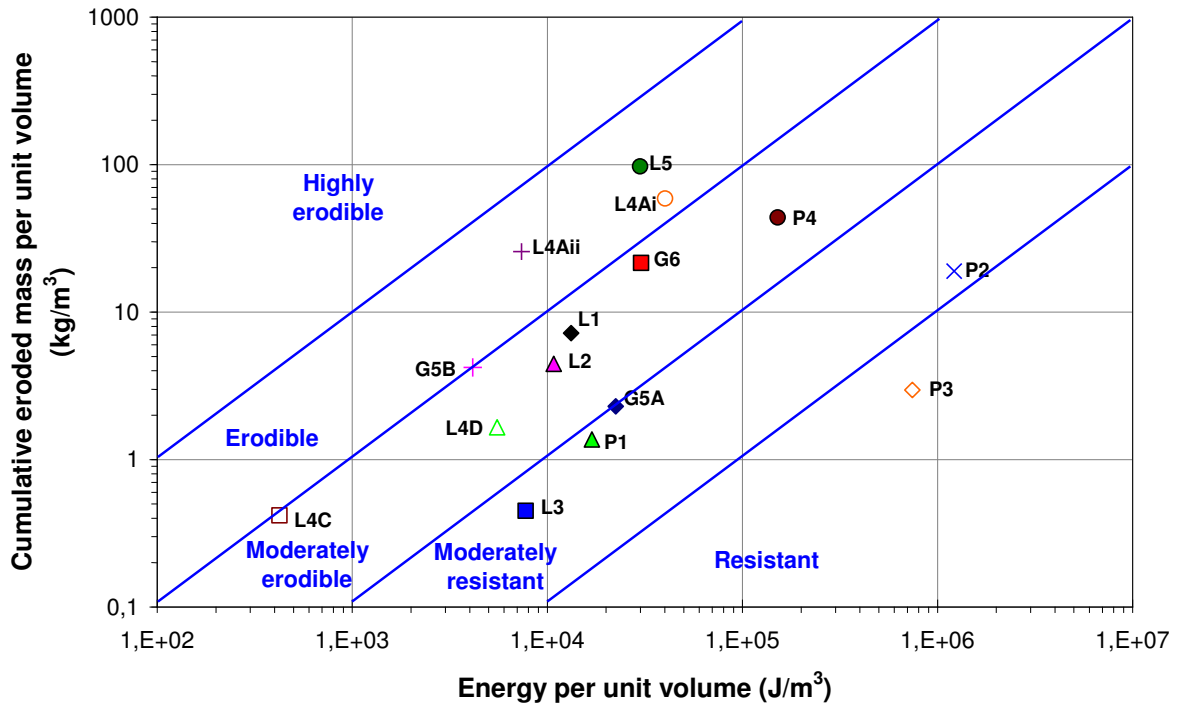


Figure II.58 Proposed classification diagram of suffusion susceptibility - energy-based approach (G5A – L5)

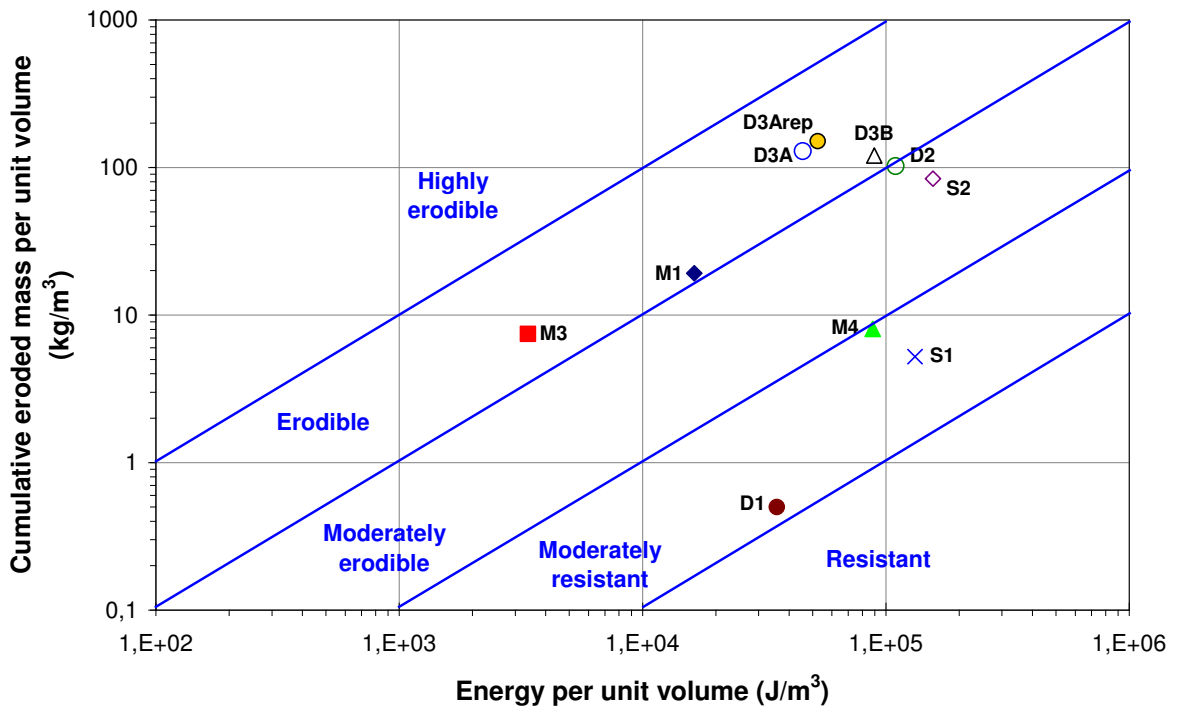


Figure II.59 Proposed classification diagram of suffusion susceptibility - energy-based approach (D1 – S2)

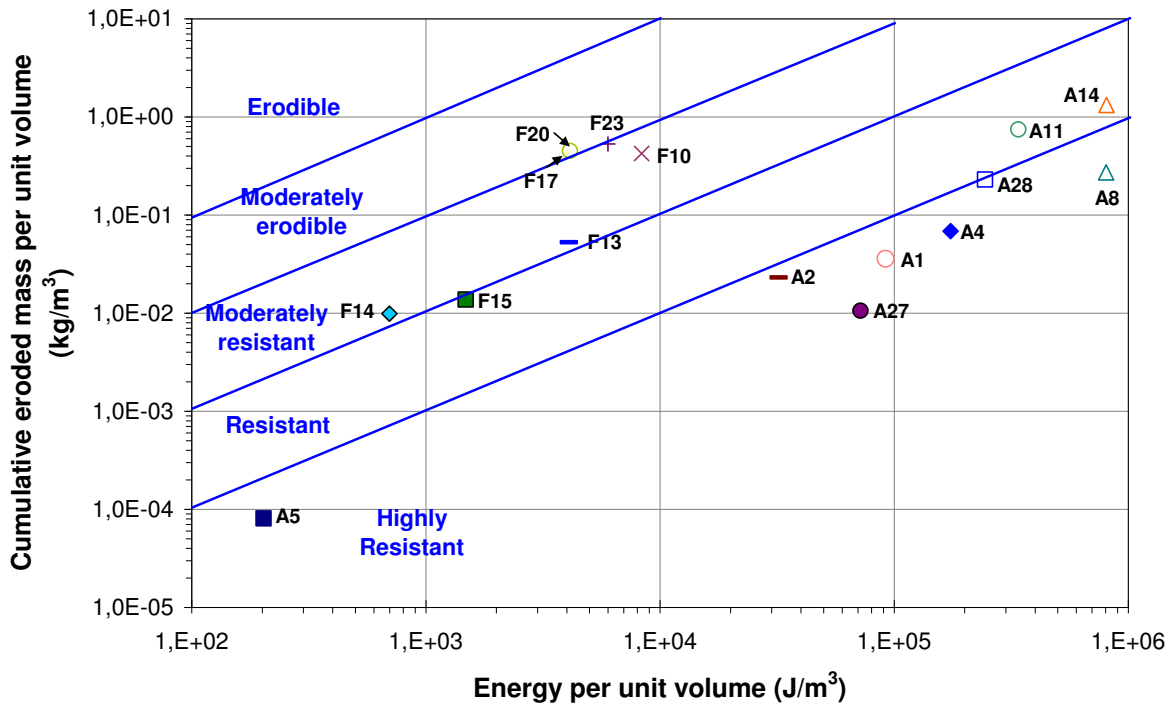


Figure II.60 Proposed classification diagram of suffusion susceptibility - energy-based approach (A1 – F23)

Table II.6 Proposed classification of suffusion resistance index, I_β

Suffusion resistance index, I_β	Description of erosion rate	Ranking of erosion
$I_\beta < 2$	Highly erodible	1
$2 \leq I_\beta < 3$	Erodible	2
$3 \leq I_\beta < 4$	Moderately erodible	3
$4 \leq I_\beta < 5$	Moderately resistant	4
$5 \leq I_\beta < 6$	Resistant	5
$I_\beta \geq 6$	Highly resistant	6

Table II.7 and Table II.8 show the comparison of the description of erosion rate of tested specimens based on two methods: erosion coefficient k_d versus critical hydraulic shear stress τ_c and energy-based approach. It is worth noting that the suffusion susceptibility of several soils based on the method of k_d - τ_c could not be estimated due to their difficulty to determine the k_d value. They are the specimens under single-stage hydraulic gradient or imposed controlled flow rate condition test. Since the different methodologies were used on the both methods, the suffusion susceptibility of a given soil cannot be always the same. In several soils, the description of erosion rate is different under the two methods: *M1*, *M4*, *A-90a*, *A-90a_rep* and *R2-90a*. From Table II.8, it can be shown the specimen *M1* has different description of erosion rate in two methods, “moderately erodible” for k_d versus τ_c method whereas “erodible” for energy-based approach. Due to a large uncertainty in k_d versus τ_c method with aforementioned reasons, the proposed classification of suffusion susceptibility based on energy-based method is preferred.

Table II.7 Comparison of proposed classification of suffusion susceptibility based on $kd-\tau_c$ method and energy-based method (G5A to B-97b)

Tested gradations	Tested specimens	Suffusion sensibility classification	
		kd versus τ	Energy-based approach
G5	G5A	Moderately resistant	Moderately resistant
	G5B	Moderately erodible	Moderately erodible
G6	G6	Moderately erodible	Moderately erodible
P1	P1	Moderately resistant	Moderately resistant
P2	P2	Moderately resistant	Moderately resistant
P3	P3	Resistant	Resistant
P4	P4	Moderately erodible	Moderately erodible
L1	L1	Moderately erodible	Moderately erodible
L2	L2	Moderately erodible	Moderately erodible
L3	L3	Moderately resistant	Moderately resistant
L4	L4Ai	Erodible	Erodible
	L4Aii	Erodible	Erodible
	L4C		Moderately erodible
	L4D		Moderately erodible
L5	L5	Erodible	Erodible
D1	D1	Moderately resistant	Moderately resistant
D2	D2	Moderately erodible	Moderately erodible
D3	D3A	Erodible	Erodible
	D3Arep	Erodible	Erodible
	D3B	Erodible	Erodible
M1	M1	Moderately erodible	Erodible
M3	M3	Erodible	Erodible
M4	M4	Moderately erodible	Moderately resistant
S1	S1	Moderately resistant	Moderately resistant
S2	S2	Moderately erodible	Moderately erodible
A	A-90 _a	Moderately resistant	Resistant
	A-90 _a rep	Moderately resistant	Resistant
	A-90 _b	Moderately resistant	Moderately resistant
	A-90 _c		Moderately resistant
B	B-90 _a	Erodible	Erodible
	B-90 _c		Moderately resistant
	B-90 _e		Moderately erodible
	B-90 _f		Moderately erodible
	B-90 _h	Moderately resistant	Moderately resistant
	B-90 _k		Erodible
	B-97 _a	Moderately erodible	Moderately erodible
	B-97 _b	Moderately erodible	Moderately erodible

Table II.8 Comparison of proposed classification of suffusion susceptibility based on $kd-\tau_c$ method and energy-based method (C-90a to F23)

Tested gradations	Tested specimens	Suffusion sensibility classification	
		kd versus τ	Energy-based approach
C	C-90 _a	Erodible	Erodible
	C-97 _a	Moderately erodible	Moderately erodible
	C-97 _b	Erodible	Erodible
Chav-1	Chav-1	Moderately resistant	Moderately resistant
Chav-2	Chav-2 _i	Moderately erodible	Moderately erodible
	Chav-2 _{ii}	Resistant	Resistant
R1	R1-90 _b	Resistant	Resistant
R2	R2-90 _a	Moderately erodible	Erodible
	R2-90 _b	Erodible	Erodible
	R2-97 _b	Moderately erodible	Moderately erodible
	R2-97 _d		Moderately erodible
	R2-97 _f		Moderately erodible
	R2-97 _g		Erodible
	K10L90	A1	
A2			Highly resistant
A4			Highly resistant
A5			Highly resistant
A8			Highly resistant
A11			Resistant
A14			Resistant
K20L80	A27		Highly resistant
	A28		Highly resistant
KPr25F75	F10		Moderately resistant
	F13		Moderately resistant
	F14		Moderately resistant
	F15		Moderately resistant
	F17		Moderately erodible
	F20		Moderately erodible
	F23		Moderately resistant

Now we investigate the effect of hydraulic loading history on suffusion susceptibility classification which is based on energy approach. Table II.9 shows several specimens having the same grain size distribution but different hydraulic loading history. Figure II.61 shows diagram of classification of suffusion susceptibility with respect to the effect of hydraulic loading history.

Table II.9 Given grain size distributions with different hydraulic loading histories

Tested gradations	Tested specimens	Initial dry density (kN/m ³)	Applied hydraulic gradient, <i>i</i> (m/m)	Test duration per stage (min)
L4	L4Ai	16	0.1 - 4	60
	L4Aii	16	0.1 - 3	20
A	A-90 _a	17.39	0.1 - 15	10
	A-90 _b	17.39	1 - 15	10
B	B-90 _a	17.39	0.1 - 6	10
	B-90 _h	17.39	0.2 - 10	60
	B-97 _a	18.74	0.1 - 12	10
	B-97 _b	18.74	1 - 9	10
C	C-97 _a	18.74	0.1 - 9	10
	C-97 _b	18.74	1 - 7	10

To investigate the effect of hydraulic loading history on suffusion susceptibility, it can be distinguished into two groups: i) the same hydraulic gradients with different duration per stage, ii) different hydraulic gradients with the same duration per stage.

The soils *L4-A* and *B-90* are subjected to the same hydraulic gradients with different duration per stage (see Table II.9). The time series of hydraulic conductivity and erosion rate, the variation of erosion rate versus hydraulic shear stress and the variation of cumulative eroded mass versus energy of soils *L4-Ai* and *L4-Aii* are shown in **Annex**. Given different duration per stage, soils subjected to faster rate of hydraulic gradient increase (*L4-Aii* and *B-90a*) resulted in soils more erodible than those subjected to longer rate (*L4-Ai* and *B-90h*). Even though the specimens *L4-Ai* and *L4-Aii* have the same description of erosion rate but it can be noticed from Figure II.61, the specimen *L4-Aii* is more erodible than *L4-Ai*. However, in case of a soil *B-90*, the specimen *B-90a* is defined as “erodible” whereas *B-90h* is “moderately resistant”. Thus at given gradient these soils that may commonly be stable may become unstable if the same gradient injected rapidly. Therefore for given soil the susceptibility can be different under different hydraulic loading histories.

The different multi-stage hydraulic gradients *a* and *b* with the same duration per stage are applied to the soils *A-90*, *B-97* and *C-97*. Multi-stage hydraulic gradient *a* applies small initial increment 0.1 whereas *b* applies large initial hydraulic gradient 1 (see Figure II.8). Given the same duration per stage, soils subjected to hydraulic gradients *b* (*A-90b*, *B-97b* and *C-97b*) resulted in soils more erodible than those subjected to hydraulic gradients *a* (*A-90a*, *B-97a* and *C-97a*) as shown in Figure II.61. It could be explained when large multi-stage hydraulic gradient *b* were imposed to the specimens by progressively increasing the hydraulic gradient, this may not allow enough time for the fine fraction to filtrate and clog the filter. This result is in accordance with the test results of Tomlinson and Vaid (2000). For a given soil, two different rates of hydraulic gradient increase were imposed: 1) normal rate of increase of 2 cm increments every 10 minutes and 2) rate of increase of 23 cm in 1 minute. In term of critical hydraulic gradient, a very rapid rate of increase of 23 cm in 1 min resulted lower critical hydraulic gradient, equals to one third of the value of normal rate. The reason of this occurrence may be caused by the possibility of filtration process. Under seepage flow, the finer fraction is not allowed to filtrate within the soil when fast rate of hydraulic gradient

increase is applied. Therefore for given soil the susceptibility can be different under different hydraulic loading histories.

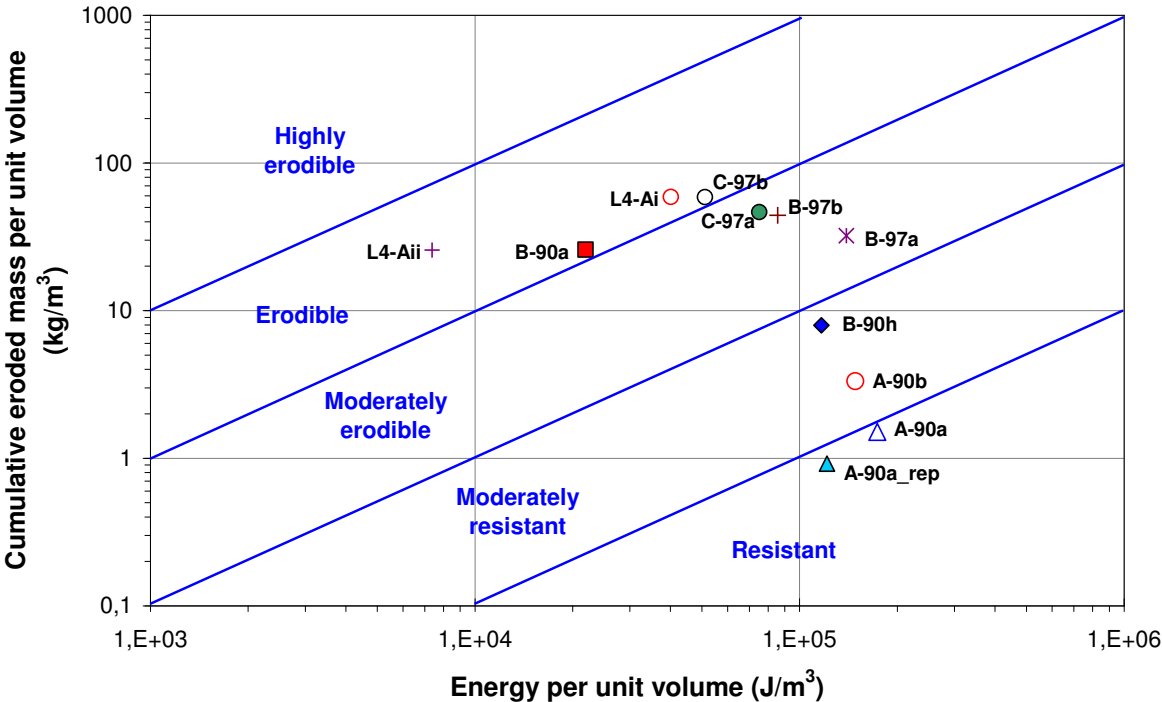


Figure II.61 Effect of hydraulic loading history on suffusion susceptibility classification

As indicated by the aforementioned results, a systematic method to suffusion susceptibility classification can be proposed. Two successive steps can be distinguished: (1) the assessment of the soil susceptibility to suffusion (based on the gradation-based criteria only) and (2) the susceptibility classification (by seepage test). The first step is carried out to compare the recent gradation-based criteria with the result of tested soils, with the aim to propose a new threshold in the recent criteria (see Section 3.8.2).

When a soil is susceptible to erosion, the soil susceptibility has to be characterized by imposing seepage flow in suffusion tests. The test should be performed by progressively increasing the applied hydraulic gradient and it should be carried on until the hydraulic conductivity value reaches constant.

With the objective to characterize independently the hydraulic loading and the induced erosion, the cumulative eroded dry mass and the cumulative energy expanded by the seepage flow, E_{flow} are computed.

Finally with the aim to classify suffusion susceptibility, the first time hydraulic conductivity reaches constant value can be determined as the time to suffusion susceptibility classification of a soil on the diagram cumulative eroded dry mass vs. cumulative expanded energy.

2.9 Comparison of gradation-based criteria and suffusion resistance index (I_β)

2.9.1 Kezdi (1979) criterion versus suffusion resistance index (I_β)

Figure II.62 shows suffusion resistant index (I_β) with respect to ratio of D_{15c}/d_{85f} for all the specimens. Values in the x-axis correspond to description of erosion rate (see Table II.6) that can be grouped into two susceptibility: “unstable” (I_β from 2 to 4) and “stable” ($I_\beta > 4$). According to criterion of Kezdi (1979), a soil having ratio of $D_{15c}/d_{85f} \leq 4$ is considered as stable soil. However after a series of seepage tests, it is found that several specimens even though as geometrically are unstable but they result in “stable” condition. From these results, the gradation-based criterion, however, demonstrates not able to take into account other important parameters such as grain shape and hydraulic loading history.

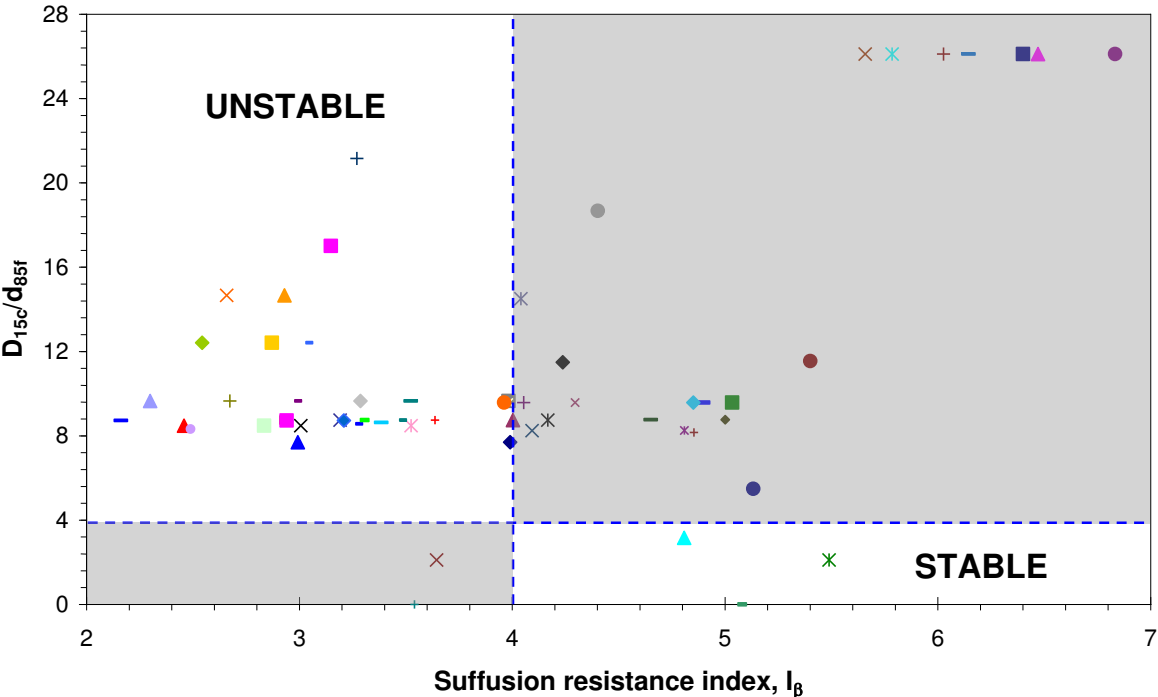


Figure II.62 Suffusion resistance index (I_β) versus D_{15}/d_{85}

2.9.2 Kenney and Lau (1985) criteria versus suffusion resistant index (I_β)

Figure II.63 displays suffusion resistance index (I_β) versus H/F minimum for all the specimens. Similar to Figure II.62, values in the x-axis correspond to description of erosion rate: “unstable” (I_β from 2 to 4) and “stable” ($I_\beta > 4$). According to criterion of Kenney and Lau (1985), a soil considered as “unstable if it has the ratio of H/F minimum < 1 . However from the results of a series of seepage tests, it is found that several soils are “stable” although they are “unstable” as geometrically. These results show that important parameters such as grain shape and hydraulic loading history are not taken into account in the gradation-based criterion.

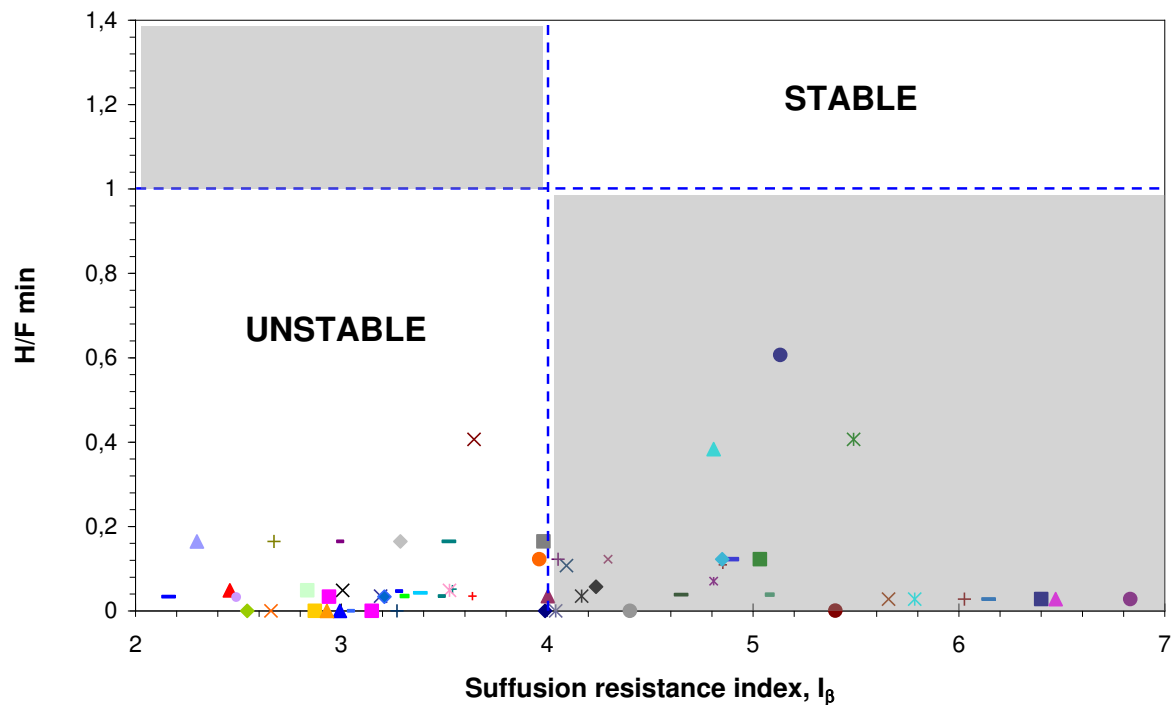


Figure II.63 Suffusion resistance index (I_{β}) versus H/F_{min}

2.9.3 Wan and Fell (2008) criterion versus suffusion resistance index (I_{β})

The diagram of suffusion resistant index (I_{β}) with respect to Wan and Fell criterion for the specimens is presented in Figure II.64. The Wan and Fell criterion is suitable only for widely-graded soils having fine content larger than 15%. The tested specimens here can be identified as gap-graded soils and only a few widely-graded soils. It is shown that almost all specimens considered as “stable” according to the criterion of Wan and Fell whereas after the seepage test they are considered as unstable soils ($I_{\beta} \leq 4$). All the gap-graded soils resulted in different classification, for instance *B-90a* is “stable” according the Wan and Fell criterion but the seepage test resulted in “unstable” soil. However the widely-graded soils (*R1*, *Chav*) resulted the same classification. Thus these results can confirm the validity of Wan and Fell criterion.

2.9.4 Chang and Zhang (2013) criterion versus suffusion resistant index (I_{β})

Chang and Zhang (2013) proposed geometric criterion for gap-graded soils. Given soils with the percentage of fine fraction < 0.063 mm, $P < 10\%$, the soil is defined as “internally stable” if gap ratio, $Gr < 3$ (Gap graded soils: $P < 10\%$ is internally stable if $Gr < 3$). However, from a series of seepage test on 16 gap-graded soils (Table II.10), given soils with $P < 10\%$ and $Gr < 3$ resulted in the suffusion susceptibility “moderately erodible to erodible”. In agreement with proposed suffusion resistant index (I_{β}): “internally stable” is defined from highly resistant to moderately resistant and “internally unstable” is defined from moderately erodible to highly erodible, thus the 16 gap-graded soils are defined as “internally unstable”. Due to this result, the author proposes a modification in the gap ratio threshold of Chang and Zhang (2013) criterion to $Gr \leq 2.14$ defined as “internally stable”.

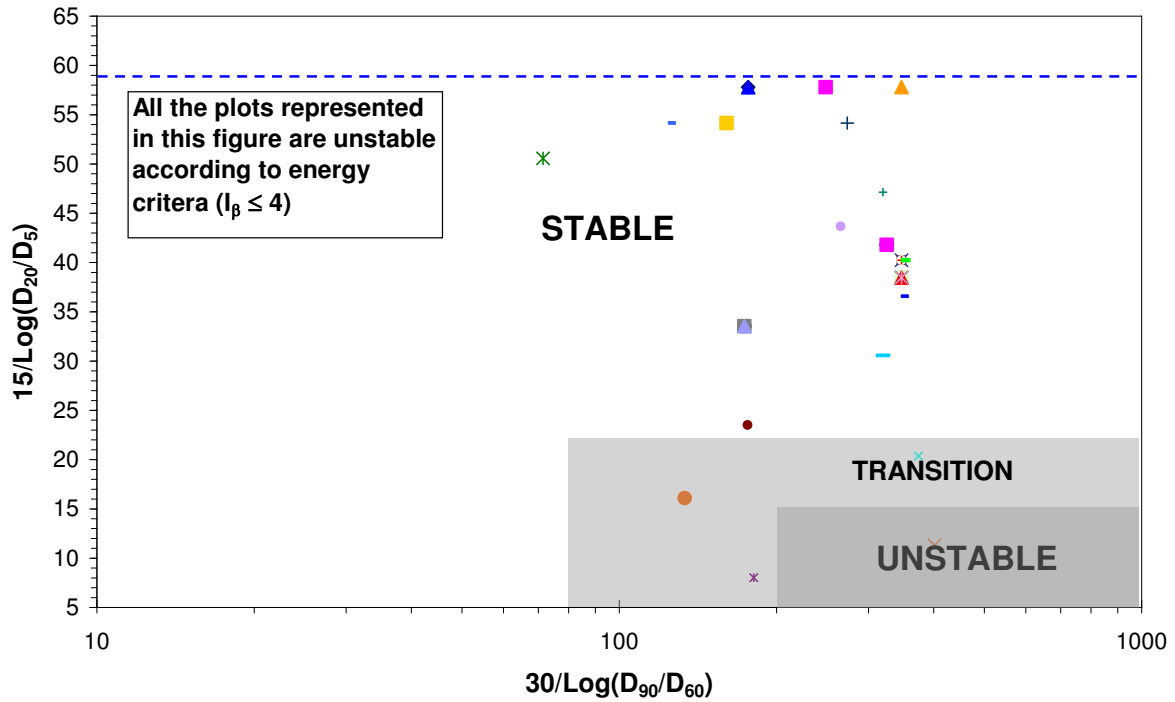


Figure II.64 Suffusion resistance index (I_{β}) versus Wan and Fell criterion

Table II.10 Chang and Zhang (2013) criterion versus suffusion resistant index (I_{β})

Tested gradations	Tested specimens	P (%)	Gr	Chang and Zhang criteria (2013)	Description of erosion rate
					Energy-based approach
L1	L1	2.706	2.143	stable	Moderately erodible
L2	L2	4.188	2.143	stable	Moderately erodible
L4	L4Ai	1.922	2.143	stable	Erodible
	L4Aii	1.922	2.143	stable	Erodible
	L4C	1.922	2.143	stable	Moderately erodible
	L4D	1.922	2.143	stable	Moderately erodible
L5	L5	3.075	2.143	stable	Erodible
B	B-90 _a	1.533	2.14	stable	Erodible
	B-90 _e	1.533	2.14	stable	Moderately erodible
	B-90 _f	1.533	2.14	stable	Moderately erodible
	B-90 _k	1.533	2.14	stable	Erodible
	B-97 _a	1.533	2.14	stable	Moderately erodible
	B-97 _b	1.533	2.14	stable	Moderately erodible
C	C-90 _a	1.779	2.14	stable	Erodible
	C-97 _a	1.779	2.14	stable	Moderately erodible
	C-97 _b	1.779	2.14	stable	Erodible

2.10 The effect of fine content and density

To investigate the effect of fine content to suffusion susceptibility, the gradation distributions A, B and C with 20%, 25% and 29% fine content respectively are performed. Figure II.65 displays diagram of classification of suffusion susceptibility with respect to the effect of fine content. As depicted in Figure II.65, specimens A are less erodible than specimen B and C. It is indicated that the lower fine content soils tend to require larger energy to the onset and development of erosion. It can be explained the reason of less fine content more resistant to suffusion is since the larger amount of coarse particles in specimen A having the same soil density with specimen B and C makes its constriction size so smaller that induces fine particles within the void of coarser particle more resistant to erosion. This result is in good agreement with the test results presented by Ke and Takahashi (2012). Given three different fine contents: 16.7%, 20%, and 25%, it is demonstrated that the samples with the lowest fine content (16.7%) required a larger critical hydraulic gradients for the onset of internal erosion for relative density of 0.2 and 0.6 respectively. Thus fine content can affect suffusion susceptibility on a soil.

With respect to soil density, the density seems to induce a slight increase of the soil’s strength facing suffusion process. The specimens B and C demonstrate that given any hydraulic loading history, soils having higher soil density (B-97a, B-97b, C-97a, C-97b) are more resistant than B-90a and C-90a.

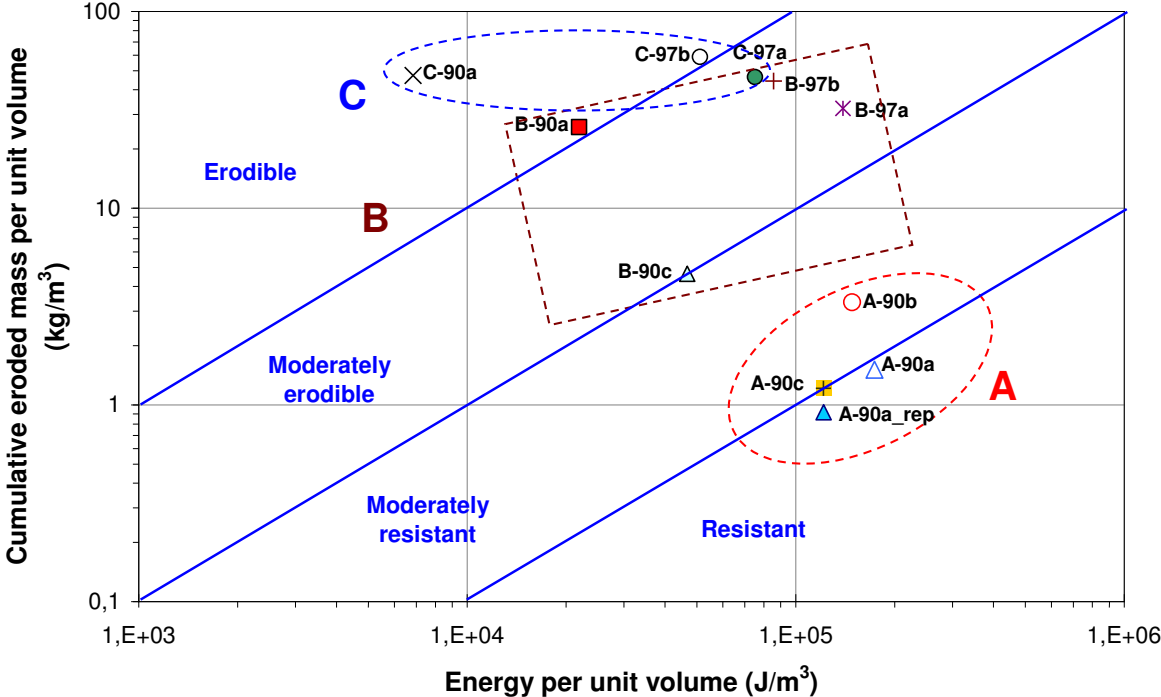


Figure II.65 Effect of fine content on suffusion susceptibility classification

2.11 Synthesis

As indicated by the aforementioned results, a systematic method to suffusion susceptibility classification can be proposed. Two successive steps can be distinguished: (1) the assessment of the soil susceptibility to suffusion (based on the gradation-based criteria only) and (2) the suffusion susceptibility classification (by seepage test). To characterize soil response and the action of hydraulic loading, specimens are subjected to a water flow in downward direction.

The results of the series of the tests demonstrate that soil response of the specimens subjected to multi-stage hydraulic gradients is different from that of the specimens subjected to single-stage hydraulic gradient or injected flow rate condition. The comparison of the three hydraulic loadings can be summarized as follow:

- (1) The tested specimens subjected to multi-stage hydraulic gradients have a clear typical trend of an initial decrease of hydraulic conductivity before it turns to progressively increases and finally reaches a constant value whereas hydraulic conductivities of the specimens subjected to single-stage hydraulic and injected flow rate condition decrease during the given times.
- (2) The method by applying multi-stage hydraulic gradients is more possible to determine erosion coefficient k_d than the two other methods (single-stage hydraulic gradient and injected flow rate). Thus, the likelihood to follow all the evolutions of suffusion is more possible only with multi-stage hydraulic gradient.
- (3) Critical hydraulic gradient the specimens injected by multi-stage hydraulic gradients (a) is larger than that of the specimens injected by single-stage hydraulic gradient (b) ($i_{cr} b > i_{cr} a$). Under hydraulic loading history a , suffusion starts easier than in the case of hydraulic loading history b .
- (4) The erosion coefficient k_d of the specimens subjected to hydraulic gradient a is smaller than those of hydraulic gradient b ($k_d a < k_d b$). In regard with fine content, the k_d value specimen A (20%) is smaller than that of specimen B (25%) and C (29%).
- (5) The critical hydraulic shear stress of the specimens subjected to hydraulic gradient a is smaller than those of hydraulic gradient b ($\tau_c a < \tau_c b$). It seems that the development of suffusion appears smaller under hydraulic loading history a in term of both hydraulic gradient and hydraulic shear stress. Given soil density and hydraulic loading history, the critical hydraulic shear stress τ_c of specimen $A-90a$ is smaller that of $B-90a$, $\tau_c B-97a < \tau_c C-97a$, and $\tau_c B-97b < \tau_c C-97b$. Thus, it seems that specimens with lower fine content are more resistant.

With the objective to take into account the complexity of suffusion process that cannot be satisfied with hydraulic shear stress method or flow power-based method, an energy-based approach is used. As this method can follow all the evolution of suffusion process from initiation to development, thus the determination of erosion coefficient is more possible than that of the methods of hydraulic shear stress and flow power. With the objective to propose a classification of suffusion susceptibility, we propose a classification of suffusion susceptibility based on energy approach (a diagram and index of suffusion resistance, I_β) that is divided into six categories of soil susceptibility from highly resistant to highly erodible. With the energy approach, the suffusion susceptibility classification of a soil is considered at the points highlighted by arrows that correspond to the end of development of suffusion (i.e. time from which hydraulic conductivity is stabilized) whereas the points before and after the arrows do not represent the soil susceptibility. The after-arrow points also do not represent the soil susceptibility since they correspond to the steady state. If the series of final points is taken into account, the soil susceptibility may become less erodible. For some tests without arrows, their susceptibility is defined at the last point. For the specimens subjected to single-stage

hydraulic gradient and imposed controlled flow rate condition test, the last point is taken into account as a representative of the soil susceptibility.

In order to follow the process of suffusion with respect to the transport of the fine fraction within the soil, a test on grain size distribution after test was carried out. After seepage test, the soil was divided into two layers: top and bottom with the same portions. Given the specimen *A-90b* consisting 20% fine fraction, fine fraction in the top layer decreases whereas in the bottom layer increases. It seems that the water flow imposed during seepage test can detach and transport some fine fraction to the bottom layer. The percentage of fine fraction in the bottom layer higher than that of the initial condition can be attributed to the supply of fine fraction from the top layer whereas only small quantity of fine fraction erosion in the bottom layer. Thus the supply and filtration induce the increase of the fine fraction in the bottom layer. However, given the specimens *B-90a* (25% fine fraction) and *C-97a* (29% fine fraction), the percentage of fine fraction in both top and bottom layer decreases (less than that of initial condition). In the bottom layer, even though there is a supply of fine fraction from the top layer, the percentage of fine fraction still decreases. This can be attributed to a significant erosion of fine fraction in the bottom layer.

From the point of view of the effect of hydraulic loading history on suffusion susceptibility, it can be summarized as follow: i) given different duration per stage, soils subjected to faster rate of the increase of hydraulic gradient resulted in soils more erodible than those subjected to longer rate. ii) given the same duration per stage, soils subjected to hydraulic gradients *b* resulted in soils more erodible than those subjected to hydraulic gradients *a*. Therefore for given soil the sensibility can be different under different hydraulic loading histories.

With respect to the effect of fine content to suffusion susceptibility, it is indicated that the lower fine content soils (*A-20%*) tend to require larger energy to the onset and development of erosion. It can be explained the reason of less fine content more resistant to suffusion is since the larger amount of coarse particles in specimen *A* having the same soil density with specimen *B* and *C* makes its constriction size so smaller that induces fine particles within the void of coarser particle more resistant to erosion. Thus fine content can affect suffusion susceptibility on a soil. With respect to soil density, the density seems to induce a slight increase of the soil's strength facing suffusion process. The specimens *B* and *C* demonstrate that given any hydraulic loading history, soils having higher soil density are more resistant.

CHAPTER III SMALL SCALE MODEL OF DIKE

3.1 Introduction

This chapter is dedicated to investigate the effect of suffusion on the hydraulic and mechanical response of soil locally and in whole structure of a small scale model of dike. One unstable soil is chosen from the tested soils performed in previous chapter. To characterize soil response owing to the action of hydraulic loading, the soil is subjected to a single-stage hydraulic gradient. During the test, the following measurements are carried out to follow the evolution of suffusion and the response of the soil structure:

- the pore water pressure in the body of dike,
- the settlement in the crest of dike,
- the flow rate in the downstream side,
- the displacement in the body of dike from digital image processing Particle Image Velocimetry (PIV) technique),
- and eroded mass.

Finally change in the grading and spatial fine distribution is characterized after the tests by taking soil samples from different locations in the body of the dike.

However, to investigate the impact of suffusion on the hydraulic properties of the small scale dike model, the results presented in this chapter was not sufficient enough to a conclusion. Thus simulations by Plaxis were needed to complete the conclusion. Total heads within the body of dike from the dike test (measured values) were compared to those from the simulation. Thus from this information, it can be deduced whether suffusion can affect the hydraulic characteristic of the soil or not.

This chapter comprises three sections: (i) the description of tested gradation distributions and tested specimens, (ii) the apparatus for small scale model dike test and test procedure and (iii) results and discussion.

3.2 Seepage test

3.2.1 Description of the device

A schematic testing apparatus of a half-dike model as shown in Figure III.1 was used to investigate the hydraulic and mechanical response of soil due to suffusion. It comprises a transparent box, a water supply system, a soil collection system, a water collection system and data acquisition system.

Transparent box

The dike specimens were made in a transparent box having a width of 1540 mm, height of 720 mm and breadth of 150 mm. Its transparent wall makes possible the observation of the detachment and transport of fine fraction in the body of the dike and also the displacement of the whole structure (Figure III.2). In the bottom side of the box is equipped with 7 pressure ports connected to piezometers as shown in Figure III.3a. A series of pressure ports is also installed in the back side of transparent box to measure local hydraulic gradients within the body of the dike as presented in Figure III.3b. To keep water from evaporation in the pipes, a cigarette filter is used. The box has inlet and outlet holes on the both sides to provide a water system, in the right side is water supply system connected to water container and in the left side is connected to funnel-shaped drainage system. The vertical sidewall between dike soil and upstream water contains fibre mess (Figure III.4) allowing water to seep into the dike, but avoiding the fine fraction of the soil to migrate into the upstream retaining reservoir.

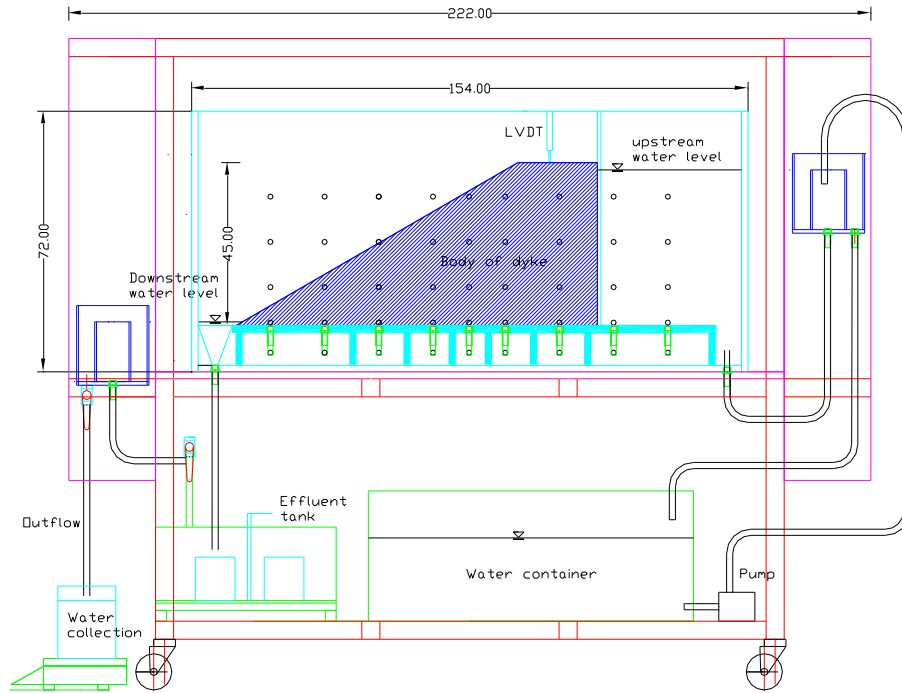


Figure III.1 Schematic diagram of the dike apparatus



Figure III.2 Front view of transparent box



(a)



(b)

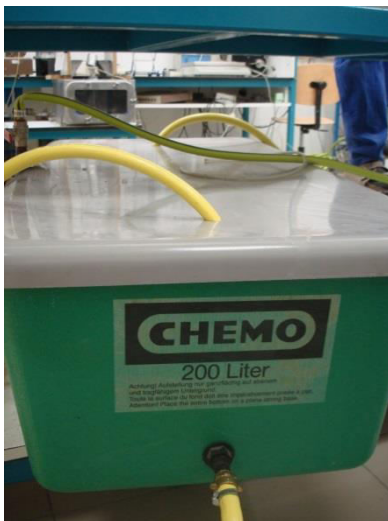
Figure III.3 Pressure ports: a) in the bottom side, b) in the back side of the box



Figure III.4 Fibre mess to separate dike soil and upstream water reservoir

Water supply system

In order to saturate the pore water pressure pipes and the tested soil and to provide hydraulic loading into the dike model, water can be poured into both upstream and downstream sides through inlet and outlet hole until the targeted water level in the box is reached. To anticipate large amount water imposed during the seepage test, a water tank of 200 litres is used to supply the water with the aid of a pump (Figure III.5). To maintain the constant upstream water level, an upstream overflow outlet as shown in Figure III.6 is used. Once the targeted water level is reached and to maintain the water level constant, the overflow outlet redirect water back to the water tank.



(a)



(b)

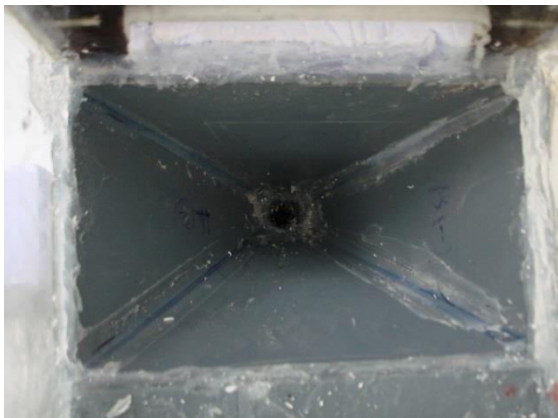
Figure III.5 Water supply system: a) 200 lt capacity water tank, b) pump and connection gates



Figure III.6 Upstream overflow outlet to maintain upstream water level

Water and soil collecting system

During the test, the water seeping through the body of the dike eventually passes the funnel-shaped drainage outlet as shown in Figure III.7a. In order to prevent clogging of the outlet by the coarse soil fraction, a 1.25 mm wire mesh is put just at the top of the funnel-shaped outlet. From this outlet, discharged eroded mass and water flow are delivered into an effluent tank comprising a 8 beaker rotating sampling device (Figure III.7b). The eroded mass is then caught by the beakers while water is flowing through a downstream overflow outlet to be finally collected and continuously weighted on a balance, as depicted in Figure III.8, to determine the water flow rate. The downstream overflow outlet similar to the upstream one is used to maintain downstream water level.

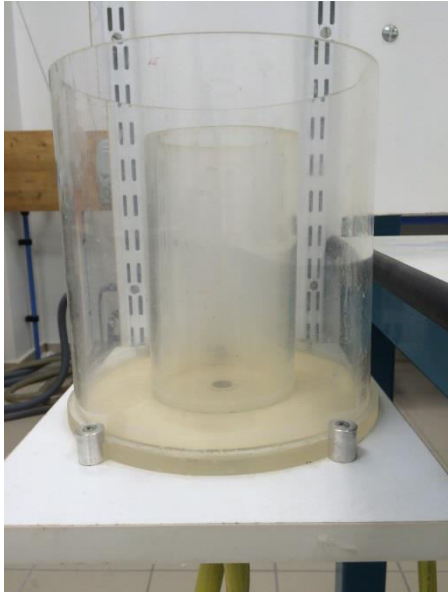


(a)



(b)

*Figure III.7 Soil collecting system: a) funnel-shaped draining outlet
b) effluent tank with 8 beaker rotating sampling device*



(a)



(b)

**Figure III.8 Water collecting system: a) downstream water outlet
b) flow rate measurement equipped with a balance**

Data acquisition

The LVDT, measuring the displacement of the crest of the dike, and the balance, from which is determined the flow rate, are directly connected to a computer to perform the data acquisition. The other measurements, concerning the evolution of the displacement of the body of the dike and the variation of local water head within the body of the dike (see Figure III.9), are determined from image processing. In this objective, pictures are regularly taken with two digital cameras. One camera placed in front of the box is used to estimate the displacement field. The other camera focuses on the panel of piezometer (Figure III.9), to compute de water head at each pressure port.



Figure III.9 Measurement system: water head pipes

3.3 Properties of tested soil

With the aim to investigate the hydraulic and mechanical response of soil due to suffusion, the soil *B-90* is selected. This selection is based on the assessment of soil susceptibility based with description of erosion rate from “moderately resistant” to “erodible” (see Table II.7). Figure III.10 shows the grain size distribution of tested soil consisting of sand and gravel from Sabliere Palvadeau (Figure III.11). The soil is identified as gap-graded distribution with 25% fine content. With a larger particle size, gravel works as the coarse particle, while sand soil as erodible fine particles. The coarse particle is classified as an angular to sub-angular material. The parameters of the tested soil can refer to Table III.1.

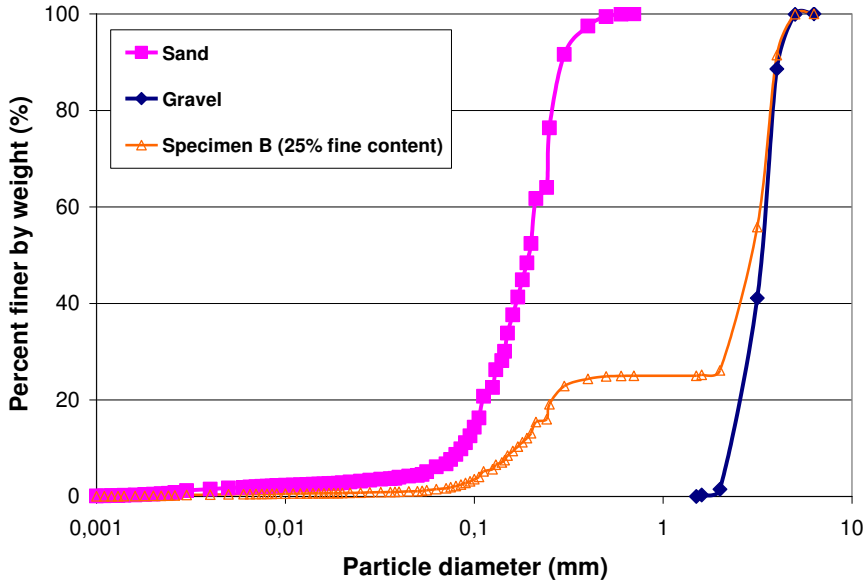


Figure III.10 Grain size distribution of tested soil



Figure III.11 Picture of sand and gravel from Sabliere Palvadeau

Table III.1 shows the properties of the specimens tested with two different soil densities. In addition, two different initial conditions were considered: pre-saturated and not pre-saturated. One repeatability test was carried out for the pre-saturated condition. A lower soil density specimen was added to investigate the effect of soil density. The last letter ‘s’ and ‘u’

correspond to saturated and unsaturated condition respectively, whereas ‘rep’ corresponds to the repeatability test.

Table III.1 Properties of tested specimens

Tested Specimen	ρ_d (g/cm ³)	Pre-saturated (YES or NO)	Duration of seepage test (min)
B-90 _s	1.739	YES	120
B-90 _{s-rep}	1.739	YES	360
B-75 _s	1.449	YES	140
B-90 _u	1.739	NO	260

3.4 Mechanical properties resulted from triaxial compression tests

The properties of shear strength and stiffness of the soil were based on the result of triaxial compression tests. In these triaxial tests, the soil was tested with three different confining pressure 75, 100 and 150 kPa corresponding to maximum stress deviator 297.7; 397.2 and 587.9 kPa respectively. Figure III.12 and Figure III.13 display young’ modulus and dilatancy angle of tested specimens whereas Figure III.14 shows the diagram of *t-s* for shear strength parameters.

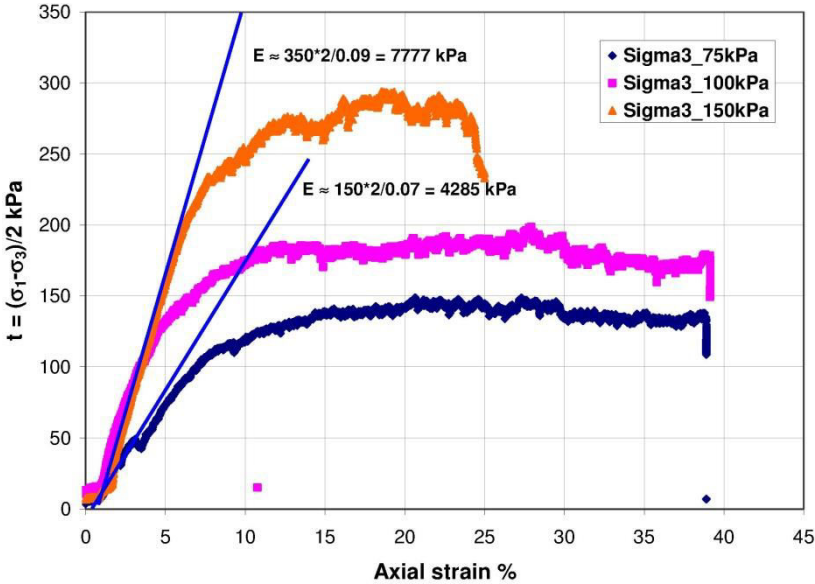


Figure III.12 Drained triaxial compression on tested soil: determination of Young’s modulus of tested soil

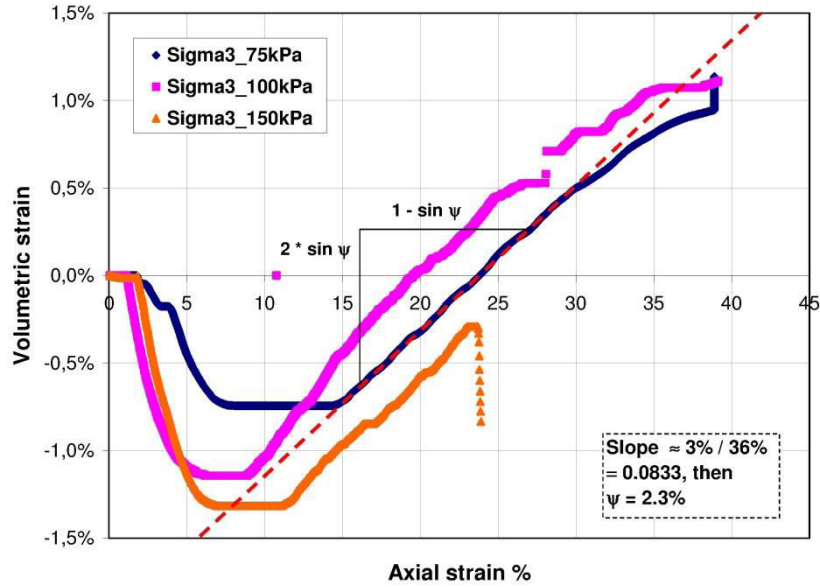


Figure III.13 Drained triaxial compression on tested soil: determination of dilatancy angle of tested soil

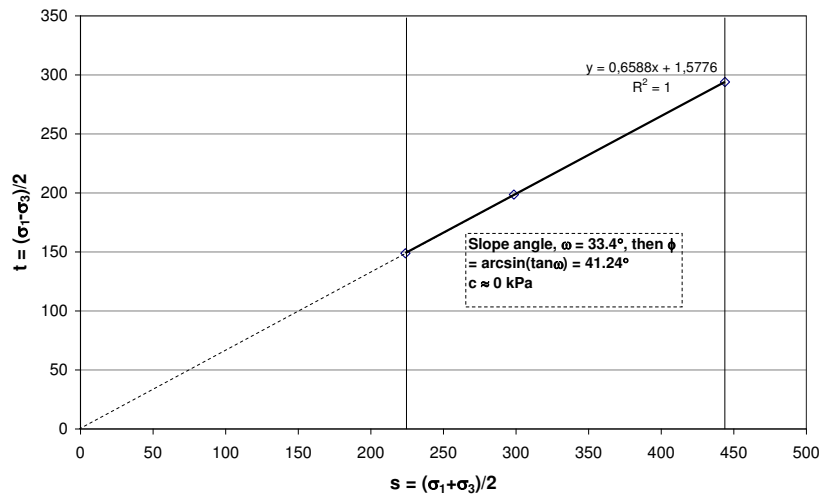


Figure III.14 Shear strength parameters of tested soil

3.4.1 Experimental procedures

A series of small scale dike tests was carried out in two steps: specimen preparation and seepage test.

Preparing specimen

The specimen preparation is divided into three steps: saturation on pore water pressure ports, production of the specimen and saturation of the specimen.

1. The filling of the transparent box with water until exceeding the upper row of the pressure ports is done to saturate all the ports as depicted in Figure III.15. The saturation is

correctly achieved once all the piezometers in the back side of the apparatus have the same water elevation than the one inside the box. Dewatering of the transparent box can be done after mixed tested-soil is prepared and ready to use.

2. The finer grain and gravel are first mixed with a moisture content of 7.8 % using a mixing machine for a duration of 5 minutes. After dewatering the box, the specimens are then built by a manual compaction technique. The dike structure is divided into five layers. Each layer is manually compacted with the aim to easily reach the targeted soil density. To obtain the desired slope of the dike, a series of pieces of wood is used to build the slope of the dike as shown in Figure III.16. The dimension of the dike is 100 cm in width, 45 cm in height, 15 cm in breadth, 22 cm in crest width and 30 degree in slope angle. Then, just after removing the wood pieces forming the slope, the box is filled at a very small rate by injecting water from both the upstream and downstream side of the soil specimen to saturate it, as shown in Figure III.17. To avoid seepage flow during saturation process due to the difference of water level, the opening of water gates for the two sides should be carefully operated to have the same water level in the upstream and downstream sides. The saturation is then left for one night (Figure III.18).



Figure III.15 Saturation process of water pressure ports

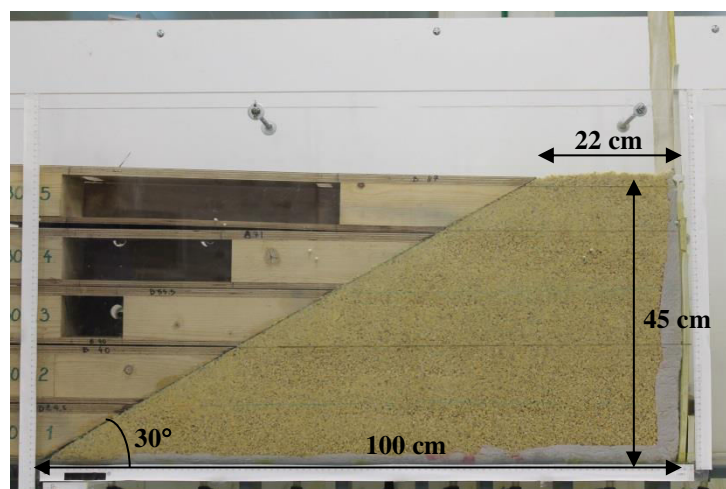


Figure III.16 Production of specimen

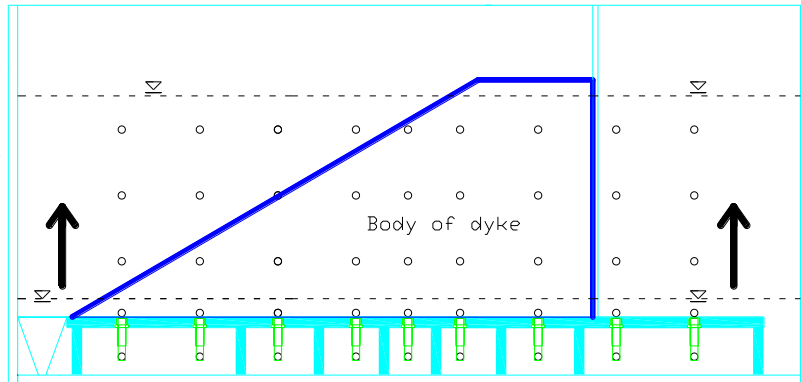


Figure III.17 Schematic diagram of the method to saturate the specimen



Figure III.18 Saturation process of the specimen

Seepage test

The specimen is subjected to a constant single-hydraulic gradient.

- In case of a pre-saturated soil specimen, the seepage test is started by dewatering the downstream side of the dike and keeping constant the upstream water level (Figure III.19).
- If the pre-saturation phase has been discarded, the seepage test is directly started after removing the wood pieces forming the slope by filling the upstream side of the dike of water up to the desired water level. In Figure III.20 is displayed a picture of the small dike during a seepage test. All the aforementioned measurements are commenced just before the dewatering process (or the filling of the upstream retaining reservoir if the pre-saturation of the specimen is discarded). The downstream overflow water is recorded in this process, and eroded mass is captured by beakers every 20 minutes. The flow rate in the downstream side is determined by the measured water mass divided by time.

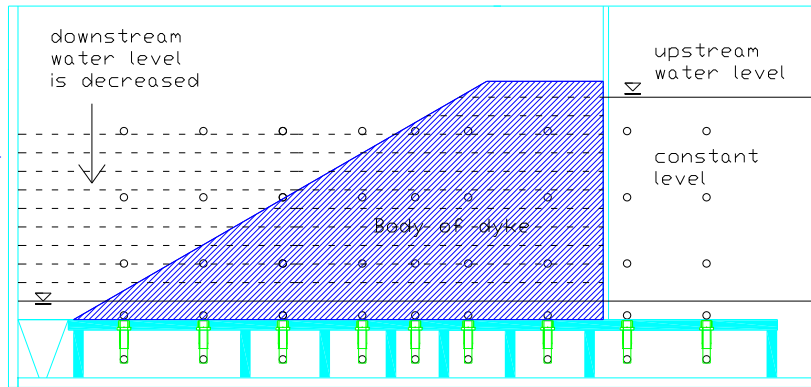


Figure III.19 Schematic diagram of seepage test method

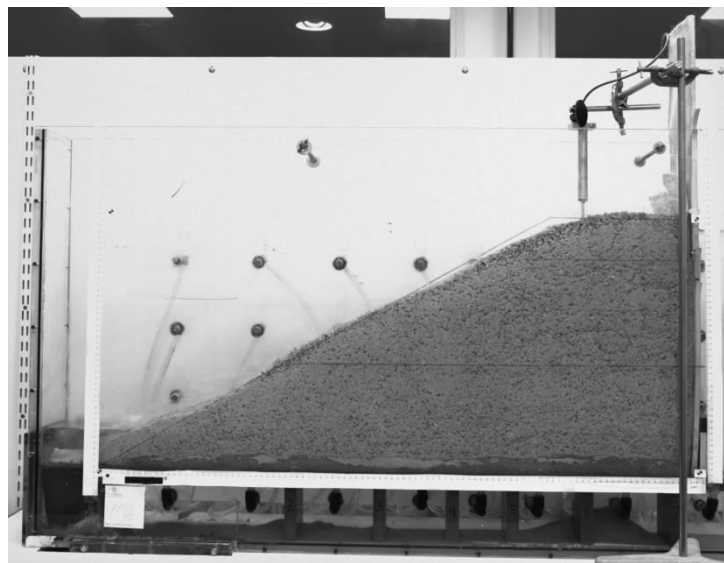


Figure III.20 Picture of a dike model after a seepage test: the dike is deformed because of settlements and sliding occurring during the test

3.5 Experimental results

The investigation on suffusion mechanisms in this dike model is based on the following results: time series of i) volumetric flow rate, ii) cumulative eroded mass, iii) water head within the body of the dike, iv) displacement during saturation and the seepage test and finally v) the post-tests spatial fine distribution of fines. Detailed results from specimens *B-90s*, *B-75s* and *B-90u* are not displayed in this chapter, but they will be presented in the **Annex** section.

3.5.1 Settlement during saturation phase

During the preparation of the specimens with partially saturated soils, apparent cohesion due to water menisci in between the particles help in stabilizing the dike model. During the saturation process, this capillary cohesion vanishes resulting in a softening of the soil and a vertical settlement of the dike model. The magnitude of the settlement depends on the soil density or the degree of compaction. Figure III.21 shows the vertical settlement at the crest of the dike during injection of water in the saturation process for three pre-saturated tests. The settlement for specimen *B-90s* is displaced 13 mm after 8 minutes. The same magnitude is

observed in the repeatability test of the specimen *B-90s-rep* whereas the specimen *B-75s*, with a lower soil density shows a larger settlement equals to 68 mm.

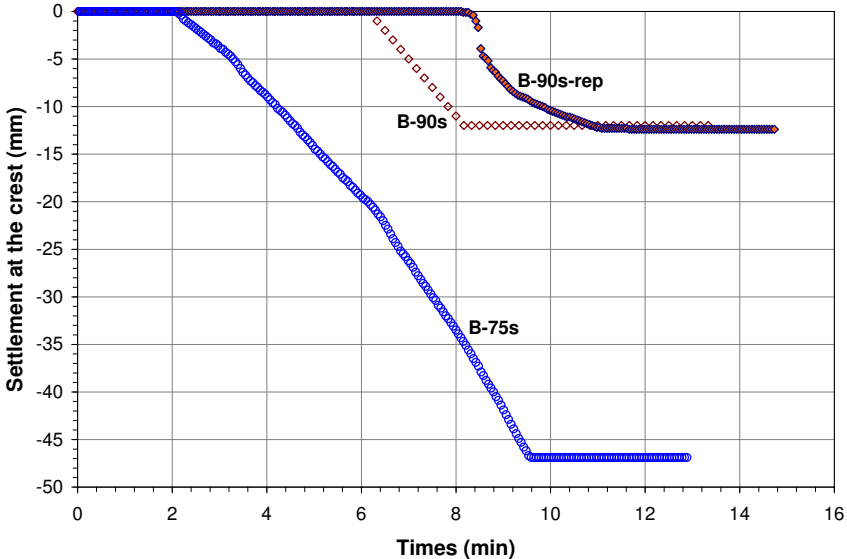


Figure III.21 Settlement of the dike crest during the saturation process

3.5.2 Settlement during seepage test

Figure III.22 displays the diagram of time series of the vertical settlement measured at the crest of the dike for four tests. In two pre-saturated soils, during the first eight minutes of the process of dewatering downstream side, the significant settlement occurred at the crest of the dike (*B-90s-rep* and *B-75s*). However, at different result is observed for the specimen *B-90s*. Even though some quantity of eroded mass is observed during the test, the settlement at the crest is almost nil. In case of specimen *B-90u*, the significant settlement at the crest is also observed (Figure III.23).

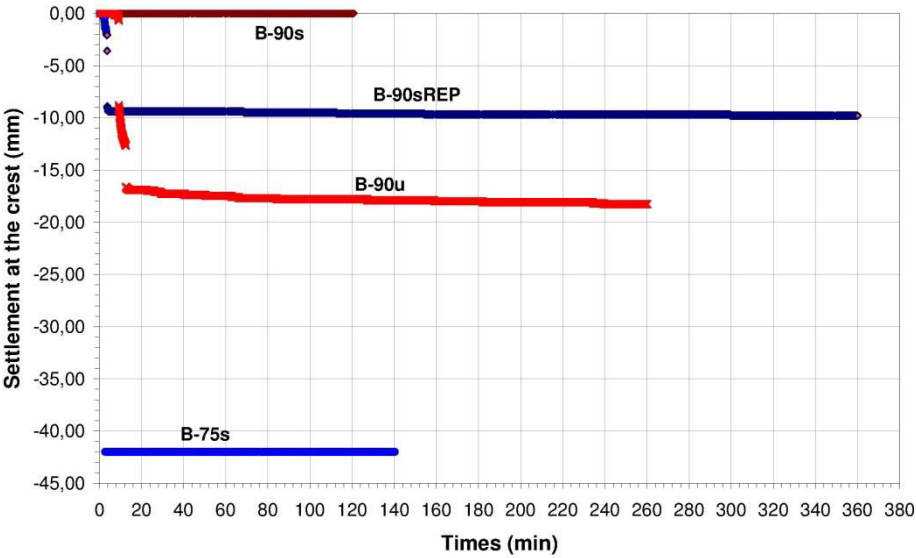


Figure III.22 Settlement of the dike crest during seepage test

3.5.3 Cumulative loss mass

The diagram of cumulative dry eroded mass versus times is presented in Figure III.23 and Figure III.24. The difference between the plots in the two last figures corresponds to the amount of eroded mass in the first 20 minutes. The all large eroded mass resulted from the emptying downstream reservoir (first 8 minutes) cannot be captured by the beaker thus soil particle settle down in the effluent tank.

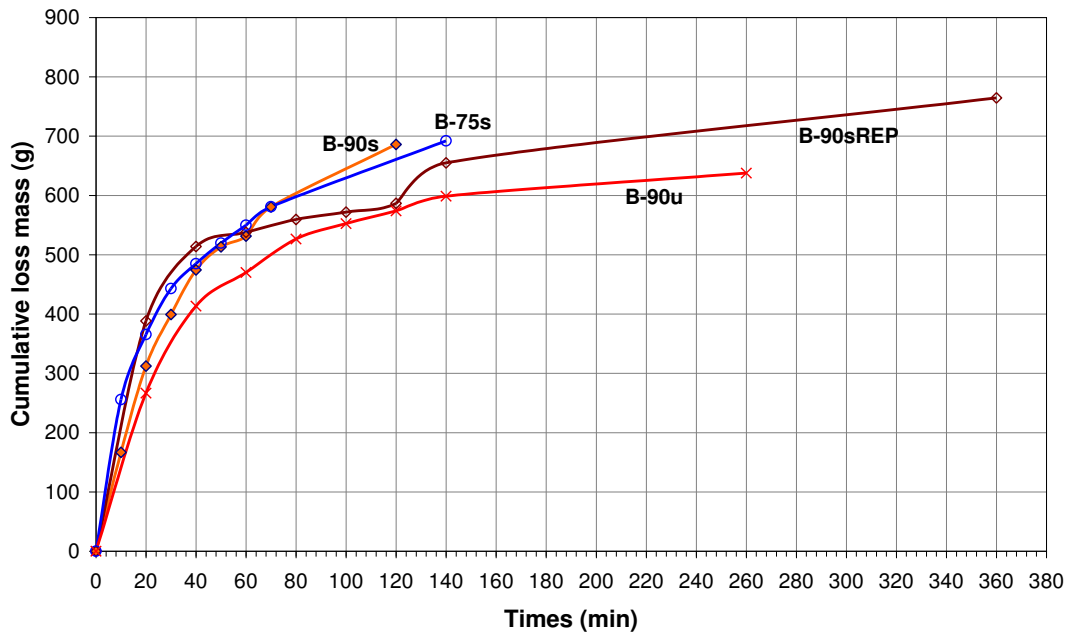


Figure III.23 Cumulative dry eroded mass versus times (captured by beakers only)

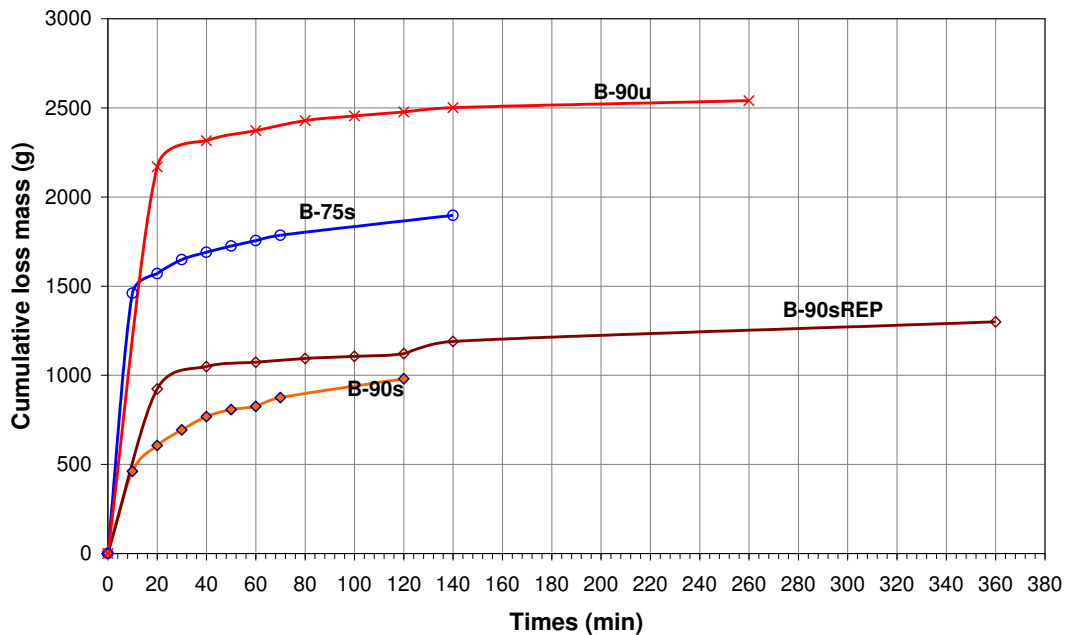


Figure III.24 Cumulative dry eroded mass versus times (beakers + outside beakers)

Figure III.24 displays the total eroded mass captured from both the beaker and the effluent tank. It is underlined that this happened only for the first 20 minutes. Decreasing downstream water level in the first eight minutes resulted in the largest eroded mass equals to 900 grams for specimen *B-90s-rep* (Figure III.24). As commonly observed during suffusion tests performed in laboratory erodimeters, the erosion rate under a constant water head drop is initially high and the decreases with time, probably due to the finite quantity of fines in the soil mobilizable under a given head drop. Indeed, a slight increase of the head drop, as for instance at $t=120$ min for the test *B-90s-rep*, results in a temporary increase of the erosion rate.

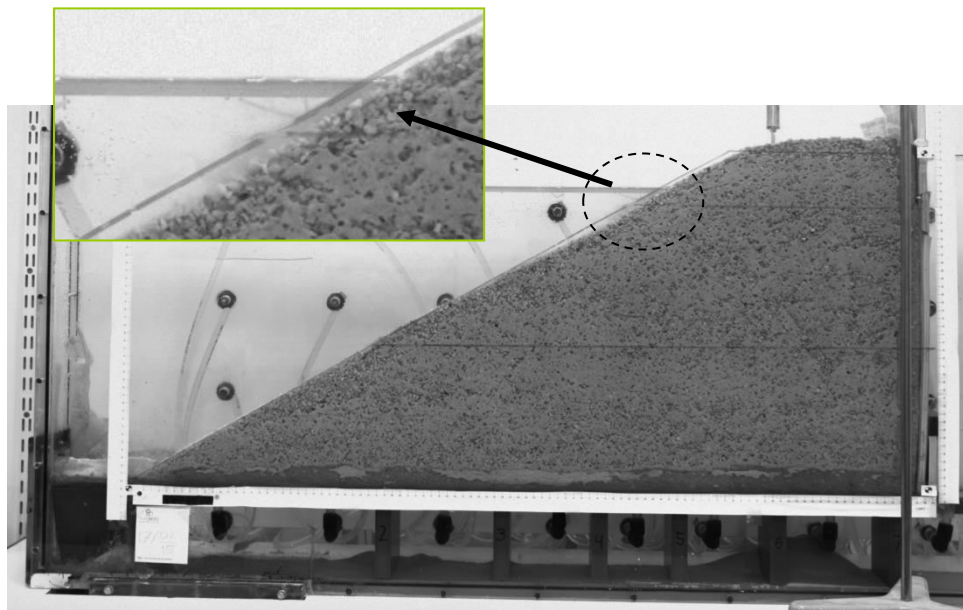


Figure III.25 The onset of suffusion (B-90_{s-rep})

The onset of suffusion could be clearly seen when the difference of total head was 5 cm as shown in Figure III.25. During the emptying of downstream water level, it could be obviously noticed by direct observation that the location of detached finer fraction was just above or just on the seepage line. In case of specimen *B-90s-rep*, the increase of larger eroded mass reoccurred after the upstream water level was increased in minute 120. For the next two-hour imposed seepage flow after minutes 140, the eroded mass was only 110 grams that might be caused by filtration process within the soil. This filtration corresponds to the decrease of flow rate as shown in Figure III.27. The same magnitude with slight increase of eroded mass after 40 minutes is observed in the specimens *B-90s*, *B-75s* and *B-90u*.

3.5.4 Downstream flow rate

The variation of the flow rate in downstream side is shown in Figure III.26. During the first 8 minutes, in general the flow rates sharply increase due to the emptying of downstream reservoir to the bottom level equals to 0 cm in case of pre-saturated tests (*B-90s*, *B-90s-rep* and *B-75s*). The large flow rate was attributed to the process of emptying downstream reservoir and seepage flow from upstream reservoir. For the corrected flow rate attributed to

seepage flow from upstream side only can be seen in Figure III.27. It is worth stressing that the significantly increase of flow rate in the specimens *B-90s*, *B-90s-rep* and *B-75s*, at $t = 60$ min, $t = 120$ min, and $t = 80$ min respectively (see Figure III.27) were due to the increase of upstream water level. The slight increase of flow rate until 40 to 60 minutes (depending on the test) may be attributed to the removal of the fine soil fraction in some parts of the dike leading locally to an increase of the hydraulic conductivity. Given In the specimen *B-90s-rep*, the flow rate had slight decrease until the test was stopped after 6 hour-test with the flow rate equals to 1.2 l/min.

However, the specimen *B-90u* progressively increases in first 40 minutes and then followed by constant values. The filling of upstream reservoir from bottom level to the level just below the crest of the dike in the first 14 minutes generates the large eroded mass (see Figure III.24) and thus a sharp increase of flow rate. Given the same soil density, it is noticed that non pre-saturated soil *B-90u* has a larger flow rate two to three time as much as pre-saturated soils *B-90s* and *B-90s-rep*. It can be attributed to the large erosion of fine fraction that induces the large flow rate.

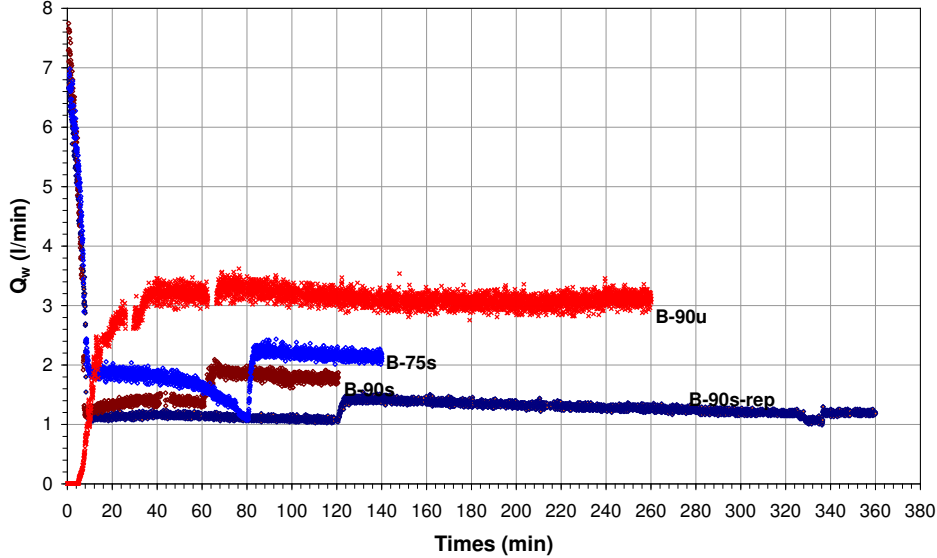


Figure III.26 The variation of downstream flow rate during the test

Figure III.27 shows the corrected downstream flow rate during the first 10 minutes. This corrected flow rate is attributed only to seepage water coming from the upstream side. The computation of corrected flow rate is shown in Figure III.28. To find the corrected flow rate curves, it is assumed that initially the whole flow rate is due to dewatering. It is assumed that the flow rate is decreasing linearly down to 0 l/min until the time when the downstream water level reached its final lowest position. The integration of this flow rate due to dewatering (the area below the curve) corresponds to the initial volume of water in the downstream reservoir. Finally the corrected flow rate is obtained by subtracting the “subtracted Q” to the “measured Q”.

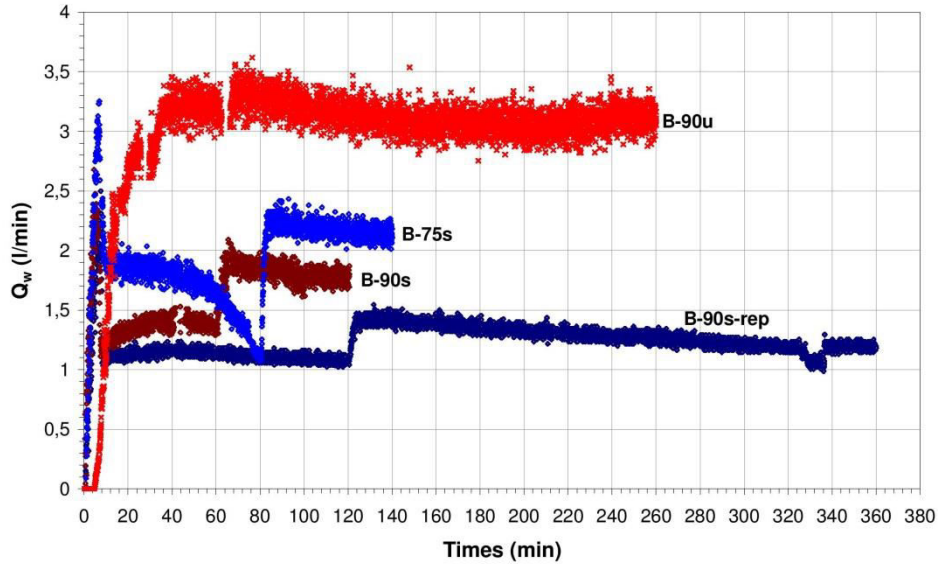


Figure III.27 The variation of corrected downstream flow rate during the test

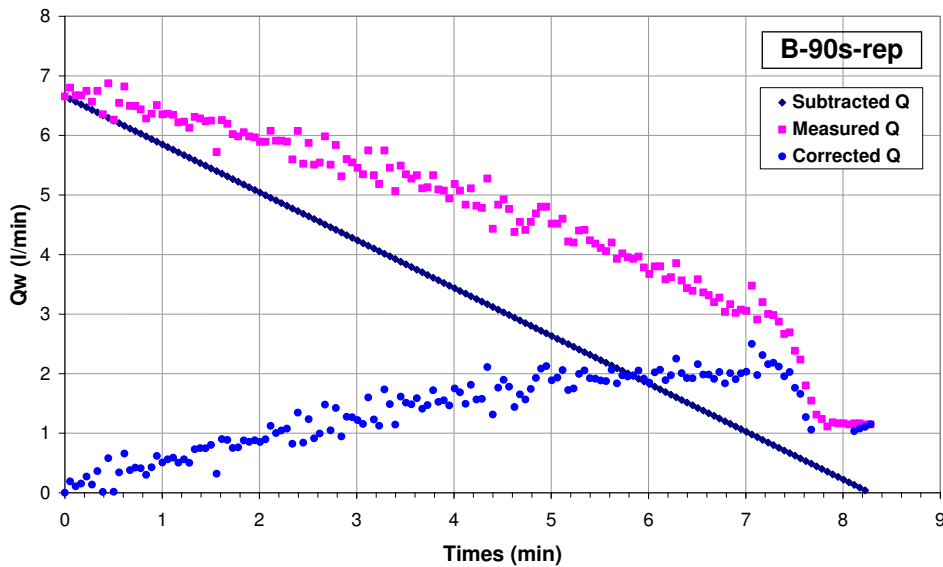


Figure III.28 Initial downstream flow rate versus corrected downstream flow rate

3.5.5 Spatial distribution of fine and density after seepage test

The development of suffusion in a soil can be indicated by spatial distribution of fine fraction after seepage tests. Spatial distribution of fines after tests is determined by taking samples from the body of the dike using a cylindrical mold having a volume of 79.481 cm^3 . Figure III.29 shows several locations of grading analyses for the specimen *B-90s-rep* and summarizes the percentage of fine and the soil density after test. It is worth noting that along the downstream slope (X1, X3, X6 and X12) the fine fraction percentage was lower than that of the initial condition. It can be explained that in the slope in the boundary between soil and water, the flow velocity is large enough to discharge the soil thus the percentage of fine fraction decreases even though there may be a supply of fine fraction from the upstream side. In addition, the decrease of fine fraction was also observed in some places in the bottom of

the dike. This decrease can be attributed to preferential flow. However, an increase of fine fraction equals to 27.10% appears in location X5. The variation of spatial distribution of fine fraction after test may relate to the evolution of water head within the body of the dike discussed in section 3.6.10. It is observed that soils near the bottom layers have a larger dry soil density ($\rho_d > 1.65 \text{ g/cm}^3$) than above layers.

Similar to *B-90s-rep*, the lower percentage along downstream slope and in the bottom of the dike were observed in the specimen *B-90s*, *B-75s* and *B-90u* (see Annex section).

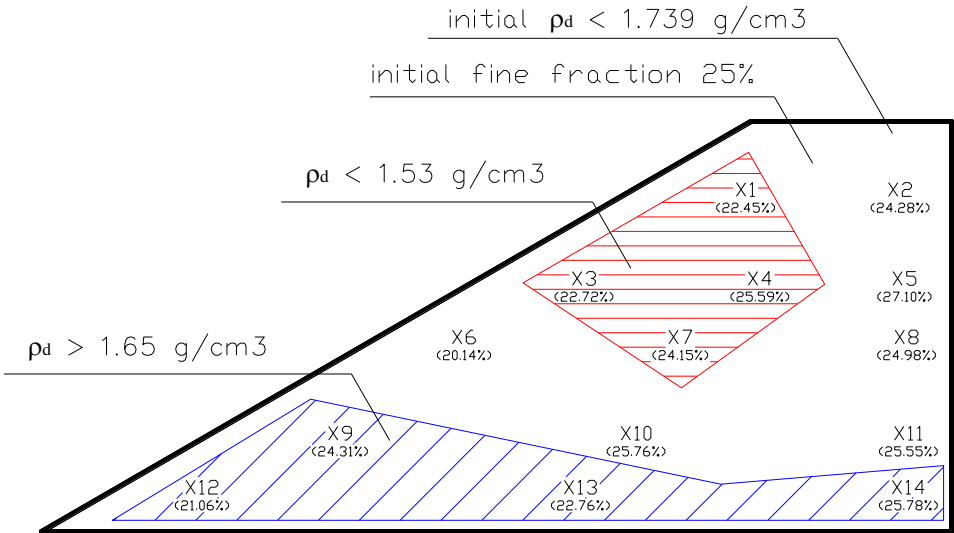


Figure III.29 Fine fraction and dry density in several locations after the seepage test (*B-90_{s-rep}*)

3.5.6 Displacement during seepage test

In order to follow the deformation of the dike, image processing with the PIV technique was carried out, and movement of the body of the dike along the downstream slope is exhibited. Figure III.30 Sliding in the downstream slope $t = 2.25$ to 2.50 min (*B-90s-rep*) Figure III.30 to Figure III.31 depicts the displacement along the downstream slope in minutes 3.75 and 6.75 resulted from PIV analysis whereas Figure III.32 shows the shape of the downstream slope at different time. It can be noticed that there was progressively slight sliding along downstream slope. The displacement may be attributed to: 1) water pressure, and/or 2) mass loss of fine fraction near the downstream slope (Figure III.24).

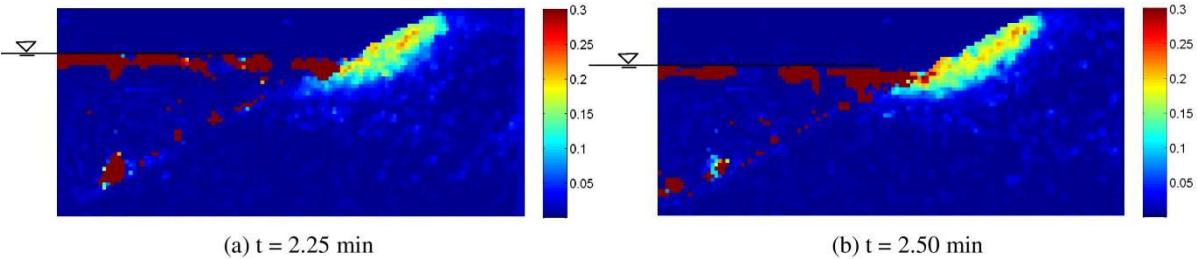


Figure III.30 Sliding in the downstream slope $t = 2.25$ to 2.50 min (*B-90_{s-rep}*)

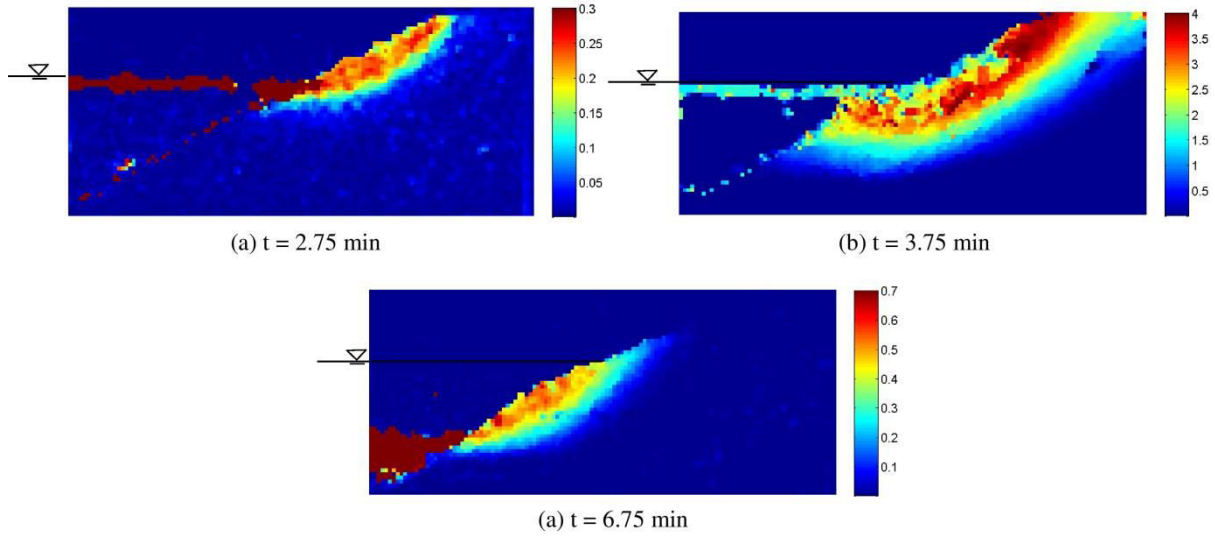


Figure III.31 Sliding in the downstream slope $t = 2.75$ to 6.75 min ($B-90_{s-rep}$)

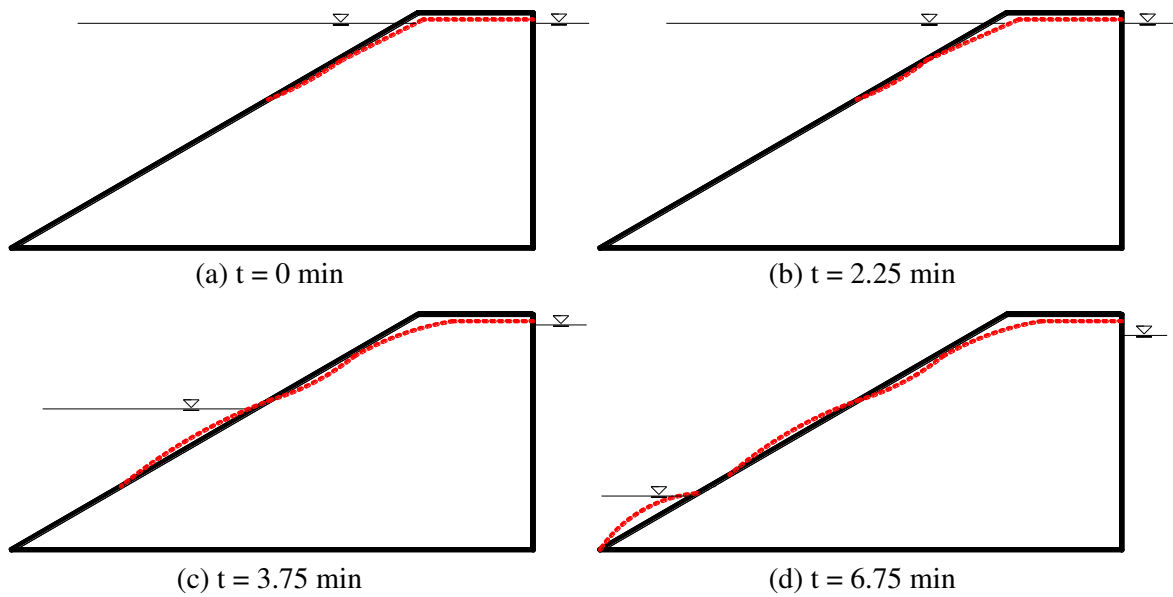


Figure III.32 Evolution of the shape of the downstream slope during the seepage test ($B-90_{s-rep}$)

3.5.7 Expended energy and erodibility classification

With the aim to compare the suffusion susceptibility of the soil constituting the dike models to the susceptibility identified from the triaxial erodimeter tests (see section 2.8.2), the energy-based approach is carried out. Figure III.34 shows the diagram of cumulative eroded mass versus cumulative expended flow energy of the tested soils whereas Figure III.35 displays the diagram of classification of its suffusion susceptibility.

The flow energy is computed as potential energy ($m \cdot g \cdot h$) where m is overflow water mass at downstream side (kg), g is gravitational acceleration (m/s^2) and h is water head difference between upstream and downstream side (m). Cumulative eroded mass here is eroded mass considered as mass in “beakers and outside beakers”. As energy and eroded mass defined per

unit volume, seepage area is defined following the phreatic line of seepage as shown in Figure III.33.

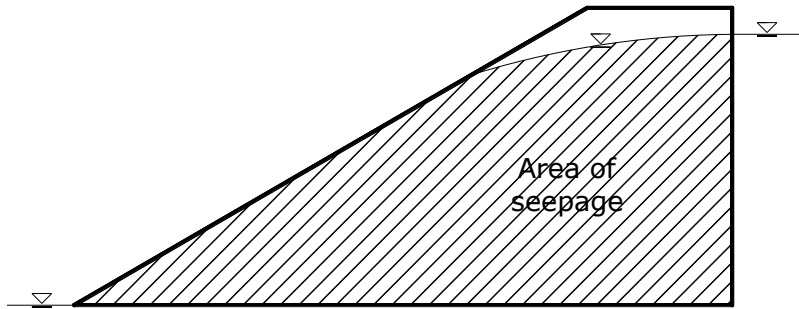


Figure III.33 Area of the soil where water go through (B-90_{s-rep})

From the dike test, all the soils are considered as erodible soil which is the same with the result from the triaxial erodimeter test. The repeatability test of the specimen B-90s as shown in Figure II.27 is fairly good, as the magnitude of the slopes is similar. Given gradation, the lower soil density B-75s is more erodible than the specimens B-90s and B-90s-rep.

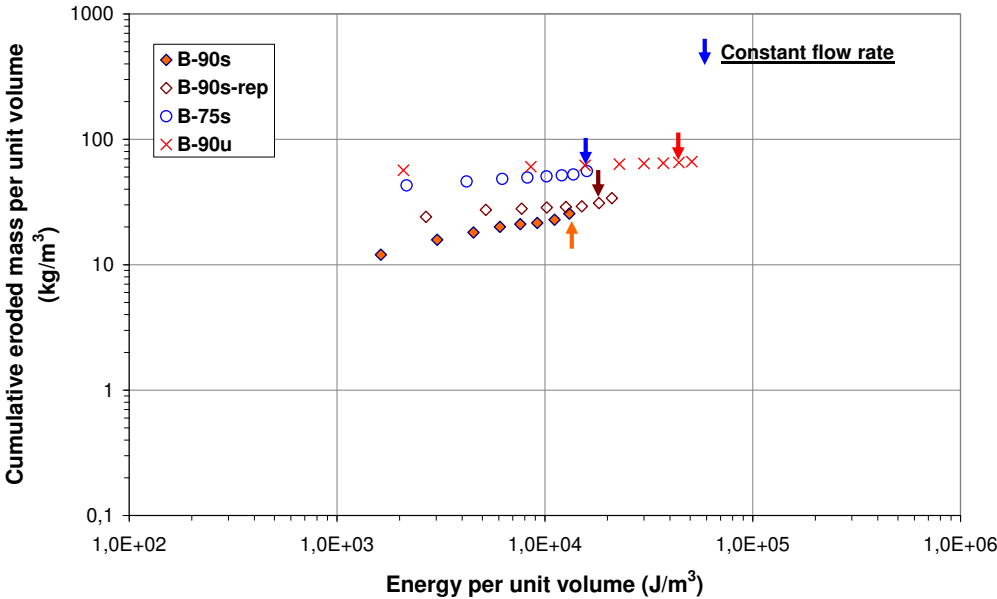


Figure III.34 Cumulative eroded dry mass versus cumulative flow energy

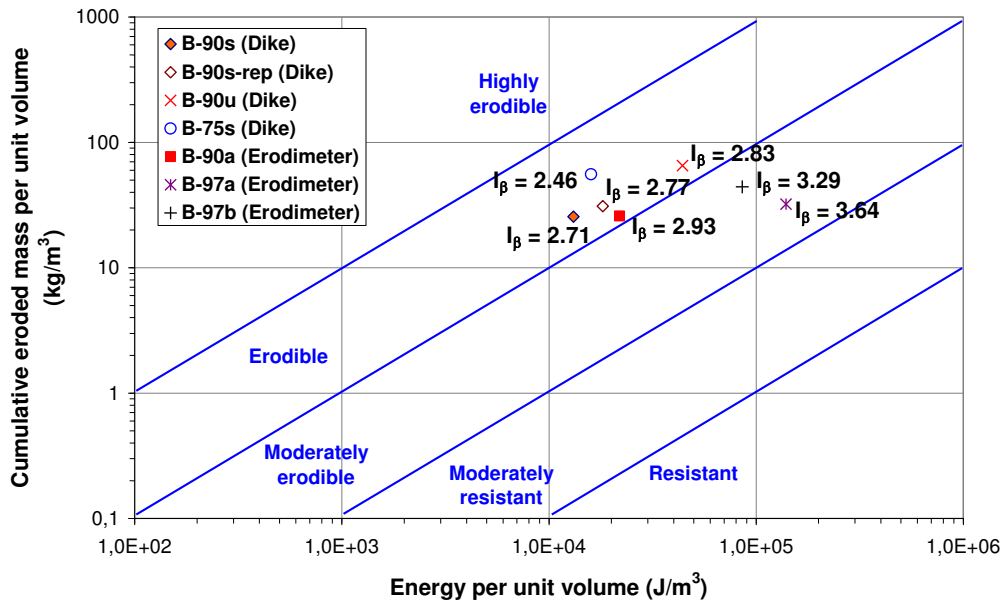


Figure III.35 Classification of suffusion susceptibility - energy-based approach

3.6 Numerical simulation

3.6.1 Introduction

In order to compare the result of the dike test and to provide a supportive interpretation, a simulation with the aid of Plaxis was carried out. The effect of the water seepage within the body of the dike on the hydraulic characteristic of the dike soil and the safety factor of the whole structure was investigated using Plaxis. In term of hydraulic loading on the dike, the evolution of seepage flow was executed with Plaxflow as a part of Plaxis. Internal erosion of the soil is not described with Plaxis, consequently these simulations assumed the soil is undisturbed by drag forces all along the seepage flow. To have the simulation easily followed by readers and to give a brief sight on Plaxis, step-by-step procedures are given.

Finally, the comparison of total head within the body of dike between measured value (from the dike test) and simulation value was realized. The evolution of the deviation between two values and safety factor during times was presented to characterize suffusion mechanism and to improve the understanding of the effect of suffusion on mechanical and hydraulic soil structure properties.

3.6.2 Methodology

Following procedures are described as methodology to given results of the evolution of total head within the body of the dike and the safety factor of the whole structure of the dike. In other words, different procedures may give different results.

3.6.3 Geometry (specimen B-90s)

To simulate the dike test in Plaxis, the first step the geometry of the dike should be realized. The geometry is inputted from “general setting” to model the geometry and to set the area where the geometry will be drawn. The geometry is modelled as plain strain and a fairly refined mesh is generated by using 15 nodes triangular finite elements, since such nodes provide more accurate results in complex problems such as bearing capacity and stability analyses. The area must be set large enough to accommodate the geometry in “dimension”

section. To model as close as the real dike test, as shown in Figure III.36, the half-shape dike has impervious boundaries except the slope, the crest and the left side of the dike. The small scale model of dike has a dimension 45 cm in height, 100 cm in length, 15 cm in width (perpendicular to the picture), 22 cm crest length and 30 degree slope.

For the boundary condition, the dike is modelled as full fixity in the base of geometry and roller condition for upstream side as depicted in Figure III.37. A full fixity means no displacement in the direction of axis-x and axis-y while roller condition corresponds to displacement only in the direction of axis-y.



Figure III.36 The front view of tested specimen

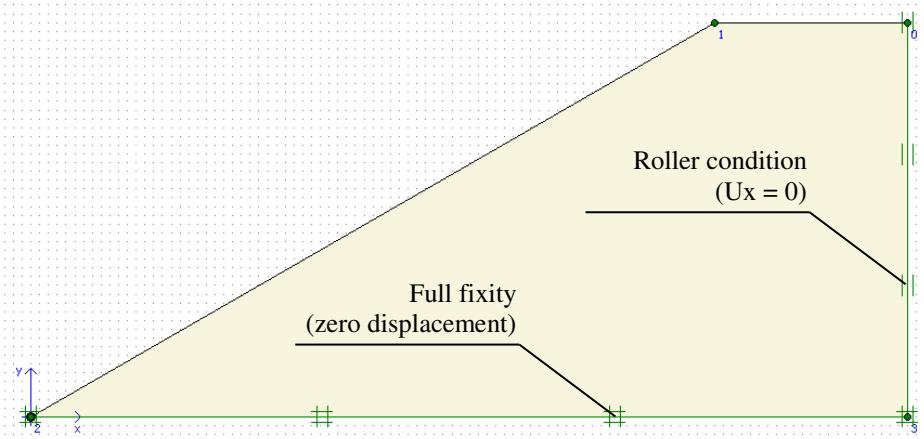


Figure III.37 The geometry condition of dike model

3.6.4 Input of soil properties

Table III.2 summaries the properties of tested soil as inputted in the *Plaxis*.

Material model:

The material considered as sandy gravel was modelled as advanced soil model with “hardening soil” model that the soil is described much more accurately than “mohr-coulomb”

model. Since such soil can dissipate the excess pore water pressure quickly the material is considered as drained.

Permeability:

Hydraulic conductivity (k) values was deduced by trial and error whereas the others were fixed as shown in Table III.2 with the objective to result in the same volumetric flow rate in the downstream side in the dike test. Due to difficulty to determine k value in horizontal direction, such value was assumed ten times larger than that of vertical direction. With $K_x = 1.2E-3$ m/s and $K_y = 1.2E-4$ m/s, the resulted flow rate is similar to the flow rate of experimental study (around 1.2 l/min) as displayed later in Figure III.27 and Figure III.46 .

Table III.2 Tested soil properties

Parameter	Name	Value	Unit
Material model	<i>Model</i>	Hardening-soil	-
Type of material behaviour	<i>Type</i>	Drained	-
Soil unit weight above phreatic level	γ_{unsat}	18.74	kN/m ³
Soil unit weight below phreatic level	γ_{sat}	20.80	kN/m ³
Permeability in horizontal direction	K_x	1.2E-3	m/s
Permeability in vertical direction	K_y	1.2E-4	m/s
Triaxial loading stiffness	$E50^{ref}$	5400	kN/m ²
Oedometer loading stiffness	E_{oed}^{ref}	5400	kN/m ²
Triaxial unloading stiffness	E_{ur}^{ref}	17550	kN/m ²
Poisson's ratio	ν	0.3	-
Cohesion	C_{ref}	0	kN/m ²
Friction angle	ϕ	41	°
Dilatancy angle	ψ	2.3	°
Initial void ratio	e_{init}	0.236	-
Void ratio minimum	e_{min}	0.217	-
Void ratio maximum	e_{max}	0.410	-
Change of permeability	c_k	1,00E+15	-

Stiffness parameter and dilatancy angle:

Being modelled as “hardening soil”, this model uses three different input stiffnesses: triaxial loading stiffness $E50^{ref}$, triaxial unloading stiffness E_{ur}^{ref} and the oedometer loading stiffness E_{oed}^{ref} . However, it is underlined that since only $E50^{ref}$ was realized, thus for E_{ur}^{ref} and E_{oed}^{ref} , they were deduced from empirical expression with E_{ur}^{ref} equals to three times as larger as $E50$ and E_{oed}^{ref} equals to $E50^{ref}$. The average value of $E50^{ref}$ is shown in Figure III.12 whereas the dilatancy angle is displayed in Figure III.13.

3.6.5 Initial phase

The test procedure consists of saturation process and seepage test. In Plaxis, these two processes are executed by *staged construction* phases. It is worth noting the saturation process

and seepage test are separated in calculation. In other words, they are executed in two different calculations. However, before the two processes are started, an initial condition or *initial phase* must be set. *Initial phase* is a soil condition from which other phase is based on. *Initial phase* in saturation process is where the soil is in dry condition without the existence of water whereas that of the seepage test is where the water level just in the crest level.

Figure III.38a shows the initial condition for saturation process. As seepage flow is not allowed to flow to the base of the dike, thus the base of geometry must be modelled as closed flow boundary, presented by a black line. Then water level is increased until reaching level just below the dike crest level as shown in Figure III.38b. The increase of water level was executed by *staged construction* loading input with the duration was set 24 hours.

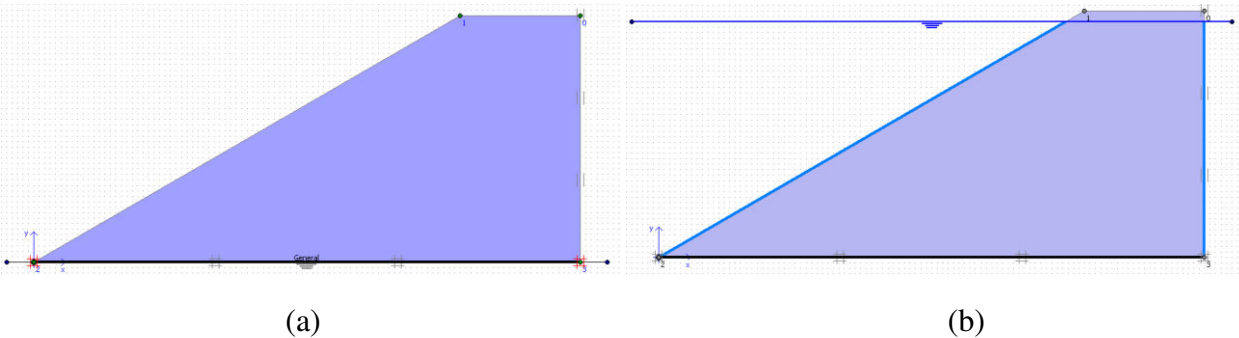


Figure III.38 Two initial conditions: (a) saturation phase, (b) seepage test

3.6.6 Seepage test phase

After one night saturation, seepage test is then carried out. The *initial phase* for seepage test is shown in Figure III.38b (the final stress state of saturation phase constitutes the initial stress state for the seepage test). The test is conducted by maintaining upstream water level constant and decreasing downstream water level to the base level as shown in Figure III.39. The time series of the evolution of water level in both sides is presented in Table III.3. For the calculation, the water level in downstream side (Column “A0” in Table III.3) was divided into four stages: decreasing of the water level from 39 cm (first stage identified as “phase 7” in Table III.3) to 27 cm (second stage identified as “phase 9” in Table III.3) after that to 0 cm (third stage identified as “phase 11” in Table III.3), corresponding to the dewatering of the downstream side of the dike, and finally the water is maintained to 0 cm until the fourth stage (identified as “phase 13” in Table III.3) to represent the pursue of the seepage test after the dewatering of the downstream side..

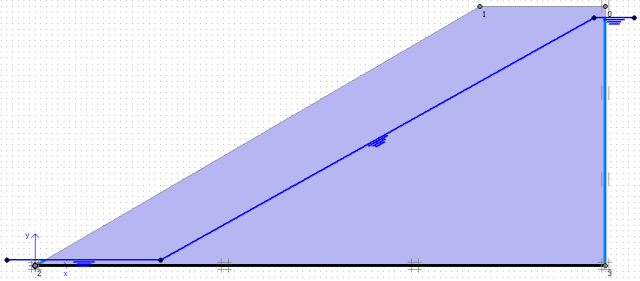


Figure III.39 Seepage test on tested dike

3.6.7 Calculation phase

In the calculation section, the variation of water level in seepage flow and its effect to the safety factor (FoS) of the dike were executed through several phases. Table III.3 summaries the computation phases of seepage test with the *initial phase* as depicted in Figure III.38a.

Due to non-horizontal soil surface of the dike (downstream slope), the execution of K0 procedure cannot be done in the *initial phase* to calculate the initial stress field. Thus the initial stresses must be computed by means of ‘gravity loading’ in the *Phase 1*. To find out the FoS of only self-weight of the dike, *phi/c reduction* calculation is executed from phase 1. The FoS of the dike without the presence of water flow should be larger than one (*Phase 2*).

The next step (*Phase 5*) is decreasing downstream water level corresponding to the duration of 1.25 minutes (*Phase 7*). *Phase 9*, *Phase 11* and *Phase 13* correspond to the duration of 3.75 minutes, 17 minutes and 6 hours respectively. All these phases: 7, 9, 11 and 13 were executed by Plaxflow as staged construction. Every staged construction was then continued by calculation type of *phi/c reduction* to execute the FoS due to the change of water level.

Table III.3 Computation stages of tested dike

Identification	Phase no.	Start from phase	Time (min)	Upstream H1 (cm)	Downstream A0 (cm)	Calculation
Initial phase	0	0				
Phase 1	1	0				Gravity loading
Phase 2	2	1				FoS - Phase 1
Phase 3	3	1	8.5	43	43	Saturation process
Phase 4	4	3				FoS - Phase 3
Phase 5	5	3	1440	43	43	Saturation process
Phase 6	6	5				FoS - Phase 5
Phase 7	7	5	1.25	43	39	Seepage flow 1
Phase 8	8	7				FoS - Phase 7
Phase 9	9	5	3.75	44	27	Seepage flow 2
Phase 10	10	9				FoS - Phase 9
Phase 11	11	5	17	41	0	Seepage flow 3
Phase 12	12	11				FoS - Phase 11
Phase 13	13	11	360	41	0	Seepage flow 4
Phase 14	14	13				FoS - Phase 13

3.6.8 Numerical results

From the calculation phase, the results consist of i) displacements both in the saturation process and the seepage test, ii) the safety factor, iii) the variation of water total head and iv) the flow rate.

3.6.9 Settlement in saturation process

The calculation of settlement in Plaxis results differently from the experimental study of the dike test. The dike settled during the saturation process if any (the case of settlement during the seepage test itself if saturation process was omitted (test *B90u*), is not discussed here after). During the saturation process, the magnitude of settlement was 13 mm for test *B90s-rep* (Figure III.40). The reason is the apparent cohesion due to water menisci in the initial unsaturated tested soil disappear when soil is saturated water can break capillary

pressure between the grains in unsaturated tested soil (see section III.5.1 Settlement during saturation phase). As the shear strength of the soil decreases the dike settles under its self-weight.

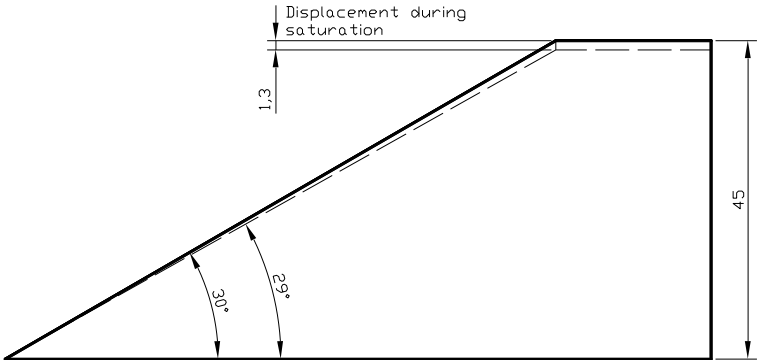


Figure III.40 Settlement measured experimentally on the test B-90s-rep of the dike during the saturation process

However, in numerical study with Plaxis the settlement was executed in two different phases: firstly due to the self-weight (gravity loading) of the soil considered as dry, and secondly due to the presence of water (saturation). *Phase 1* was dedicated to gravity loading and executed by calculation type *plastic analysis* (elastic-plastic deformation analysis). The settlement from *Phase 1* is shown in Figure III.41a. The movement of the settlement presented by arrow was in downward direction. However, upward direction movement, due to reduction of the vertical effective stress, is identified in *Phase 3* that corresponds to saturation process as shown in in Figure III.41b although its magnitude is almost zero. Thus the total magnitude of the settlement of the dike by Plaxis version equals to subtraction of the settlement of gravity loading from that of saturation process. The settlement is only 0.163 mm.

It can be noticed there is a big difference magnitude of settlement between the experimental study (13 mm) and numerical study by Plaxis. Indeed, apparent cohesion due to capillary menisci is not described by Plaxis (at least with the model chosen), consequently it is not possible to describe the slight collapse observed experimentally during the saturation. In term of eroded mass, it is worth stressing that there was no eroded mass captured during saturation process, thus soil erosion cannot be at the origin of the difference between experimental and numerical settlement during this latter process.

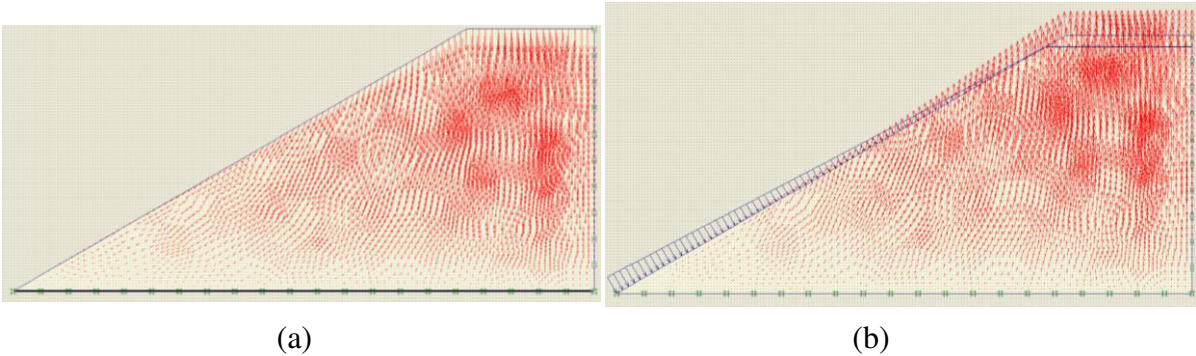


Figure III.41 Settlement of the dike simulated with Plaxis due to (a) gravity loading, (b) saturation phase

3.6.10 Flow network

Figure III.42 to Figure III.44 show equipotential drops computed with Plaxflow for several elapsed times. The total heads at pressure ports (identified with bold letters in Figure III.42 to Figure III.44) is almost constant from minute 17 (Figure III.42) to 360 (Figure III.44), i.e. once the downstream water level has been lowered down to the toe of the dike.

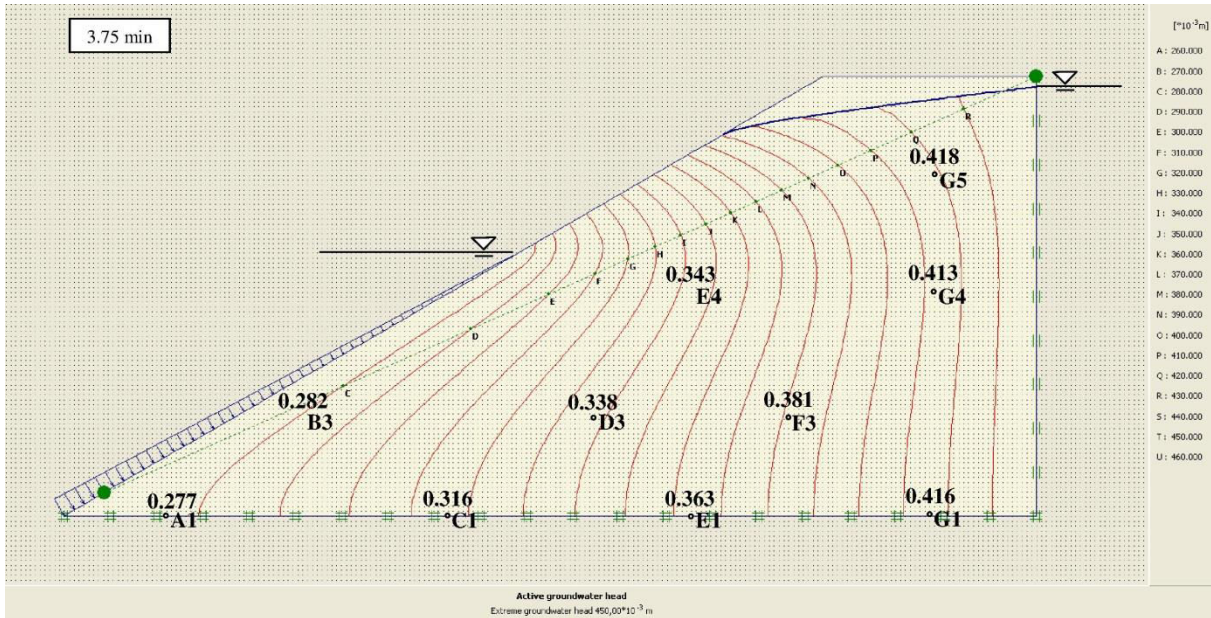


Figure III.42 Equipotential drops of the dike (in meter) at minutes 3.75, computed with Plaxflow

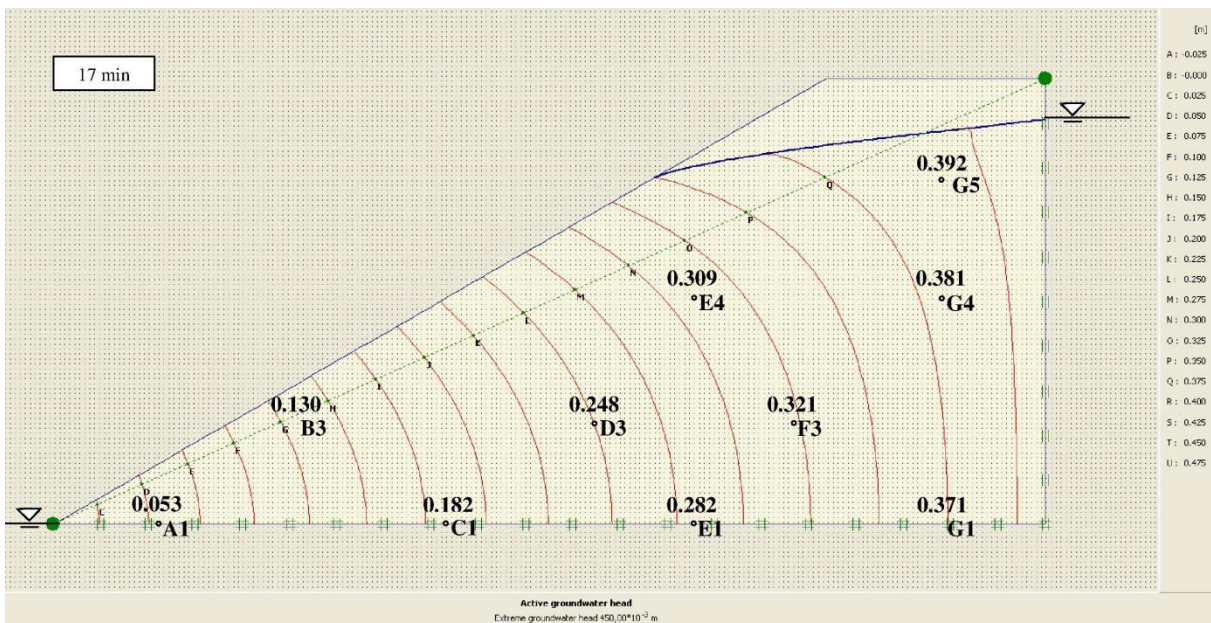


Figure III.43 Equipotential drops of the dike (in meter) at minutes 17, computed with Plaxflow

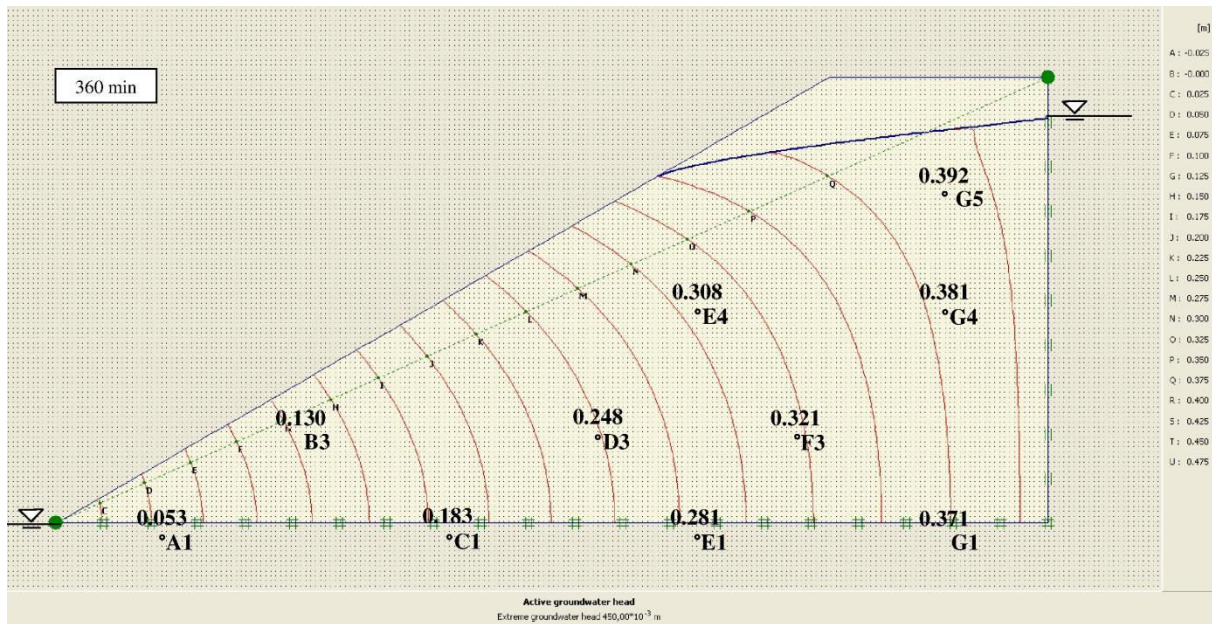


Figure III.44 Equipotential drops of the dike (in meter) at minutes 360, computed with Plaxflow

3.6.11 Global safety factor

In each calculation stage with Plaxis, it is possible to compute global safety factor through *staged-construction* phases. This computation uses the *Phi/c reduction method*. In the *Phi/c reduction* approach the strength parameters $\tan\phi$ and c of the soil are reduced until failure of the structure occurs. The total multiplier ΣMsf is used to define the value of the soil strength parameters at a given stage in the analysis:

$$\Sigma Msf = \frac{\tan \varphi_{input}}{\tan \varphi_{reduced}} = \frac{c_{input}}{c_{reduced}}$$

where the strength parameters with the subscript 'input' refer to the properties entered in the material sets and parameters with the subscript 'reduced' refer to the reduced values used in the analysis, ΣMsf is set to 1.0 at the start of a calculation to set all material strengths to their unreduced values.

At the failure stage of the slope, the total safety factor is given as follows:

$$FoS = \text{available strength} / \text{strength at failure} = (\Sigma Msf) \text{ at failure}$$

Table III.4 summaries the displacement and global safety factor of each stage of calculation. It can be noticed that the global safety factors decrease when the difference water level between the upstream and downstream side is larger (*Phase 9* and *Phase 11*). The FoS that equals to 1 can be reached when the head difference between upstream and downstream sides is 4 cm (*Phase 7*) as shown in Figure III.45.

Table III.4 Displacement and global safety factor

	Phase	Time (min)	Displacement (cm)	FoS
1	Gravity loading		$1.96 \cdot 10^{-1}$	
2	FoS - Phase 1			1.3188
3	Saturation process from base to level 43 cm	8.5	$0.225 \cdot 10^{-1}$	
4	FoS - Phase 3			1.4966
5	Saturation process for one night	1440	$0.103 \cdot 10^{-10}$	
6	FoS - Phase 5			1.4966
7	Seepage flow with downstream water level = 39 cm	1.25	$0.140 \cdot 10^{-1}$	
8	FoS - Phase 7			1.0
9	Seepage flow with downstream water level = 27 cm	3.75	$0.250 \cdot 10^{-1}$	
10	FoS - Phase 9			0.1498
11	Seepage flow with downstream water level = 0 cm	17	$0.883 \cdot 10^{-4}$	
12	FoS - Phase 11			0.5842
13	Seepage flow with downstream water level = 0 cm	360	$0.128 \cdot 10^{-16}$	
14	FoS - Phase 13			0.5842

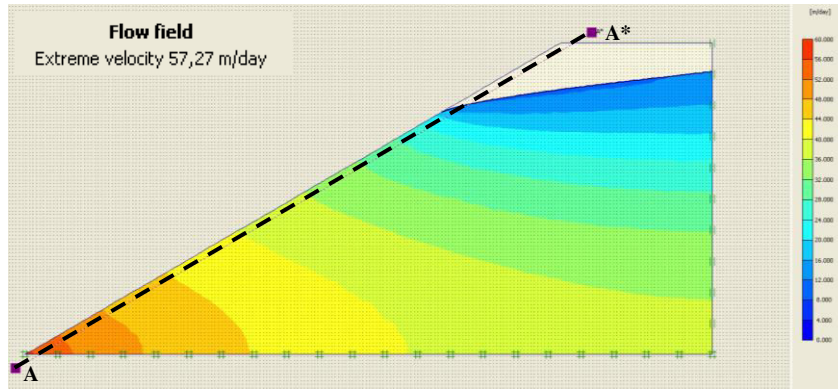


Figure III.45 Condition where FoS = 1.00

3.6.12 Comparison between experimental and numerical results

3.6.13 Downstream flow rate

With the aim to reach the same flow rate through the dike between experimental study and numerical study, permeability properties (hydraulic conductivity) in Plaxis were fixed after successive trials until the flow rate given by the dike simulation resulted in the same magnitude flow rate of the dike test. We just imposed a ratio between the horizontal conductivity k_x and the vertical one k_y equal to 10. Given hydraulic conductivities $k_x = 1.2E-3$ m/s and $k_y = 1.2E-4$ m/s as the input to Plaxis, the flow rate of the simulation resulted in similar magnitude of flow rate to the one measured during the experimental study 1.2 l/min (see Figure III.27). Figure III.47 shows the comparison of flow rate between experimental study and numerical study for several elapsed times for the specimen *B-90s-rep*. It can be noticed that the values between two approaches are not significantly different.



(a)



(b)

Figure III.46 Flow field at 360 minutes:
(a) Flow velocity, (b) flow rate section A-A*

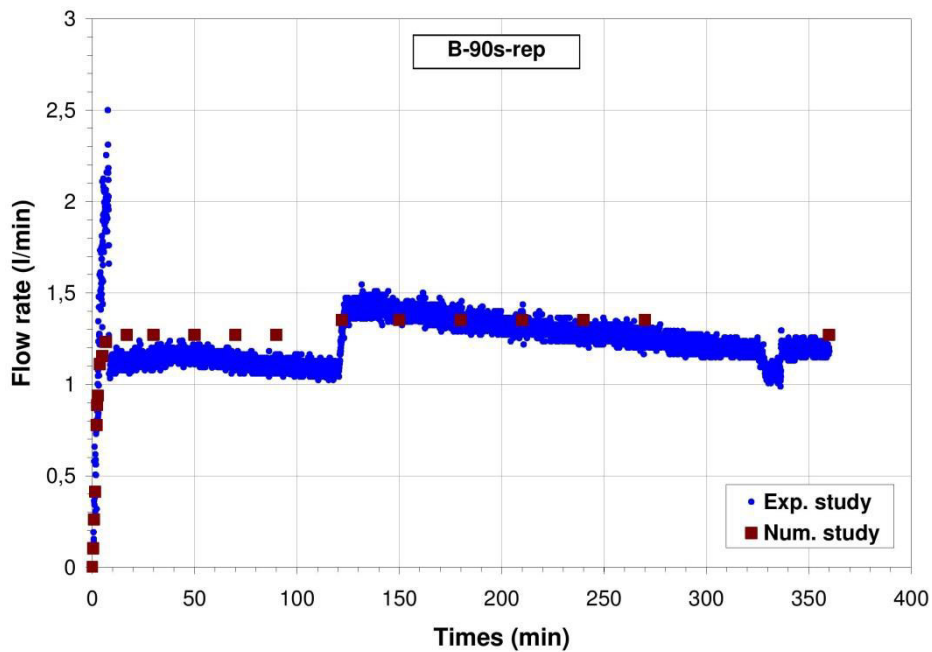


Figure III.47 Comparison of downstream flow rate between experimental study and numerical study (B-90s-rep)

3.6.14 Initiation of sliding and slip surface

Figure III.48 to Figure III.52 display the displacement along the downstream slope from the experimental study and numerical study, respectively. From the two pictures, it is shown that the numerical analysis gives much less displacement than the experimental study. It is due to the Plaxis can only take into account static equilibrium whereas during sliding phase, the soil is in dynamic condition.

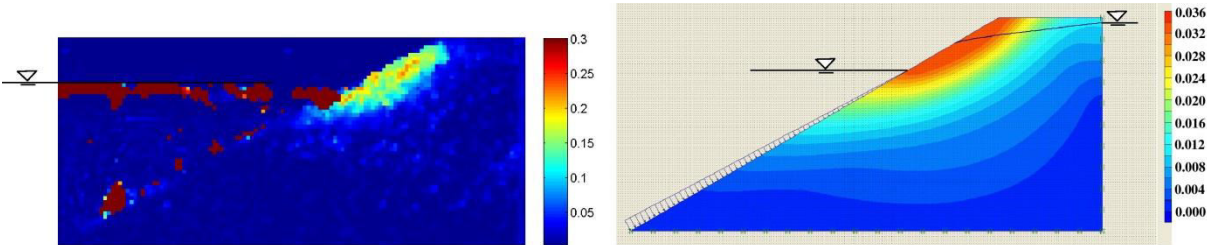


Figure III.48 Displacement of at minutes 2.25 in cm (experimental vs. numerical study)

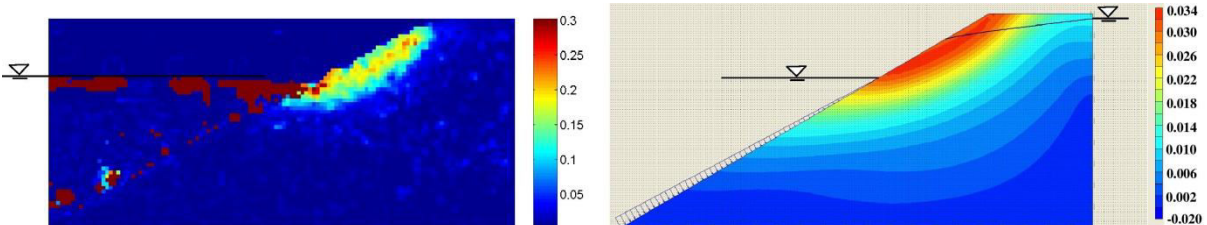


Figure III.49 Displacement of at minutes 2.50 in (experimental vs. numerical study)

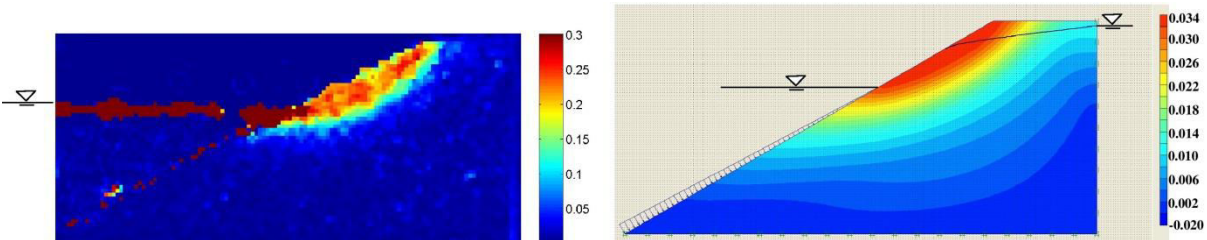


Figure III.50 Displacement of at minutes 2.75 (experimental vs. numerical study) in cm

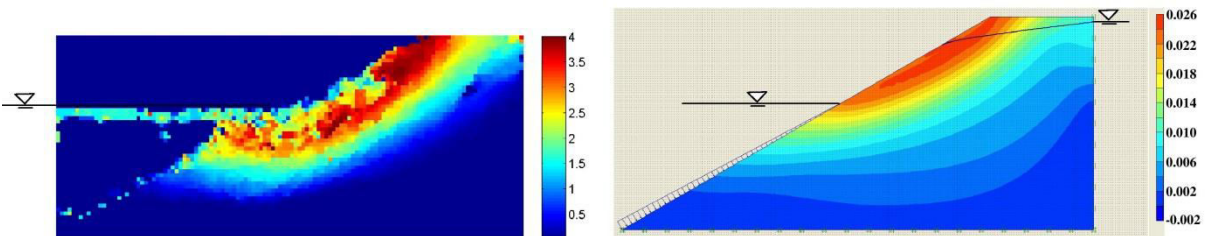


Figure III.51 Displacement of at minutes 3.75 (experimental vs. numerical study) in cm

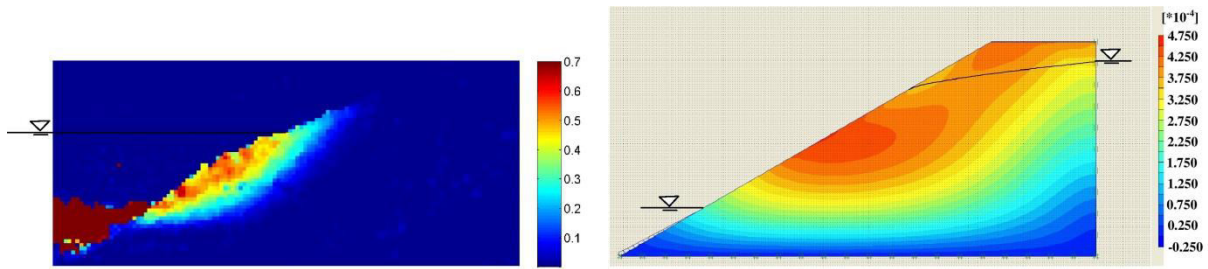


Figure III.52 Displacement of at minutes 6.75 (experimental vs. numerical study) in cm

3.6.15 Local hydraulic head

Figure III.53 to Figure III.55 depict the evolution of the equipotential drops resulted from simulation (presented by red line) for three different durations: at 3.75 minutes, 17 minutes and 6 hours. In the pictures the pressure ports represented by bold fonts (for instance **A1**, or **G4**) are plotted with total head values given from the dike test and simulation. Values in bracket correspond to the deviation values between the dike test and simulation. The positive values in green colour are when the measured values from the dike test are higher than the values from the simulation whereas values in red colour represent the inverse. The minus values of total head deviation in the base of dike (Figure III.53) may be attributed to preferential flow, thus the total head at these pressure ports drop quickly. It can be noticed during elapsed time water head deviation in the location near the downstream slope, *B3* and *E4* changed a lot from positive to negative values (see the evolution from Figure III.53 to Figure III.55). It may be attributed to loss of fine particle that induce the drop of water head. After six hour-test (Figure III.55), it is shown that almost all of the total head deviations within the body of dike are negative compared to the first minute-test (Figure III.53). It may be due to decrease of fine fractions. Only *G4* point is positive that can be attributed to increase of fine fractions 27.10% near that point (Figure III.29).

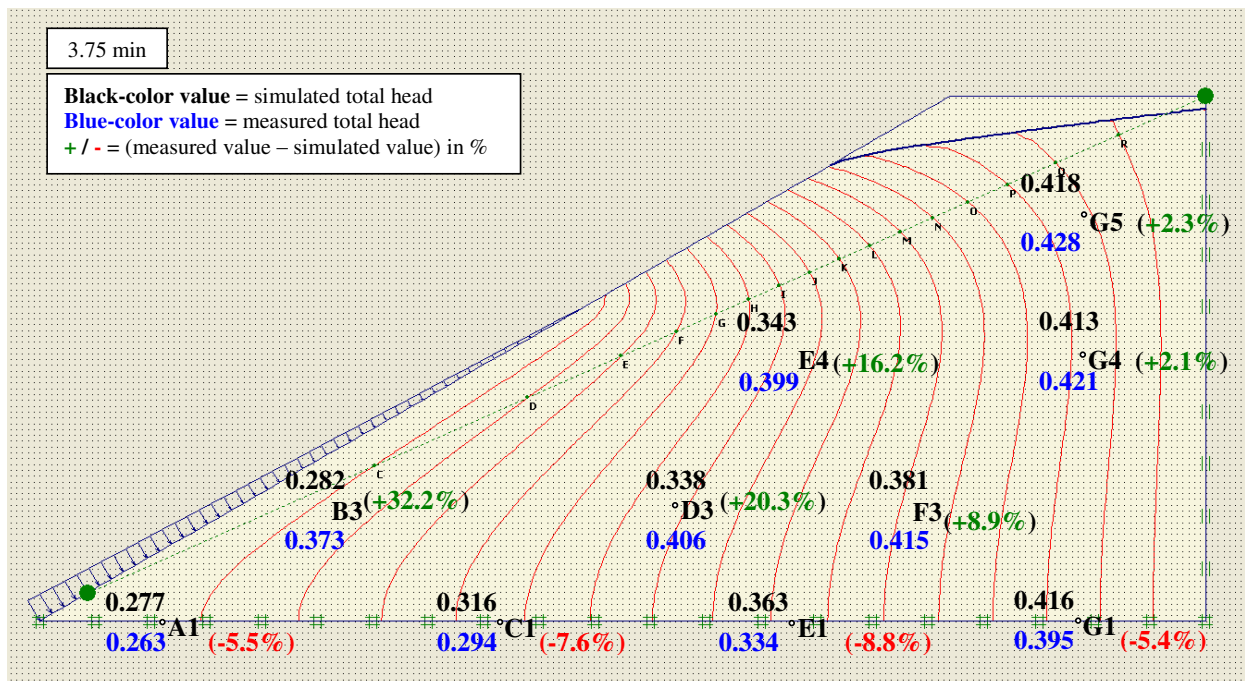


Figure III.53 Measured and simulated values of total head (in meter) at 3.75 minutes

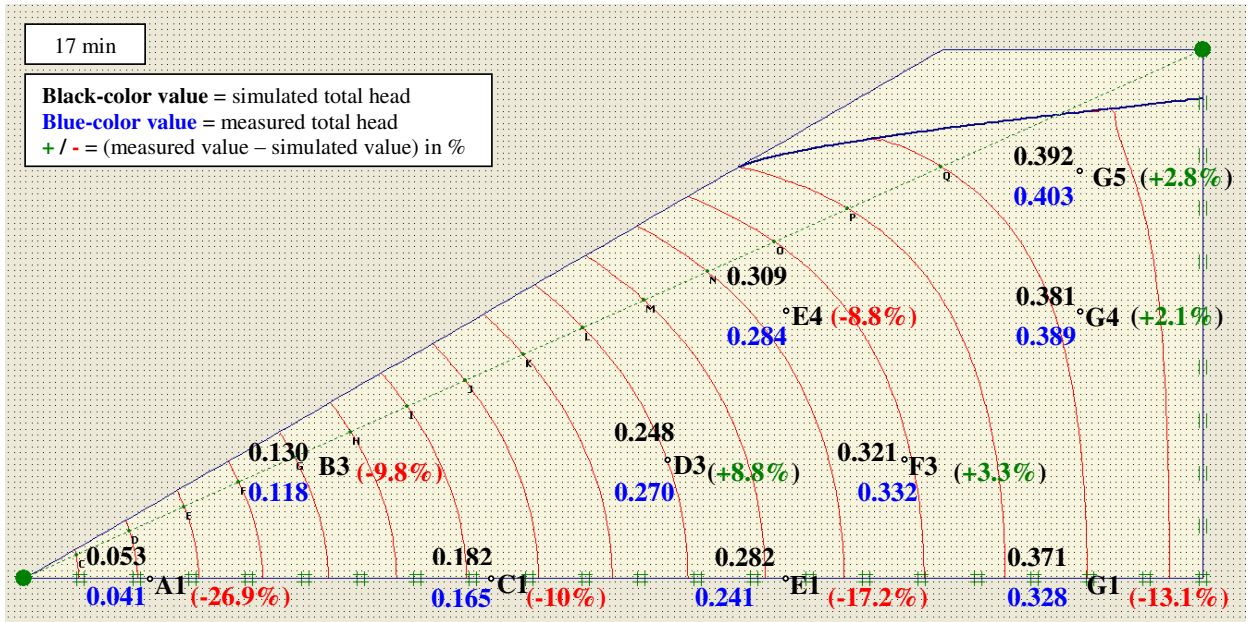


Figure III.54 Measured and simulated values of total head (in meter) at 17 minutes

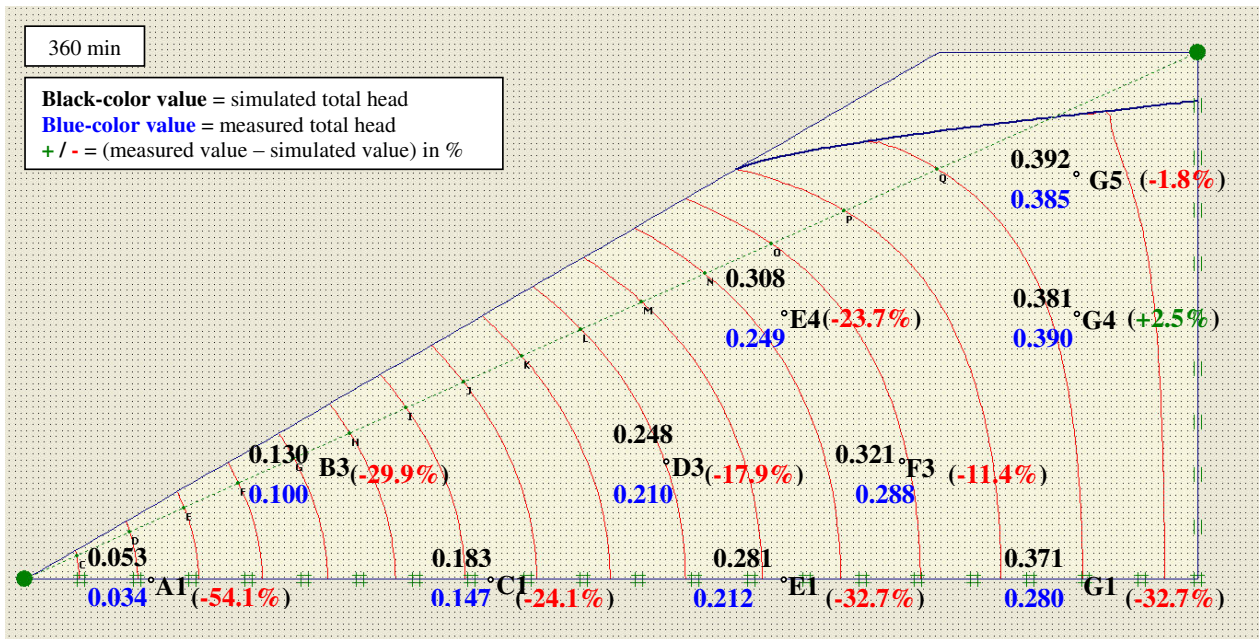


Figure III.55 Measured and simulated values of total head (in meter) at 6 hours

Figure III.56 to Figure III.58 show the diagram of the comparison of total water head at the pressure ports between experimental study and numerical study. In general during elapsed times, total heads from experimental study lower than those of numerical study. For instance at pressure port *E1* next to the downstream slope, the water head is much lower (experimental study) than that of the numerical study. This can be attributed to the decrease of fine fraction along the downstream slope that soils at the pressure port cannot maintain the water head.

Figure III.59 to Figure III.60 displays the diagram of time series of the evolution of deviation values of water head (values in the bracket in %). In general, the pressure ports show the decrease of the deviation values during the times whereas only *G4* shows the contrary. In minutes 17 as presented in Figure III.60, a slight increase of deviation appears in *A1* and *C1*. This increase may be attributed to the transport of fine fraction from the upstream side and then filtrated near the downstream side. However after six-hour duration, all the water head tubes except *G4* show the decrease of the deviation. From this evolution, it can be concluded that seepage flow has detached and transported the fine fraction to the downstream side and induce the drop of water head within the soil (see spatial distribution at the post-test in Figure III.29). Thus suffusion can affect the hydraulic properties of a soil.

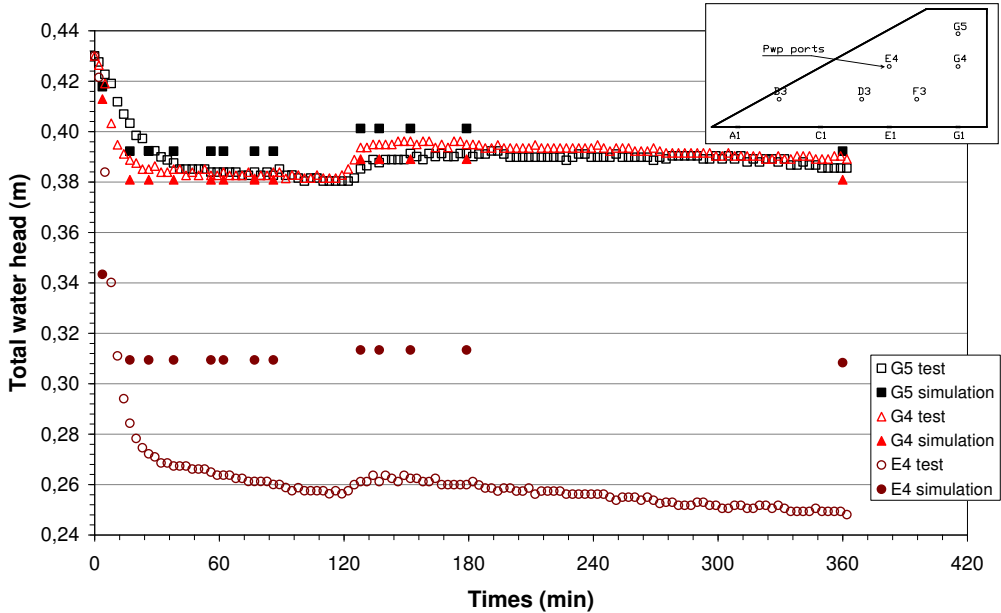


Figure III.56 Comparison of total water head within the dike between real test and simulation G5-E4 (B-90_{s-rep})

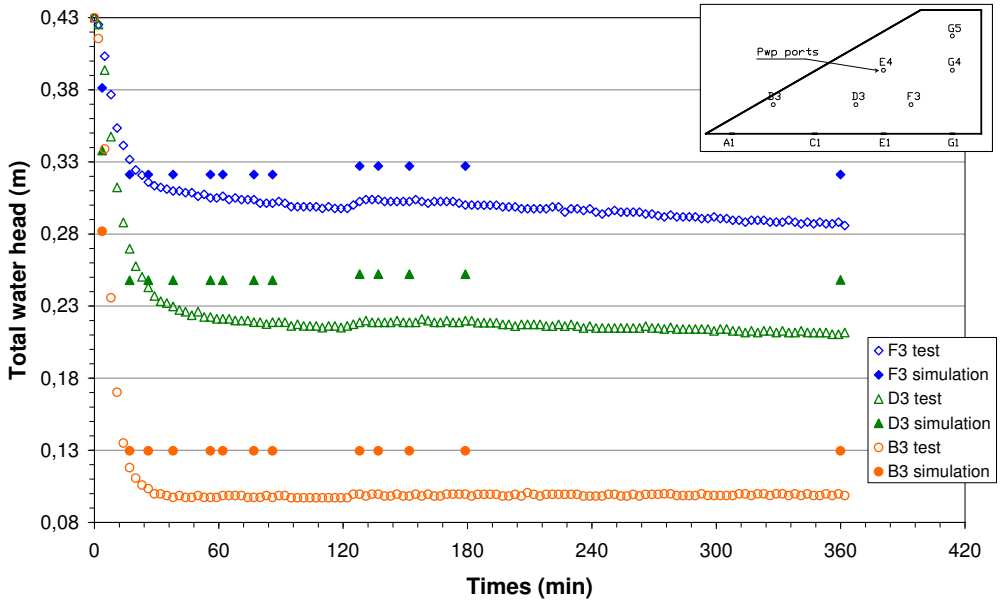


Figure III.57 Comparison of total water head within the dike between real test and simulation F3-B3 (B-90_{s-rep})

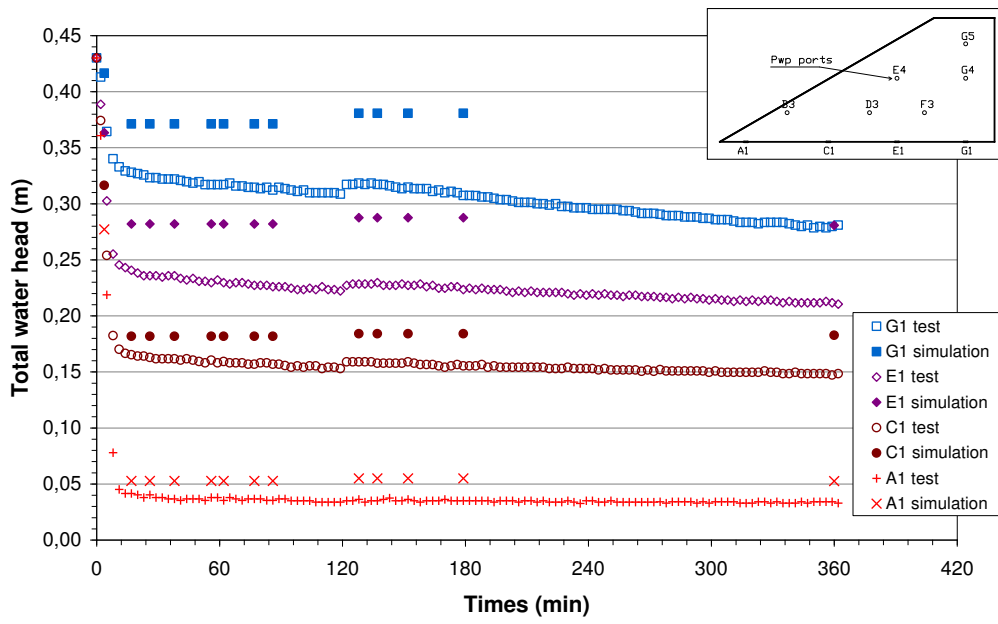


Figure III.58 Comparison of total water head within the dike between real test and simulation G1-A1 (B-90_{s-rep})

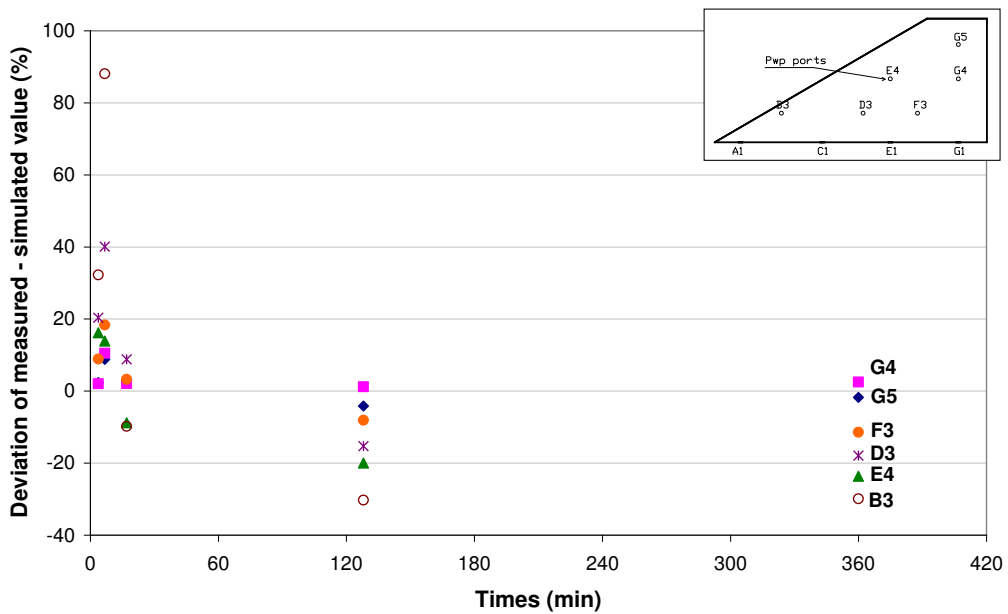


Figure III.59 Time series of evolution of deviation values within the dike soil (G5-B3)

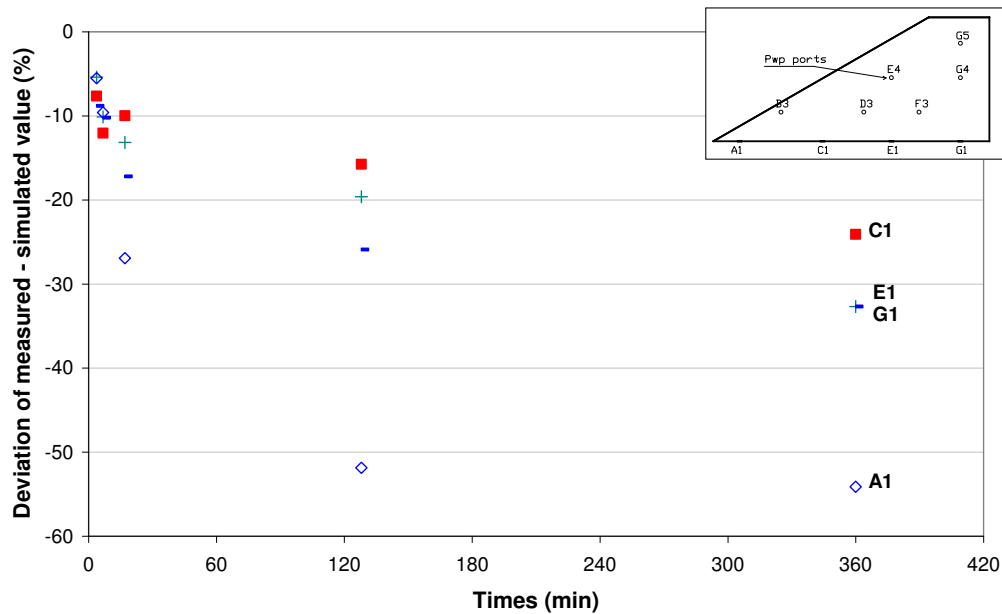


Figure III.60 Time series of evolution of deviation values within the dike soil (G1-A1)

3.7 Synthesis

The tests on the dike model were planned to study the development and the effect of suffusion on a water retaining structure made of soil. The objective was also to investigate the possibility to apply, to a soil structure, the soil characterizations relative to suffusion performed from laboratory erodimeter tests. As similitude laws were not respected, the objective is not to transfer the results obtained at the scale of this dike model to real structures. In the later goal, more advance tests would be necessary, for instance in a centrifuge.

The experimental results showed the suffusion effectively occurred in the dike model preferentially near the downstream slope and at the base of the dike, according to the post-test gradation analyses. Close to the downstream slope of the dike the soil is directly in contact with the atmosphere and auto-filtration cannot happen. The bottom of the dike is in contact with the bottom wall of the cell, and even if the bottom wall has been equipped with small roughness, preferential flow seems still to occur favoring the erosion of this region. Despite this heterogeneous development of suffusion within the dike model, the susceptibility to suffusion identified with the erodimeter in chapter II seems to hold if the energy approach is directly applied to the dike itself. In comparison with erodimeter test, in the dike model, the volume of soil, the average direction of seepage path and the boundaries conditions are different. However, the characterization of the dike with respect to suffusion itself, interpreted globally (i.e. from the total eroded mass, and the total dissipation of seepage energy) lead to results which are of the same order of magnitude as the one identified with a one-dimensional flow in the erodimeter device. The confirmation of this possible direct implement of suffusion characterization from laboratory erodimeter to soil structures using the energy approach would require more tests and more comparisons with different configurations. But, in case of a confirmation, it would constitute a simple tool directly applicable for engineers. More advance interpretations could be also carried out at the scale of the structure by estimating locally the energy dissipation due to the water seepage to refine the potential zones of erosion (especially when the structure is itself strongly heterogeneous).

Concerning the mechanical stability of the dike model, three tests (B-90s-rep, B-75s, and B-90u), among the four, presented an important sliding during the establishment of the water seepage (either by emptying the downstream reservoir, tests B-90s-rep and B-75s, or directly by filling the upstream reservoir, test B-90u). Hence, the occurrence of such a sliding is quite well reproducible. The reason of the lack of sliding for test B-90s is not very clear. Settlement during the saturation process, flow rate of the water seepage, eroded mass, and pressure field during the seepage test are similar to results obtained for the others tests (refer to the figures shown in the Annex), consequently the difference may be related to the soil itself that would be able to develop a shear strength higher than what was expected (possibly in relation with a problem concerning the soil preparation). In all cases, we prefer to discard this test and the discussion is only based on tests B-90s-rep, B-75s, and B-90u. Besides, a numerical simulation of the dike model was performed with Plaxis reproducing the different steps experienced by the test B-90s-rep. For this simulation, the coupling between the constitutive behavior of the soil and the redistribution of the interstitial water pressure during the seepage has been taken into account. However, there is no erosion law introduced in Plaxis and mechanical and hydraulic soil properties are assumed constant and equal to the initial one all along the seepage test. Therefore, if the simulation results to a different response of the structure than the one observed experimentally, then this difference can be identified as an induced effect of internal erosion. However, despite some slight differences in the pressure field between the experimental and the numerical ones (possibly related to local changes of hydraulic conductivity due to the partial washing, locally, of the fine fraction, and also due to the difficulty of the determination of the anisotropy of the hydraulic conductivity fixed here arbitrarily), the simulation was able to predict quite accurately the initiation (time initiation, and sliding region) of the main sliding observed experimentally. Consequently, even if the suffusion may degrade locally the mechanical properties of the soil constituting the dike model, the realized experiences do not allow to conclude about this point since, here, the redistribution of the interstitial water pressure (due to seepage) and then of the effective stresses is enough to trigger the observed sliding, as shown from Plaxis simulations.

It has been chosen here to work only on a half dike (with a single slope on the downstream side) to limit the size of the physical model. However, this solution results in high interstitial pressure near the downstream slope leading to its failure. Before making new tests, further numerical studies would be required to improve the design of the dike model (mainly its geometry) to avoid such instability of the downstream slope. One alternative could consist to increase the effective stress, or to select a more resistant soil, together with keeping a limited size of the physical model.

CONCLUSION AND PERSPECTIVES

1-Conclusion

Hydraulic structures such as dams and levees or dikes are subjected to some seepage passing through them. This can lead to a generation of the detachment and transport of certain constituent particles of the structures or their foundations. This problem is called internal erosion. Suffusion, as one type of internal erosions, refers to detachment and transport of finer particles through a coarser soil matrix due to seepage flow. The development of suffusion can modify hydraulic and mechanical characteristic of soils. This may trigger significant instabilities.

This research aims for investigating the initiation and development of the mechanism of suffusion under two experimental studies (triaxial erodimeter and small scale model of dike) and numerical study. The objectives of this research are: (1) to characterize suffusion mechanisms, (2) to provide a new methodology for identification of suffusion susceptibility of soils, (3) to propose suffusion susceptibility classification, (4) to establish better understanding of the mechanism of initiation and development of suffusion process on the body of dikes, in small scale model, and (5) to characterize the effects of suffusion on mechanical and hydraulic soil properties. This research comprises (1) modified triaxial erodimeter tests are performed in order to characterize the suffusion susceptibility of a soil. The soil specimens (50 tests) are subjected to downward seepage flow to erode the soils, (2) small scale model dike tests (4 tests) are carried out to characterize the effects of suffusion on the hydraulic behaviour of soils, (3) numerical simulation using Plaxis program to compare with experimental study of small-scale model of dike.

In order to investigate the mechanism of suffusion on cohesionless soils and to provide a classification of suffusion susceptibility, a series of tests is performed using an erodimeter. In a first time the susceptibility classification is carried out by taking into account only the grain size distribution thanks to different existing gradation based-criteria. To characterize soil response and the action of hydraulic loading, specimens are subjected to a water flow in downward direction. Three kinds of hydraulic loading history on several grain size distributions are used here with the aim to investigate the effect of hydraulic loading history.

The response of the specimens is investigated through the changing of hydraulic conductivity and erosion rate versus time respectively, and also the changing of erosion rate versus hydraulic shear stress or stream power in order to characterize the suffusion mechanism. As to the present a classification of suffusion susceptibility has not been yet established, the first approach (to classify suffusion susceptibility) using previous methods proposed by several researchers in case of interface erosion to investigate the evolution of erosion rate versus hydraulic shear stress can be conducted. Determination of erosion coefficients k_d and α (where k_d is erosion rate coefficient and α is ratio of cumulative eroded mass to cumulative expanded energy) is also presented. Afterward the energy-based approach based on two independent cumulative quantities is used. The effect of hydraulic loading history to the initiation and development of suffusion is also investigated. Finally based on the results, the classification of suffusion susceptibility and the methodology to evaluate the suffusion susceptibility are proposed.

From the results of the series of the tests, it is found that soil response of the specimens subjected to multi-stage hydraulic gradients is different from that of the specimens subjected to single-stage hydraulic gradient or injected flow rate condition. For all the tested specimens subjected to multi-stage hydraulic gradients, an evolution into three predominant phases can

be drawn: filtration, process of erosion and finally failure (represented by constant value of hydraulic conductivity). However, hydraulic conductivities of the specimens subjected to single-stage hydraulic and injected flow rate condition decrease during the given times. With the objective to classify the suffusion susceptibility of soils, the method by applying multi-stage hydraulic gradients is more possible to determine erosion coefficient k_d than the other methods (single-stage hydraulic gradient and injected flow rate). From the determination of the critical hydraulic gradient, it can be deduced that critical hydraulic gradient the specimens injected by multi-stage hydraulic gradients (a) is larger than that of the specimens injected by single-stage hydraulic gradient (b) ($i_{cr} b > i_{cr} a$). Under hydraulic loading history a , suffusion starts easier than in the case of hydraulic loading history b . With respect to hydraulic loading history, the erosion coefficient k_d of the specimens subjected to hydraulic gradient a is smaller than those of hydraulic gradient b ($k_d a < k_d b$). It can be noticed that the critical hydraulic shear stress of the specimens subjected to hydraulic gradient a is smaller than those of hydraulic gradient b ($\tau_c a < \tau_c b$) with the second approach. It seems that the development of suffusion appears smaller under hydraulic loading history a in term of both hydraulic gradient and hydraulic shear stress. In regard with fine content, the k_d value specimen A (20%) is smaller than that of specimen B (25%) and C (29%). In addition, given soil density and hydraulic loading history, the critical hydraulic shear stress τ_c of specimen $A-90a$ is smaller than that of $B-90a$, $\tau_c B-97a < \tau_c C-97a$, and $\tau_c B-97b < \tau_c C-97b$. Thus, it seems that specimens with lower fine content are more resistant.

With the objective to take into account the complexity of suffusion process, an energy approach is used in order to take into account the whole hydraulic loading history based on the energy dissipated by the fluid seepage. The determination of erosion coefficient (from the plot of linear approximation of cumulative eroded mass and cumulative energy) is more possible than that of the methods of hydraulic shear stress and flow power. All tests in single stage hydraulic gradient condition tests and constant flow rate condition tests can be studied with energy based method, but they do not work if tests are carried out under hydraulic shear stress method or flow power based method. With respect to the proposition of suffusion susceptibility classification, the points highlighted by arrows correspond to the end of development of suffusion (i.e. time from which hydraulic conductivity is stabilized) that is considered as the soil susceptibility. It is worth noting that the points before and after the arrows do not represent the soil susceptibility. The eroded mass in the beginning may be attributed to loss mass during saturation phase and during filtration process. The after-arrow points also do not represent the soil susceptibility since they correspond to the steady state. If the series of final points is taken into account, the soil susceptibility may become less erodible. For some tests without arrows, their susceptibility is defined at the last point. For the specimens subjected to single-stage hydraulic gradient and imposed controlled flow rate condition test, the last point is taken into account as a representative of the soil susceptibility.

From the post-test, the soil was divided into two layers: top and bottom with the same portions. Given the specimen $A-90b$ consisting 20% fine fraction, fine fraction in the top layer decreases whereas in the bottom layer increases. It seems that the water flow imposed during seepage test can detach and transport some fine fraction to the bottom layer. The percentage of fine fraction in the bottom layer higher than that of the initial condition can be attributed to the supply of fine fraction from the top layer whereas only small quantity of fine fraction erosion in the bottom layer. Thus the supply and filtration induce the increase of the fine fraction in the bottom layer. However, given the specimens $B-90a$ (25% fine fraction) and $C-97a$ (29% fine fraction), the percentage of fine fraction in both top and bottom layer decreases (less than that of initial condition). In the bottom layer, even though there is a supply of fine fraction from the top layer, the percentage of fine fraction still decreases. This can be attributed to a significant erosion of fine fraction in the bottom layer.

With the objective to propose a classification of suffusion susceptibility, we propose a classification of suffusion susceptibility based on energy approach (a diagram and index of suffusion resistance, I_{β}) that is divided into six categories of soil susceptibility from highly resistant to highly erodible.

From the investigation of the effect of hydraulic loading history on suffusion susceptibility, it can be distinguished into two groups: i) the same hydraulic gradients with different duration per stage, ii) different hydraulic gradients with the same duration per stage. Given different duration per stage, soils subjected to faster rate of the increase of hydraulic gradient resulted in soils more erodible than those subjected to longer rate. The different multi-stage hydraulic gradients a and b are applied with the same duration per stage. Multi-stage hydraulic gradient a applies small initial increment 0.1 whereas b applies large initial hydraulic gradient 1. Given the same duration per stage, soils subjected to hydraulic gradients b resulted in soils more erodible than those subjected to hydraulic gradients a . Therefore for given soil the susceptibility can be different under different hydraulic loading histories.

To investigate the effect of fine content to suffusion susceptibility, the gradation distributions A , B and C with 20%, 25% and 29% fine content respectively are performed. It is indicated that the lower fine content soils tend to require larger energy to the onset and development of erosion. It can be explained the reason of less fine content more resistant to suffusion is since the larger amount of coarse particles in specimen A having the same soil density with specimen B and C makes its constriction size so smaller that induces fine particles within the void of coarser particle more resistant to erosion. Thus fine content can affect suffusion susceptibility on a soil. With respect to soil density, the density seems to induce a slight increase of the soil's strength facing suffusion process. The specimens B and C demonstrate that given any hydraulic loading history, soils having higher soil density are more resistant.

With respect to small scale model of dike, 4 tests (3 pre-saturated soils and 1 non pre-saturated soil) were carried out to investigate the effect of suffusion on the hydraulic response of soil. One unstable soil is chosen from the tested soils performed with triaxial erodimeter. To characterize soil response owing to the action of hydraulic loading, the soil is subjected to a single-stage hydraulic gradient. During the test, the following measurements are carried out to follow the evolution of suffusion and the response of the soil structure: (1) the pore water pressure in the body of dike, (2) the settlement in the crest of dike, (3) the flow rate in the downstream side, (4) the displacement in the body of dike from digital image processing (Particle Image Velocimetry (PIV) measurement), (5) and eroded mass and (6) finally change in the grading and spatial fine distribution is characterized after the tests by taking soil samples from different locations in the body of the dike. However, to investigate the impact of suffusion on the hydraulic properties of the small scale dike model, the results presented in this chapter was not sufficient enough to a conclusion. Thus simulations by Plaxis were needed to complete the conclusion.

The experimental results showed the suffusion effectively occurred in the dike model preferentially near the downstream slope and at the base of the dike, according to the post-test gradation analyses. From image processing with the PIV technique, the movement of the body of the dike along the downstream slope is observed. It can be noticed that there was progressively slight sliding along downstream slope. The displacement may be attributed to: 1) water pressure, and/or 2) mass loss of fine fraction near the downstream slope. It is worth noting that along the downstream slope the fine fraction percentage was lower than that of the initial condition. It can be explained that in the slope in the boundary between soil and water, the flow velocity is large enough to discharge the soil thus the percentage of fine fraction decreases even though there may be a supply of fine fraction from the upstream side. In

addition, the decrease of fine fraction was also observed in some places in the bottom of the dike. This decrease can be attributed to preferential flow. The variation of spatial distribution of fine fraction after test may relate to the change of water head within the body of the dike.

With the aim to compare the suffusion susceptibility of the soil constituting the dike models to the susceptibility identified from the triaxial erodimeter tests, the energy-based approach is carried out. It demonstrates that given gradation, the suffusion susceptibility has the same order of magnitude even if under different methodology or different scale. In comparison with erodimeter test, in the dike model, the volume of soil, the average direction of seepage path and the boundaries conditions are different. Given gradation, the lower soil density *B-75s* is more erodible than the specimens *B-90s*.

For this simulation, the coupling between the constitutive behavior of the soil and the redistribution of the interstitial water pressure during the seepage has been taken into account. However, there is no erosion law introduced in Plaxis and mechanical and hydraulic soil properties are assumed constant and equal to the initial one all along the seepage test. During elapsed times, the total heads from experimental study are lower than those of numerical study. At pressure ports next to the downstream slope for instance, the water head of experimental study is lower than that of the numerical study. This can be attributed to the decrease of fine fraction along the downstream slope that soils at the pressure port cannot maintain the water head. From this evolution, it can be deduced that seepage flow has detached and transported the fine fraction to the downstream side and induce the drop of water head within the soil and slight slide. However, despite some slight differences in the pressure field between the experimental and the numerical ones, the simulation was able to predict quite accurately the initiation (time initiation, and sliding region) of the main sliding observed experimentally. Consequently, even if the suffusion may degrade locally the mechanical properties of the soil constituting the dike model, the realized experiences do not allow to conclude about this point since, here, the redistribution of the interstitial water pressure (due to seepage) and then of the effective stresses is enough to trigger the observed sliding, as shown from Plaxis simulations.

2-Perspectives

From the results of the two experimental studies, erodimeter test and small scale model of dike, it is demonstrated that the suffusion susceptibility has the same order of magnitude. However to confirm this result would require more tests and more comparisons with different configurations. More advance interpretations could be also carried out at the scale of the structure by estimating locally the energy dissipation due to the water seepage to refine the potential zones of erosion (especially when the structure is itself strongly heterogeneous).

As the realized dike tests do not allow to conclude on the effect of suffusion to instability of the dike, thus several alternatives can be tested: (1) selecting a more resistant soil with keeping the same geometry or (2) changing to the more stable geometry of the physical model with the same soil. Before making new tests, further numerical studies would be required to improve the design of the dike model (mainly its geometry) to avoid such instability of the downstream slope.

As the result of the small scale model of dike cannot be transferred to real structures since similitude laws were not respected, more advance tests for instance in a centrifuge would be necessary.

REFERENCES

- Acosta et al. (2013). Safety of a protection levee under rapid drawdown conditions. Coupled analysis of transient seepage and stability. Proceedings of the 18th International Conference on Soil Mechanics and Geotechnical Engineering, Paris : 3305-3308.
- Adel, H. D., Bakker, K. J., and Breteler, M. K. (1988). Internal stability of minestone. Proceedings of International Symposium on Modelling Soil-Water-Structure Interactions, Balkema, Rotterdam, 225–231.
- Arulanandan K, Perry EB (1983) Erosion in relation to filter design criteria in earth dams. *Journal of Geotechnical Engineering* 109(5): 682-696.
- Bandini, P. & Sathiskumar, S. (2009) Effects of silt content and void ratio on the saturated hydraulic conductivity and compressibility of sand-silt mixtures. *J. Geotech. Geoenviron. Eng. Div., ASCE*, 135, n° 12, 1976- 1980.
- Beek, V.M.van, Bezuijen, A., Zwanenburg, C. (2010) Piping: Centrifuge experiments on scaling effects and levee stability. *Physical modelling in Geotechnics – Springman, Laue & Seward (eds)*, ISBN 978-0-415-59288-8, 183-189.
- Bendahmane F, Marot D, Alexis A (2008) Experimental parametric Study of Suffusion and Backward Erosion. *Journal of Geotechnical and Geoenvironmental Engineering - ASCE* 134(1): 57-67.
- Berrones and Acosta (2011). Internal Erosion Due to Water Flow Through Earth Dams and Earth Structures. *Soil erosion studies*. InTech publisher, Croatia.
- Briaud, J.L. (2005) Erodibility of fine grained soils and new soil test. *Erosion of Soils and Scour of Foundation*, ASCE, pp1-10, ISBN 978-0-7844-0781-3
- Briaud (2008) Case Histories in Soil and Rock Erosion: Woodrow Wilson Bridge. Brazos River Meander. Normandy Cliffs. and New Orleans Levees. *Journal of Geotechnical and Geoenvironmental Engineering – ASCE* 134(10): 14425-1447.
- Building Research Establishment (2002) Reservoir safety – Floods and reservoir safety integration, Final Report vol 2 of 3.
- Burenkova VV (1993) Assessment of suffusion in noncohesive and graded soils”. *Proc. 1st Conf Geo-Filters, Kralruhe, Germany*: 357-360. Rotterdam: Balkema.
- Chang DS, Zhang LM (2011) A Stress-controlled erosion apparatus for studying internal erosion in soils. *Geotechnical Testing Journal*, 34(6): 579-589
- Chang (2012) Internal erosion and overtopping erosion of earth dams and landslide dams. PhD Thesis. The Hong Kong University of Science and Technology
- Chang, D.S., Zhang, L.M, Xu, T.H. (2012) Laboratory Investigation of Initiation and Development of Internal Erosion in Soils under Complex Stress States, *Proceeding ICSE6*, 895-902.
- Chang DS, Zhang LM (2013) Extended internal stability criteria for soils under seepage. *Soils and Foundations* 53(4): 569-583.
- Chapuis, R. P. (1992) Similarity of internal stability criteria for granular soils. *Canadian Geotechnical Journal*, 29(4): 711–713.
- Chapuis (1996) Migration of lines in 0-20mm crushed base during placement, compaction and seepage under laboratory conditions. *Can. Geotech Journal*, 33: 168-176

- Charles J A (1998) Internal erosion in European embankment dams. Progress report ICOLD European Club, 1-8.
- Charles et al. (2011) Lessons from Historical Dam Incidents. Environment agency Bristol.
- Comité Français des Grands Barrages (1997) Internal erosion typology, detection repair. Barrages & Reservoirs, 6: 126pp.
- Costa, John E. (1985) Floods from Dam Failures, U.S. Geological Survey Open-File Report 85-560, Denver, Colorado, 54 p.
- Engemoen, W.O., and Redlinger, C.G. (2009). – Internal Erosion Incidents at Bureau of Reclamation Dams. USSD Annual Conference. Nashville, Tennessee, USA: 731-745.
- Fell, R., et al. (2003) Time for Development of Internal Erosion and Piping in Embankment Dams, Journal of Geotechnical and Geoenvironmental Engineering, ASCE Vol. 129(4): 307-314.
- Fell R, Fry JJ, editors (2007) The state of the art of assessing the likelihood of internal erosion of embankment dams, water retaining structures and their foundations. Internal erosion of dams and their foundations. Taylor & Francis Publisher.
- Fell R, Fry JJ (2013) Erosion in geomechanics applied to dams and levees: 1-99. Bonelli S. Editor. ISTE – Wiley.
- Foster, M.A, Fell, R. (1999) A framework for estimating the probability of failure of embankment dams by piping using event tree methods. UNICIV Report No. R-377. School of Civil and Environmental Engineering, The University of New South Wales, Sydney, Australia 2052. ISBN: 85841 343 4.
- Foster, M.A (1999) The probability of failure of embankment dams by internal erosion and piping. PhD Thesis. School of Civil and Environmental Engineering, The University of New South Wales.
- Foster et al. (2000) The statistics of embankment dam failures and accident. Can. Geotech Journal, 37: 1000-1024.
- Fry, J.J, Vogel, A., Royet, P., Courivaud, J.R (2012) Dam failures by erosion lessons from ERINOH data bases. Proceeding ICSE6, Paris : 273-280
- Garner SJ, Fannin RJ (2010) Understanding internal erosion: a decade of research following a sinkhole event. The International J. on Hydropower & Dams 17: 93-98.
- Hanson, G. J. (1989) Channel erosion study of two compacted soils. Transactions of the ASAE 32(2): 485–490.
- Hanson GJ, Simon A (2001) Erodibility of cohesive streambeds in the loess area of the Midwestern U.S.A. Hydrological Processes 15(1):23-38.
- Horikhosi et al. (2012) Physical modelling test on the slope destabilization induced by internal erosion. ICSE6, 879-886.
- Horikoshi, A, Takahashi, A (2014) Physical model tests on suffusion-induced change of spatial distribution of fine fraction in embankments. Proceeding ICSE7, Perth : 163-170.
- ICOLD (1995) Dam Failures, Statistical Analysis, Commission Internationale des Grands Barrages, Bulletin 99, Paris, 73 pp.

- Indraratna et al. (2011) Assessing the potential of internal erosion & suffusion of granular soils. *Journal of Geotechnical and Geoenvironmental Engineering* 137: 550-554.
- Istomina VS (1957) Filtration Stability of Soils. Gostroizdat, Moscow, Leningrad (in Russian).
- Ke L, Takahashi A (2012) Strength reduction of cohesionless soil due to internal erosion induced by one dimensional upward seepage flow. *Soils and Foundations* 52(2012): 698–711.
- Kenney TC, Lau D (1985) Internal stability of granular filters. *Canadian Geotechnical Journal* 22: 215-225.
- Kézdi (1979) Soil physics selected topics. Elsevier Scientific Publishing Co. Amsterdam.
- Koolgaard, E.B and Chadwick, W.L (1988) Development of dam engineering in the United States. Pergamon press, USA.
- Kovacs G (1981) Seepage hydraulic. Elsevier Scientific Publishing Co. Amsterdam.
- Lafleur J, Mlynarek J, Rollin AL (1989) Filtration of broadly graded cohesionless soils. *Journal of Geotechnical Engineering* 115(12): 1747-1768.
- Li M (2008) Seepage induced failure of widely graded cohesion-less soils. PhD. Thesis. Department of Civil Engineering. The University of British Columbia. Vancouver. BC.
- Li M, Fannin J (2008) Comparison of two criteria for internal stability of granular soil. *Canadian Geotechnical Journal* 45: 1303-1309.
- Li, M., Fannin, R.J. (2012) A theoretical envelope for internal instability of cohesionless soil. *Géotechnique*, 62(1), pp.77–80
- Luo YL, Qiao L, Liu XX, Zhan ML, Sheng JC (2013) Hydro-mechanical experiments on suffusion under long-term large hydraulic heads. *Natural Hazards* 65:1361–1377.
- Marot D, Regazzoni PL, Wahl T (2011) Energy based method for providing soil surface erodibility rankings. *Journal of Geotechnical and Geoenvironmental Engineering – ASCE* 137(12): 1290-1294.
- Marot D, Bendahmane, F, Nguyen, H.H (2012a) Influence of angularity of coarse fraction grains on internal erosion process. *La Houille Blanche, International Water Journal* 6(2012): 47–53.
- Marot D, Le VD, Garnier J, Thorel L, Audrain P (2012b) Study of scale effect in an internal erosion mechanism. *European Journal of Environmental and Civil Engineering* 16(1): 1–19.
- Moffat R. (2002) A laboratory study of particle migration in cohesionless soils. Thesis. Department of Civil Engineering, The University of British Columbia.
- Moffat R, Fannin J (2006) A large permeameter for study of internal stability in cohesionless soils. *Geotechnical Testing Journal* 29(4): 273-279.
- Moffat R, Fannin RJ, Garner. SJ (2011) Spatial and temporal progression of internal erosion in cohesionless soil. *Canadian Geotechnical Journal* 48(3): 399-412.
- Moffat R. and Herrera P. (2014). Hydromechanical model for internal erosion and its relationship with the stress transmitted by the finer soil fraction. *Acta Geotechnica*, online first published 2014. DOI: 10.1007/s11440-014-0326-z.
- Nguyen HH, Marot D, Bendahmane F (2012) Erodibility characterisation for suffusion process in cohesive soil by two types of hydraulic loading. *La Houille Blanche, International Water Journal* 6: 54-60.

- Perzmaier S (2007) Hydraulic criteria for internal erosion in cohesionless soil. In *Internal erosion of dams and their Foundations*. Editors R. Fell and J.J. Fry. Taylor & Francis: 179-190.
- Reddi LN, Lee I, Bonala MVS (2000) Comparison of internal and surface erosion using flow pump test on a sand-kaolinite mixture. *Geotechnical Testing Journal* 23(1): 116-122.
- Sail Y, Marot D, Sibille L, Alexis A (2011) Suffusion tests on cohesionless granular matter. *European Journal of Environmental and Civil Engineering* 15(5): 799-817.
- Scholtes, L., Hicher, P. Y., and Sibille L. (2010). Multiscale approaches to describe mechanical responses induced by particle removal in granular materials. *C. R. Mecanique*, 338(10-11): 627–638.
- Schuler, U. (1995). How to deal with the problem of suffosion. *Research and Development in the Field of Dams, SNCLD, Crans-Montana, Switzerland*, 145–159.
- Schuler, U. and Brauns, J (1997). The safety of geotechnical filters. *Hydropower and Dams*, Issue six.
- Sherard, J. L. (1979). Sinkholes in dams of coarse broadly graded soils. *Proceedings of 13th ICOLD, New Dehli, India*, 25–34.
- Shire T. and O’Sullivan C. (2013). Micromechanical assessment of an internal stability criterion, *Acta Geotechnica*, 8:81-90.
- Skempton AW, Brogan JM (1994) Experiments on piping in sandy gravels. *Géotechnique* 44(3): 440-460.
- Sibille L, Lominé F, Poullain P, Sail Y, Marot D (2014) Internal erosion in granular media: direct numerical simulations and energy interpretation. *Hydrological Processes*, in press
- Sterpi D (2003) Effects of the erosion and transport of fine particles due to seepage flow. *International Journal of Geomechanics – ASCE* 3(1): 111-122.
- Tanaka T., Nagai, S., Doi, H., Hirose, T (2014) Experimental findings regarding piping failure of embankments. *Proceeding ICSE7, Perth* : 87-93.
- Terzaghi, K. (1939). Soil mechanics: a new chapter in engineering science. *Journal of the Institution of Civil Engineers*, 12(7): 106–141.
- Thoman, R. W., and Niezgodna, S. L. (2008). Determining erodibility, critical shear stress, and allowable discharge estimates for cohesive channels: case study in the Power River Basin of Wyoming. *Journal of Hydraulic Engineering*, 134(12): 1677–1687.
- Tomlinson, S.S and Vaid, Y.P (2000) Seepage forces and confining pressure effects on Piping Erosion. *Canadian Geo Journal* : 1-13.
- US Army corps of engineering (2012) Best Practices in Dam and levee safety risk analysis. Presentation.
- US.Department of the Interior (2012) Internal erosions risks.
- Wan CF, Fell R (2004) Investigation of rate of erosion of soils in embankment dams. *Journal of Geotechnical and Geoenvironmental Engineering – ASCE* 130(4):373-380.
- Wan CF, Fell R (2008) Assessing the potential of internal instability and suffusion in embankment dams and their foundations. *Journal of Geotechnical and Geoenvironmental Engineering – ASCE* 134(3): 401-407.

LIST OF PUBLICATION

- Marot D., Rochim A., Nguyen H.H., Bendahmane F., Sibille L. (2014) Méthodologie de caractérisation de la sensibilité des sols aux processus d'érosion interne. XIII^{èmes} Journées Nationales Génie Côtier - Génie Civil, 2-4 juillet, Dunkerque.
- Marot D., Rochim A., Nguyen H.H., Bendahmane F., Sibille L. (2014). Systematic methodology for characterization of suffusion sensibility. 7th International Conference on Scour and Erosion (ISCE-7). 2-4 December 2014, Perth, Australia.
- Rochim A., Marot D., Sibille L. (2015). Soil sensibility characterization of granular soils due to suffusion. 2nd International Conference on Advances in Civil, Structural and Construction Engineering – CSCE. 18-19 April 2015, Rome, Italy.
- Rochim A., Marot D., Sibille L., Bendahmane F. (2015). The effect of fine content and history of hydraulic loading on the characterization of suffusion sensibility of cohesionless soil. 6th International Symposium on deformation characteristics of geomaterials. 15-18 November 2015, Buenos Aires, Argentina
- Rochim A., Marot D., Sibille L. Le V.T. (2016). A possible characterization of suffusion susceptibility independent of the hydraulic loading history? Submitted for 8th International Conference on Scour and Erosion (ISCE-8). 12-15 September 2016, Oxford, UK.
- Le V.T., Marot D., Rochim A., Bendahmane F., Nguyen H.H. (2016). Suffusion susceptibility characterization by triaxial erodimeter and statistical analysis. Submitted for 8th International Conference on Scour and Erosion (ISCE-8). 12-15 September 2016, Oxford, UK.
- Marot D., Rochim A., Nguyen H.H., Bendahmane F., Sibille L. Assessing the susceptibility of gap graded soils to internal erosion: proposition of a new experimental methodology. Soumis à la revue Natural Hazards (en cours de 2^{ème} lecture).
- Rochim A., Marot D., Sibille L., Le V.T. Effect of hydraulic loading history on the characterization of suffusion susceptibility of cohesionless soils. Article en préparation pour soumission à la revue Journal of Geotechnical and Geoenvironmental Engineering (ASCE)
- Le V.T., Marot D., Rochim A., Bendahmane F., Nguyen H.H. Investigation of suffusion susceptibility by triaxial erodimeter tests and statistical analysis. Article en préparation pour soumission à la revue Canadian Geotechnical Journal

Annex 1 – Summary of suffusion test performed

Tested specimens: G5A, G5B, G6, P1, P2, P3 and P4	
Figure 1	Variation of hydraulic conductivity (G5A to P4)
Figure 2	Time series of erosion rate (G5A to P4)
Figure 3	Erosion rate versus hydraulic shear stress (G5A to P1)
Figure 4	Erosion rate versus hydraulic shear stress (P2 to P4)
Figure 5	Erosion rate versus flow power (G5A to P1)
Figure 6	Erosion rate versus flow power (G6)
Figure 7	Erosion rate versus flow power (P2 to P4)
Figure 8	Cumulative eroded mass versus energy (G5A to P4)
Tested specimens: L1, L2, L3, L4Ai, L4Aii, L4C, L4D and L5	
Figure 9	Variation of hydraulic conductivity (L1 to L5)
Figure 10	Variation of hydraulic conductivity (L4C and L4D)
Figure 11	Time series of erosion rate (L1 to L5)
Figure 12	Erosion rate versus hydraulic shear stress (L1 to L3)
Figure 13	Erosion rate versus hydraulic shear stress (L4Ai to L5)
Figure 14	Erosion rate versus hydraulic shear stress (L4C and L4D)
Figure 15	Erosion rate versus flow power (L1 to L3)
Figure 16	Erosion rate versus flow power (L4Ai to L5)
Figure 17	Erosion rate versus flow power (L4C and L4D)
Figure 18	Cumulative eroded mass versus energy (L1 - L5)
Tested specimens: D1, D2, D3B, M1, M3, M4, S1 and S2	
Figure 19	Variation of hydraulic conductivity (D1 to S2)
Figure 20	Time series of erosion rate (D1 to S2)
Figure 21	Erosion rate versus hydraulic shear stress (D1 and S1)
Figure 22	Erosion rate versus hydraulic shear stress (D2, D3B and S2)
Figure 23	Erosion rate versus hydraulic shear stress (M1, M3 and M4)
Figure 24	Erosion rate versus flow power (D1 and S1)
Figure 25	Erosion rate versus flow power (D2, D3B and S2)
Figure 26	Erosion rate versus flow power (M1, M3 and M4)
Figure 27	Cumulative eroded mass versus energy (D1 - S2)
Tested specimens: B-90f, C-90a, Chav-1, Chav-2i, Chav-2ii, R1-90b, R2-97f and R2-97g	
Figure 28	Variation of hydraulic conductivity (C-90a and R1-90b)
Figure 29	Variation of hydraulic conductivity (Chav-1, Chav-2i and Chav-2ii)
Figure 30	Variation of hydraulic conductivity (B-90f, R2-97f and R2-97g)
Figure 31	Time series of erosion rate (C-90a to R1-90b)
Figure 32	Time series of erosion rate (B-90f to R2-97g)
Figure 33	Erosion rate versus hydraulic shear stress (C-90a and Chav-2i)
Figure 34	Erosion rate versus hydraulic shear stress (R1-90b, Chav-1 and Chav-2ii)
Figure 35	Erosion rate versus hydraulic shear stress (B-90f, R2-97f and R2-97g)
Figure 36	Erosion rate versus flow power (C-90a and Chav-2i)
Figure 37	Erosion rate versus flow power (R1-90b, Chav-1 and Chav-2ii)
Figure 38	Erosion rate versus flow power (B-90f, R2-97f and R2-97g)
Figure 39	Cumulative eroded mass versus energy (B-90c to R2-97g)

Annex 2 – Properties of the suffusion test

Tested gradations	Tested specimens	Hydraulic loading	Duration per stage
G5	G5A	i = 1-2-3-4-5-6-7-8-9-10-11-12-13-14-15-16	30
	G5B	i = 0.1-0.2- ... -0.9-1-1.2-1.4- ... -2-2.5-3-3.5-4-5-6-7-8-9	30
G6	G6	i = 0.1-0.25-0.4-0.55-0.7-0.85-1-1.25- ... -2-2.5- ... -5-6-7- ... -12	15
P1	P1	i = 1-2-3-4-5-6-7-8-9-10-11-12-13-14-15-16	30
P2	P2	i = 1-2-3-4-5-6-7-8-9-10-11-12-13-14-15	30
P3	P3	i = 1-2-3-4-5-6-7-8-9-10	30
P4	P4	i = 1-2-3-4-5-6-7-8-9	30
L1	L1	i = 0.1-0.2-0.4-0.8-1-2-3	60
L2	L2	i = 0.1-0.2-0.4-0.8-1-2-3	60
L3	L3	i = 0.1-0.2-0.4-0.8-1-2-3	60
L4	L4Ai	i = 0.1-0.2-0.4-0.8-1-2-3-4	60
	L4Aii	i = 0.1-0.2-0.4-0.8-1-2-3	20
	L4C	i = 0.8	60
	L4D	i = 2	60
L5	L5	i = 0.1-0.2-0.4-0.8-1-2-3	60
D1	D1	i = 0.1-0.2-0.4-0.8-1-2-3-4-5- ... -16	20
D2	D2	i = 0.1-0.2-0.4-0.8-1-2-3-4-5-6-7	20
D3	D3B	i = 0.5-1-1.5-2.5-3.5-4.5-5.5-6.5	20
M1	M1	i = 0.1-0.2-0.4-0.8-1-2-3-4-5	20
M3	M3	i = 0.1-0.2-0.4-0.8-1-2-3-4-5-6	20
M4	M4	i = 0.1-0.2-0.4-0.8-1-2-3-4-5-6-7-8	20
S1	S1	i = 0.1-0.2-0.4-0.8-1-2-3-4-5-6-7-8-9	20
S2	S2	i = 0.1-0.2-0.4-0.8-1-2-3-4-5-6-7-8-9	20
B	B-90 _c	i = 4	30
	B-90 _e	q = 1.641 (ml/min)	30
	B-90 _f	q = 12 (ml/min)	30
C	C-90 _a	i = 0.1-0.2-0.3-0.4-0.5-0.65-0.8-1-1.25- ... -2-2.5-3-3.5-4	10
Chav-1	Chav-1	i = 0.1-0.2-0.4-0.8-1-2-3-4-5- ... -10-12-14	20
Chav-2	Chav-2 _i	i = 0.1-0.2-0.4-0.8-1-2-3-4-5-6-7-8-9	20
	Chav-2 _{ii}	i = 0.1-0.2-0.4-0.8-1-2-3-4-5- ... -10-12-14-16	20
R1	R1-90 _b	i = 1-2-3-4-5-6-7-8-9-10-11	10
R2	R2-97 _f	q = 12 (ml/min)	30
	R2-97 _g	q = 48 (ml/min)	30

Annex 3 – Tested specimens: G5A, G5B, G6, P1, P2, P3 and P4

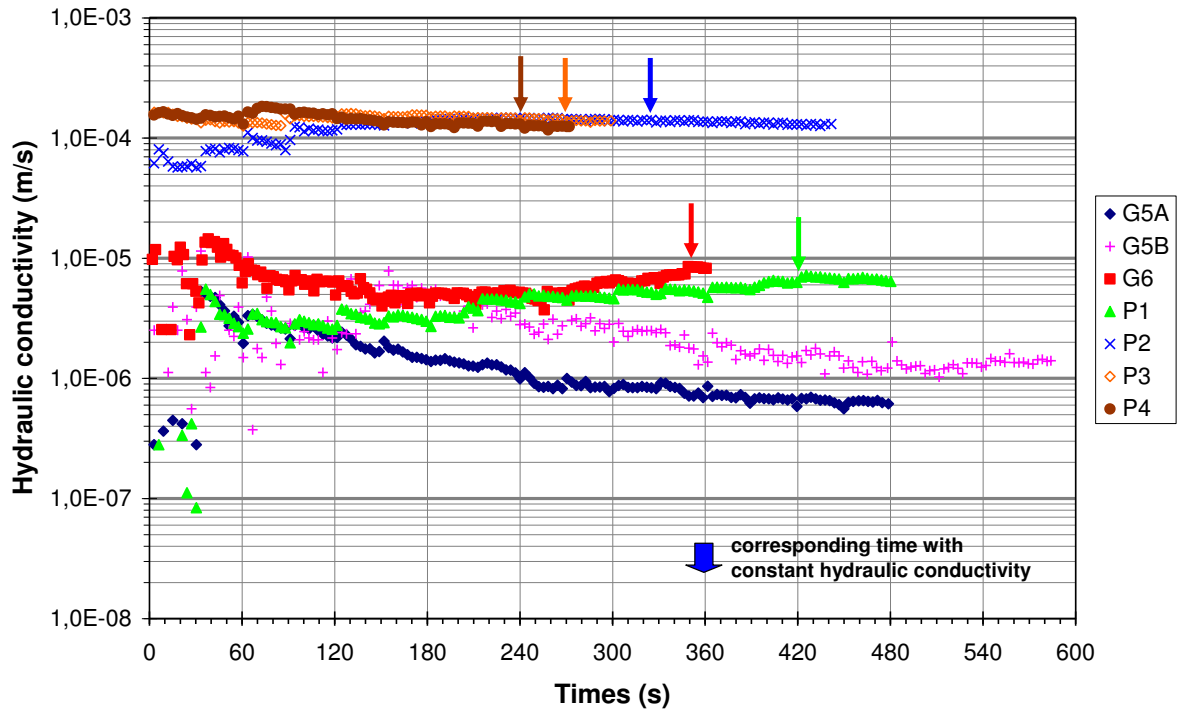


Figure 1 Variation of hydraulic conductivity of tested specimens subjected to multi-stage hydraulic gradients (G5A to P4)

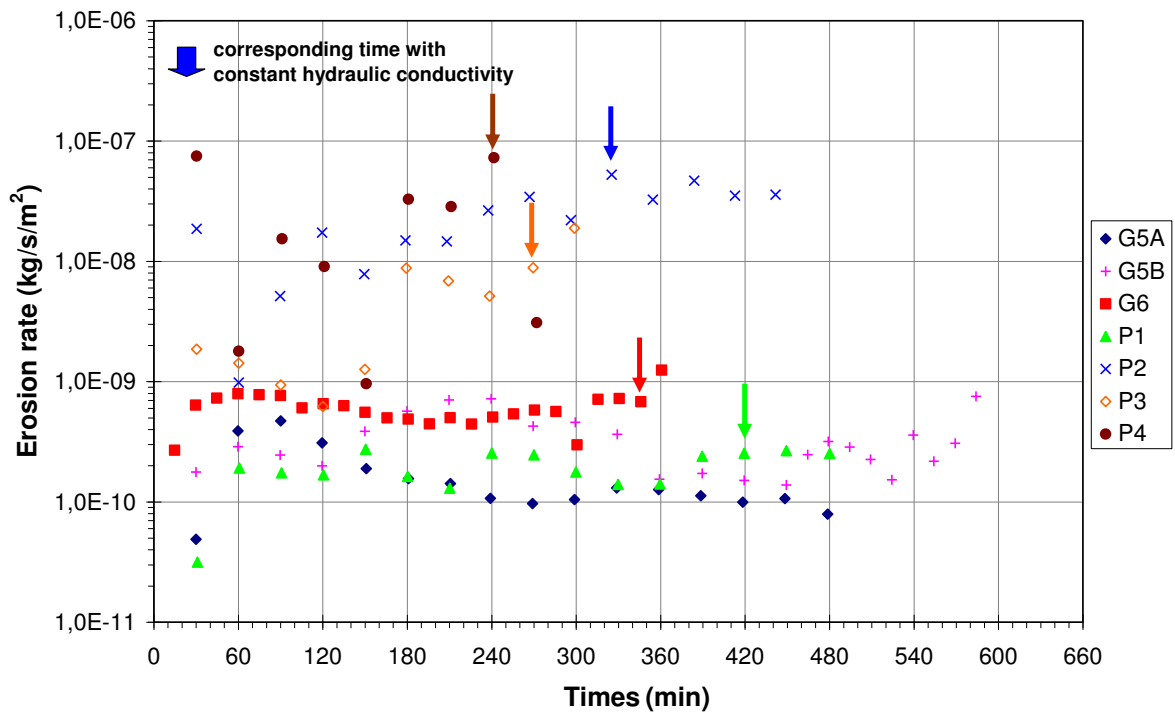


Figure 2 series of erosion rate – specimens subjected to multi-stage hydraulic gradients (G5A to P4)

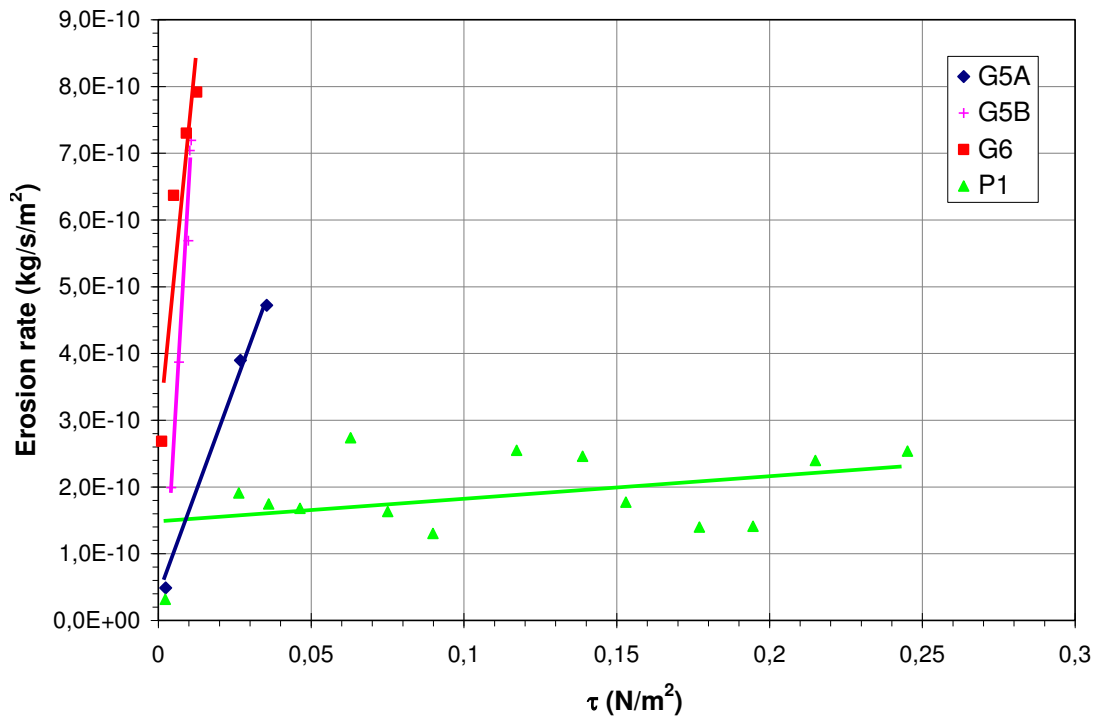


Figure 3 Erosion rate versus hydraulic shear stress – specimens subjected to multi-stage hydraulic gradients (G5A to P1)

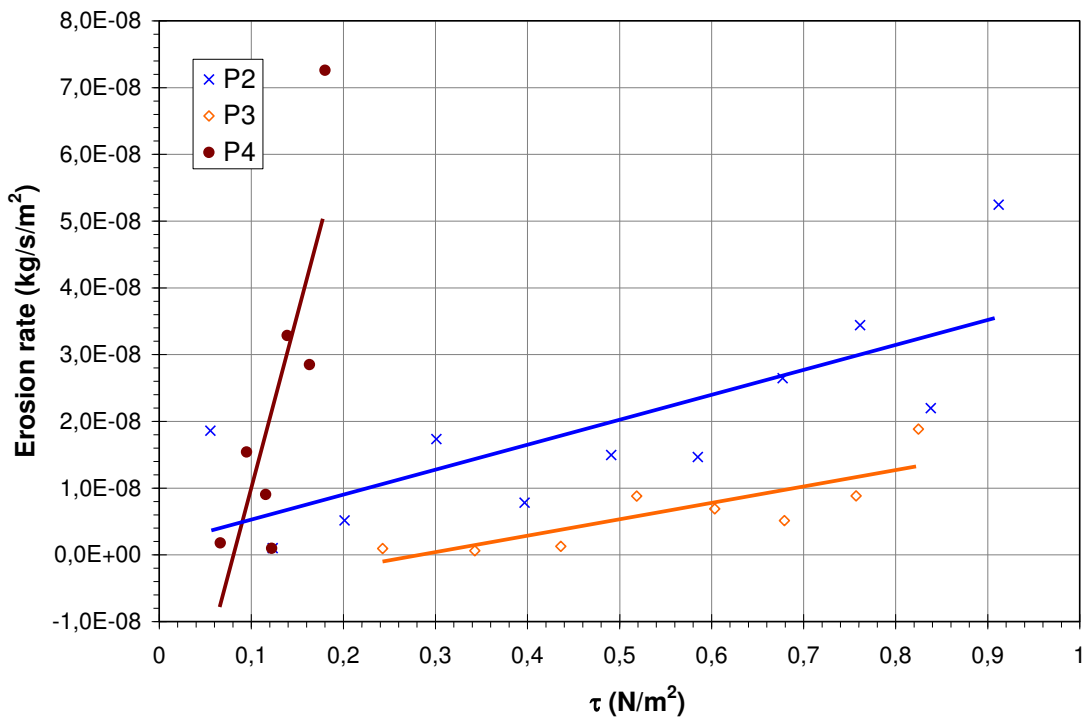


Figure 4 Erosion rate versus hydraulic shear stress – specimens subjected to multi-stage hydraulic gradients (P2 to P4)

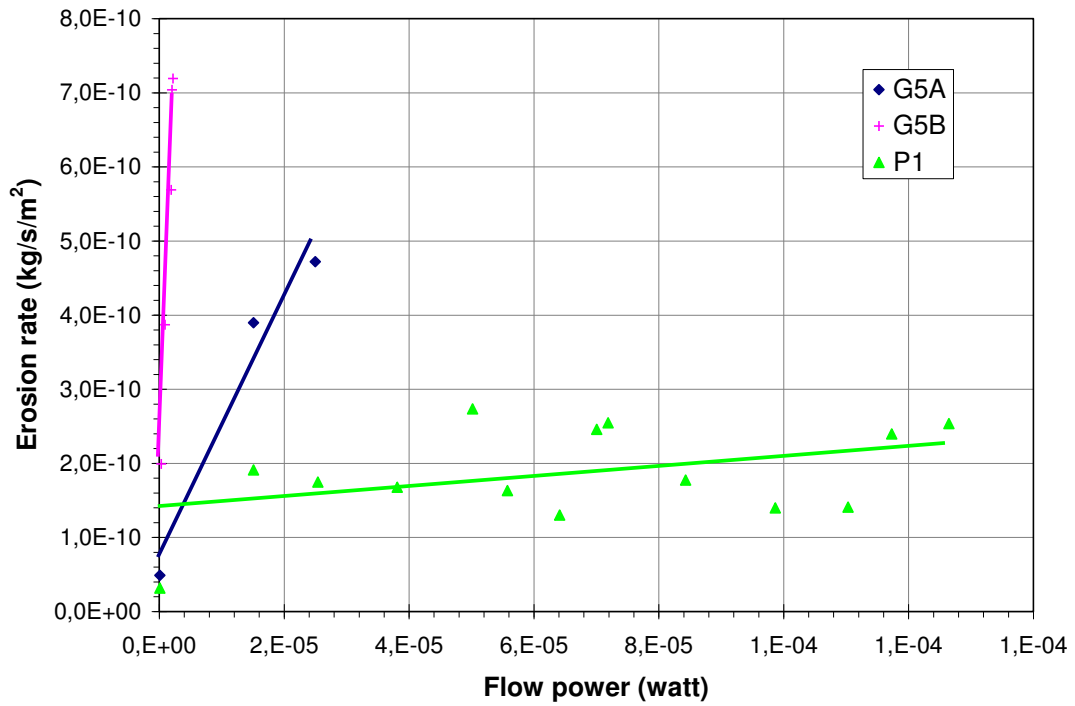


Figure 5 Erosion rate versus flow power – specimens subjected to multi-stage hydraulic gradients (G5A to P1)

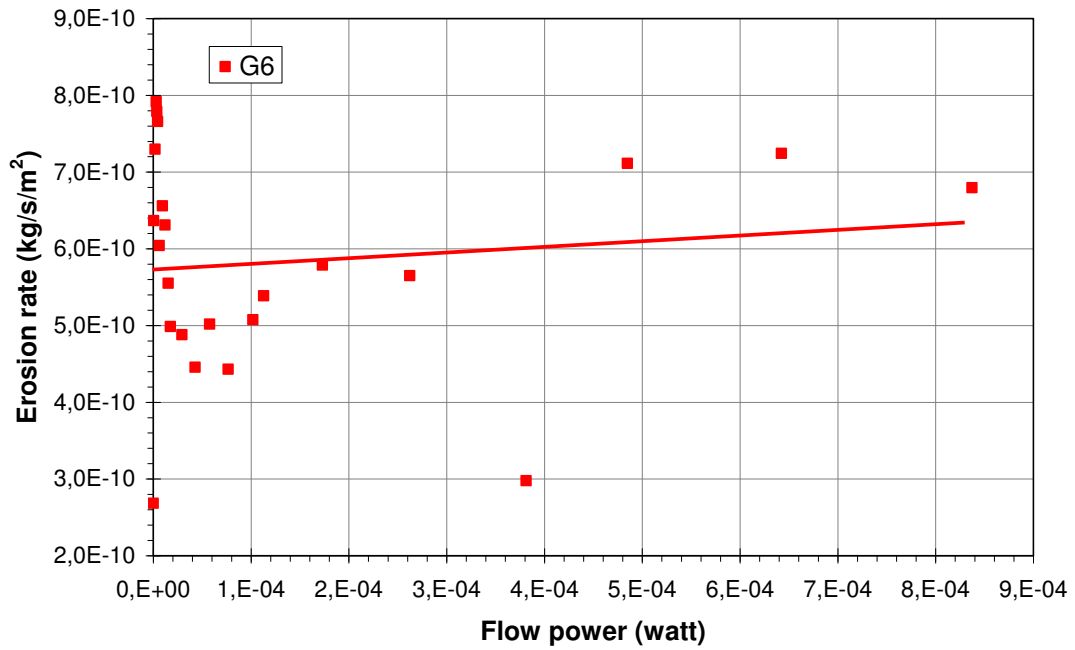


Figure 6 Erosion rate versus flow power – specimens subjected to multi-stage hydraulic gradients (G6)

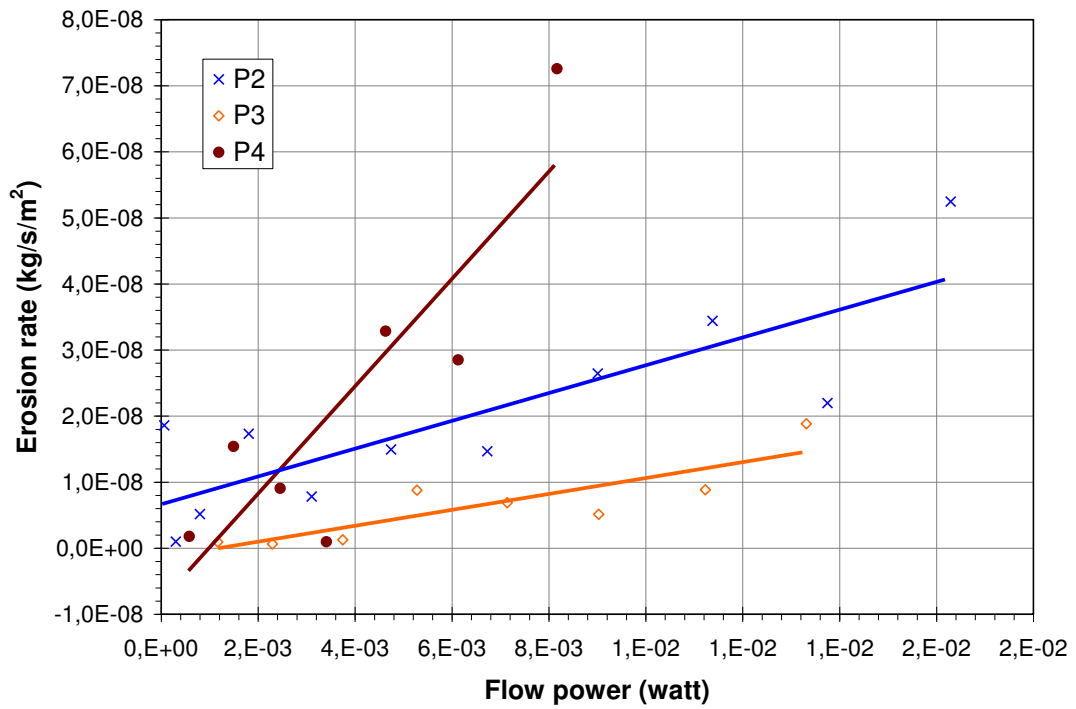


Figure 7 Erosion rate versus flow power – specimens subjected to multi-stage hydraulic gradients (P2 to P4)

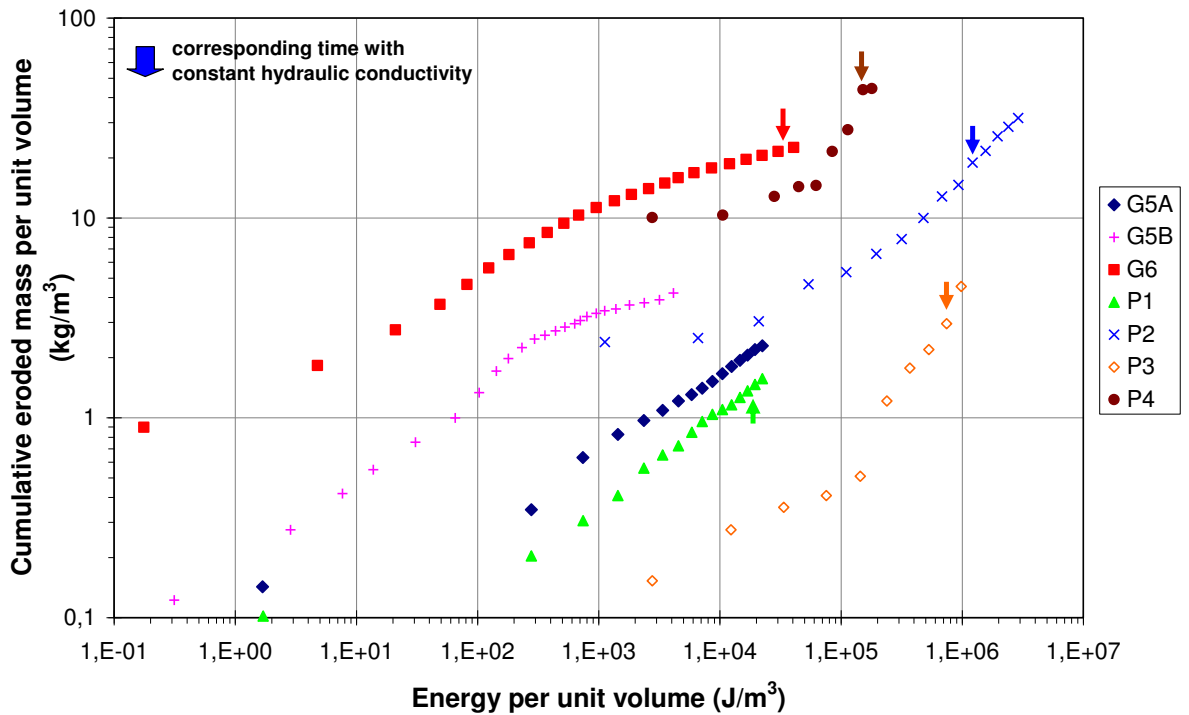


Figure 8 Cumulative eroded dry mass per unit volume versus cumulative expanded energy per unit volume (G5A to P4)

Annex 4 – Tested specimens: L1, L2, L3, L4Ai, L4Aii, L4C, L4D and L5

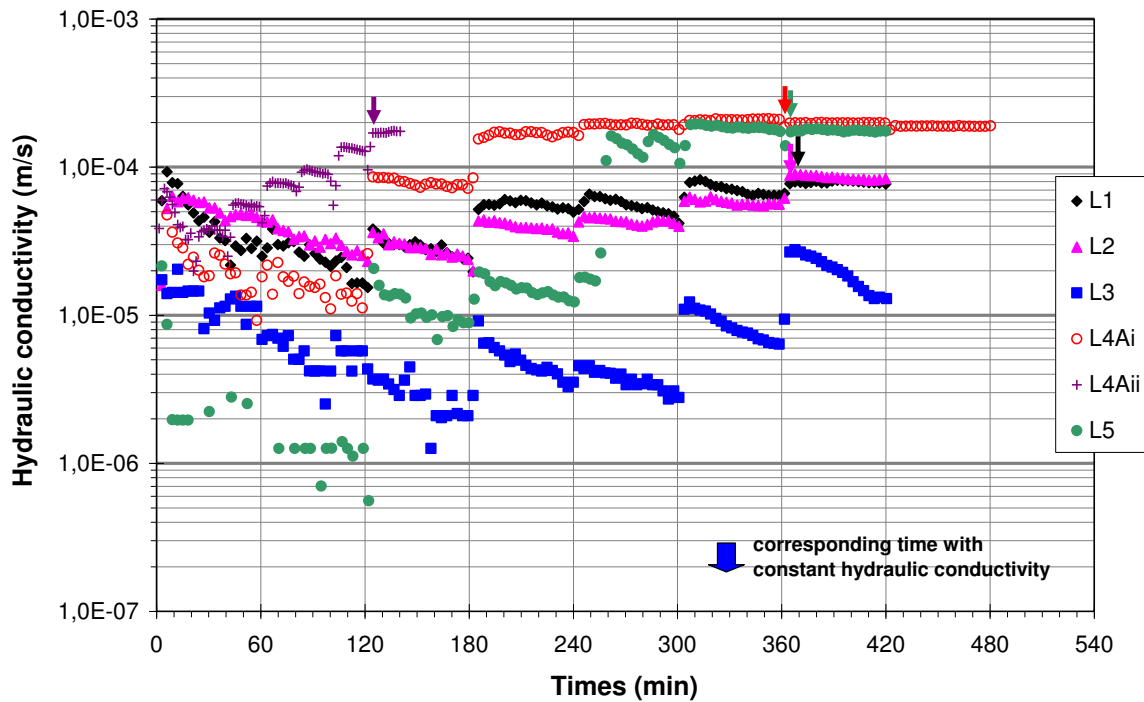


Figure 9 Variation of hydraulic conductivity of tested specimens subjected to multi-stage hydraulic gradients (L1 to L5)

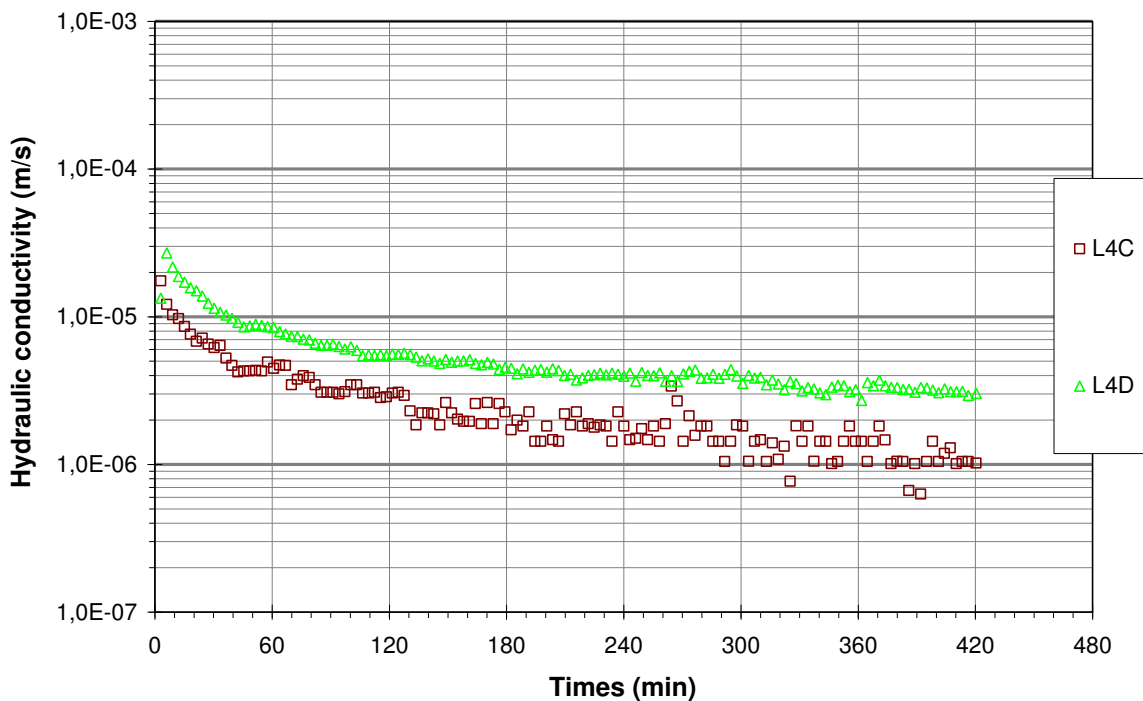


Figure 10 Variation of hydraulic conductivity of tested specimens subjected to single-stage hydraulic gradient (L4C and L4D)

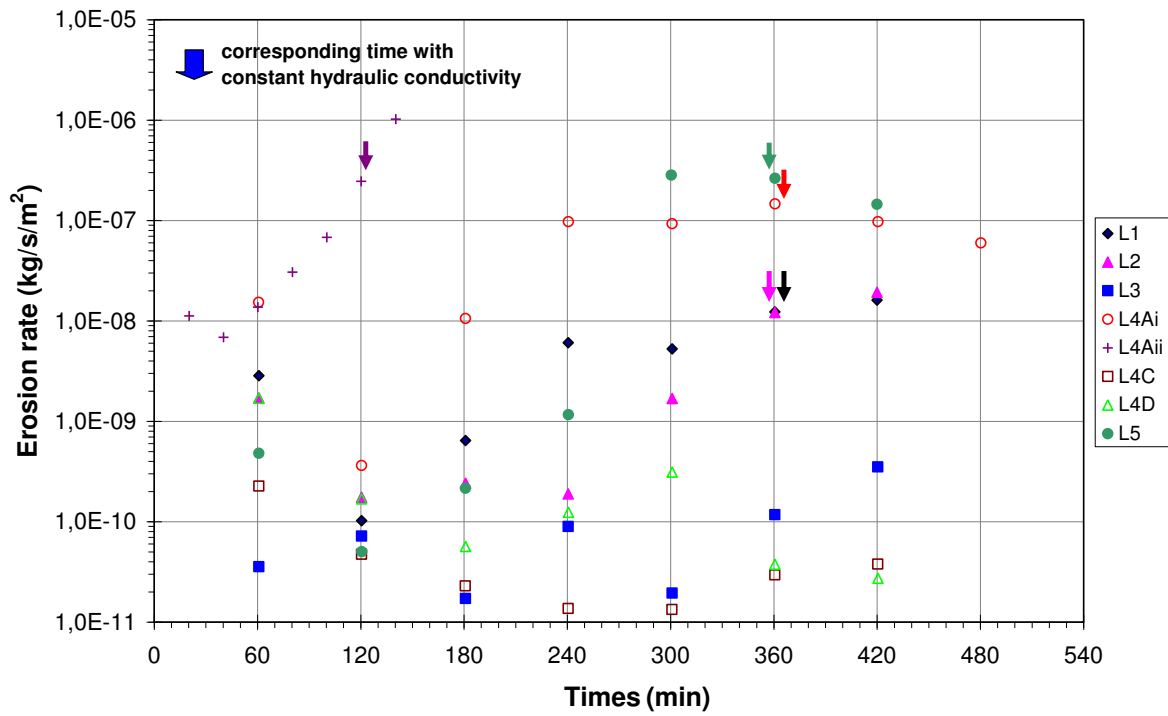


Figure 11 Time series of erosion rate – specimens subjected to single and multi-stage hydraulic gradients (L1 to L5)

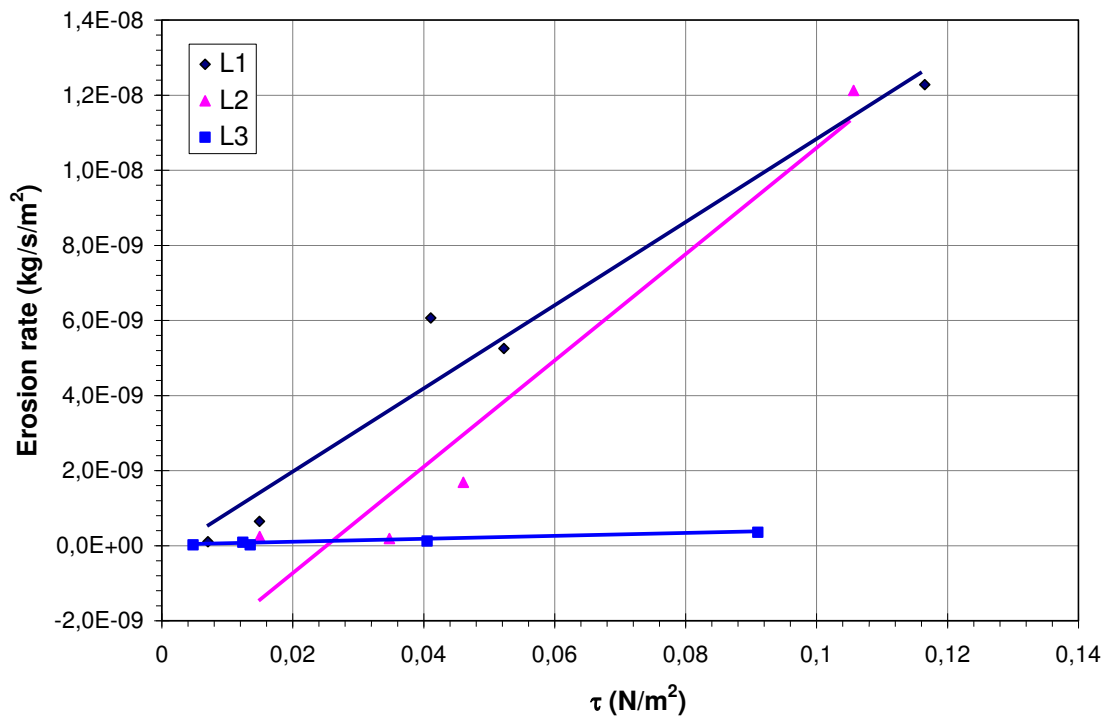


Figure 12 Erosion rate versus hydraulic shear stress – specimens subjected to multi-stage hydraulic gradients (L1 to L3)

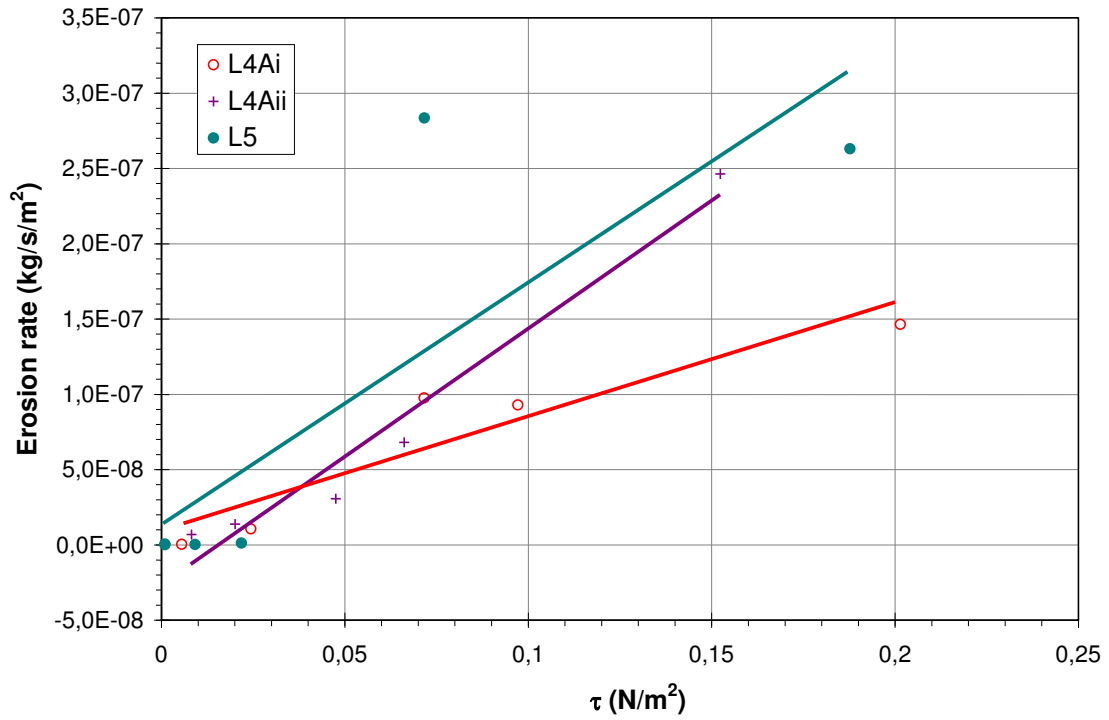


Figure 13 Erosion rate versus hydraulic shear stress – specimens subjected to multi-stage hydraulic gradients (L4Ai to L5)

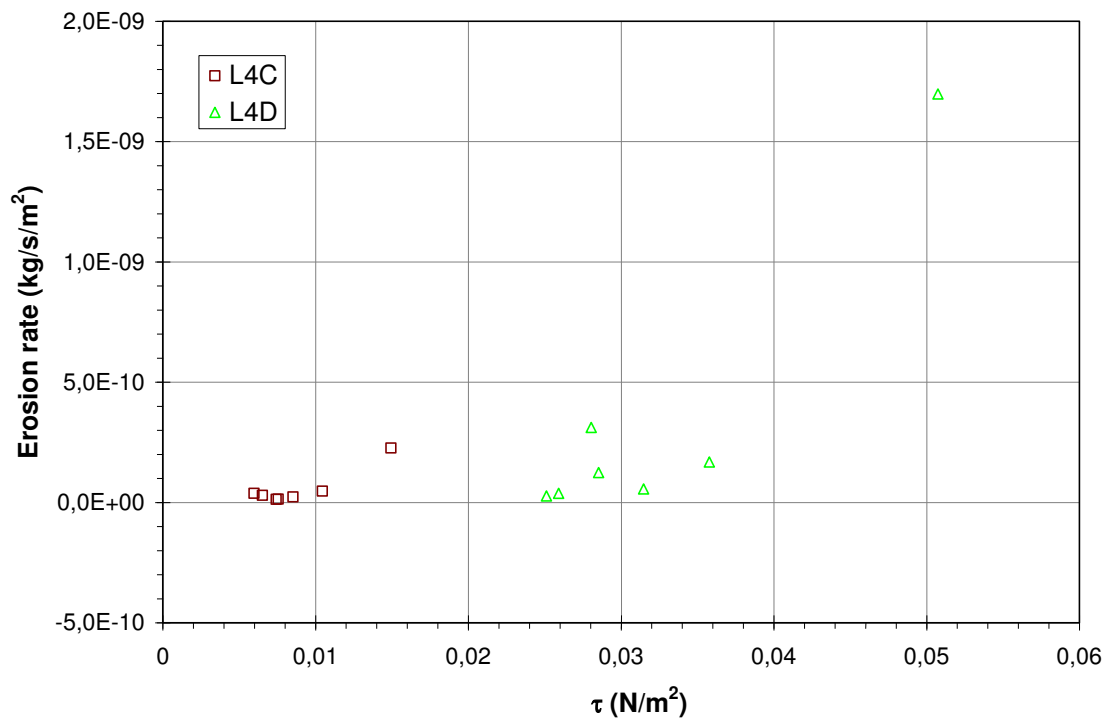


Figure 14 Erosion rate versus hydraulic shear stress – specimens subjected to single-stage hydraulic gradient (L4C and L4D)

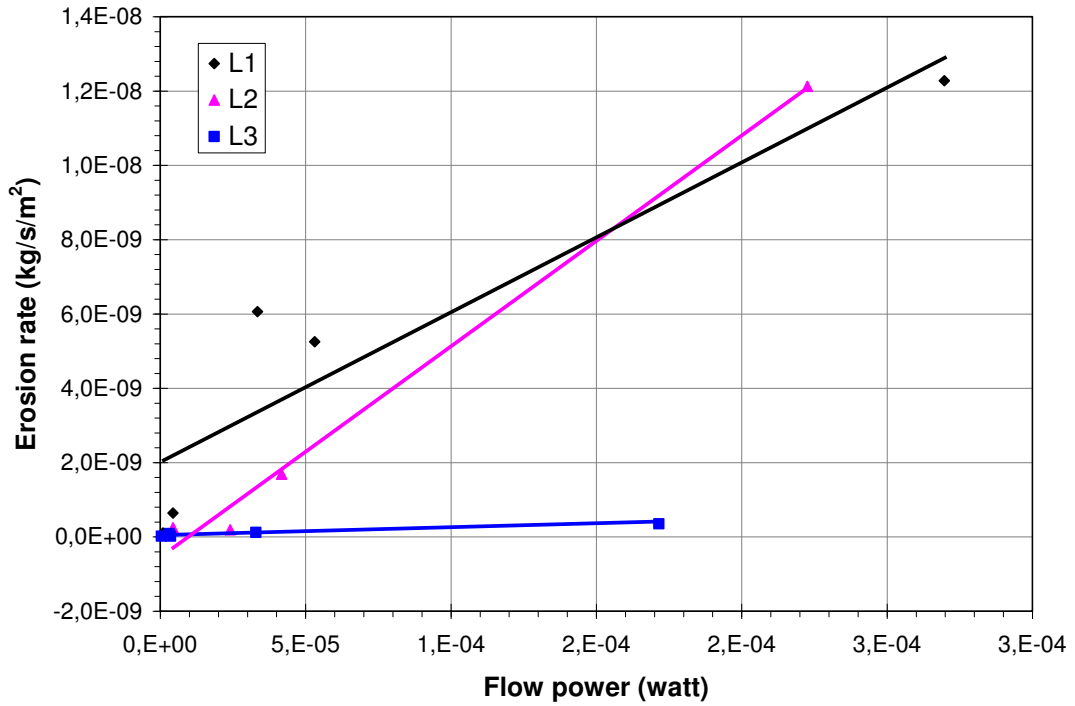


Figure 15 Erosion rate versus flow power – specimens subjected to multi-stage hydraulic gradients (L1 to L3)

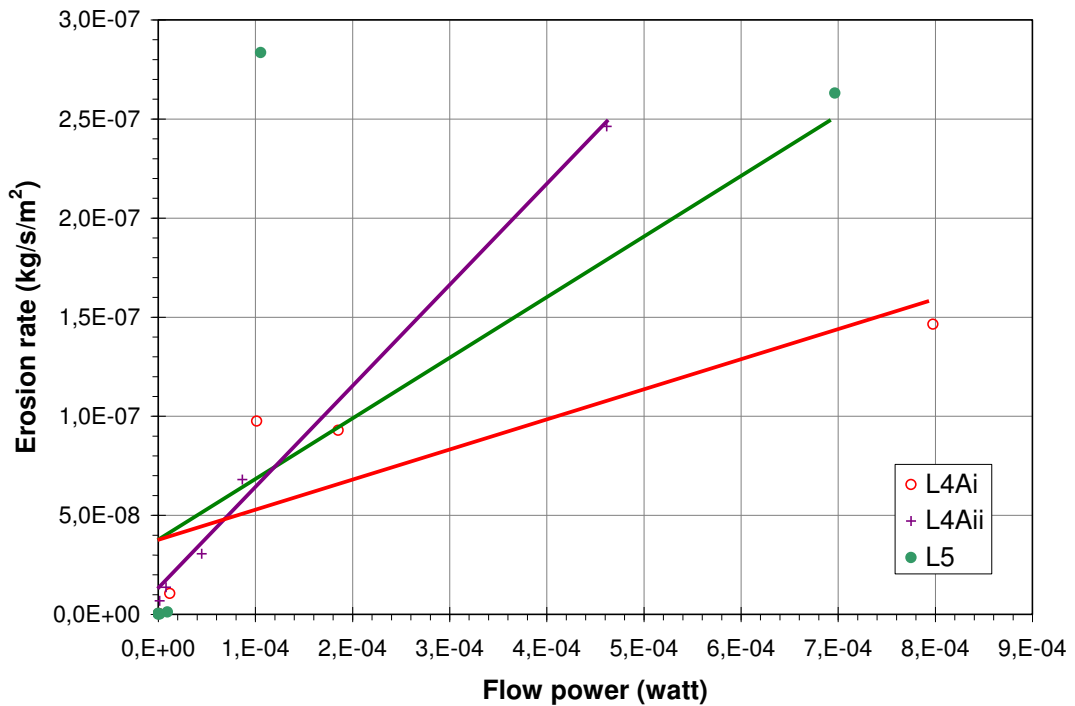


Figure 16 Erosion rate versus flow power – specimens subjected to multi-stage hydraulic gradients (L4Ai to L5)

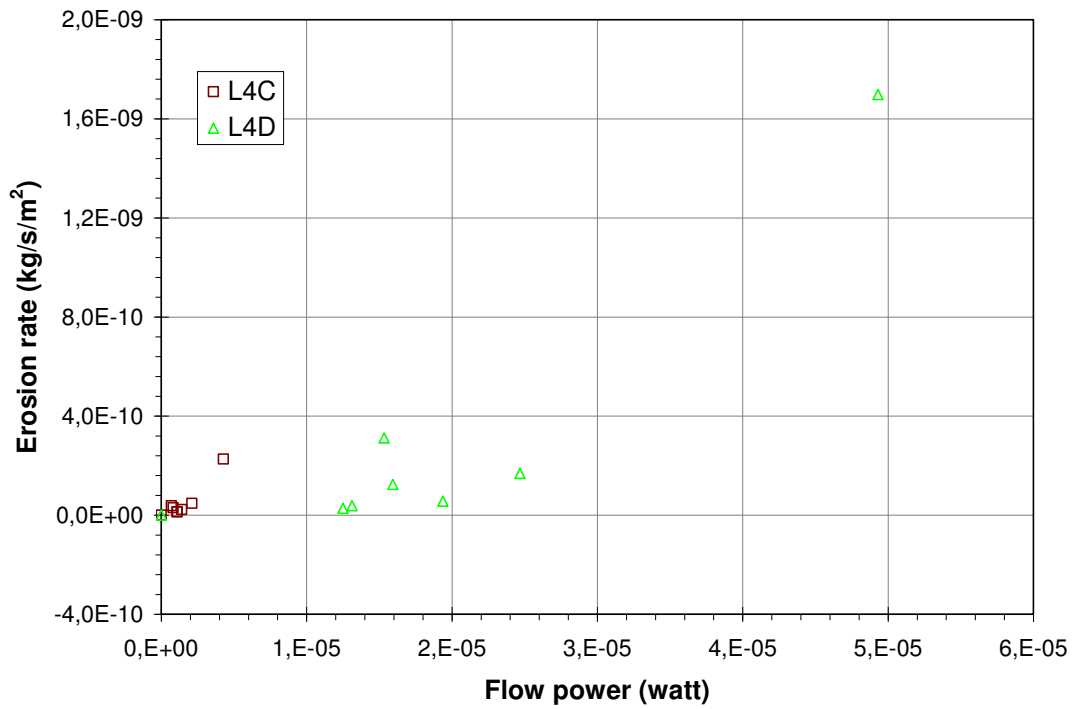


Figure 17 Erosion rate versus flow power – specimens subjected to single-stage hydraulic gradients (L4C and L4D)

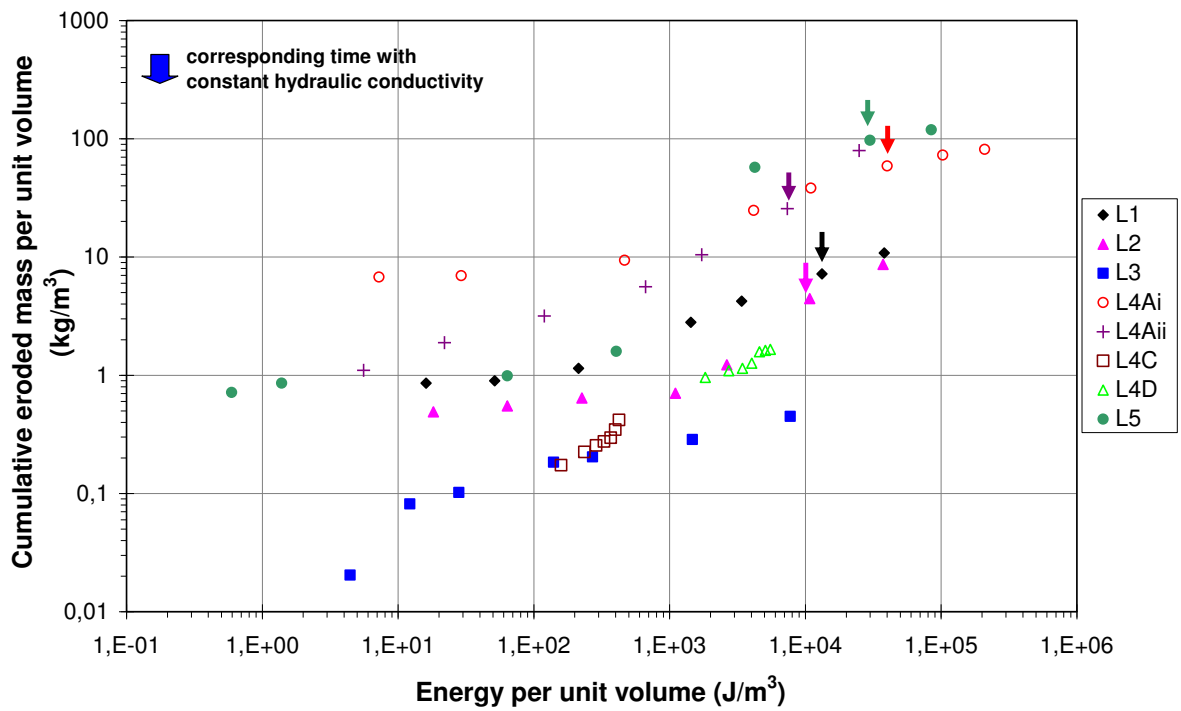


Figure 18 Cumulative eroded dry mass per unit volume versus cumulative expanded energy per unit volume (L1 to L5)

Annex 5 – Tested specimens: D1, D2, D3B, M1, M3, M4, S1 and S2

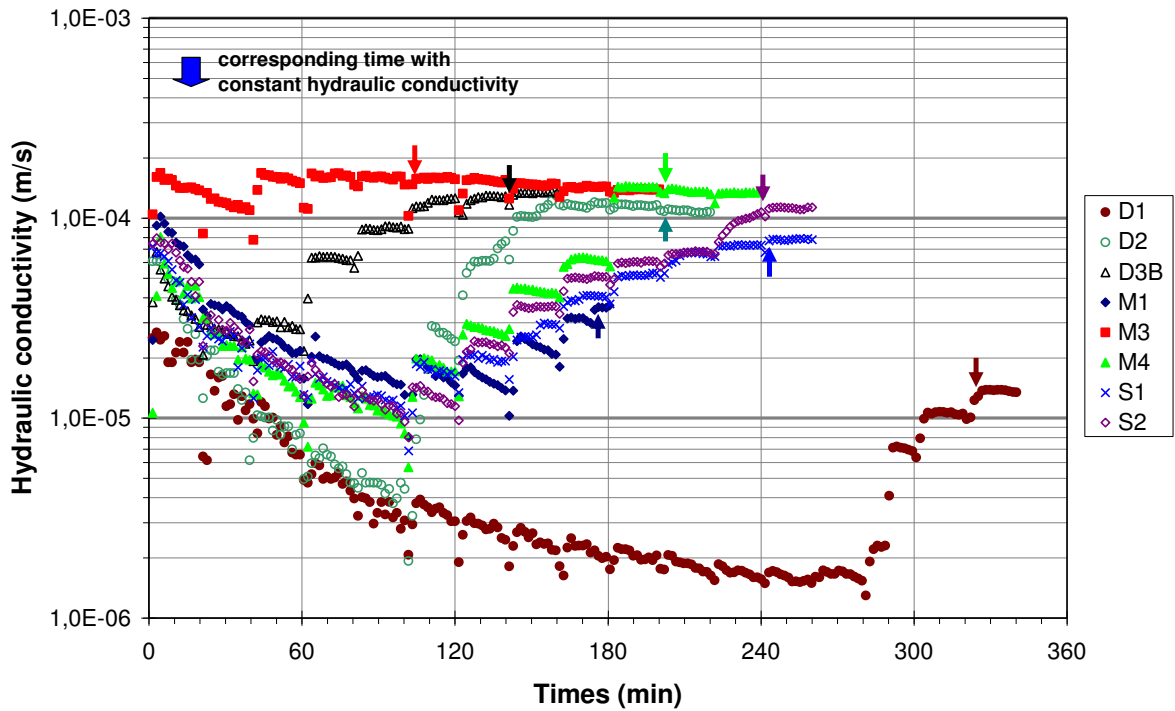


Figure 19 Variation of hydraulic conductivity of tested specimens subjected to multi-stage hydraulic gradients (D1 to S2)

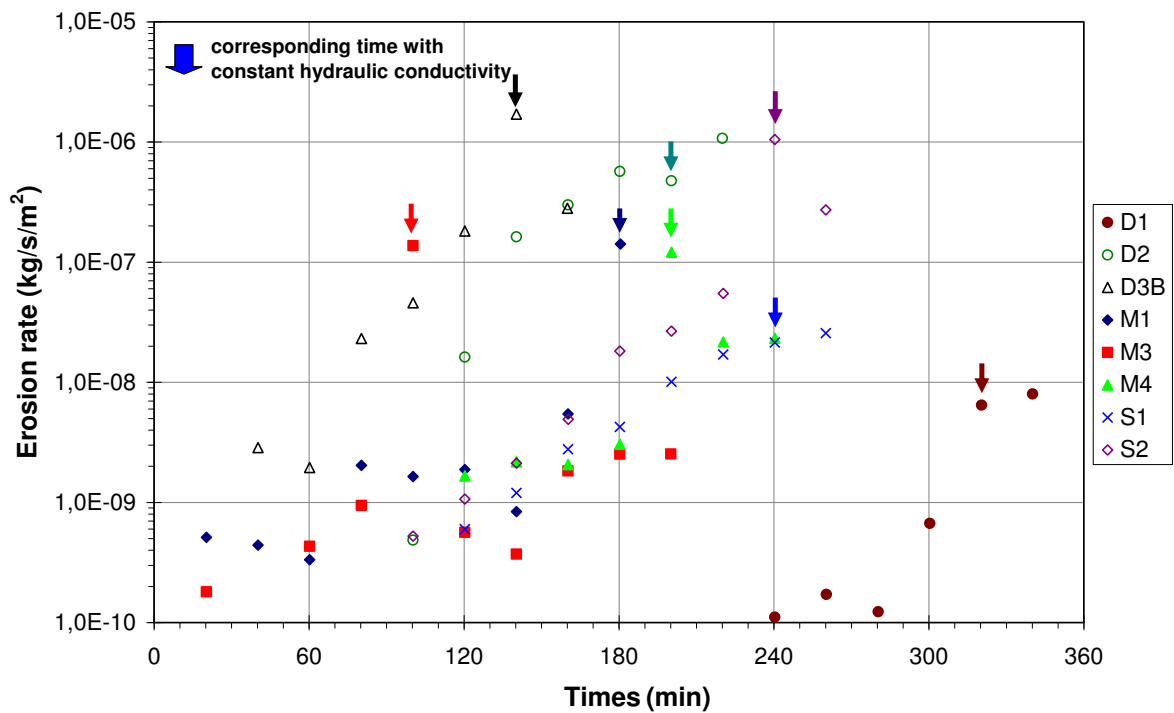


Figure 20 Time series of erosion rate – specimens subjected to multi-stage hydraulic gradients (D1 to S2)

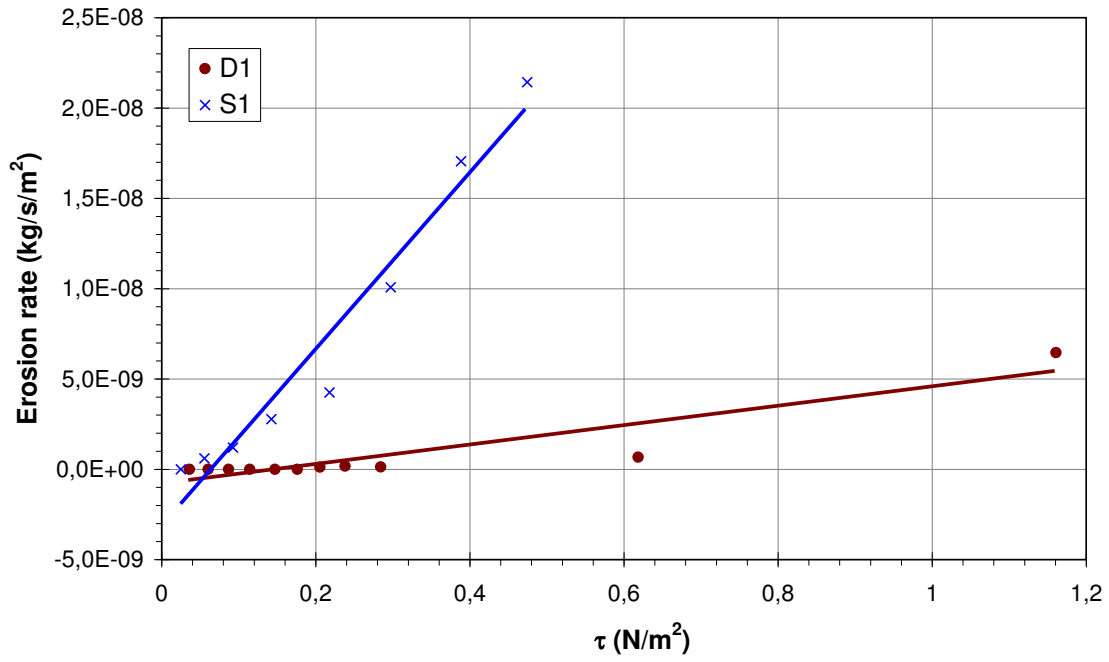


Figure 21 Erosion rate versus hydraulic shear stress – specimens subjected to multi-stage hydraulic gradients (D1 and S1)

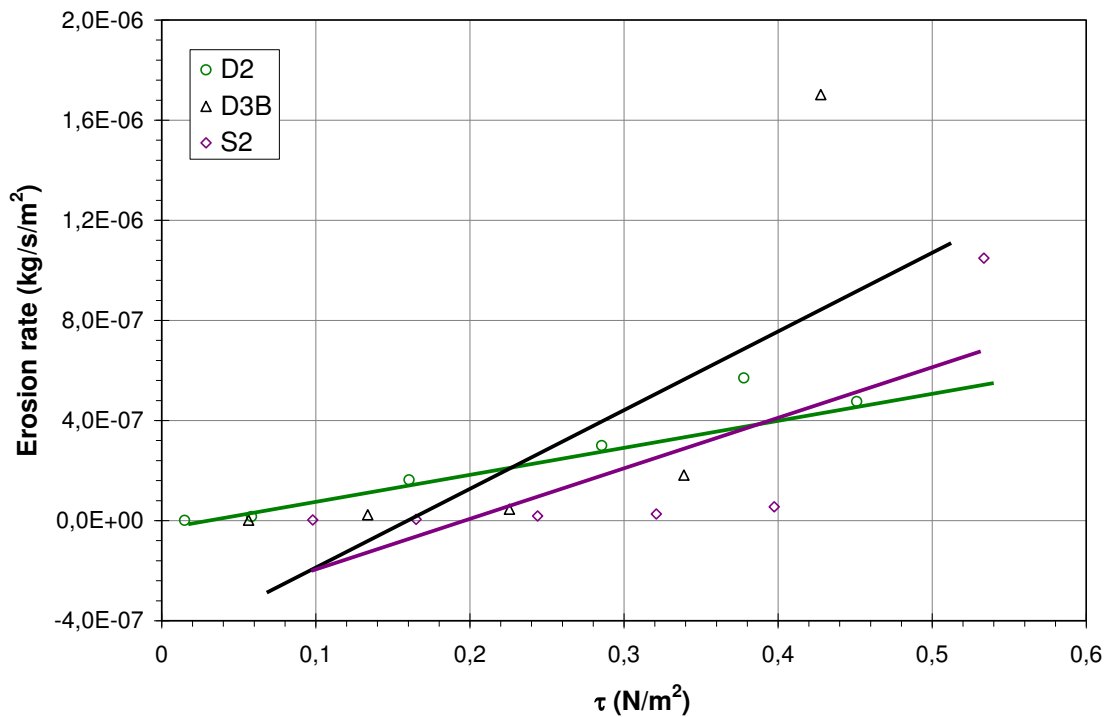


Figure 22 Erosion rate versus hydraulic shear stress – specimens subjected to multi-stage hydraulic gradients (D2 to S2)

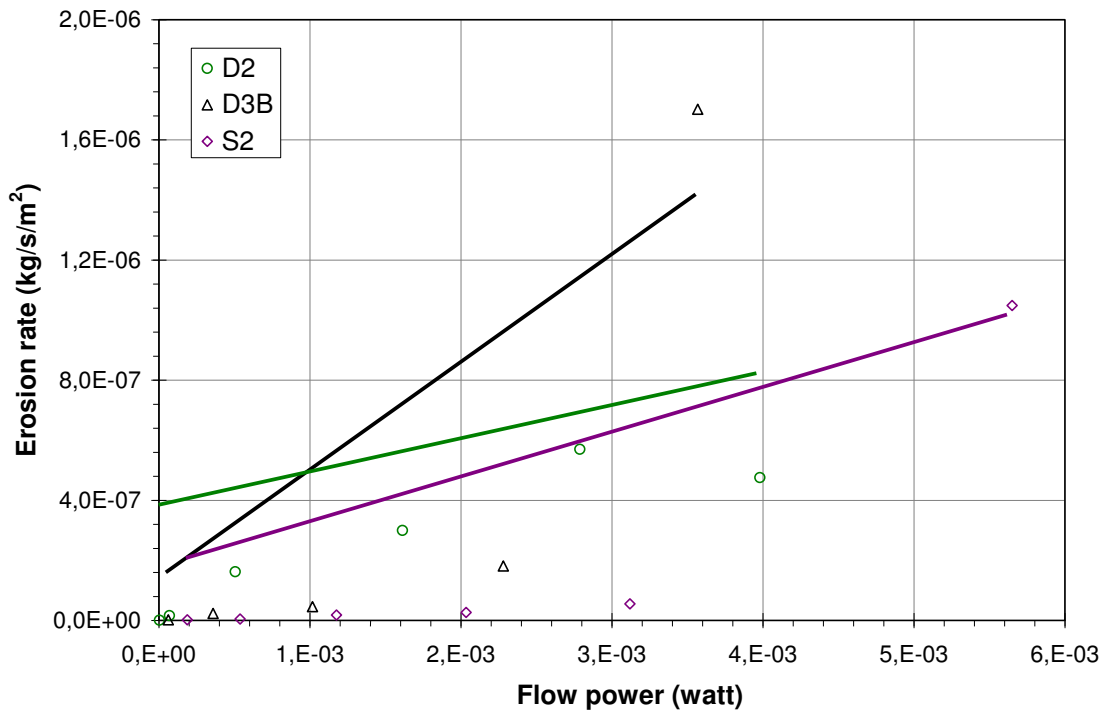


Figure 25 Erosion rate versus flow power – specimens subjected to multi-stage hydraulic gradients (D2 to S2)

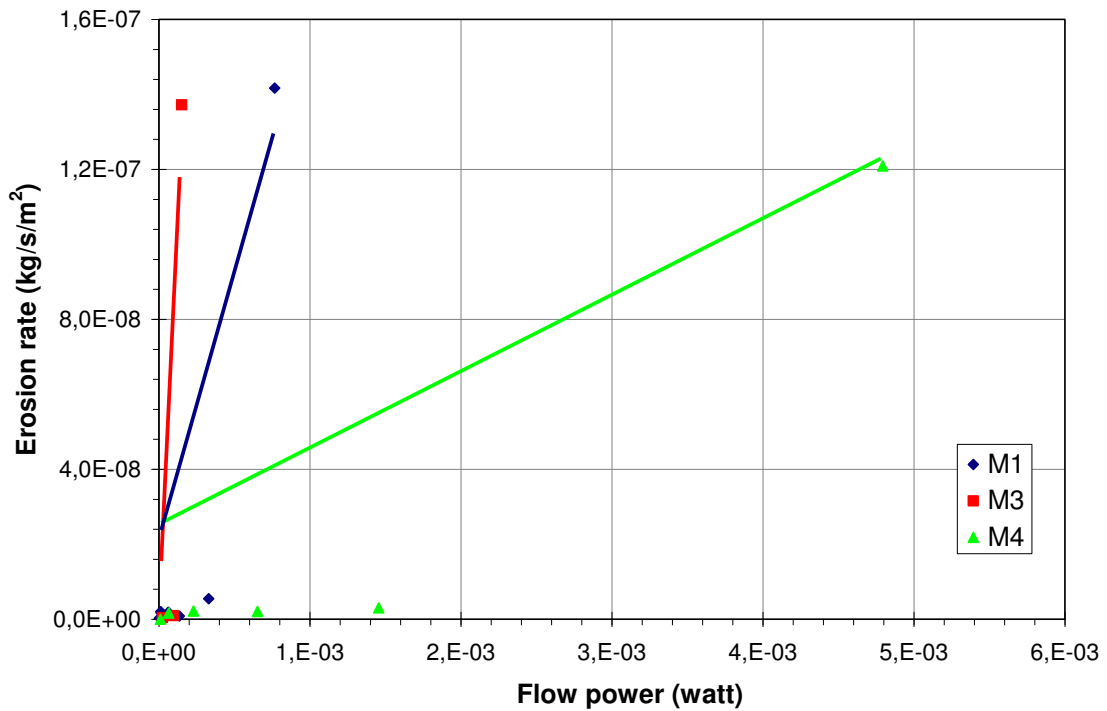


Figure 26 Erosion rate versus flow power – specimens subjected to multi-stage hydraulic gradients (M1 to M4)

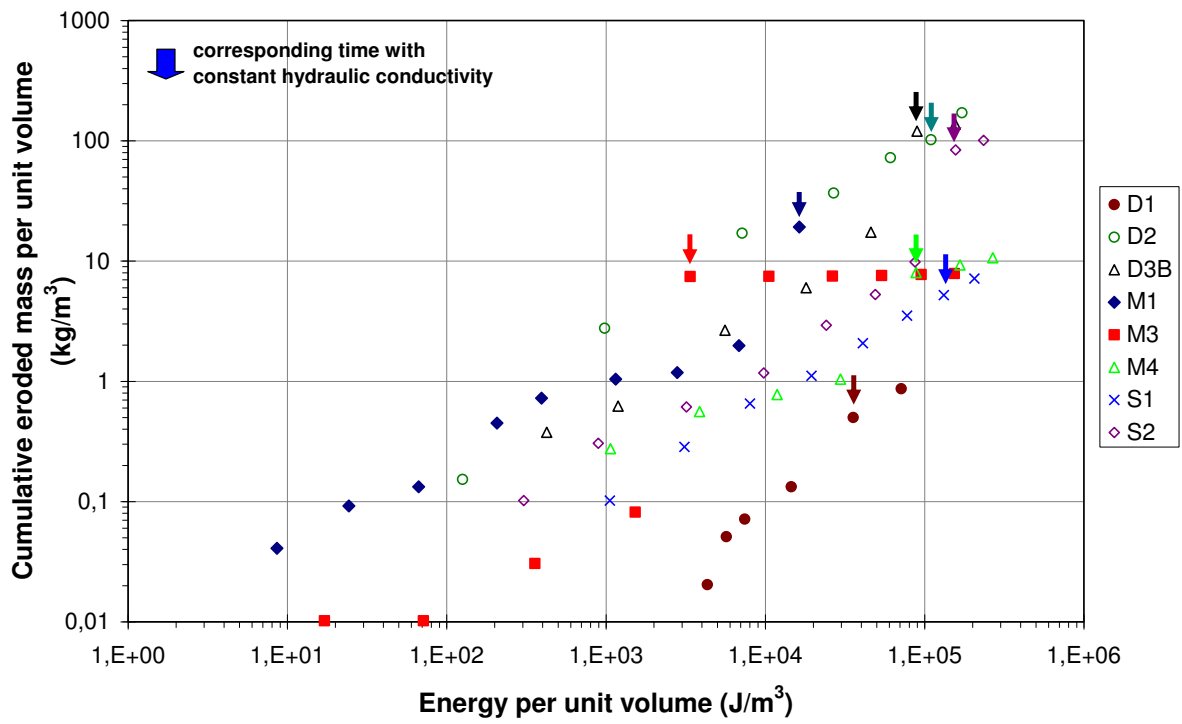


Figure 27 Cumulative eroded dry mass per unit volume versus cumulative expanded energy per unit volume (D1 to S2)

Annex 6 – Tested specimens: B-90f, C-90a, Chav-1, Chav-2i, Chav-2ii, R1-90b, R2-97f and R2-97g

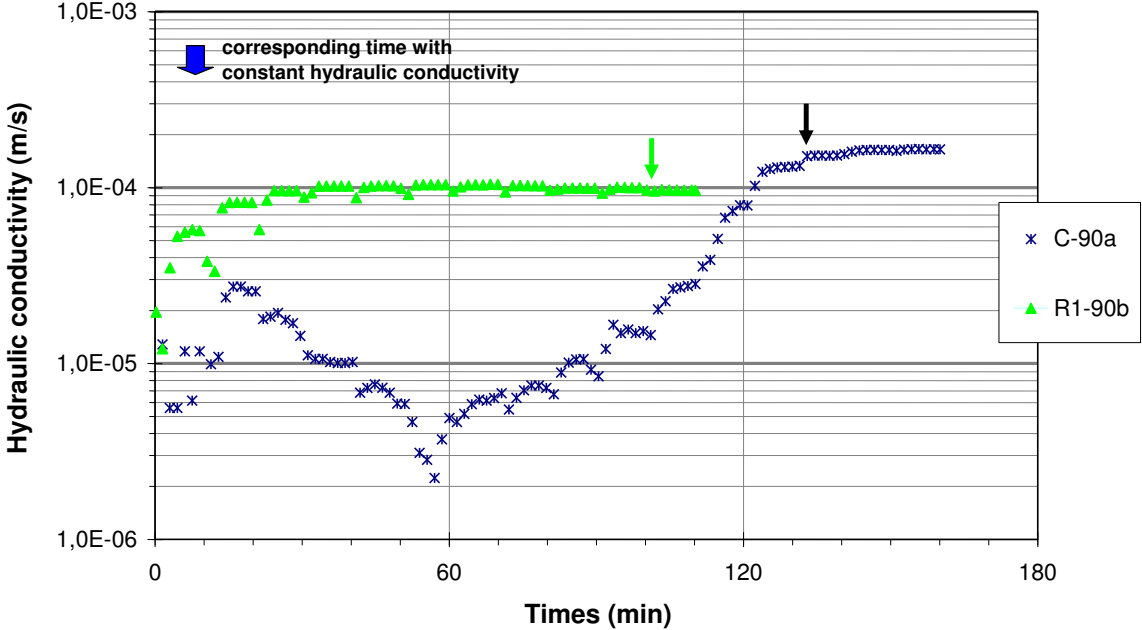


Figure 28 Variation of hydraulic conductivity of tested specimens subjected to multi-stage hydraulic gradients (C-90a and R1-90b)

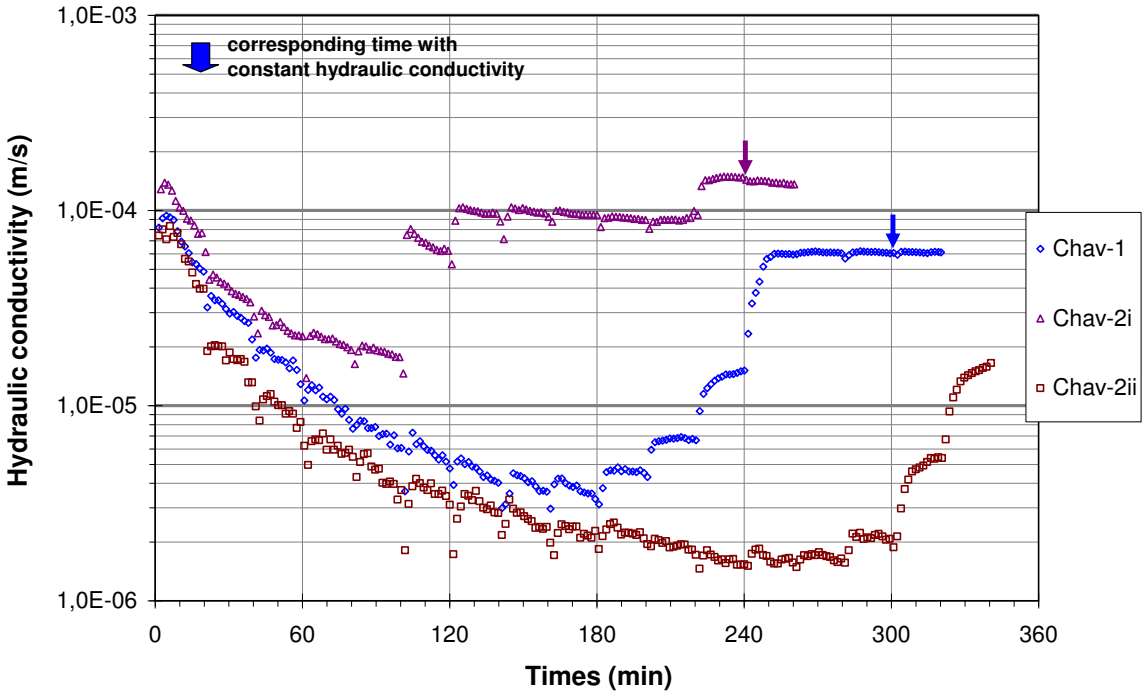


Figure 29 Variation of hydraulic conductivity of tested specimens subjected to multi-stage hydraulic gradients (Chav-1 to Chav-2ii)

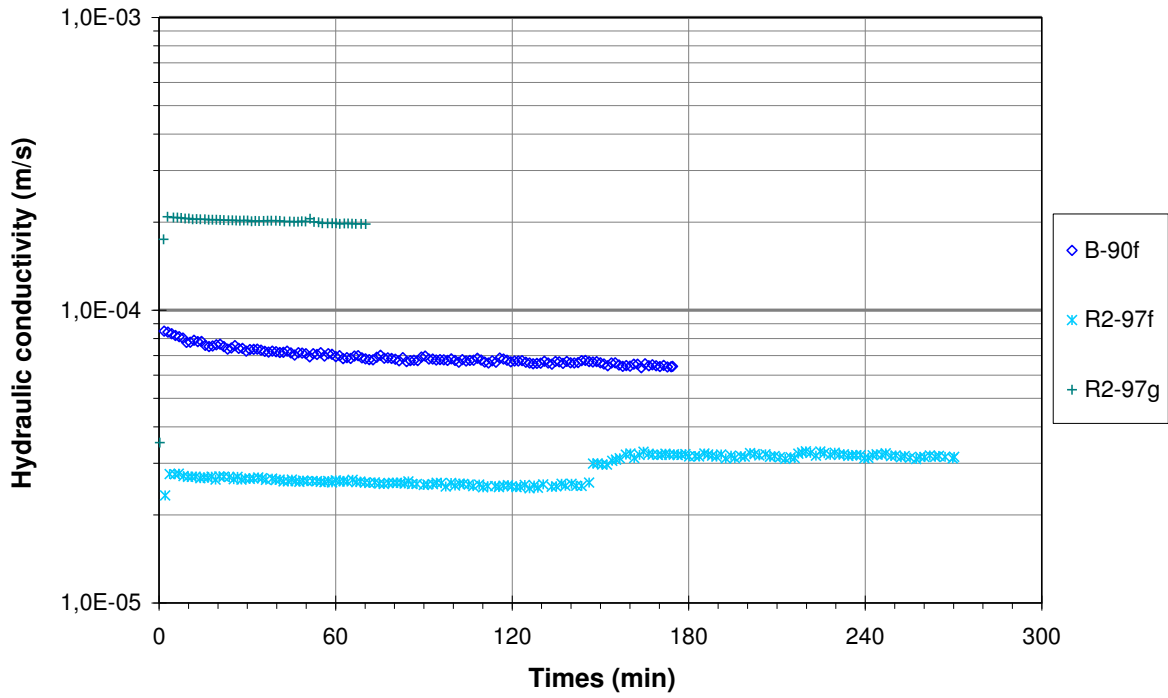


Figure 30 Variation of hydraulic conductivity of tested specimens subjected to controlled flow rate condition (B-90f to R2-97g)

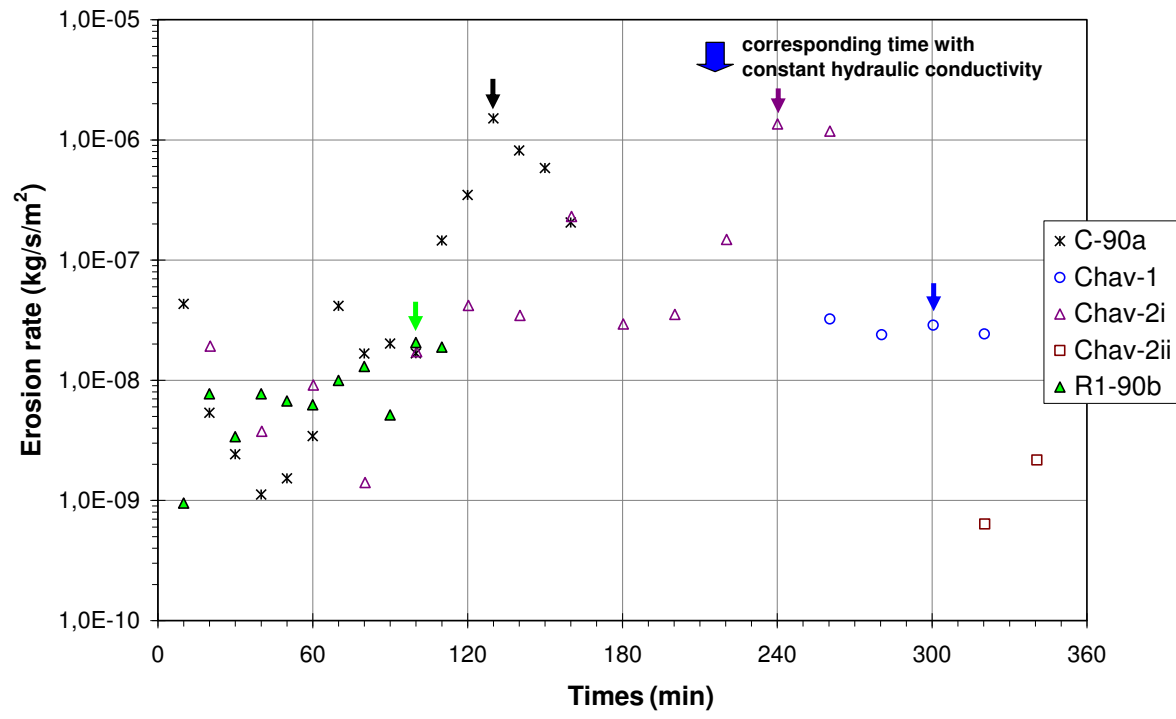


Figure 31 Time series of erosion rate – specimens subjected to multi-stage hydraulic gradients (C-90a to R1-90b)

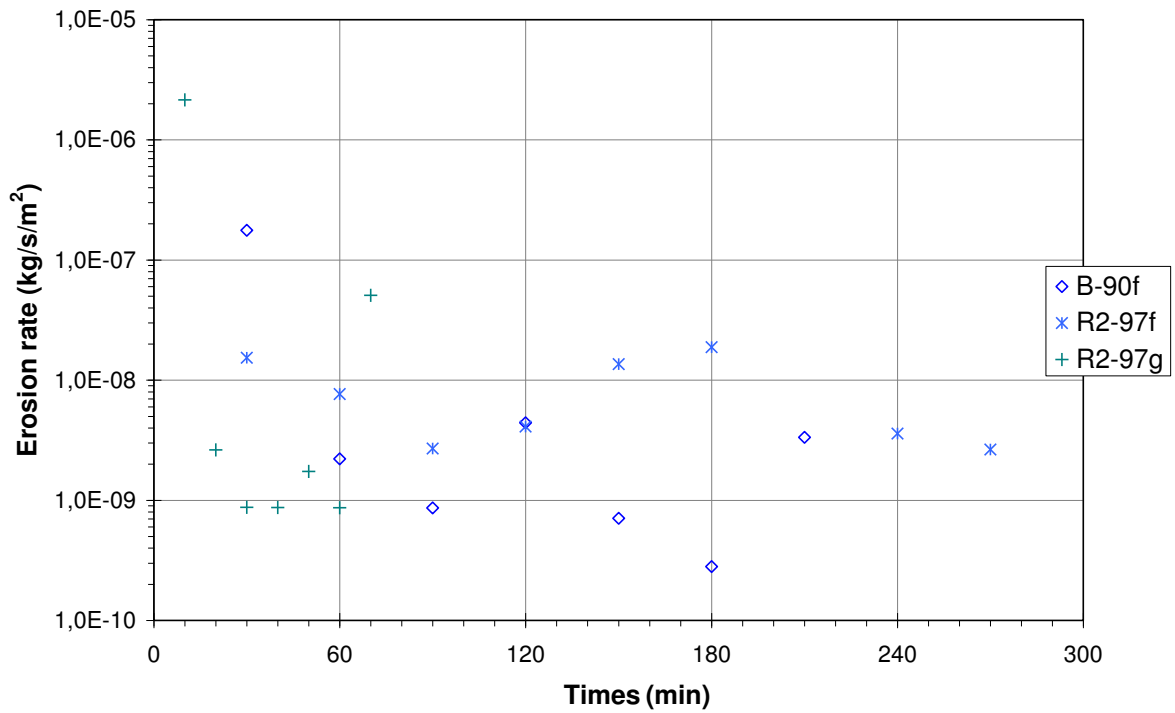


Figure 32 Time series of erosion rate – specimens subjected to controlled flow rate condition (B-90f to R2-97g)

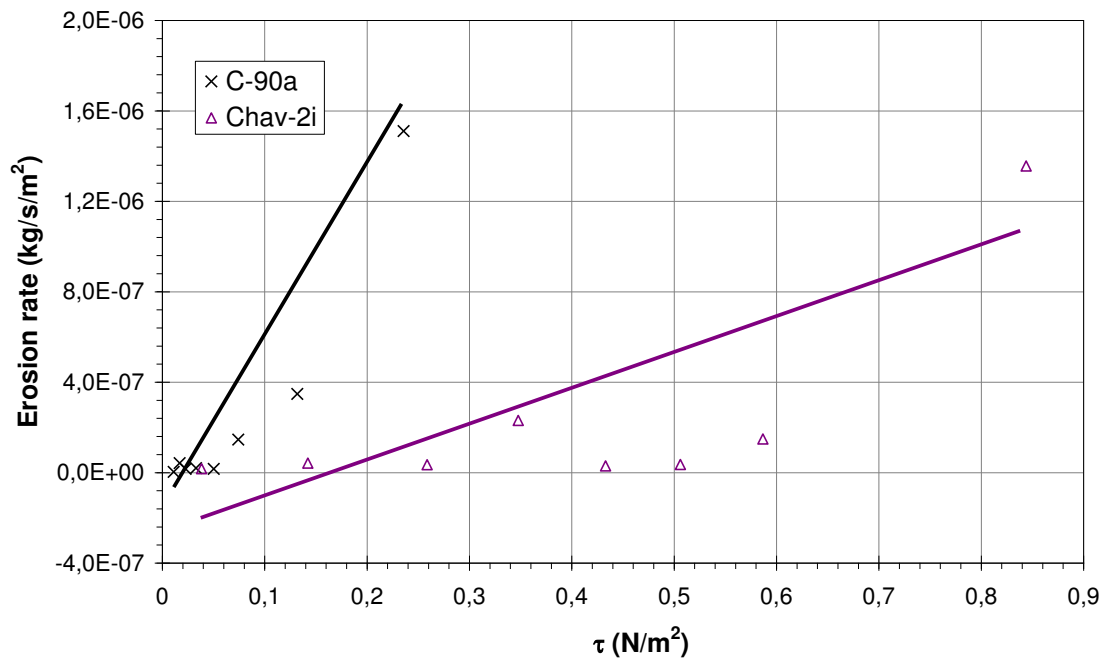


Figure 33 Erosion rate versus hydraulic shear stress – specimens subjected to multi-stage hydraulic gradients (C-90a and Chav-2i)

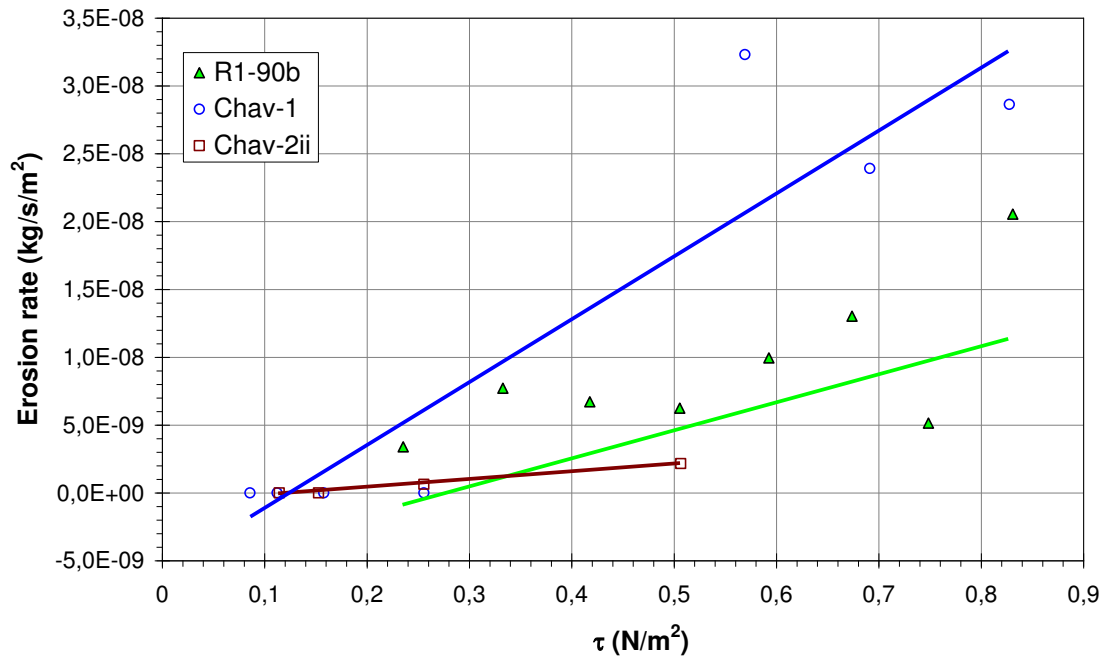


Figure 34 Erosion rate versus hydraulic shear stress – specimens subjected to multi-stage hydraulic gradients (R1-90b to Chav-2ii)

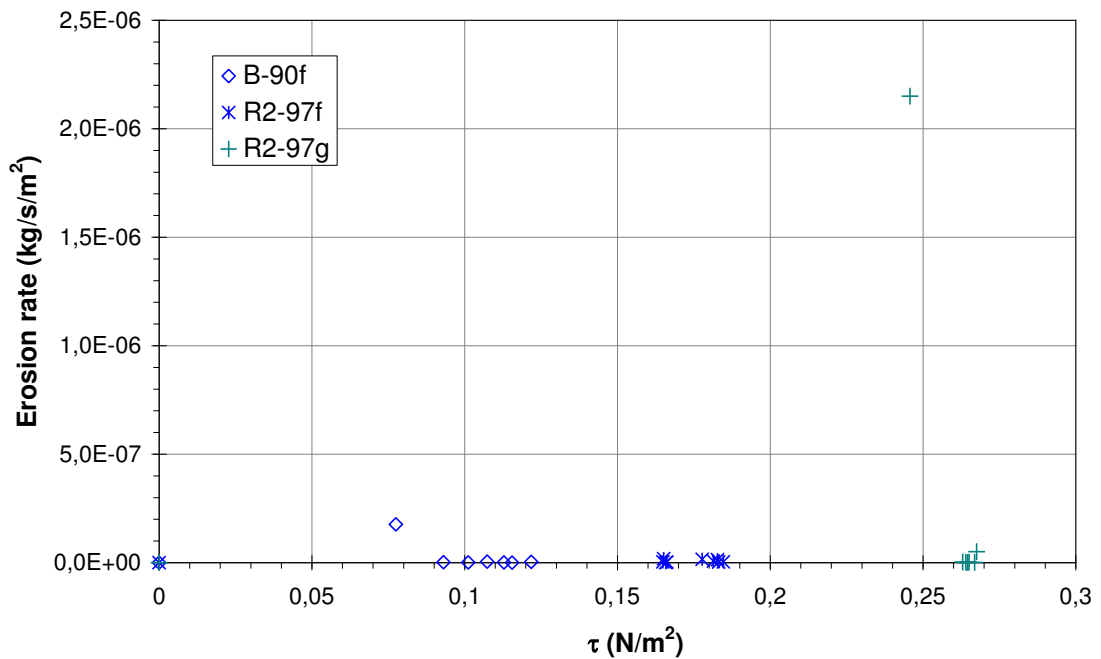


Figure 35 Erosion rate versus hydraulic shear stress – specimens subjected to controlled flow rate condition (B-90f to R2-97g)

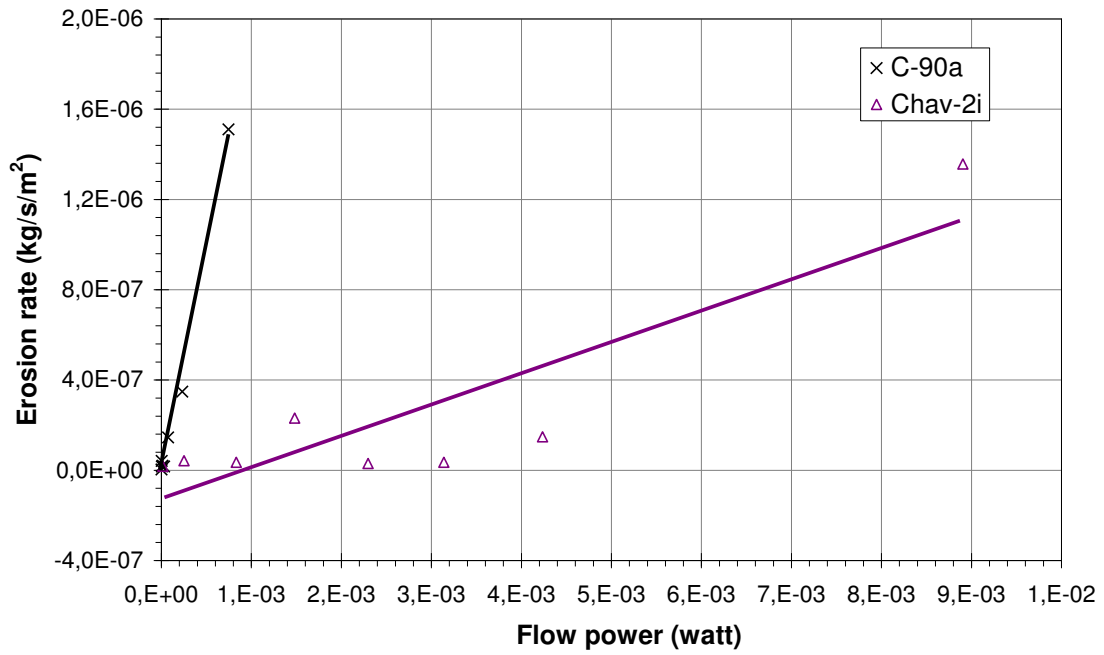


Figure 36 Erosion rate versus flow power – specimens subjected to multi-stage hydraulic gradients (C-90a and Chav-2i)

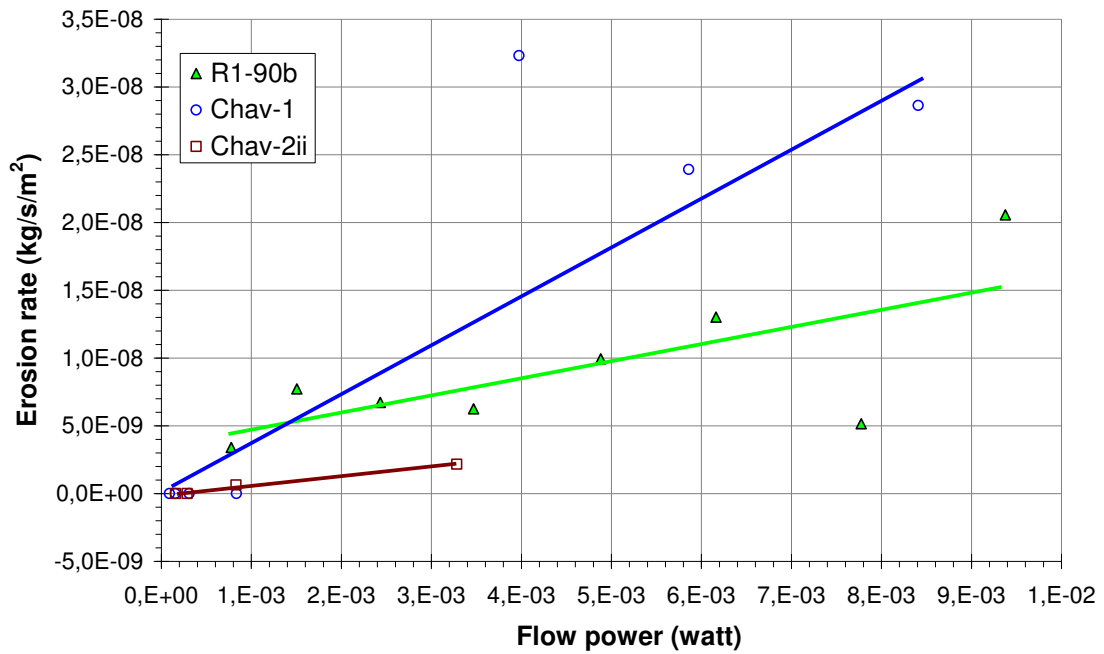


Figure 37 Erosion rate versus flow power – specimens subjected to multi-stage hydraulic gradients (R1-90b to Chav-2ii)

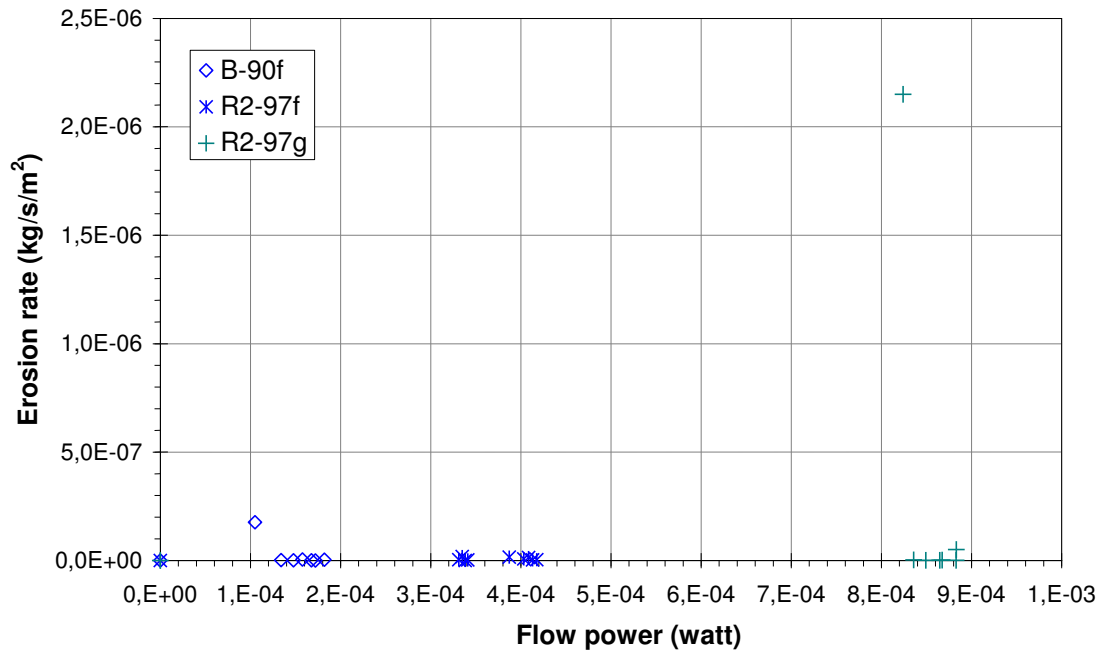


Figure 38 Erosion rate versus flow power – specimens subjected to controlled flow rate condition (B-90f to R2-97g)

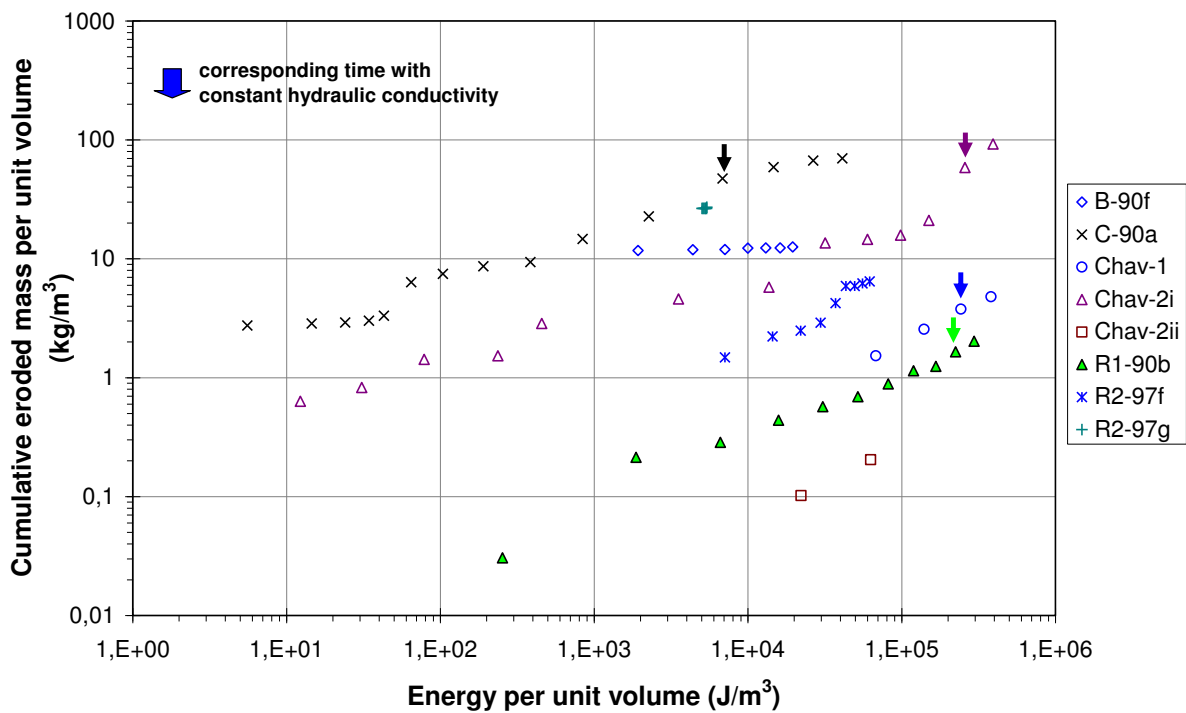


Figure 39 Cumulative eroded dry mass per unit volume versus cumulative expanded energy per unit volume (B-90f to R2-97g)

Annex 7 – Small scale model of dike: Summary of small scale model of dike

Small scale model of dike : specimen B-90s	
Figure 40	Measured and simulated values of total head (in meter) at 2.5 minutes
Figure 41	Measured and simulated values of total head (in meter) at 10 minutes
Figure 42	Measured and simulated values of total head (in meter) at 79 minutes
Figure 43	Comparison of total water head within the dike G5-E4
Figure 44	Comparison of total water head within the dike F3-B3
Figure 45	Comparison of total water head within the dike G1-A1
Figure 46	Time series of evolution of deviation values within the dike soil G5-B3
Figure 47	Time series of evolution of deviation values within the dike soil G1-A1
Figure 48	Comparison of downstream flow rate
Figure 49	Fine fraction in several locations after the seepage test
Table 1	Displacement and global safety factor
Small scale model of dike : specimen B-75s	
Figure 50	Sliding in the downstream slope at several times
Figure 51	Evolution of the shape of the downstream slope during the seepage test
Figure 52	Displacement of at minute 2.83 (experimental vs. numerical study) in cm
Figure 53	Measured and simulated values of total head (in meter) at minute 1
Figure 54	Measured and simulated values of total head (in meter) at minute 3
Figure 55	Measured and simulated values of total head (in meter) at minute 78
Figure 56	Comparison of total water head within the dike G5-E4
Figure 57	Comparison of total water head within the dike F3-B3
Figure 58	Comparison of total water head within the dike G1-A1
Figure 59	Comparison of downstream flow rate
Figure 60	Fine fraction in several locations after the seepage test
Small scale model of dike : specimen B-90u	
Figure 61	Sliding in the downstream slope at several times
Figure 62	Evolution of the shape of the downstream slope during the seepage test
Figure 63	Measured and simulated values of total head (in meter) at minute 7.5
Figure 64	Measured and simulated values of total head (in meter) at minute 9.5
Figure 65	Measured and simulated values of total head (in meter) at minute 100
Figure 66	Measured and simulated values of total head (in meter) at minute 240
Figure 67	Comparison of total water head within the dike G5-E4
Figure 68	Comparison of total water head within the dike F3-B3
Figure 69	Comparison of total water head within the dike G1-A1
Figure 70	Comparison of downstream flow rate
Figure 71	Fine fraction in several locations after the seepage test

Annex 8 – Small scale model of dike: specimen B-90s

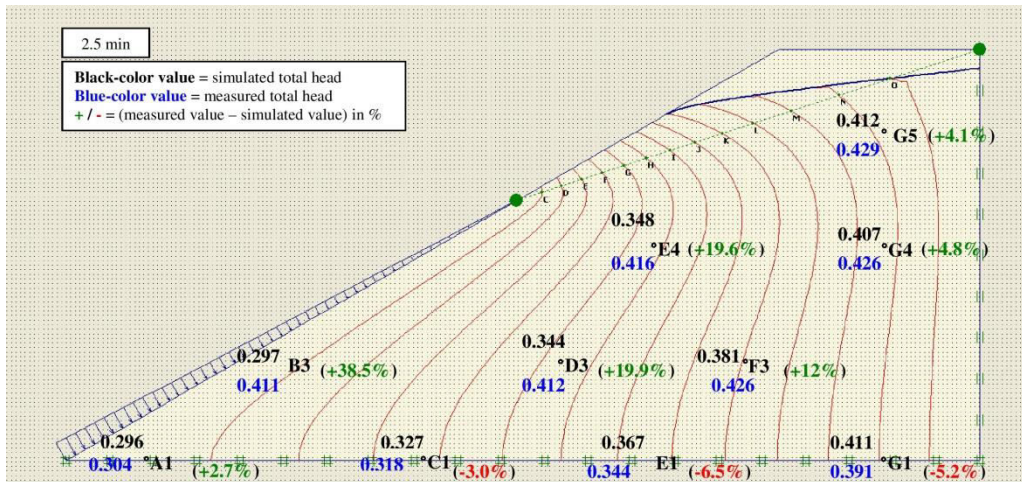


Figure 40 Measured and simulated values of total head (in meter) at minute 2.5 (B-90_s)

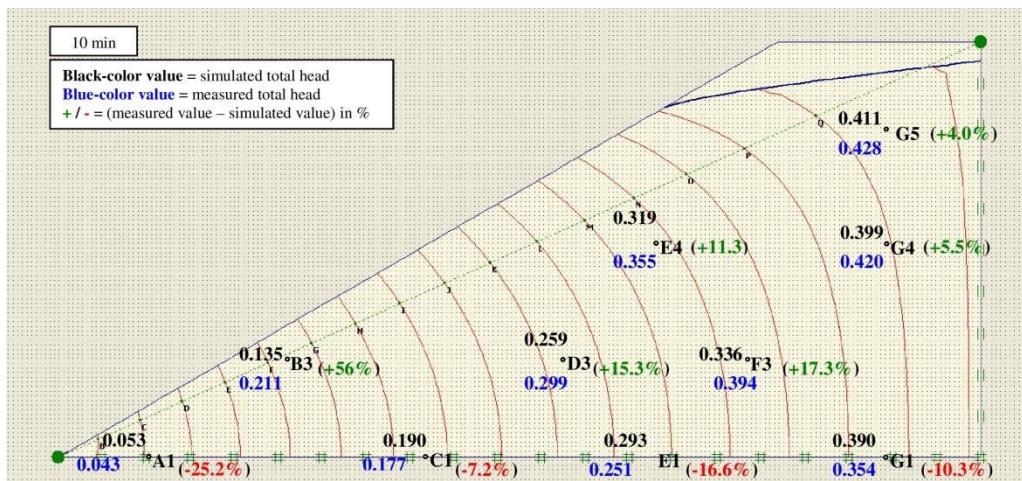


Figure 41 Measured and simulated values of total head (in meter) at minute 10 (B-90_s)

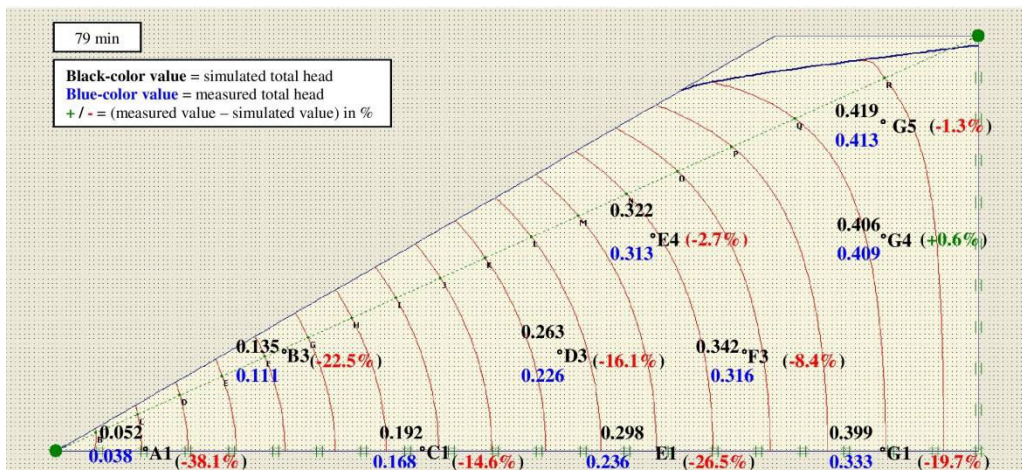


Figure 42 Measured and simulated values of total head (in meter) at minute 79 (B-90_s)

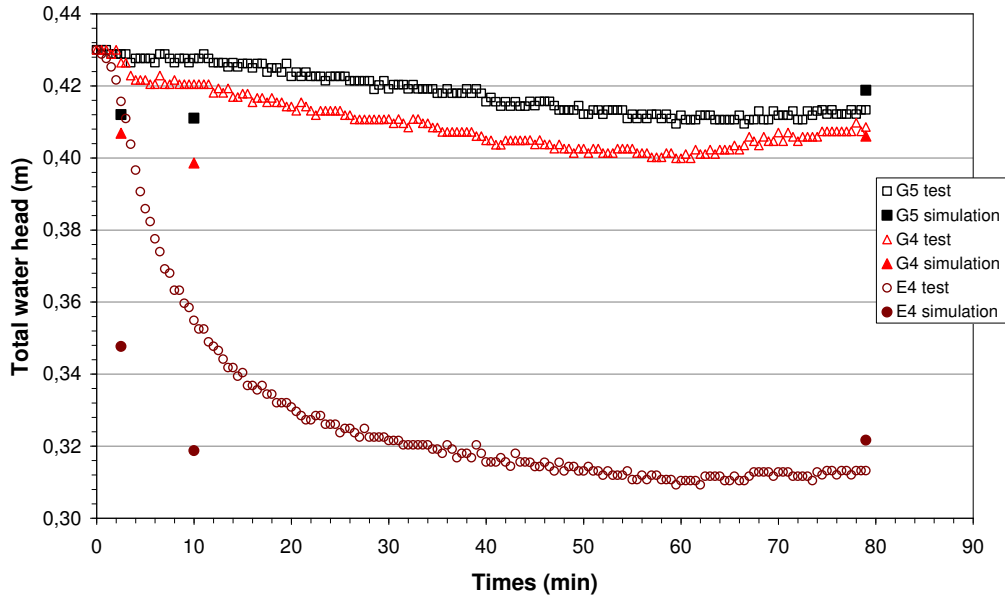


Figure 43 Comparison of total water head within the dike between real test and simulation G5-E4 (B-90_s)

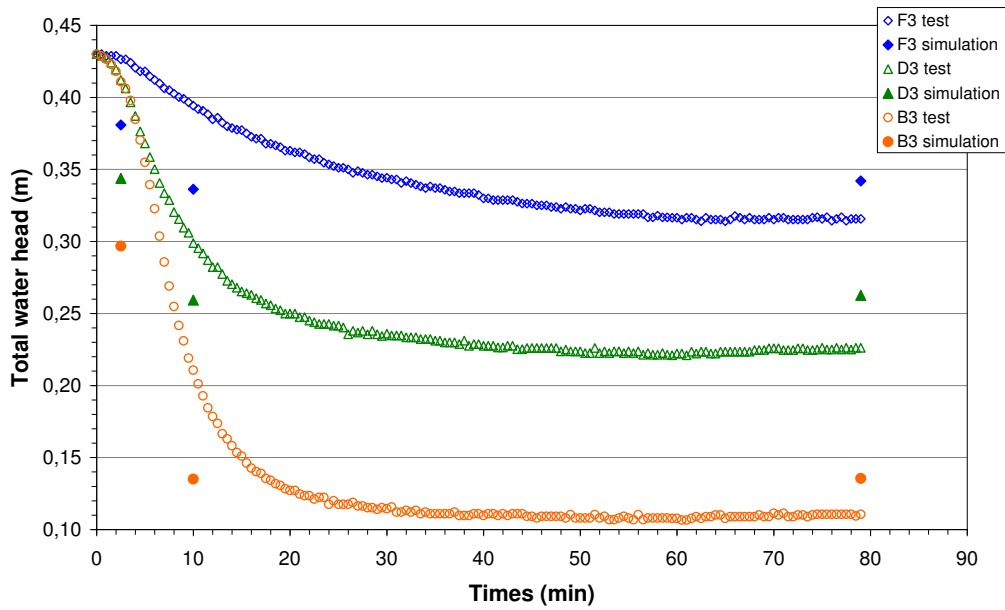


Figure 44 Comparison of total water head within the dike between real test and simulation F3-B3 (B-90_s)

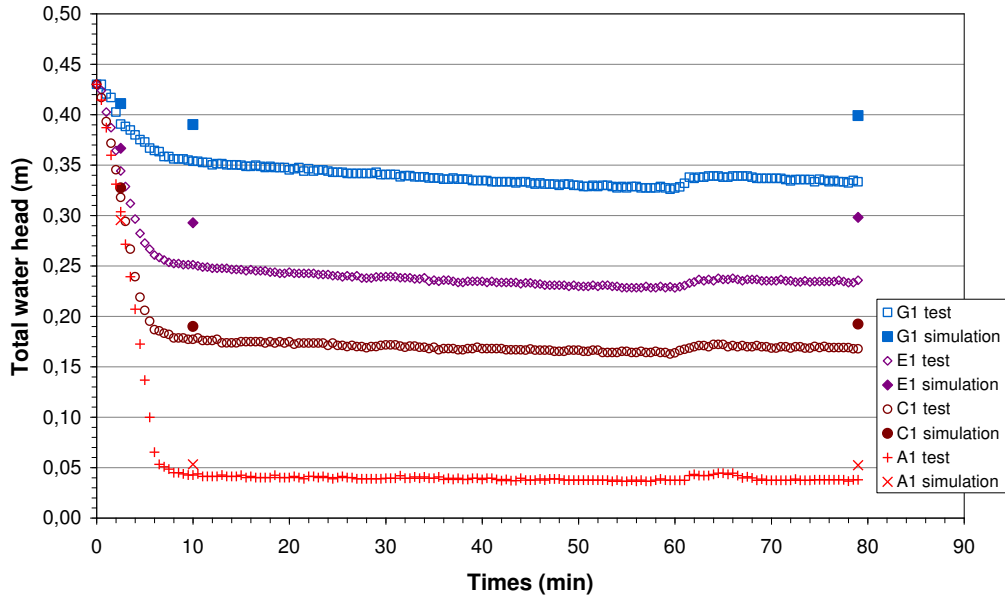


Figure 45 Comparison of total water head within the dike between real test and simulation G1-A1 (B-90_s)

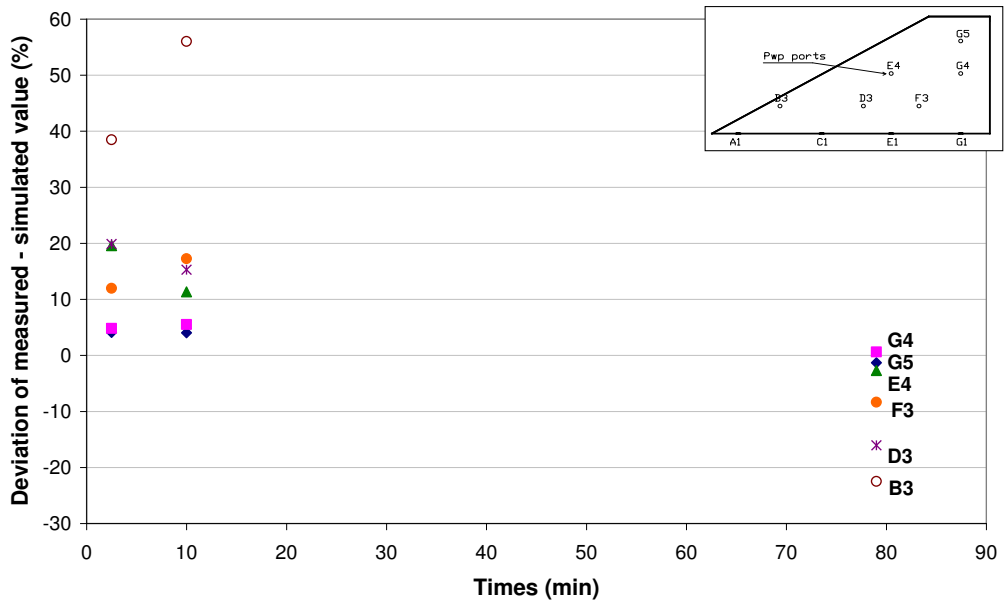


Figure 46 Time series of evolution of deviation values within the dike soil G5-B3 (B-90_s)

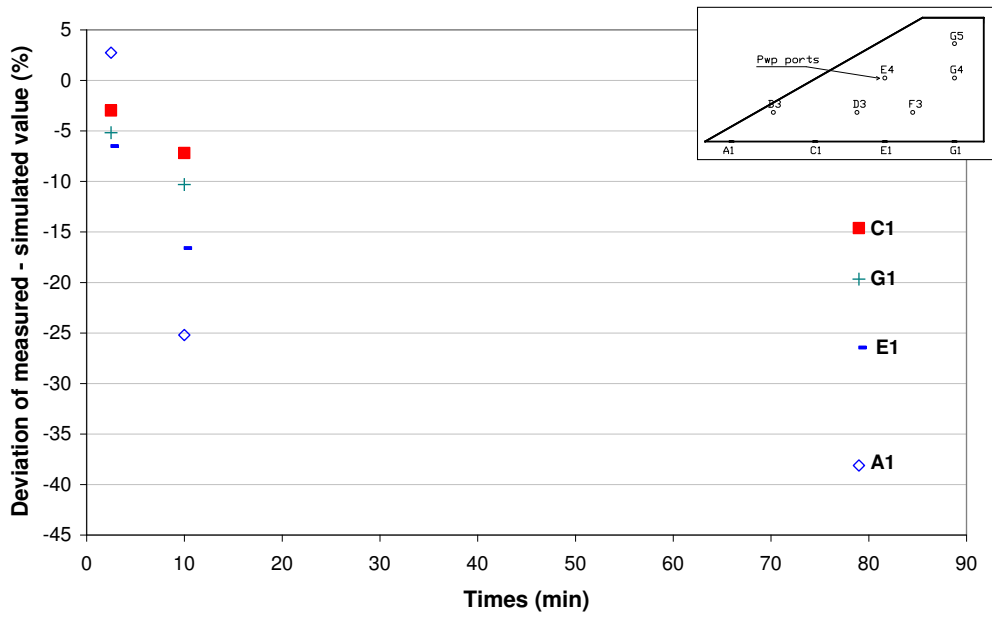


Figure 47 Time series of evolution of deviation values within the dike soil G1-A1 (B-90_s)

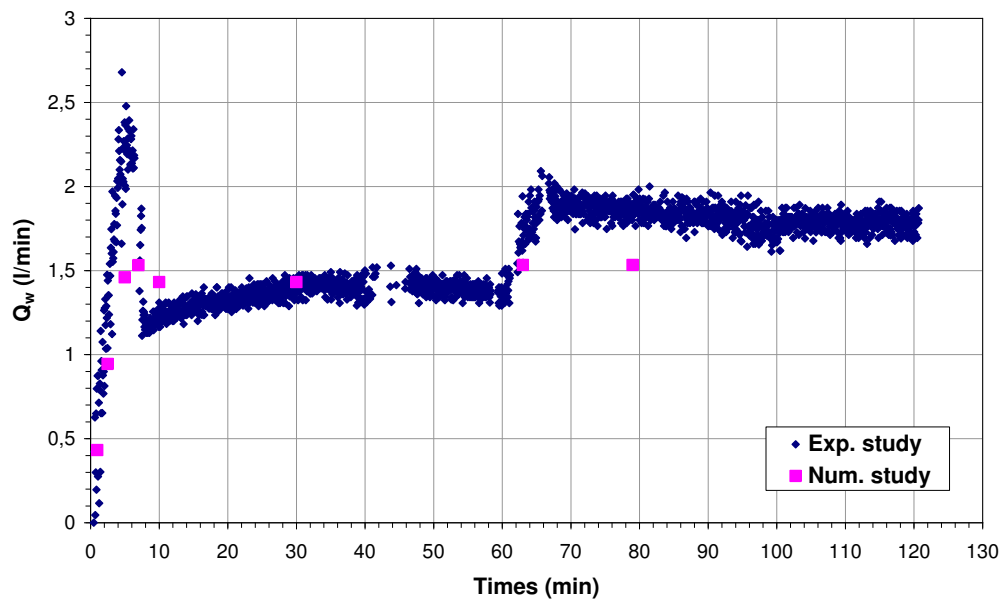


Figure 48 Comparison of downstream flow rate between experimental study and numerical study (B-90_s)

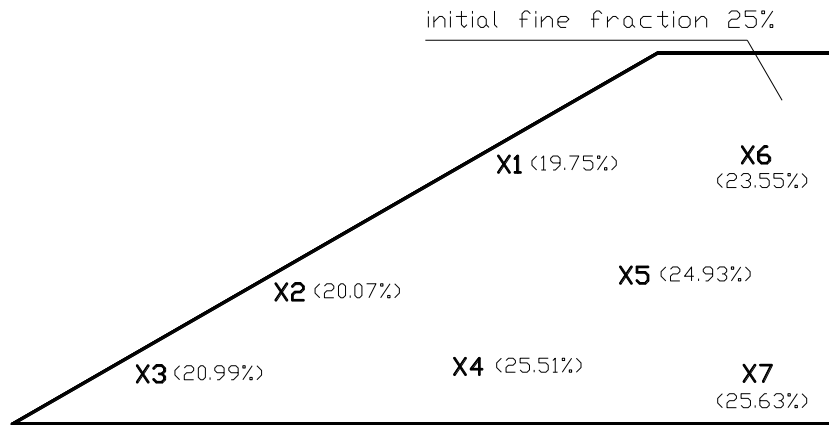


Figure 49 Fine fraction in several locations after the seepage test (B-90_s)

Table 1 Displacement and global safety factor

Phase	Time (min)	Displacement (cm)	FoS
1 Gravity loading		$1.96 \cdot 10^{-1}$	
2 FoS - Phase 1			1.3188
3 Saturation process from base to level 43 cm	8.5	$0.225 \cdot 10^{-1}$	
4 FoS - Phase 3			1.4966
5 Saturation process for one night	1440	$0.103 \cdot 10^{-10}$	
6 FoS - Phase 5			1.4966
7 Seepage flow with downstream water level = 29 cm	2.5	$0.316 \cdot 10^{-1}$	
8 FoS - Phase 7			0.5170
9 Seepage flow with downstream water level = 0.5 cm	10	$1.08 \cdot 10^{-4}$	
10 FoS - Phase 9			0.5285
11 Seepage flow with downstream water level = 0.5 cm	79	$0.452 \cdot 10^{-16}$	
12 FoS - Phase 11			0.3478

Annex 9 – Small scale model of dike: specimen B-75s

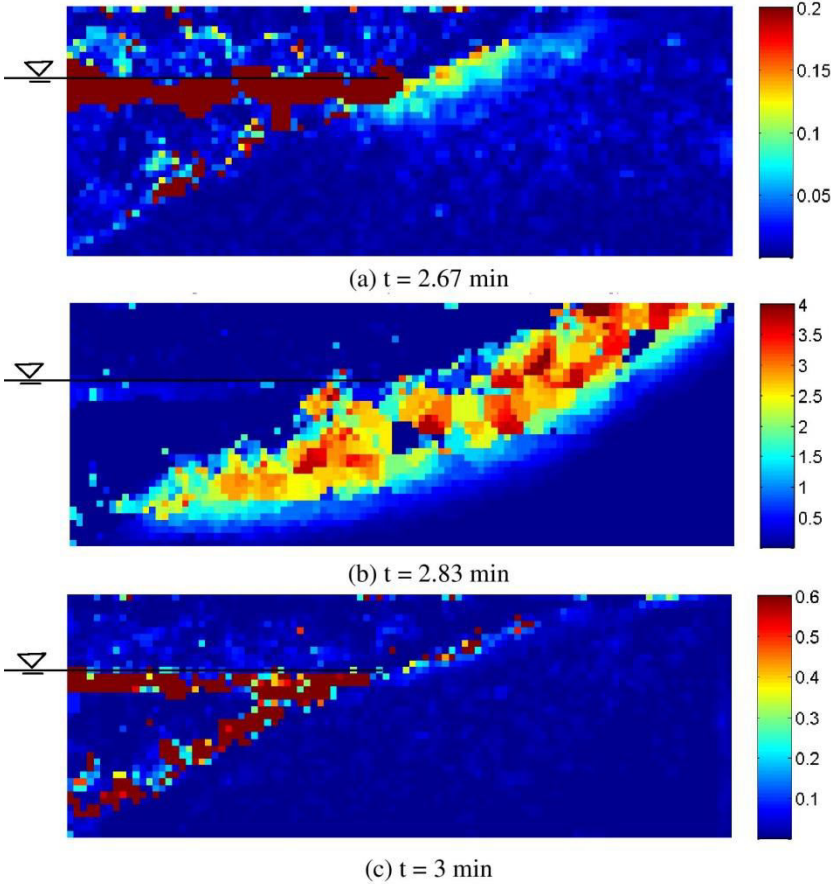


Figure 50 Sliding in the downstream slope at several times (B-75_s)

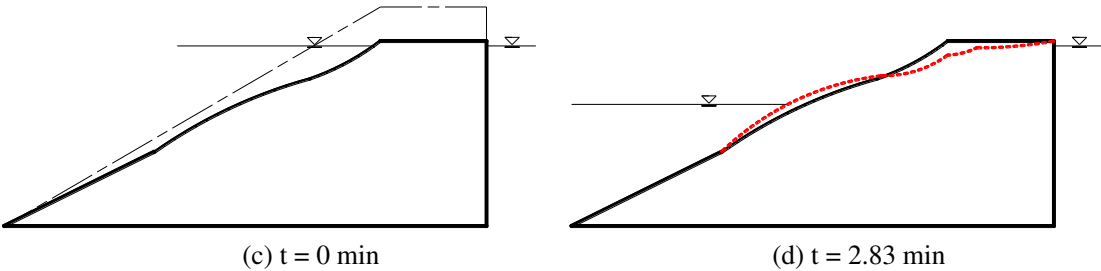


Figure 51 Evolution of the shape of the downstream slope during the seepage test (B-75_s)

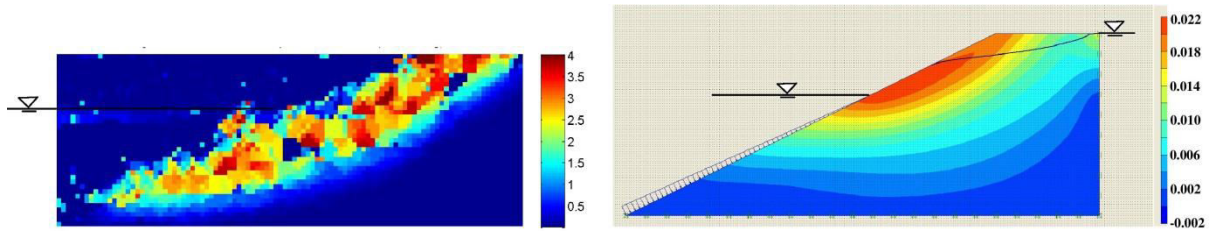


Figure 52 Displacement of at minute 2.83 (experimental vs. numerical study) in cm

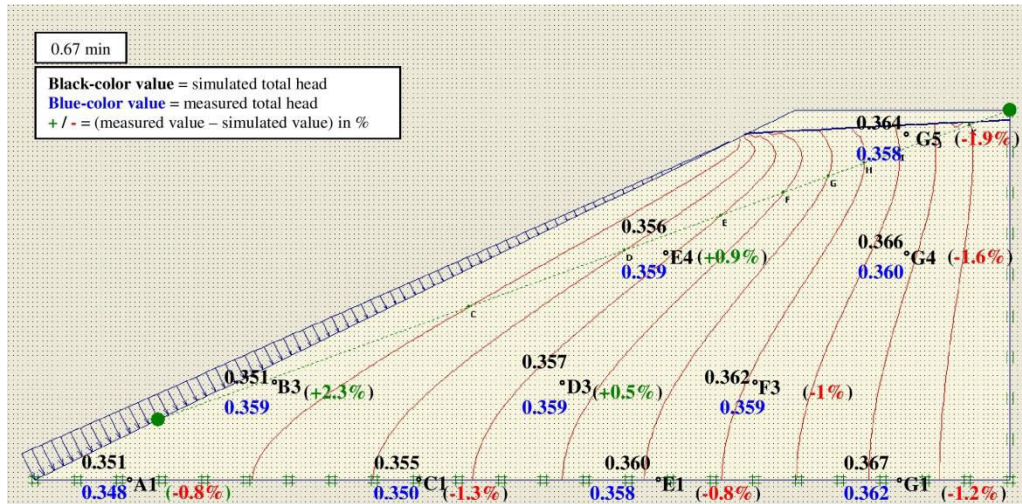


Figure 53 Measured and simulated values of total head (in meter) at minute 1 (B-75_s)

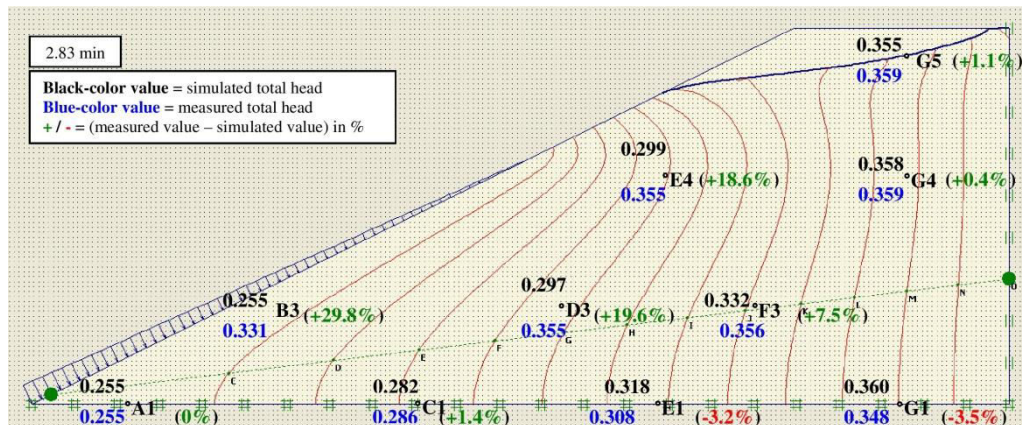


Figure 54 Measured and simulated values of total head (in meter) at minute 3 (B-75_s)

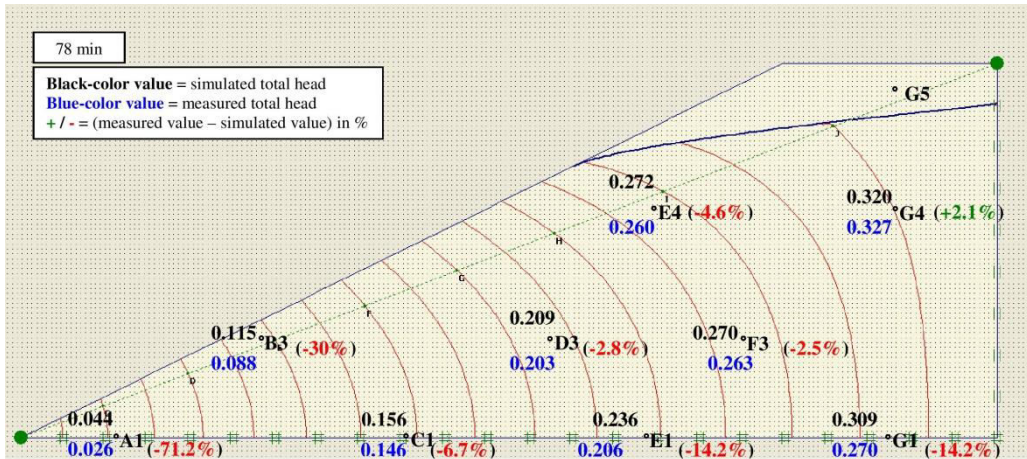


Figure 55 Measured and simulated values of total head (in meter) at minute 78 (B-75_s)

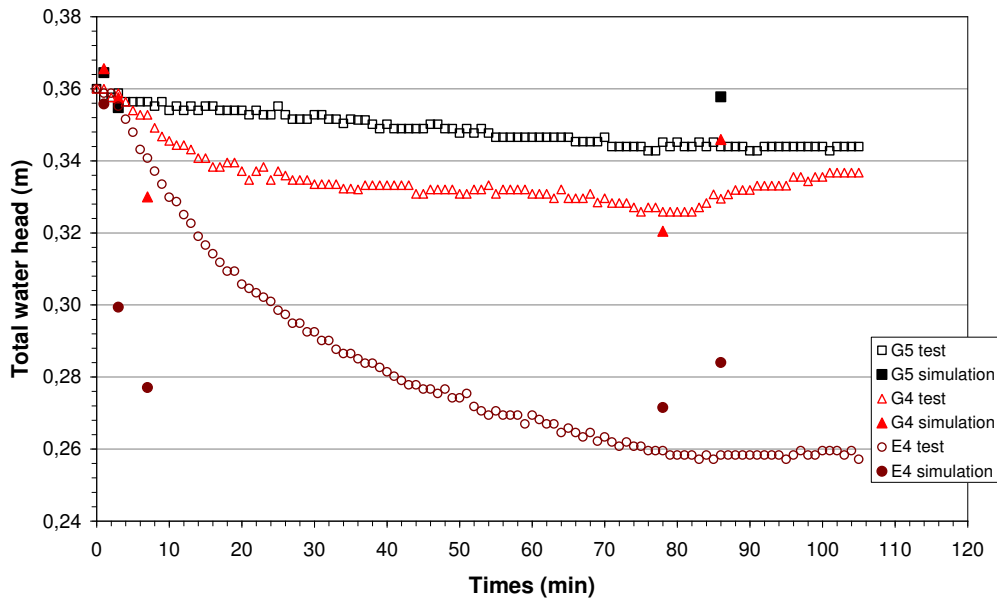


Figure 56 Comparison of total water head within the dike between real test and simulation G5-E4 (B-75_s)

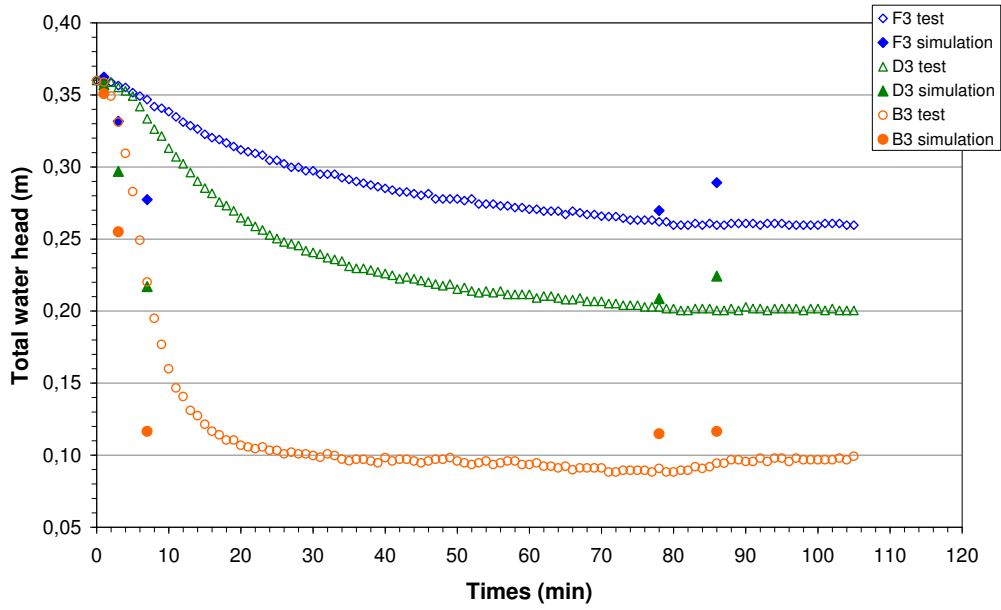


Figure 57 Comparison of total water head within the dike between real test and simulation F3-B3 (B-75_s)

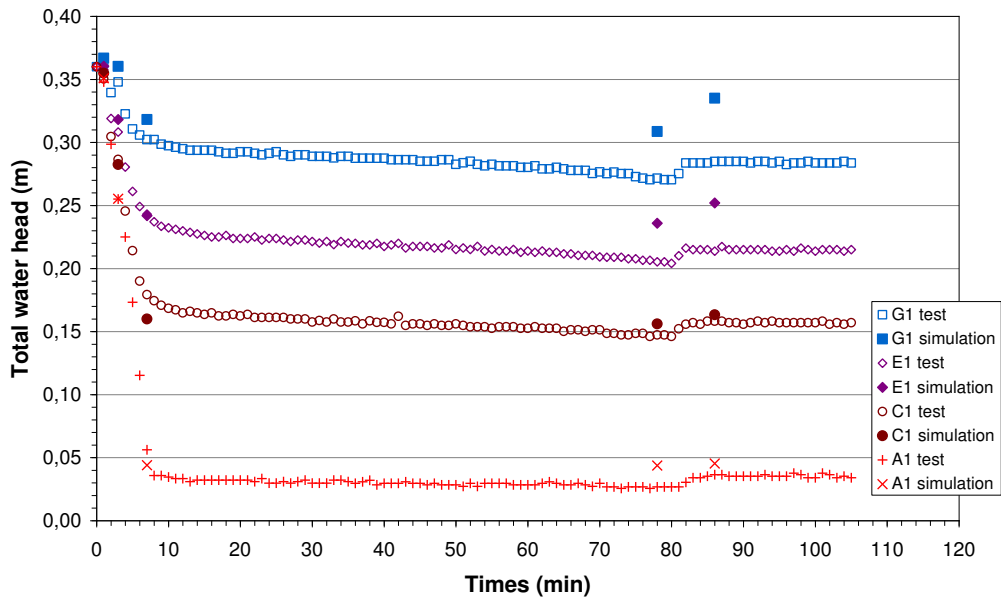


Figure 58 Comparison of total water head within the dike between real test and simulation G1-A1 (B-75_s)

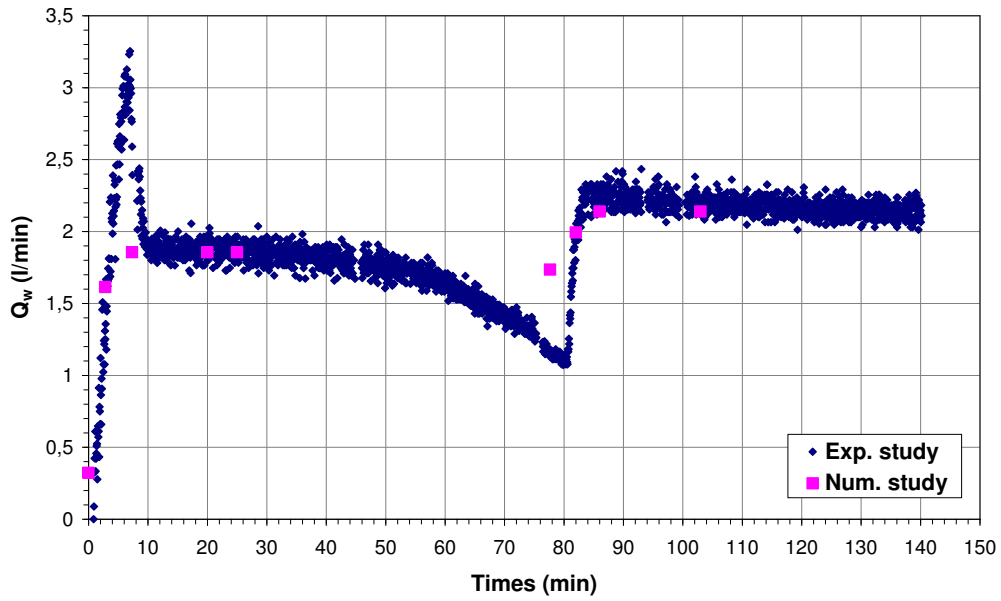


Figure 59 Comparison of downstream flow rate between experimental study and numerical study (B-75s)

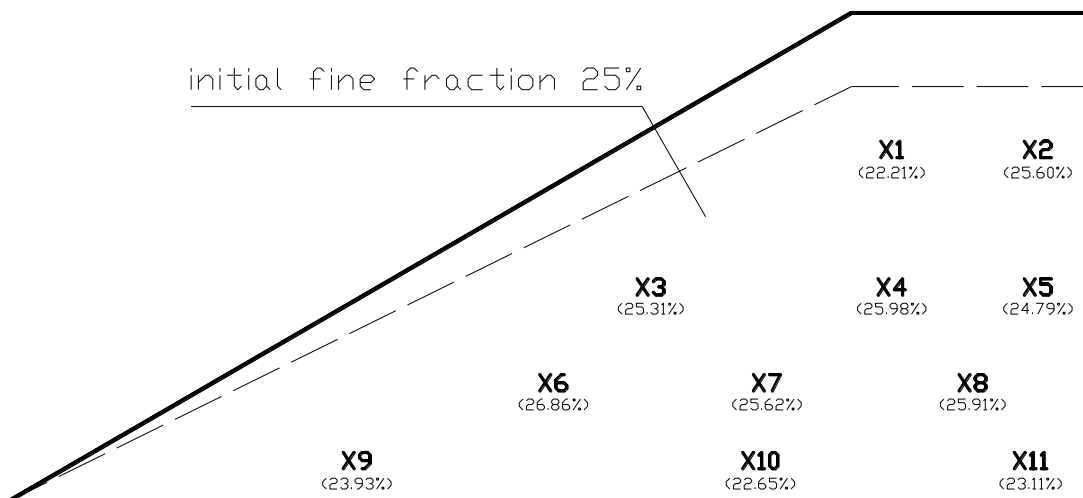


Figure 60 Fine fraction in several locations after the seepage test (B-75_s)

Annex 10 – Small scale model of dike: specimen *B-90u*

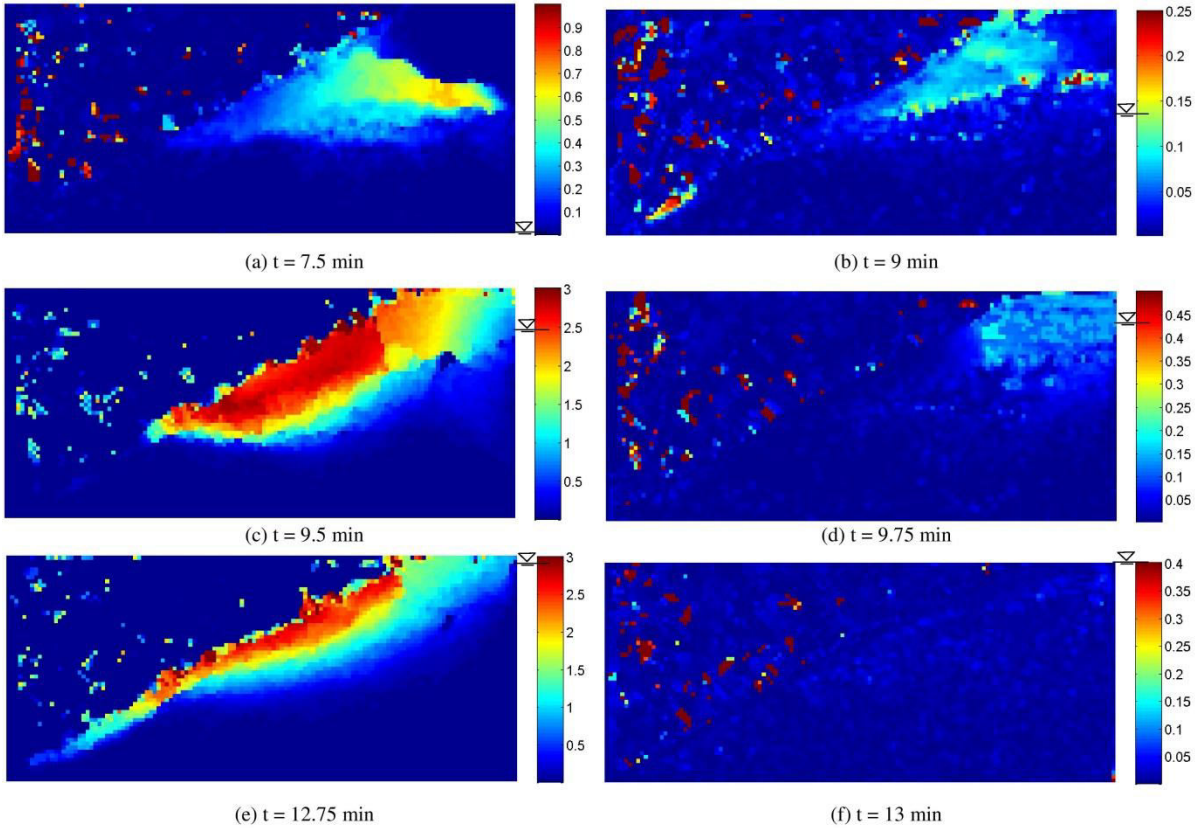


Figure 61 *Sliding in the downstream slope (B-90_u)*

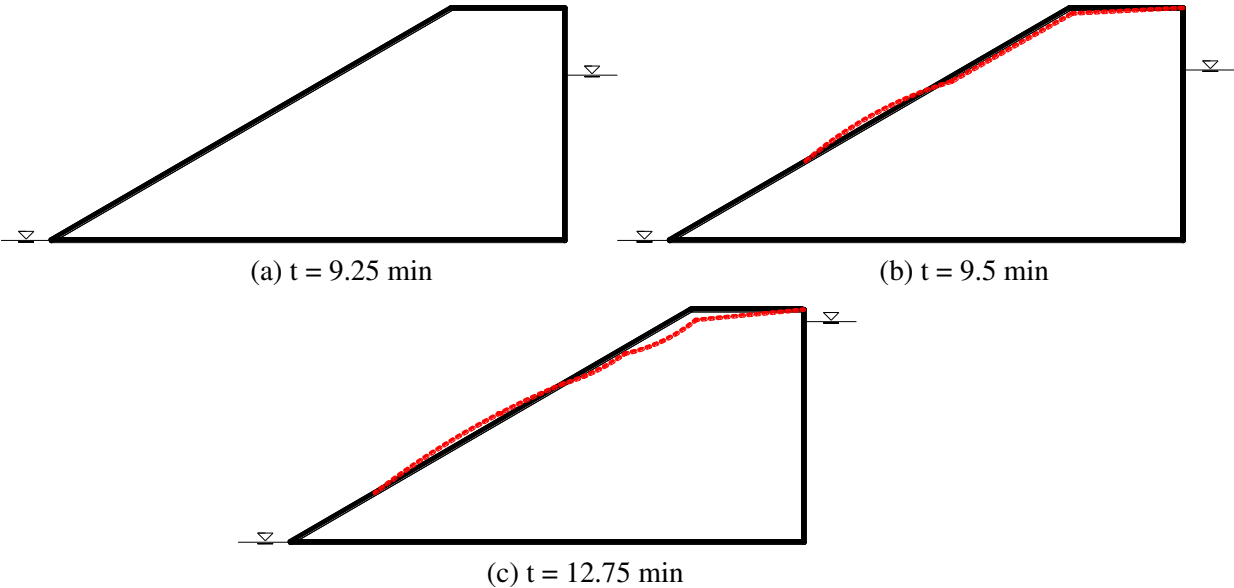


Figure 62 *Evolution of the shape of the downstream slope during the seepage test (B-90_u)*

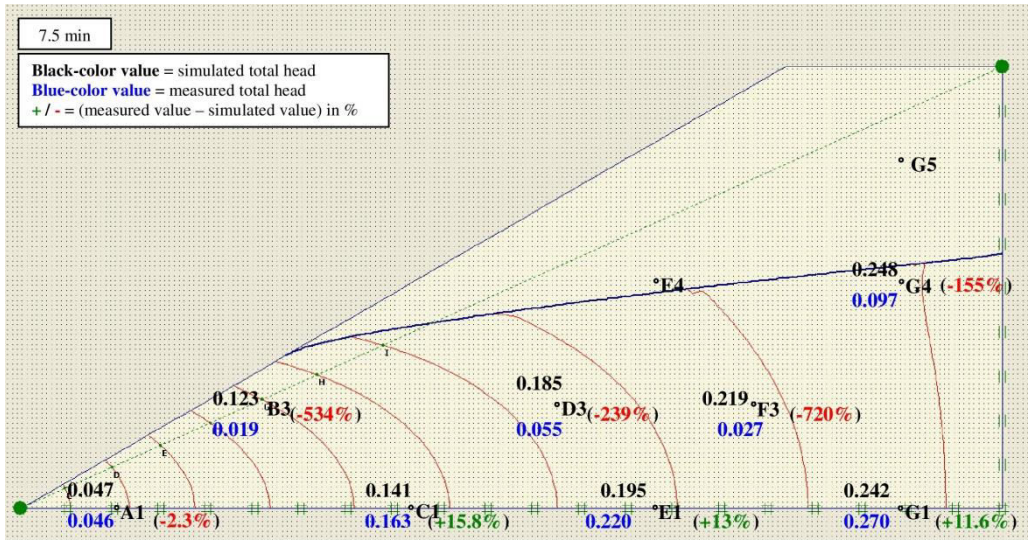


Figure 63 Measured and simulated values of total head (in meter) at minute 7.5 (B-90u)

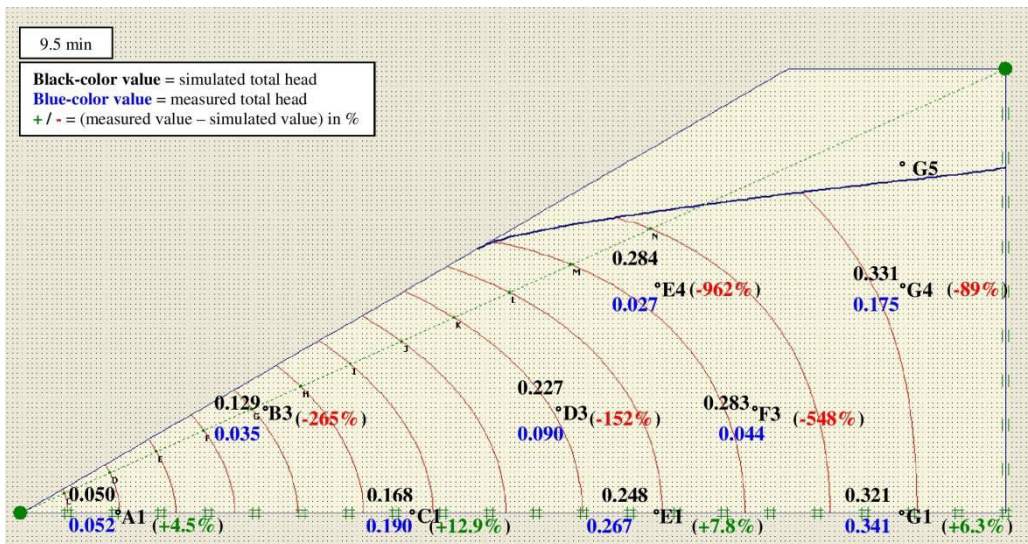


Figure 64 Measured and simulated values of total head (in meter) at minute 9.5 (B-90u)

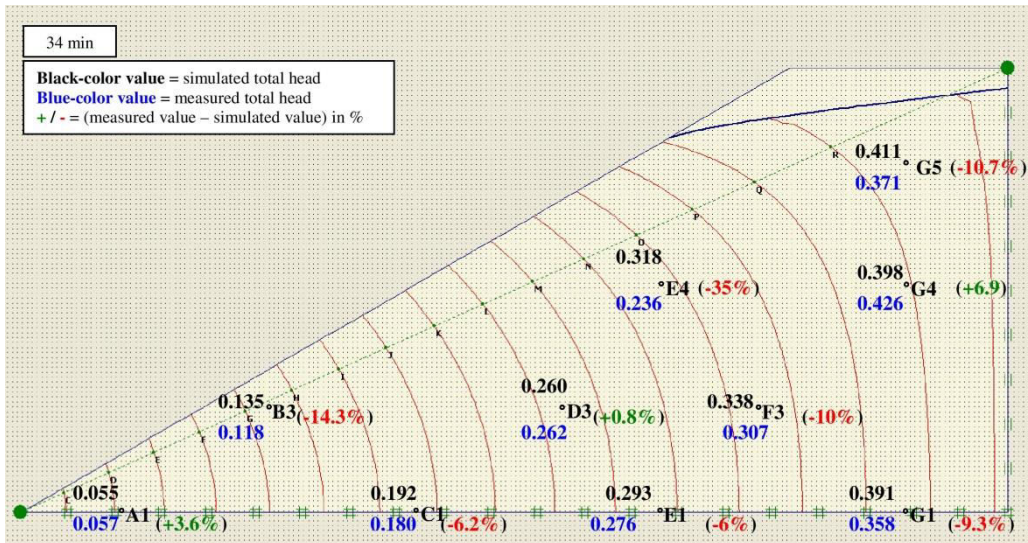


Figure 65 Measured and simulated values of total head (in meter) at minute 100 (B-90u)

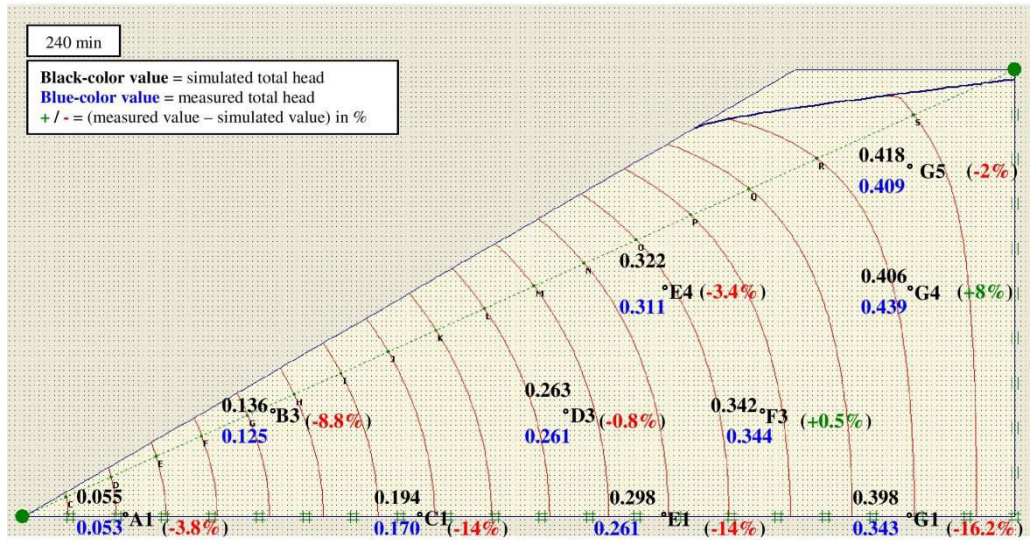


Figure 66 Measured and simulated values of total head (in meter) at minute 240 (B-90_u)

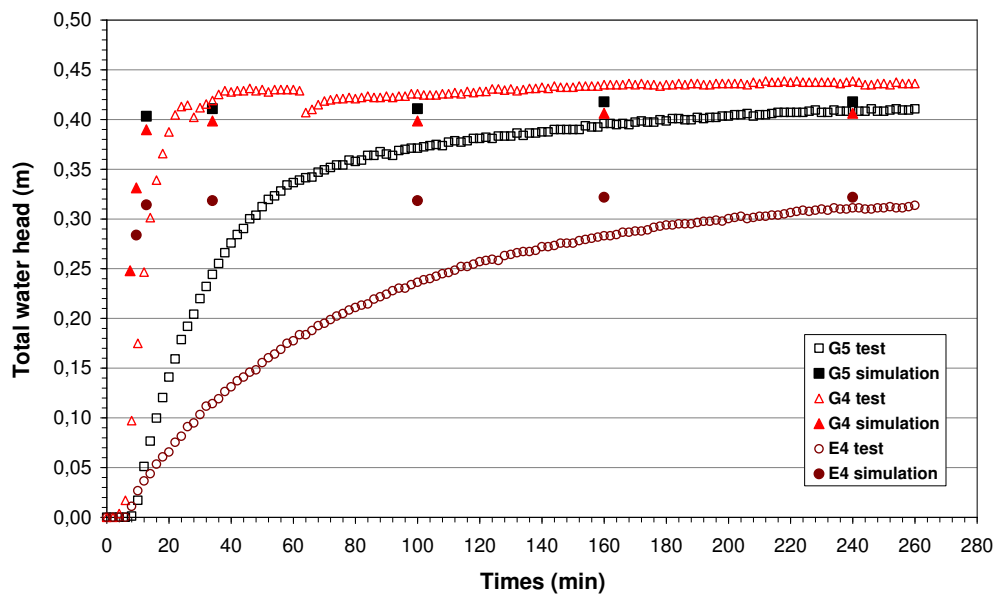


Figure 67 Comparison of total water head within the dike between real test and simulation G5-E4 (B-90_u)

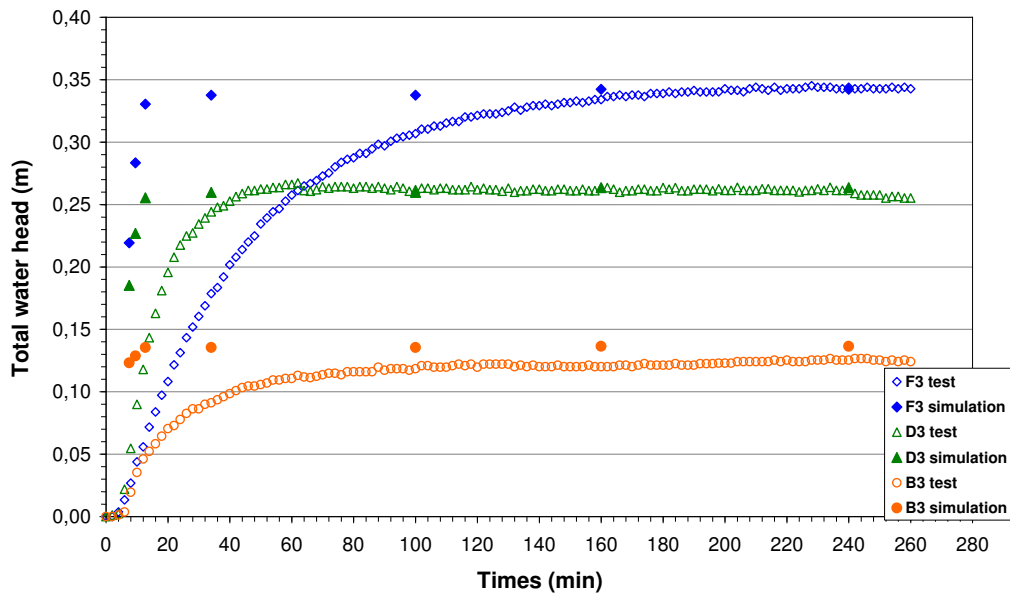


Figure 68 Comparison of total water head within the dike between real test and simulation F3-B3 (B-90_u)

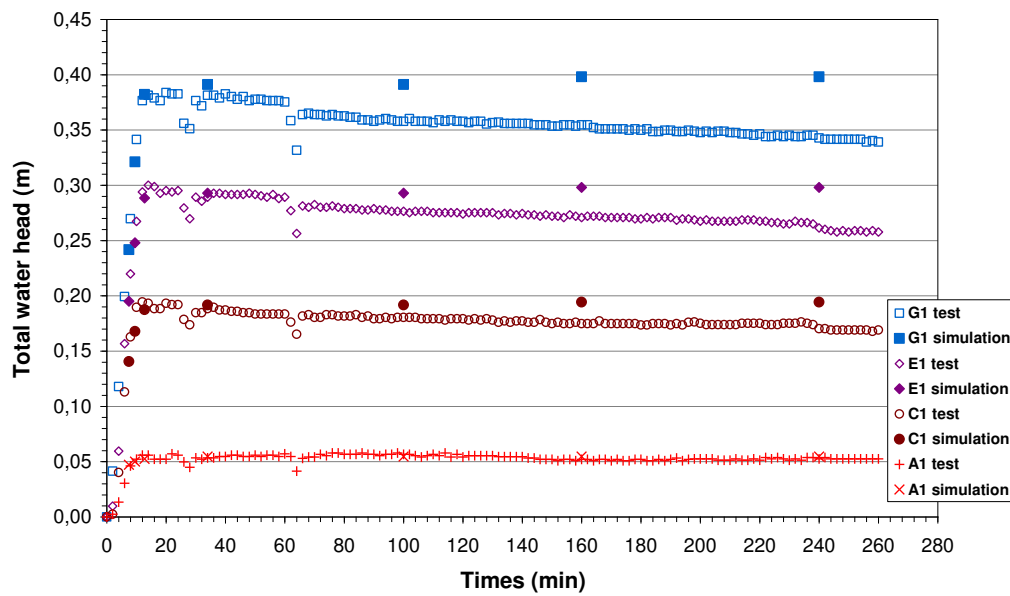


Figure 69 Comparison of total water head within the dike between real test and simulation G1-A1 (B-90_u)

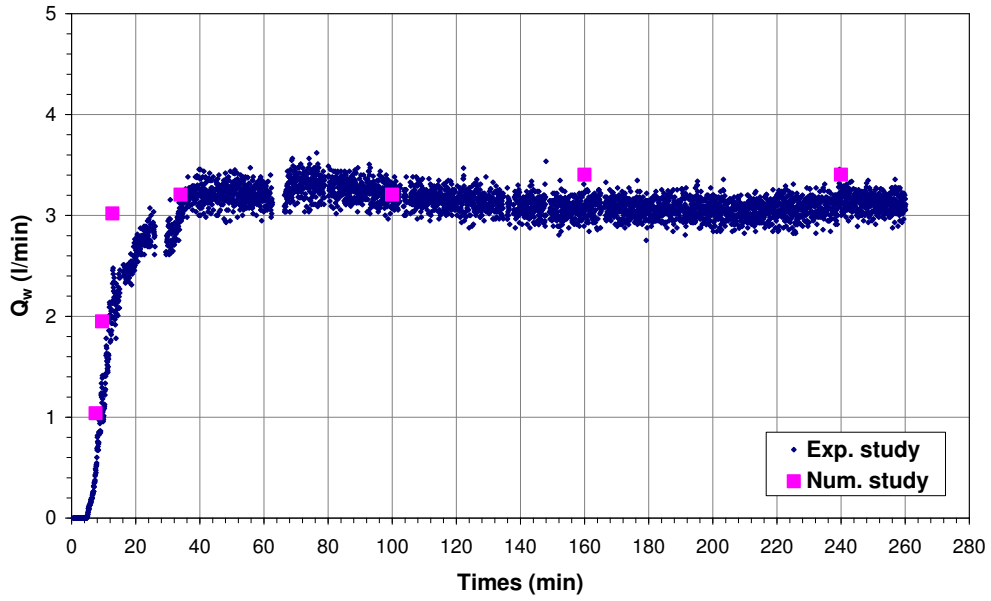


Figure 70 Comparison of downstream flow rate between experimental study and numerical study (B-90_u)

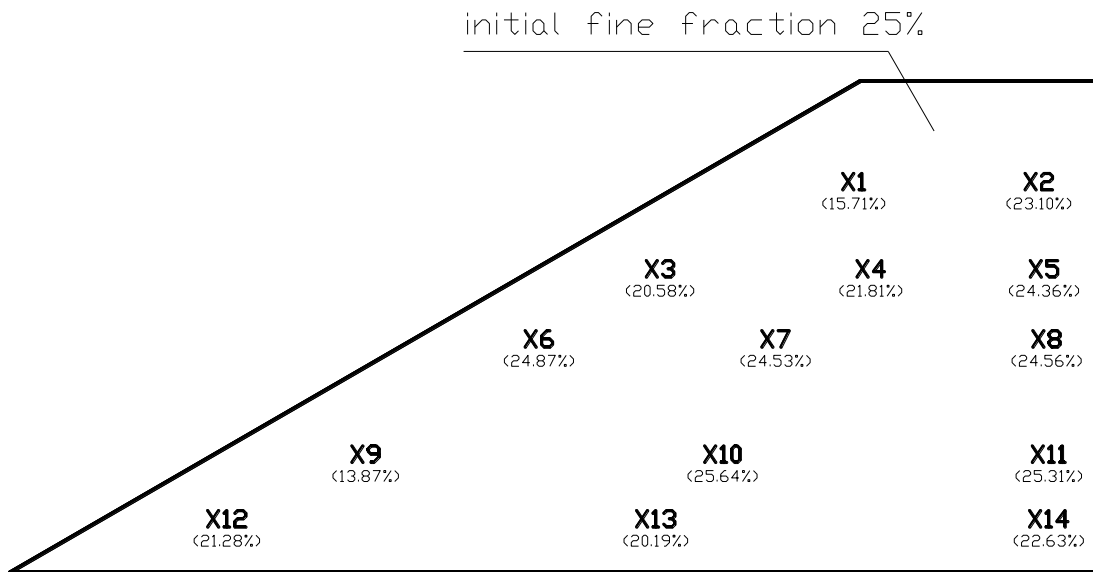


Figure 71 Fine fraction in several locations after the seepage test (B-90_u)

Thèse de Doctorat

Abdul ROCHIM

Characterization of suffusion susceptibility of granular soils

Caractérisation de la sensibilité à la suffusion des sols pulvérulents

Résumé

Une majeure partie des ruptures d'ouvrages hydrauliques en terre (digues, levées, ou barrages) est due aux mécanismes d'érosion interne. Parmi ces mécanismes, la suffusion mobilise la fraction fine des sols constituant l'ouvrage ou le sol de fondation. Ce phénomène est complexe car il combine trois processus : détachement, transport et l'éventuelle filtration d'une partie des grains transportés. Aucune classification de la sensibilité des sols à la suffusion n'est décrite dans la littérature. À l'aide d'un appareillage spécifique, une campagne d'essais de suffusion est menée. Une étude approfondie est également réalisée pour caractériser l'effet de l'historique de chargement hydraulique. L'analyse des résultats montre que les méthodes d'interprétation basées sur le gradient hydraulique ou sur la contrainte de cisaillement hydraulique ne permettent pas d'obtenir une caractérisation unique du processus de suffusion pour différents historiques de chargement hydraulique. La nouvelle analyse basée sur l'énergie dissipée par l'écoulement du fluide interstitiel permet la proposition d'une classification de sensibilité des sols à la suffusion. Des essais sur un modèle physique réduit de digue sont également réalisés. Les premiers résultats soulignent la possibilité d'aboutir à la même classe de sensibilité à la suffusion à l'échelle du modèle physique. Cette caractérisation expérimentale est complétée par des simulations numériques avec le code Plaxis. L'ensemble de ces travaux souligne la complexité des phénomènes mis en jeux et ouvre des perspectives de recherche sur l'applicabilité aux ouvrages des caractérisations réalisées en laboratoire.

Mots clés

Géotechnique, digue, érosion interne, suffusion, expérimentations, énergie d'écoulement, modèle physique, simulation numérique

Abstract

Most of instabilities of hydraulic earth structures (dikes, levees or dams) are due to internal erosion processes. Among these processes, suffusion concerns the fine fraction from structure made of soils or from soil of foundations. This process is complex as it combines three processes: detachment, transport and possibly the filtration of some transported particles. No susceptibility classification for suffusion process exists in literature. Thanks to a specific device, a series of suffusion tests is performed. An advanced study is also realized about the effect of hydraulic loading history. The results show that methods characterizing the erosion susceptibility based on hydraulic gradient or rate of erosion don't lead to a unique characterization of suffusion process for different histories of hydraulic loading. Thanks to a new analysis based on energy expended by the seepage flow to characterize the hydraulic loading, we propose a susceptibility classification for suffusion process. Some tests are performed with a small scale model of dike. First results show that it is possible to obtain the same soil susceptibility classification at the scale of this physical model. The experimental characterization is completed by some numerical simulations with Plaxis software. All these results highlight the complexity of studied processes and open the way to further research opportunities concerning the applicability to earth structures of laboratory characterizations of internal erosion.

Key Words

Geotechnics, dike, internal erosion, suffusion, testing, seepage energy, physical model, numerical simulation